GROWTH AND CHARACTERIZATION OF SOME AMINO ACID DOPED NLO MATERIALS CRYSTALS

Thesis submitted to the

SAURASHTRA UNIVERSITY

For

The degree of

DOCTOR OF PHILOSOPHY

in

PHYSICS

by

DIPAKKUMAR J. DAVE

M. Sc.

Guided by

Dr. M. J. Joshi

Professor

Department of Physics

Suarashtra University

Rajkot 360 005

March 2011

Statements Under O. Ph.D.7 of Saurashtra University

The contents of this thesis is my own work carried out under the supervision of ***Dr. M. J. Joshi*** and leads to some contributions in Physics supported by necessary references.

(Dipakkumar J. Dave)

This is to certify that the present work submitted for Ph. D. Degree of the Saurashtra University, Rajkot, by ***Shri Dipakkumar J. Dave*** has been the result of about six years of work under my supervision and is a valuable contribution in the field of "Solid State Physics and Materials Science".

(Dr. M. J. Joshi)
Professor
Department of Physics
Saurashtra University
Rajkot-360 005

Dedicated

to

My Beloved Family

सक्तुमिव तितउना पुनन्तो

यत्र धीरा मनसा वाचमकृत ।

अत्रा सखायः सखानि जानते

भद्रै षां लक्ष्मीर्निहिताधि वाचि ॥

ऋग्वेद १०–७१–२

As a hopper separates grains from husk, intellectuals in their subjects use a hopper of knowledge to purify their speeches where the other intellectuals understand and appreciate this. A generous Goddess always remains with their speeches.

Rig Veda 10-71-2

ACKNOWLEDGEMENT

The author expresses his deep sense of gratitude and sincere thanks to his guide **Dr. Mihir J. Joshi**, Professor, Department of Physics, Saurashtra University, Rajkot, who introduced him to the field of "*Crystal Growth*", particularly, in the recent field of "Growth of Non Linear Optical Materials Crystals", and guided in the most profound manner with continuous encouragement, inspiration and love during the work and made himself available for guidance and discussion in the odd hours of the days.

The author is highly indebted to **Prof. Hiren H. Joshi**, Head of the Physics Department, Saurashtra University, Rajkot, and the former head of the department **Prof. K. N. Iyer**, for their keen interest and providing the necessary facilities to work. The author wishes to express his gratitude to Prof. B. S. Shah and Prof. B. J. Mehta for their fruitful suggestions during the work.

The author expresses his sincere thanks to other faculty members of the Physics Department, Prof. H.P. Joshi, Prof. D.G. Kuberkar, Dr .G. J. Baldha, Dr. K. B. Modi and Dr. J. A. Bhalodia for their kind help and cooperation during the experimental work.

The author is grateful to his senior research colleagues Dr. Vimal S. Joshi (Principal, R.K. Parikh Arts and Science College, Petlad), Dr. R. M. Dabhi, Dr. H. J. Pandya Dr. K. C. Joseph, Dr. B. B. Parekh, Dr. S. R. Suthar and Dr. S. J. Joshi and also the present co-workers**,** Mr**.** K.D. Parikh, Mr. Poorvesh M. Vyas, Ms. Kashmira P. Tank, Ms. Sonal R. Vasant, Mr. C. K. Chauhan, Mr. Hiren Jani , Mr. R.R. Hajiyani , Mr. Ravi Mansuria and Mr. Ravindra Gohel for their friendly support and kind cooperation throughout the research work.

The present author wishes to express his special heartfelt gratitude to **Ms. Sonal R. Vasant** for helping him in meticulous proof reading, setting alignments, and compilation of the thesis chapters. This work is time consuming,

laborious, tire some and prone to errors and she supported the author throughout the thesis compilation even from early morning to late evening hours, without which it would have been difficult for the author to bring the thesis in this shape easily. The author expresses his special thanks to **Shri K.D. Parikh** for his unending support in compilation of some thesis chapters and helping him in certain data analysis. The author also thanks Dr. Bharat B. Parekh (Pt. Deendayal Petroleum University, Gandhinagar) to help him in designing the experiments in the early stages.

The author seek blessings of the **Pujya Shri Tyagvallabh Swamiji** of Atmiya Education Campus(Rajkot) and also extends his sincere thanks to Dr. A. U. Patel, Principal, M&N Virani Science College, Rajkot, and his other colleagues Dr. B. A. Joshi, Dr. B. S. Trivedi ,Dr. P.C. Shah and Mr. B. G. Panelia. The author also expresses his sincere thanks to Mr. V. K. Lakhani, Mr. Nimish Vasoya, Mr. Tushar K. Pathak , Mr. Ashish Tanna and other co-workers from the Department of Physics, Saurashtra University, Rajkot, for their excellent moral support.

The author is highly thankful to Prof. P. Sagayaraj (Physics Department, Loyola College, Chennai) and his student Mr. Rajesh for helping in getting SHG data in time. The author expresses his gratitude to Prof. Vrinda Thakar (Bioscience Department) and her student Dr. Kinjal Bhatt for taking photographs on microscope and Prof. H.S. Joshi and Prof. Viresh Shah (Chemistry Department) and their students Dr. Dushyant Purohit and Dr. Mathukiya for various experimental help. Also, thanks to the Glass Blower Shri Ranjitbhai for the special design of dialatometer he made.

Author also thanks to workshop staff as well as non- teaching staff and the office staff of the Physics department for their kind cooperation.

The author heartily expresses his gratitude to his beloved father **Mr. Jayantilal Dave**, wife **Mrs. Alka Dave**, daughter Nandini and son Tirth, Father-

in-law, Mother- in -law and all other family members for their unending moral support and love, without which it was difficult to culminate this research work.

At last the author also expresses his heartfelt gratitude towards **Mrs. Shilpa M. Joshi**, Dada and the whole family of his guide for the moral support and the affection throughout the work.

Dipakkumar J. Dave

Rajkot

Date:07/03/2011

Abstract

The recent advances in science and technology have brought a great demand of various crystals with numerous applications. A field of multidisciplinary nature in science and technology has been emerged, known as crystal growth, which deals with the crystal growth methods, crystals characterizations and crystal growth theories. There are different kinds of crystals having various applications grown by different techniques. Broadly speaking, there are three main categories of crystal growth processes. (1) $S \rightarrow S$, process involving solid-solid phase transitions, (2) $L \rightarrow S$, process involving liquid-solid phase transitions, and (3) $V \rightarrow S$, process involving vapor (gas)-solid phase transitions.

Potassium Dihydrogen Phosphate (KDP) and Potassium Dideuterium Phosphate (KD*P) are among the most widely-used commercial NLO materials. They are commonly used for doubling, tripling and quadrupling of Nd:YAG laser at the room temperature. In addition, they are also excellent electro-optic crystals with high electro-optic coefficients, widely used as electro-optical modulators, Q-switches, and Pockels Cells, etc.

The thesis consists of nine chapters as follows.

Chapter I gives a brief review of the NLO effect and NLO materials, in which some theoretical aspects of nonlinear optics (NLO), the importance and the role

of NLO materials in rapidly developing field of science and technology, recent advances and future challenges along with necessary literature survey are included. The significance of the present study is also covered.

Chapter II In this chapter a brief survey of different crystal growth techniques, crystal growth theories and solution growth techniques is given. The author has employed the slow solvent evaporation technique for the growth of pure and 0.3 wt %, 0.4 wt % and 0.5 wt %. L-histidine, L-threonine and DL-methionine doped KDP crystals. The study of solubility curves for pure KDP solution and various amounts of amino acids added solutions are presented. The kinetics of nucleation is also discussed and it has been observed that the induction period as well as nucleation parameters are higher for doped crystals in comparison to the pure KDP crystals.

Chapter III The author has employed CHN analysis, paper chromatography and FT-IR spectroscopy studies of pure and L-histidine, L-threonine and DL-methionine (amino acids) doped KDP crystals are reported, which confirms the successful achievement of doping in KDP .In CHN analysis presence of C and N are detected in all doped samples and not in the pure sample, the proportion of C and N also increases with increase in doping level. In the paper chromatograph of doped samples, characteristically, purple spot is observed. From FTIR analysis, the functional groups and their interactions in the crystal are confirmed

through hydrogen bonds. The functional groups representing amino acids are obviously absent in the pure KDP samples.

Powder XRD is used to study the variation in the unit cell parameters and the possibility of presence of any extra phase due to doping of amino acids in KDP crystals. All samples have showed the single phase nature and not much variation in unit cell parameters of KDP is observed due to doping.

Chapter IV describes the thermo-gravimetric analysis (TGA) of pure and L-histidine, L-threonine and DL- methionine doped KDP crystals. The TGA is carried out from room temperature to 800 ^{o}C. It has been observed that amino acids doped KDP crystals exhibit slightly less thermal stability compared to pure KDP crystals. This the little disadvantage of doping. The Coats and Redfern relation is employed to evaluate kinetic and thermodynamic parameters of the decomposition reaction, the values of both kinetic and thermodynamic parameters are found to be decreased due to doping of various amino acids.

Chapter V covers the dielectric study of L-histidine, L-threonine and DL-methionine doped KDP crystals. In the beginning, a brief review of dielectric study is presented. The dielectric study is carried out on pure and doped KDP crystals at room temperature by varying the frequency of applied field in the range from 100 Hz to 100 kHz. The values of dielectric constant and dielectric loss decrease with increase in frequency of applied field. It have also been observed that the values of dielectric loss and dielectric constant are less for

doped samples in comparison to the pure KDP sample and decrease with increase in doping level. The variation of a.c. resistivity with applied frequency is also presented. The low dielectric loss values in doped crystals have indicated that the doping do not introduce major defects in the crystals. The lowering of dielectric constant values due to doping makes the crystals good candidates for electro-optic applications, which needs lower dielectric constants.

Chapter VI describes the nonlinear optical properties of grown pure and amino acids doped KDP crystals and UV-Vis measurements. The Kurtz and Perry powder method has been used to determine the second harmonic generation of laser beam. A Q-switched, mode locked Nd:YAG laser of 6 mJ/pulse at 1064 nm fundamental radiation is passed through the powdered samples filled in a fine capillary and the radiation emitted by the samples is detected by photodiode detector. The second harmonic radiation intensity is compared with the standard KDP sample. Thus the figure of merit of the SHG for the sample is estimated. It has been found that as the doping of amino acids increases in KDP crystals the SHG efficiency increases. It is beneficial to add amino acids in KDP crystals. The UV-Vis spectra of pure and doped KDP crystals suggest that the optical transmission increases on doping of amino acid. The UV- cut off limit slightly decreases on doping; however, in case of L-threonine doping it remains unaltered. The slight loss of UV cut off limit is the disadvantage of doping, but L-threonine doping is the better option.

Chapter VII In this chapter the dislocation etching study of L-histidine, L-threonine and D L-methionine (amino acid) doped KDP crystals has been explained. The chemical etching technique is quite simple and provides very interesting results regarding the delineation of dislocations on the crystalline plane. Many times the impurity plays important role in dislocation etch-pitting. The etching is carried out at different temperatures on {110} plane of pure and amino acid doped KDP crystals by using glacial acetic acid as the etchant. Flat bottom rhombus type etch pits are obtained. The reactivity at line defects and kinetics of the motion of ledges of etch pits is studied by applying the Arrhenius law. Various kinetic and thermodynamic parameters are obtained. The effect of the doping on the kinetic and thermodynamic parameters is observed in comparison to the pure KDP crystals. Doping do influences the etching behavior of amino acid doped KDP in comparison to pure KDP, but the change in concentration of dopant does not have any systematic effect on etching parameter values. Impurity is expected to produce shallow flat bottomed etch pits. Therefore, the doping of different amino acid is expected to alter chemical etch pitting behaviors. This study is conducted for pure and all three amino acids doped KDP crystals with doping of amino acids in different concentrations.

Chapter VIII deals with the micro-indentation hardness of pure and L-histidine, L-threonine and DL-methionine doped KDP crystals. For any device application, various mechanical properties are very important. The variation of Vickers micro-hardness with applied load is studied. As the applied load increases the Vickers

micro-hardness decreases. Also, as doping increases the Vickers micro-hardness decreases, which indicates that the crystals are becoming soft. Meyer's relation is applied to the results. The Hays and Kendall law is also applied to the results. The cracking phenomenon is also studied around the indentation mark. The fracture toughness values are calculated from the crack measurements. As the doping concentration increases the fracture toughness decreases, which suggests that the doping makes KDP crystals more fragile to produce kracks easily.

Chapter IX presents an overall view of the results and general conclusions. Also, the scope for future work is included.

CONTENTS

Papers Published in National and International Journals

(1) K. D. Parikh, B. B. Parekh, **D. J. Dave**, M. J. Joshi, *Investigation of various growth parameters, FT-IR and thermal studies of gel grown pure and mixed levo-tartrates of Calcium and Strontium tartrate. Ind*ian *J. Physics*, **80** (2006) 719.

(2) K. D. Parikh, **D. J. Dave**, B. B. Parekh, M. J. Joshi, *Thermal, FT-IR and SHG efficiency studies of L-arginine doped KDP crystals,* Bull. Mater. Sci. **30**(2007)1.

(3) **D. J. Dave**, K. D. Parikh, B. B. Parekh, M. J. Joshi, *Growth and Spectroscopic, Thermal, Dielectric and SHG studies of L- Threonine Doped KDP Crystals,* J. of Optoelectronic & Adv. Mater. **11** (2009) 602.

(4) K. D. Parikh, **D. J. Dave,** M.J. Joshi, *Crystal growth, Thermal, Optical, and Dielectric properties of L-lysine doped KDP Crystals*, Mod. Phys. Letts. B. **23** (2009) 15892.

(5) M. J. Joshi , **D. J. Dave** , K. D. Parikh, *Effect of Different Amino Acids on Various Characterization of KDP Single crystal*, Proceeding of the National Symposium on Growth of Detector Grade Single Crystals, BARC, Mumbai (2009) 50.

(6) R. R. Hajiyani, **D. J. Dave**, C., K. Chauhan, P. M. Vyas, M. J. Joshi, *Growth and characterization of Bis – Thiourea strontium chloride single crystals*, Mod. Phys. Letts B, **24** (2010) 735.

(7) K. D. Parikh, **D. J. Dave**, B. B. Parekh, M. J. Joshi, *"Growth and Characterization of L – Alanine doped KDP crystals*", Cryst. Res. Technol. **45** (2010) 603.

(8) K. D. Parikh, **D. J. Dave**, M. J. Joshi, *Dielectric and FT –IR studies of L – Arginine doped KDP crystals,* J. of Sci. **1** (2010) 53.

Research Paper in Communication

(1) **D. J. Dave**, K. D. Parikh, M. J. Joshi, *Modification of Thermal, Optical, and Dielectric properties of KDP Crystals by doping of DL – methionine",* J. of NLO Mater. and Phys.

Paper Presented at National and International Conferences

(1) Thermal, Kinetic, Thermodynamic and SEM Studies of Gel Grown Calcium Oxalate Monohydrates Singles Crystals,V. S. Joshi, B. B. Parekh, **D. J. Dave** and M. J. Joshi, International Conference on Solvo Thermal Reaction-6 (ICSTR-6), 24 - 27 August 2004, Mysore.

(2) The effect of Unripe Mango Juice on the Growth of Brushite Crystals K. C. Joseph, B. B. Parekh, **D. J. Dave** and M. J. Joshi International Conference on Solvo Thermal Reaction-6 (ICSTR-6), 24 - 27 August 2004, Mysore.

(3) Growth, Inhibition and Characterization of Hydroxyapatite Crystals B. B. Parekh, **D. J. Dave**, V. S. Joshi, A. Raut, S.Sunder,N. Pandita and M. J. Joshi, 92nd Indian Science Congress, 2-7 January, 2005, Ahmedabad.

(4) Growth of L - Histidine Doped KDP Crystals,**D. J. Dave**, B. B. Parekh, P. J. Kurani, K. D. Parikh and M.J. Joshi, Seminar on Current Trends in Material Research, February 2005, Saurashtra University, Rajkot.

(5) Growth and Characterization of L-Histidine Doped KDP Crystals, B. B. Parekh, **D. J. Dave**, K. D. Parikh and M. J. Joshi, One Day National

Seminar on Recent Advances in Condensed Matter and Space Physics, UGC-SAP, 21st March 2006, Saurashtra University, Rajkot.

(6) Measurement of Induction Period and Nucleation Kinetics of the L-histidine Doped KDP Crystals, **D. J. Dave**, B. B. Parekh, K. D. Parekh and M. J. Joshi, One Day National Seminar on Recent Advances in Condensed Matter and Space Physics, UGC-SAP, 21st March 2006, Saurashtra University, Rajkot

(7) Thermal Studies of L-Argenine Doped KDP Crystals, K. D. Parikh, B. B. Parekh, **D. J. Dave** and M. J. Joshi, One Day National Seminar on Recent Advances in Condensed Matter and Space Physics, UGC-SAP, 21st March 2006, Saurashtra University, Rajkot

(8) Growth and Characterization of L-threonine doped KDP crystals.

D. J. Dave, B. B. Parekh and M. J. Joshi,International Conference on Materials for Advanced Technologies, 2007 (ICMAT 2007), 1 – 6 July, 2007, Singapore

(9) Thermal and FT-IR Spectroscopic Studies of Bis-thiourea Strontium Chloride Crystals,R. R. Hajiyani, **D. J. Dave**, K. D. Parikh and M. J. Joshi,XXI Gujarat Science Congress, 11th March 2007, Patan.

(10) Influence of sea-water on the growth of calcite crystals, D. D. Khunti, R. M. Dabhi, **D. J. Dave** and M.J.Joshi, One Day National Seminar on Recent Trends in Material Science, 25th March, 2007, Saurashtra University, Rajkot.

(11) Growth and Characterization of L- Histidine doped KDP crystals, M. J. Joshi, **D. J. Dave**, K. D. Parikh and B. B. Parekh, 15th International Conference on

Crystal Growth (ICCG–15), 14th – 17th August, 2007 Salt Lake City, Utah, USA.

(12) Etching study of L – Histidine, DL – Methionine and L – Threonine doped KDP crystals. **D. J. Dave**, K. D. Parikh, P. M. Vyas, R. R. Hajiyani, K. B. Mehta, R. R. Gohel and M. J. Joshi,12th National Seminar on Crystal Growth (With International Participation), 21 - 23 December 2007; Centre for Crystal Growth, S. S. N College of Engineering, Chennai

(13) Growth, Thermal and Kinetic parameters of 4–(2– hydroxyphenylamino) – pent – 3 – 2 – one crystals, B. B. Parekh, P. M. Vyas, **D. J. Dave**, R. R. Hajiyani and M. J. Joshi, Seminar on Advances in Materials Research (AMR - 08), Department of Physics, Saurashtra University, Rajkot

(14) Growth, FT – IR spectroscopic, powder XRD and Chemical etching studies of L – arginine, L – lysine and L – alanine doped KDP crystals. K. D. Parikh, **D. J. Dave**, B. B. Parekh and M. J. Joshi,13th National Conference on Crystal Growth, SSN Nagar, Chennai, 27 – 29 January, 2009

(15) Study of L – arginine doped Ammonium Dihydrogen Phosphate crystals M. J. Joshi, R. R. Gohel, P. M. Vyas, **D. J. Dave**, K. D. Parikh, B. B. Parekh, International Conference on Crystal Growth (ICCG - 16), 8th – 13th August, 2010, Beijing.

Chapter-I

Brief Introduction to Nonlinear Optical Materials Crystals

Light, my light, the world – filling light

The eye – kissing light,

Heart – sweetening light!

Ah, the light dances, my darling, at the centre of my life;

The light strikes, my darling, the chord of my love;

The sky opens, the wind runs wild, laughter passes over Earth.

The butterflies spread their sails on the sea of light;

Lilies and Jasmines surge up on the crest of the waves of light;

The light is shattered into gold on every cloud,

My darling and it scatters gems in profusion

Mirth spreads from leaf to leaf, my darling,

and gladness without measure

The heaven's river has drowned its banks

and the flood of joy is aboard.

Rabindranath Tagore, 'Light'

Light is a prima donna in the nature's opera! Light signifies knowledge and life. Light played the crucial role, when the life evolved on the Mother Earth. The first optical instrument bestowed upon vertebrates and invertebrates was eye by the Mother Nature. Pre – historic humans were thrilled by natural optical phenomena like rain – bow and mirrage. As the civilizations developed, the optics and optical instruments started taking shape gradually right from common spectacles to complicated equipments

like telescopes, microscopes, interferometers, etc. Moreover, the study of various optical phenomena, for example, diffraction, interference, dispersion, polarizations, etc. has added either new branches or new dimensions to optics.

Optics, the study of light, is usually divided into three fields, each of which employs different method of theoretical treatment, these are (1) geometrical optics (2) physical optics and (3) quantum optics.

The geometrical optics is treated by the method of light rays. The physical optics is concerned with the nature of light and involves primarily the theory of waves. Whereas, the quantum optics deals with the interaction of light with the atomic entities of matter and which for an exact mathematical treatment needs quantum mechanic [1].

Later on, the new fields like magneto-optics and electro-optics were developed .The optical phenomena, which depends on an applied magnetic field are called magneto-optics and, similarly, which depends on applied electric field are called electro- optics. Nowadays, extended fields of optics, for instant, singular optics, non-imagining optics, non-linear optics, statistical otpics, etc, are available.

An optical vortex or phase singularity is a zero of an optical field- a point of zero intensity. The research into the properties of vortices has begun after the comprehensive study by Nye and Berry [2], which is known as “Singular Optics”. Light can be twisted like a corkscrew around its axis of travel and because of this; the light waves at the axis itself cancel each other out. When projected on to a flat surface, an optical vortex looks like a ring of

light, with a dark hole in the centre. This corkscrew of light with darkness at the centre is called an optical vortex.

Non – imaging optics is the branch of optics deals with the optical transfer of light radiation between a source and target. Unlike the traditional imagining optics, the techniques involved do not attempt to form an image of source, but an optimized optical system for optical radiative transfer from source to target is achieved, for example in photomultiplier tubes.

Nonlinear Optics (NLO) is the branch of optics that describes the behaviors of light in non-linear media, that is, the media in which the dielectric, polarization *P* gives response to the electric field *E* of light non-linearly. This non-linearity is only observed at very high intensity of light having values of the electric field comparable to the inter-atomic electric fields 10^8 V/m, which is provided by pulsed laser. In nonlinear optics, the superposition principle no longer holds [3, 4]. After the discovery of lasers, the dimension of optics changed completely. A review is written by Rao [5], on the completion of 50 years of discovery of lasers. There are also branches of optics like Statistical Optics [6] and Fourier Optics [7] and many more.

The present author interested to give a brief introduction to NLO and NLO crystals, which will be covered in the following section.

1.1 Origin of NLO

Before the advent of the lasers, it was assumed that the optical parameters of the medium were independent of the intensity of the light propagating in that medium. The electric field strength generated by the non-laser light sources is of the order of 10^3 V/cm, which is very much smaller than the inter-atomic fields. Whereas, the inter-atomic electric field strength of the

medium is of the order of 10^{7} to 10^{10} V/cm. Therefore, normal light source is unable to affect the atomic fields of the medium and thereby the optical properties of the medium. On the other hand, lasers generate electric field strength of the order of 10^{5} to 10^{9} V/cm, which is able to commensurate to that of the atomic electric fields of the medium. This affects the optical properties of the medium and thus generates new electromagnetic fields altered in phase, frequency and amplitude.

The first demonstration of Nonlinear Optical (NLO) frequency conversion took place as early as in 1961 by Franken et al [8]. They used quartz crystal to double the frequency of 694 nm light of Ruby laser. Inasmuch as the interaction was not phase matched, the ultraviolet output power was so small that the editors of the journal mistook for a blemish the spot on spectrograph plate that demonstrated the new effect. However, in the end 1962, the classical paper appeared in which Armstrong et al, [9] have given the theoretical underpinning for both microscopic origin of the nonlinear susceptibilities and the propagation effects governing macroscopic Nonlinear interactions between electro-magnetic waves. Later on, Nicolas Bloembergen won Nobel Prize in 1981 for his contribution in laser spectroscopy. Also, the selected papers of Bloembergen were published under the title," Encounter in the Nonlinear Optics" [10]. Then the quest began for identifying various nonlinear optical materials and which had gathered momentum in past more than one decade.

The present author feels pride to write this brief introduction to the nonlinear optics on 50^{th} year of its discovery.

In a dielectric medium when an electric field is applied, the charges are displaced slightly from their usual position. This small movement of positive charge in one direction and negative charge in other, results in a collection of induced dielectric dipole moment [11]. A light wave consists of electric and magnetic fields which vary sinusoidally at optical frequencies. The motion of charged particles in a dielectric medium in response to an optical electrical field also oscillates and forms oscillatory dipoles. At very low fields, the induced polarization is directly proportional to the electric field [12].

$$P = \varepsilon_0 \chi^{(1)} E \qquad (1.1)$$

Where, *E* is the magnitude of the applied electric field, $\chi^{(1)}$ is the linear susceptibility of the material, *P* is the polarization and ε_0 is the permittivity of free space.

The NLO phenomena occur at sufficiently intense fields. As the applied field strength increases (e.g. in lasers) the polarization response of the medium is no longer linear as shown by the equation (1.1). The induced polarization (*P*) becomes a function of the applied field and given by [13],

$$P = \varepsilon_0 \chi^{(1)} E + \varepsilon_0 \chi^{(2)} E^2 + \varepsilon_0 \chi^{(3)} E^3 + \ldots\ldots\ldots \qquad (1.2)$$

Each term is modified by the susceptibility, χ a tensor quantity. The susceptibility tensor for second-order effects $\chi^{(2)} = \chi_{ij}$ relates each of the three components of the polarization – P_x, P_y and P_z to the nine products of the two applied light fields, for a total 27 terms. For convenience, the second order susceptibility is converted into nonlinear optical coefficient d_{ijk}. Different definitions and dimensions are used; therefore, absolute value of d_{ijk} should be used with care. The most common second order effect and the most

important NLO phenomenon is the second-harmonic-generation (SHG). In the similar manner the third order susceptibility, a fourth-rank tensor and the third order coefficients are responsible for the third harmonic generation, parametric conversion, stimulated scattering, etc. there are 81 possible third order terms.

The net polarization of a material depends on its symmetry properties with respect to the orientation of the applied field. A careful examination of the symmetries in a material is indispensable in understanding its nonlinear optical properties. For instance, 11 of the point groups are “centrosymmetric”, meaning that the structure of the crystal remains unchanged along a direction reversed 180º. No second order effects can take place in centrosymmetric crystals as all components of even order of χ are zero. Obviously, an important criterion for a material to exhibit SHG is that it should be a non-centro-symmetric material.

At the molecular level equation (1.2) is expressed as [14],

$$P = \sum_{j} \alpha_{ij} E + \sum_{j<k} \beta_{ijk} E^2 + \sum_{j<k<l} \gamma_{ijkl} E^3 + \ldots\ldots\ldots \quad (1.3)$$

Where, α_{ij} = Polarizability, β_{ijk} = First hyper-polarizability (second order effects), γ_{ijkl} = Second hyper-polarizability (third order effects) and *i,j,k,l* corresponds to the molecular coordinates.

A medium exhibiting such a NLO response might consist of a crystal composed of molecules with asymmetric charge distribution. If the medium (or molecule) is centro-symmetric, then first order hyper-polarizability (β) is zero, indicating that centro-symmetric media do not show second harmonic generation. If a field +*E* is applied to the medium, equation (1.3) predicts the

first Nonlinear term as $+\beta E^2$. If a field $-E$ is applied, the polarization is still predicted to be $+\beta E^2$. Yet, if the medium is centro-symmetric the polarization should be $-\beta E^2$. This contradiction can be resolved only if β=0. Thus the centro-symmetric medium has zero β-value. In the case of third order NLO susceptibility, if $+E$ field produces polarization $+\gamma E^3$ and $-E$ field produces $-\gamma E^3$, so the second order hyper-polarizability (γ) is the first non-zero nonlinear term in centro-symmetric media [15].

1.2 Various Types of Second-Order NLO Effects

In a medium several second-order NLO effects can be observed experimentally which are summerized as follows [16].

Second Harmonic Generation (SHG)

The process of transformation of light with frequency ω into light with double frequency 2ω is referred as SHG [17]. In figure (1.1), the two photons with momenta P_1 and P_2 are absorbed and photon with momentum P is emitted. This process is spontaneous and involves three photon transitions, for instance, two photons with the same energy $h\nu$ are absorbed spontaneously to emit a photon with energy $2h\nu$.

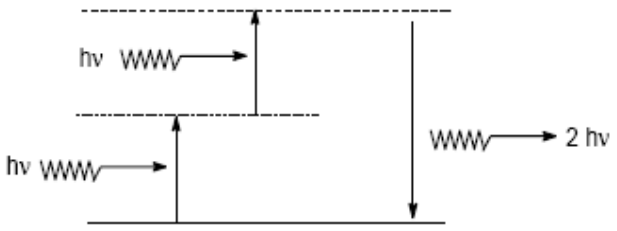

Figure 1.1 Second harmonic generation.

Frequency doubling or SHG is a special case of sum frequency generation if the two input wavelengths are the same. In figures (1.2) to (1.5)

several methods for obtaining SHG are shown schematically. The simplest scheme for frequency doubling is extra cavity doubling, where the laser beam passes through the nonlinear crystal only once. However, if the power density of laser is low, focused beam, intra-cavity doubling and external resonant cavity are normally used to increase the power density on the crystals.

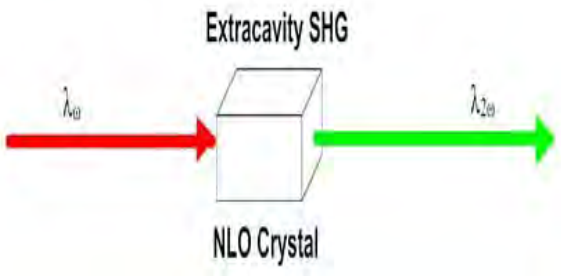

Figure: 1.2 Extra cavity SHG.

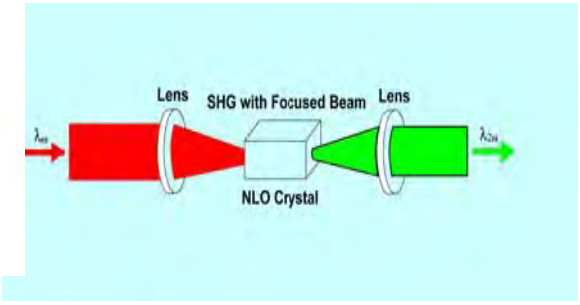

Figure: 1.3 SHG with focused beam.

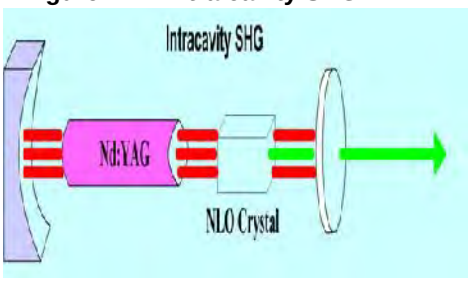

Figure: 1.4 Intra-cavity SHG.

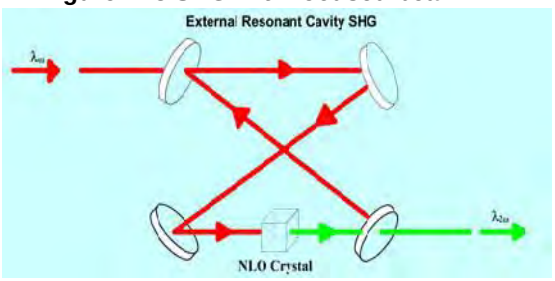

Figure: 1.5 External resonant cavity SHG.

Sum and Difference Frequency Generation or Parametric Generation

The essential goal of practical nonlinear optical frequency conversion is the efficient generation of radiation of sum, difference and second harmonic frequencies. If two monochromatic optical fields, with frequencies ω_1 and ω_2 and amplitudes E_1 and E_2, respectively, are applied to a medium with non vanishing second-order susceptibility $\chi^{(2)}$, the induced dipole response will contain, in addition to the ordinary linear response terms at frequencies ω_1

and ω_2, a Nonlinear response P_2 proportional to $\chi^{(2)} E_1 E_2$, with spectral components at $\omega_1 \pm \omega_2$, are obtained as follows:

Suppose two travelling waves are,

$$E_1(z,t) = E_1\cos(\omega_1 t + k_1 z) \quad (1.4)$$

$$E_2(z,t) = E_2\cos(\omega_2 t + k_2 z) \quad (1.5)$$

Considering the second order Nonlinearity in polarization alone is,

$$P = \chi^{(2)} E^2 \quad (1.6)$$

$$P=\chi^{(2)}[E_1^2\cos^2(\omega_1 t + k_1 z) + E_2^2\cos^2(\omega_2 t + k_2 z) +$$

$$2\,E_1\cos(\omega_1 t + k_1 z)\,E_2\cos(\omega_2 t + k_2 z)] \quad (1.7)$$

However, from above expression it can be found that the polarization consists of number of component with different frequencies as follows:

Where, first term is $=P_1\,\omega_1=\chi^{(2)} E_1^2\,[\cos 2(\omega_1 t + k_1 z)]$

And second term is $=P_2\omega_2=\chi^{(2)} E_2^2\,[\cos 2(\omega_2 t + k_2 z)]$

$$P_1\,\omega_1 + P_2\omega_2 =\chi^{(2)} E_1 E_2[\cos(\omega_1+ \omega_2)t + \cos(k_1 + k_2)z]$$

$$P_1\,\omega_1 - P_2\omega_2 =\chi^{(2)} E_1 E_2[\cos(\omega_1- \omega_2)t + \cos(k_1 - k_2)z]$$

And steady term, $P_{direct} = (\chi^{(2)}/2)\,(E_1^2 + E_2^2)$

The different components of nonlinear polarization generate electromagnetic waves having frequency different from those of the incident ones.

Sum Frequency Generation (SFG)

From equation (1.7) the sum of frequency term is obtained which is $\omega_1+\omega_2=\omega_3$ (or in form of wavelength $1/\lambda_1+1/\lambda_2=1/\lambda_3$). This is shown in figure (1.6) schematically. It combines two low energy (or low frequency) photons into a high energy photon.

Figure: 1.6 Schematic representation of Sum frequency generation.

If ω_3 and ω_1 are fixed, then ω_2 is also fixed. Notwithstanding, in the case of only ω_3 is fixed, then the other two are free to range over many values; this effect is called as the *parametric amplification*. This is used to produce coherent radiation at frequencies in ultraviolet region [18, 19]. The additional wave length made available by harmonic generation and parametric oscillation find applications in photochemistry, high resolution spectroscopy and the remote detection and identification of atmospheric pollutants by optical radar or LIDAR [20].

Optical Parametric Generation (OPG)

Optical Parametric Generation (OPG) is an inverse process of sum frequency generation. It splits one high-frequency photon (pumping wavelength, λ_p) into two low-frequency photons (signal, λ_s, and idler wavelength, λ_i). If two mirrors are added to form a cavity, an Optical Parametric Oscillator (OPO) is established. For a fixed pump wavelength, an infinite number of signal and idler wavelengths can be generated by tilting a crystal. Therefore, OPG is an excellent source for generating wide tunable range coherent radiation. The OPG is shown in figure (1.7) schematically.

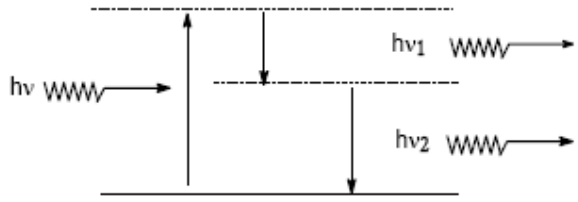

Figure: 1.7 Schematic representation of Optical Parametric Oscillator.

This is a three photon process in which one photon with energy $h\nu$ is absorbed and two photons with energies $h\nu_1$ and $h\nu_2$ are emitted.

Differential-Frequency Generation (DFG)

From the equation (1.7) the difference of frequency term is obtained which is $\omega_1-\omega_2=\omega_3$ (or in form of wavelength $1/\lambda_1-1/\lambda_2=1/\lambda_3$)

It combines two high energy photons into a low energy photon. This is shown schematically in figure (1.8).

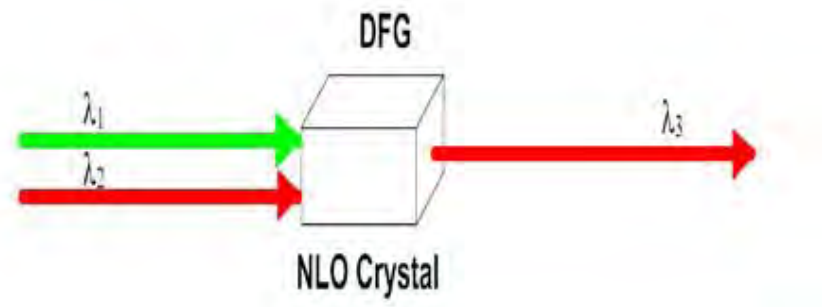

Figure: 1.8 Schematic representation of difference frequency generation.

Linear Electro-optic Effect or Pockels Effect

The Pockels effect is a linear change in the refractive index (or the optical susceptibility) of a medium in the presence of an external electric field. Here a DC field is applied to a medium through which an optical wave propagates. The change in the polarization due to the presence of these two interacting field components effectively alters the refractive index of the medium [15].

Optical Rectification

The optical rectification is defined as the ability to induce a dc voltage between the electrodes placed on the surface of the crystal when an intense laser beam is directed into the crystal [15]. Equation (1.7) shows the term responsible for optical retification.

1.3 Some Important Parameters of NLO Process

Some of the important parameters of NLO process are summarized as follows:

Phase-matching

Many of the practical problems associated with optical frequency mixing come from the distributed nature of the mixing process. Particularly, the difference in the phase velocities of the interacting waves of different frequencies in the Nonlinear medium produces a phase difference that accumulates along the length of the device and significantly limits the efficiency of the mixing process. In order to obtain high conversion efficiency, the phase vectors of input beams and generated beams have to be matched $\Delta K=k_3-k_2-k_1=2\pi(n_3/\lambda_3-n_2/\lambda_2-n_1/\lambda_1)=0$. Where, ΔK is phase mismatching, k_i is phase vector at λ_i and n_i is refractive index at λ_i. In low power case, the relationship between conversion efficiency and phase mismatching is:

$$\eta \alpha PL(d_{eff}\, Sin(\Delta KL)/\Delta KL)^2 \qquad (1.8)$$

Where, d_{eff} is the effective Nonlinear coefficient , L is the crystal length , P is the input power density and ΔK is the phase mismatching.

It is clear that the conversion efficiency will drop dramatically if ΔK increases and the same has been given in the figure (1.9).

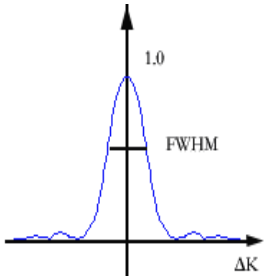

Figure: 1.9 Plot of conversion efficiency Vs *ΔK.*

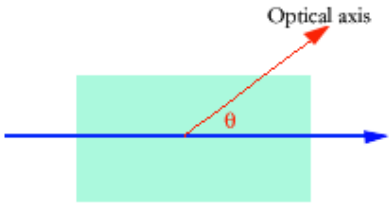

Figure: 1.10 Critical phase matching.

The phase-matching can be obtained by angle tilting; temperature tuning or other methods. The angle tilting is mostly used to obtain the phase-matching as shown in figure (1.10). If the angle between optical axis and beam propagation (θ) is not equal to 90^0 or 0^0, it is called the Critical Phase Matching (CPM). Whereas, the Non-Critical Phase-Matching (NCPM) obtained values of 90^0 and 0^0.Two types of phase-matchings are classified in consideration of polarization of lasers. If the polarizations of two input beams (for sum of frequency) are parallel to each other, it is called as the type I phase-matching. If the polarizations are perpendicular to each other, then it is called type II phase-matching. Type I and Type II phase matching conditions are shown in figures (1.11) and figure (1.12), respectively.

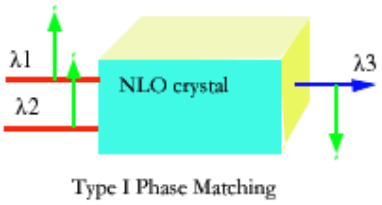

Figure: 1.11 Type I phase matching.

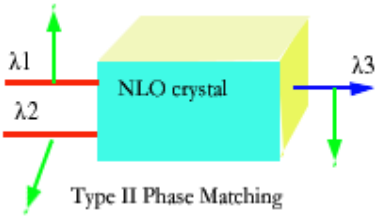

Figure: 1.12 Type II phase matching.

Conversion Efficiency

The most important aim is to obtain a high conversion efficiency of a selected NLO crystal. The conversion efficiency has the relationship with

effective nonlinear coefficient (d_{eff}), as given by equation (1.8), in general, higher the power density, longer the crystal length, larger the nonlinear coefficients and smaller the phase mismatching will result higher conversion efficiency. However, there are some limitations coming from nonlinear crystals and lasers used , for example, the d_{eff} is determined by the nonlinear crystal itself and the input power density has to be lower than the damage threshold of crystal.

1.4 Some NLO Crystal Parameters

For selecting crystals for different applications, certain crystal parameters are important to consider along with the laser parameters. Table (1.1) lists various laser and crystal parameters for selecting proper NLO crystals. Various NLO parameters are discussed in detail by Adhav [21].

Table :1.1 Different Laser and Crystal Parameters required for NLO.

Laser Parameters	Crystal Parameters
NLO Process	Phase-Matching Type and Angle
Power or Energy	Damage Threshold, D_{eff}
Divergence	Acceptance
Bandwidth	Spectral Acceptance
Beam Size	Crystal Size, Walk-off Angle
Pulse Width	Group Velocity Mismatching
Repetition Rate	Damage Threshold
Environment	Temperature Acceptance, Moisture

Crystal Acceptance

If a laser light propagates in the direction with angle $\Delta\theta$ to phase matching direction, the conversion efficiency will reduce dramatically. One

defines the acceptance angle (Δθ) as full angle at half maximum (FAHM), where θ is 0^0, is phase-matching direction.

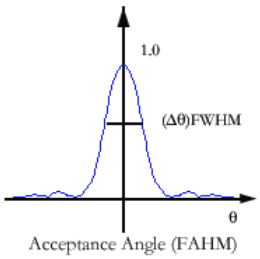

Figure: 1.13 Plot of conversion efficiency Vs acceptance angle.

Moreover, there are certain other parameters to be considered along with the crystal acceptance, which are the spectral acceptance ($\Delta\lambda$) of crystal and the spectral bandwidth of the laser as well as crystal temperature acceptance (ΔT) and the temperature change of environment.

Beam Walk-Off

Due to the birefringence in NLO crystals, the extraordinary wave (n_e) will experience Poynting vector walk-off as shown in figure (1.14), which is the angular deviation between ordinary ray and extra ordinary ray as they propagate through the crystal. If the beam size of input beam is separated at walk-off angle (ρ) in the crystal, it will cause low conversion efficiency. Therefore, for a focused beam or intra-cavity SHG experiment the walk-off is a main limitation to high conversion efficiency.

Figure: 1.14 The angular deviation between ordinary ray and extra ordinary ray.

Two other methods of phase matching avoids beam walk off by forcing all frequencies to propagate at a 90^0 angle with respect to the optical axis of

the crystal. These methods are called temperature tuning method and quasi – phase matching. In temperature tuning, the pump (laser) frequency polarization is selected orthogonal to the signal and idler frequency polarization. The birefringence in some crystals, for example, Lithium niobate is highly temperature dependent. The crystal is controlled at a certain temperature to achieve phase matching conditions. In quasi – phase matching the frequencies involved are not constantly locked in phase with each other, instead the crystal axis is altered at a regular interval. Hence, these crystals are called periodically poled. This results in the polarization response of the crystal to be shifted back in phase with the pump beam by reversing the Nonlinear susceptibility. This allows net positive energy flow from pump into the signal idler frequencies. In this case, the crystal itself provides the additional wave vector $K = 2\pi/\lambda$ to satisfy the phase matching condition. The quasi – phase matching can be expanded to chipped pulse as it is done in a dazzler.

Group Velocity Mismatching

For NLO processes of ultrafast lasers such as Ti:Sapphire and Dye lasers with femto second (fs) pulse width, the main limitation to conversion efficiency is group velocity mismatching(GVM). The GVM is caused by group velocity dispersion of NLO crystal.

Damage Threshold

Damage threshold is a property of the crystal to withstand the laser radiation without damage. The damage threshold is a function of the wavelength of fundamental and harmonic radiation, pulse duration, beam

profile and other parameters. The damage threshold of KDP at some selected wavelengths is given in table (1.2).

Table: 1.2 Damage threshold of KDP at some selected wave length.

Wave length (λ)	Damage threshold
355 nm	10 GW/cm^{2}0.03 ns 10Hz
532 nm	8GW/cm^2 0.03ns 10Hz
1064 nm	6GW/cm^2 1 ns 10Hz

1.5 Criteria for selecting NLO

For an NLO crystal device to work well without degradation of its performance over the life time of its assignment, the following criteria are required to be fulfilled [21]:

1. Reliable crystal growth technique for adequate size
2. NLO susceptibility coefficient
3. Birefringence (n_o-n_e) and optical dispersion
4. Moderate to high transparency
5. Good optical homogeneity
6. Good mechanical strength
7. Chemical stability
8. Ease of polishing and antireflection coating
9. Low linear and non-linear absorption
10. Temperature phase-matching band width
11. Fracture toughness
12. Damage threshold
13. Non-linear index of refraction
14. Brittleness.

In reality the ideal nonlinear crystal does not exist, nevertheless, the applicability of a particular crystal depends on the nonlinear process used, the desired device characteristics and the pump laser. Special material properties

that are important in one application may not be significant in another. For instance, the efficient doubling of very high power lasers having poor beam quality requires a material with large angular bandwidth. A crystal, which has a smaller nonlinearity but allows noncritical phase matching, will perform better than one, which is more nonlinear, but is critically phase matched. On the other hand, for the doubling of femto second optical pulses, the preferred material will be with a large nonlinearity so that a very thin crystal can be used to avoid dispersive broadening of the second harmonic output pulses [22].

1.6 Applications of NLO effects

NLO materials find different applications in modern technology and an attempt is made here to summarize it briefly. The NLO material with susceptibility $\chi^{(2)}$ have application in optical rectification in hybrid bistable device [17], electro-optic (Pockels) effect in modulators, variable phase retarders and frequency doubling in harmonic generation device [13], frequency mixing in parametric amplifiers and IR converters [23], AC electro-optic effect in optical bistability, AC Kerr effect in phase conjugation [19], Frequency tripling in deep UV conversion [24], laser fusion [25] and frequency conversion of ultra short pulses [26].

Whereas, Marder [27] has reviewed a variety of applications of NLO materials, such as modulation of optical signal facilitated by electro-optic effect (where the refractive index of a material changes in response to an applied electric field) , micro-fabrication , sensing , imaging and cancer therapy facilated by multi photon absorption (where molecules simultaneously absorb two or more photons of light). The two photon absorption (TPA) and femto-second laser pulses high density 3D optical

memory [28], two photons scanning microscope [29] and demonstrated the 3D micro-modification and tera bit /cm^3 3D optical data storage.

The nonlinear optical phenomenon of SHG has intrinsic sensitivity to the voltage across a biological membrane. The second order NLO process has been used to monitor membrane voltage by Bouevitch et al [30].

1.7 Materials for Nonlinear Optics

As the technological importance and applications of NLO materials is continuously increasing the quest is going on to develop the most suitable NLO material. The understanding of the nonlinear polarization mechanisms and their relation to the structural characteristics of the materials has been considerably improved. The new development of techniques for the fabrication and growth of artificial materials has dramatically contributed to this evolution. The aim is to develop materials presenting large nonlinearities, at the same time, not only all the technological requirements for applications such as, wide transparency range, fast response and high damage threshold, but also satisfying the processability, adaptability and interfacing with other materials.

Advances in the development of NLO materials can be divided into three different areas.

(i) Discovery of new NLO materials

(ii) Growth of promising NLO crystals

(iii) Improving the characteristics of NLO crystals

From materials point of view, the NLO materials can be broadly classified in three different categories as, inorganic, organic and semi-organic or metalorganic materials. Inorganic and organic possess their own set of

advantages and disadvantages [31], while in semi-organic or metalorganic materials the aim is always to combine advantages of the both. All the three types of NLO materials are briefly out lined here by.

Inorganic NLO Materials

These are covalent and ionic bulk materials where the optical nonlinearity is a bulk effect. The phenomenon of SHG in inorganic materials was first reported in 1961, which led to the development of recent NLO materials such as inorganic systems, semi conductors and inorganic photorefractive crystals. The examples of this type of crystals are lithium niobate ($LiNbO_3$), potassium niobate ($KNbO_3$), barium titanate ($BaTiO_3$), potassium titanly phosphate (KTiOPO4 KTP), potassium dihydrogen phosphate (KH_2PO_4,KDP), potassium deuterium phosphate (KD*P), ammonium dihydrogen phosphate (NH_3PO_4, ADP), lithium iodate ($LiIO_3$), etc., and a variety of semiconductors such as gallium arsenide (GaAs), cadmium sulphide (CdS), cadmium telluride (CdTe), zinc germanium phosphide ($ZnGeP_2$) and teluride (Te), Cadmium germenium arsenide ($CdGeAs_2$) and Silver gallium selenide ($AgGaSe_2$) are appropriate infrared NLO materials.

Nikogosyan [32] have carried out detailed survey of all NLO properties of various materials. BBO is an efficient NLO crystal for second, third and forth harmonic generation of Nd;YAG lasers and best NLO crystal for fifth harmonic generations. The conversion efficiency of BBO is 70% for SHG, 60 % for THG and 50% for FHG. KTP is also well-known NLO crystal with SHG coefficient about three times of KDP.

The inorganic NLO materials have some advantages like highest bulk susceptibility and compatible physical properties, on the other hand, such materials suffer from disadvantages like absorption in the visible region, poor response time and degradative photorefractive effects, low laser damage threshold (~10 MW cm^{-2}) and poor optical transparency [33].

Lithium niobate ($LiNbO_3$) crystals are one of the most investigated materials for widespread and promising applications in nonlinear optics, e.g., for parametric amplification and second-harmonic generation [34]. $LiNbO_3$ also shows photorefractive properties [35], which are characterized by a change in its refractive index that results from an optically induced separation of electrons and the linear electro-optic effect. $LiNbO_3$ crystals are attractive due to many applications such as holographic data storage, optical information processing, phase conjugation, and wavelength filters [36].

Borate family complexes are excellent nonlinear optical (NLO) materials, as they possess high chemical stability, damage threshold, optical quality and wide range of transparency. In particular, inorganic crystals like lithium triborate (LiB_3O_5, LBO), lithium tetraborate, beta barium borate (*β*-BaB_2O_4 ,BBO) and potassium pentaborate tetrahydrate (KB_5) have been widely used for NLO devices in ultra-violet laser generation. High purity single-crystal of beta barium borate (β-BaB_2O_4) has been successfully grown from Czochralski method by Itoh and Marumo [37]. The obtained crystal was confirmed to be that of the low-temperature β-phase by powder X-ray diffraction and the second harmonics generation. Due to its large SHG coefficient (d_{22} = 2.22 pm/V), wide optical transmission ranges (190–3500 nm) and high damage threshold (about 50 times higher than that of KDP), the beta

barium borate, initially, reported by Chen et al [38] and as a single crystal material, it has been extensively investigated for applications in the ultraviolet region [39]. KB_5 is a desirable NLO material, which exhibits a low angular sensitivity and hence proved to be useful for type II second harmonic generation [40]. Bhar et al [41] have found that ultraviolet radiation is generated in a lithium tetraborate ($Li_2B_4O_7$) crystals by Type-I walk-off compensated sum-frequency mixing (SFM) of the commonly available Nd:YAG laser radiation. Main inorganic materials applied in nonlinear optics are as follows:

Table (1.3): Typical application of different inorganic NLO materials.

Title	**Typical Application**
LBO	High Power laser harmonics generation and pumped by Nd:YAG laser.
BBO	Solid state and Dye laser harmonics generation.
KTP	Harmonics generation in UV and Vis region.
KDP	Harmonics generation in visible region.
$LiNbO_3$	SHG and OPO pumped by Nd:YAG laser.
$AgGaS_2$	Harmonics generation in IR region of CO_2 laser.
BSO	Photorefractive, electro-optical and acousto-optical.
KB_5	Second to sixth harmonics generation.
KTA	Harmonics generation in UV and Vis region.

As the present author deals with growth and characterization of pure and amino acids doped KDP crystals the properties of KDP crystals are discussed in a separate section. Most of these crystals are market by various firms for commercial use, since there is a great demand of good optical quality crystals.

Organic NLO Materials:

Organic materials are molecular materials that consist of chemically bonded molecular units interacting in the bulk media through weak van der Waal interactions. The organic molecules which contain both conjugated bonds and acceptor group on one side and a donor group on the other side are known as nonlinear optical (NLO) materials [12].

A typical SHG active molecule can be represented as follows:

Donor $\rightarrow$ π – conjugated system $\rightarrow$ acceptor

The π – conjugated molecules with a donor and acceptor will not display SHG activity if they possess a centre of symmetry. This symmetry requirement eliminates several materials for consideration of SHG. The π conjugated systems would be benzene, azobenzene, stilbene, tolans, biphenyl, hetrocycle, polyens, benzylidene, etc. Some accepter groups are, for instance, NO_2, NO, CN, NH_3^+, CF_3, $COCH_3$, COOH, COO^-, etc. Whereas, some donor groups are NH_2, $NHCH_3$, FCl, Br, CH_3, $COOCH_3$, $NHCOCH_3$, O^- etc.

The trade off between optical transparency and SHG efficiency is an important issue while designing devices using NLO materials. Both the second order optical nonlinearity and optical transparency are affected by the nature of conjugated bonds, length of π - conjugation and strength of electron donor/ acceptor constituents[14,42].

The second order NLO organic materials are most often based on π conjugated molecules (Chromophores) with strong electron donor and accepter group at the end of π – conjugate structure. Such molecules must be ordered in an acentric manner in a material to achieve a macroscopic second

order NLO response. Many times it is achieved by incorporating the NLO chromophores into a polymerric and pole the composite under the influence of a strong dc electric field close to the glass transition temperature Poled polymer systems are particularly interesting due to their relative ease and subsequent device fabrication by using conventional photolithography [43, 44].

The advantages of organic nonlinear optical materials are : (i) high second order nonlinear optical co-efficient, (ii) grater resistance to damage in the laser beam, (iii) birefringent nature facilitating phase-matching and (iv) possibility to chemically engineer molecular properties. However, the shortenings of organic crystals are [45,46]:

(i) Poor physicochemical stability

(ii) Low hardnees and

(iii) Cleavage tendency hindering their device application.

Moreover, organic materials have advantages like low dielectric constants, inherent synthetic flexibility, high optical damage thresholds and large NLO response over a broad frequency range comparable to those of inorganic materials.

Perumal et al [47] synthesized the 4-methoxy benzaldehyde- N-methyl-4-stilbazolium tosylate (MBST), which is a new material having high NLO property. The Kurtz powder SHG measurements on MBST showed that the peak intensity was 17 times more than that of urea. Jagannathan et al [48] have reported the SHG efficiency of 4-ethoxy benzaldehyde–n-methyl-4-stilbazolium tosylate crystals as 11 times greater than that of the urea. Also,

Jagannathan, et al [49] have reported 141 times efficiency of SHG than that of urea for 4-Dimethylamino-N-methyl-4-stilbazolium tosylate (DAST) crystals. DAST has found application in continuously tunable THz and the far infrared generation system [50]. Azariah et al [51] have found that the SHG efficiency is 1.24 times that of KDP for n-nitro-4-methoxy benzylidene aniline. Urea has been studies for several years. It is difficult to grow crystals and the polished surfaces other than cleavage surfaces which are extremely hygroscopic [52]. Devices based on urea must immerse the crystal in oil, which is usually absorbing in the UV region [53]. The efforts made to resolve the problems associated with urea are not very successful.

Organic molecules with π-electron delocalization are currently of wide interest as NLO materials in optical switches and NLO devices [13]. A large amount of organic compounds have been studied as NLO materials [14]. Historically, the optical SHG in an organic material was reported for the first time in 1964 by two research groups in 3, 4-benzopyrene by Rentzepis and Pao [54] and in hexamethylenetetramine single crystals by Heilmer et al [55].Two years later, Orlov [56] reported SHG from the hippuric acid. Further research in organic NLO was stimulated in 1970, when Davydov et al [57] reported strong SHG from organic compounds having electron donor and acceptor groups attached to a benzene ring while screening a large variety of organic compounds using the Kurtz and Perry powder method.

Semi-organic Materials

Semi-organic compounds share the properties of both organic and inorganic compounds. They are organic based materials in which the polarizable part is an organic molecule which is stoichiometrically bonded with

an inorganic ion [58]. The π -conjugated network in organic system with large nonlinearity has significant absorption in the visible region and hence for second harmonic generation (SHG) in the blue near UV region, more transparent and less extensively delocalized organics like urea or its analogs have been considered.

An interesting class of semi-organic crystals receiving wider attention in recent past is the amino acid family which includes the analogs of L-arginine, L-histidine, L-alanine, and L-lysine etc. Amino acid can be used as a basis for synthesizing organic-inorganic compounds like L-arginine phosphate and derivaties. L-arginine phosphate monohydrate (LAP) is a new nonlinear optical (NLO) material first introduced by Chinese material scientists in 1983 [59]. LAP crystals are usually grown from aqueous solution by the temperature lowering technique. LAP crystals caught the attention of many researchers because of their high nonlinearity, wide transmission range (220-1950 nm), high conversion efficiency (38.9%) and high damage threshold [60, 61]. Monaco et al [61] formed LAP and its chemical analogs from the strongly basic amino acid and various other acids. All the compounds in this class contain an optically active carbon atom and, therefore, all of them form acentric crystals. All the crystals are optically biaxial and among them several give second harmonic signals greater than quartz. It has been reported that L-arginine fluoride (LAF) [62] possesses high NLO coefficient next to LAP. LAF has a very strong type-I position, i.e., angularly insensitive compared to LAP, which makes LAF crystal attractive of certain cascade scheme for producing third harmonic. The amount of second harmonic generated in a powder LAF sample at 1064 nm relative to a quartz standard 5.6 times. Packiam Julius et

al [63] reported that the efficiency of frequency doubling of L-arginine hydrofluoride (LAHF) was 39% and was larger then KDP (22%) and LAP (33%).

The growth and properties of new semiorganic nonlinear optical crystal, tetra l-lysine alanine mono hydrochloride dihydrate (TLAMHCl) has been studied [64]. The second harmonic generation (SHG) efficiency of TLAMHCl was found to be 1.2 times that of KDP. L-lysine sulphate a semi-organic NLO material useful for frequency doubling in the IR region has been synthesized by Krishnakumar et al [65]. L-histidine salts can display high NLO properties due to the presence of imidazole group in addition to amino-carboxylate. Among the L-histidine analogs, the low temperature solution grown L-histidine tetrafluoroborate (LHFB) [66] is a promising NLO material and has superior NLO properties than LAP. The SHG intensity of L-HFB crystal is five times that of the KDP. Single crystals of L-histidinium dihydrogen orthophosphate ortho-phosphoric acid (LHP) were grown and characterized by Madhavan et al [67]. The SHG efficiency of LHP was found to be nearly 4 times that of KDP. Narayan Bhat and Dharmaprakash [68] have reported the growth of the semi-organic glycine nitrate (GSN) by slow evaporation from solution. They have determined the SHG efficiency of GSN to be 2 times that of KDP. Glycine forms the ferroelectric diglycine nitrate whose spectral transparency range is from 245 to 1900 nm.

Organo-metallic NLO Crystals

Recent interest is centered on metal complexes of certain organic ligands and among them metal complexes of thiocynate and thiourea are of special interest owing to their large nonlinearity, high laser damage threshold,

low UV-cut off and good mechanical properties. Many metal complexes of urea and urea analogs have been explored [69]. Examples of these complexes are zinc thiourea sulfate (ZTS), zinc thiourea chloride (ZTC), bis(thiourea) cadmium chloride (BTCC) and copper thiourea chloride (CTC). Bis(thiourea) cadmium chloride (BTCC) is a promising semi-organic NLO material for second-harmonic generation[70-72]. BTCC crystals have very high laser induced damage threshold values. In general, crystals of the type $M[tu]_2X_2$ (where M = Cd, Co, Hg, Pb, Ti and Zn, tu is thiourea and X is a halogen) have been found to exhibit good NLO properties [73]. In organometalic category complexes of thiourea like, Bis(thiourea) cadmium zinc chloride (BTCZC) [74] and bis(thiourea) cadmium formate [75] exhibit good NLO property . The characteristics of ATMX (where AT = allylthiourea, M = Cd or Hg, X = Cl or Br) were studied by Sun et al [76]. The second harmonic generation efficiency of these materials is higher than that of urea. Recently, Sun et al [77] have reported the crystal structure, optical and thermal characterization of tri-allyl thiourea zinc chloride (ATZC) . ATZC shows powder SHG efficiency comparative to urea.

The metal thiocyanantes and their Lewis-base adducts are one of the interesting themes of structural chemistry [78]. As second order NLO materials, the well known category of bimetallic thiocyanates such as $ZnCd(SCN)_4$, $ZnHg(SCN)_4$, $CdHg(SCN)_4$ and $MnHg(SCN)_4$ (abbreviated as ZCTC, ZMTC, CMTC and MMTC, respectively), exhibit efficient SHG at short wavelengths. Cadmium mercury thicoyanate (CMTC) crystal is one of the most efficient NLO crystals among complex crystals [79]. A novel NLO organometallic complex crystal, Cadmium mercury thiocyanate dimethyl

sulphoxide (CMTD) was reported for the first time by Dong et al in 2000 [80]. The SHG efficiency of CMTD crystal is found to be 15 times that of urea and is larger than that of a CMTC crystal. Another novel NLO crystal manganese mercury thiocyanate (MMTC) was reported by Wang et al [81]. The thermal analysis of MMTC shows that it possesses better physicochemical stability than that of CMTC.

1.8 KDP as a NLO Crystal

Potassium dihydrogen phosphate (KDP) single crystals have a high laser damage threshold, a large nonlinear optical coefficient, good structural and mechanical properties. KDP crystals find several device applications. The electro-optic effect in KDP is used to obtain phase and amplitude modulations [82, 83]. The acousto-optic tunable filters have been developed using KDP [84]. A three wave interaction involving 200 fs pulse at 527 nm and 0-9 ps pulses at 1055 nm was obtained with energy conversion efficiency of 30-40% in 2.5 mm and 3 mm thick KDP crystals. The yielding ~ 200 fs pulses at 351 nm were with milijoule energy [85]. For the inertial confinement fusion (ICF) experiments the performance of large aperture switches based on KDP have been assessed for high power laser experiments [86-88]. Rapid growths of large size (40-55 cm) KDP crystals [89] as well as rapid growth of KDP crystals with additives [90] have facilitated to obtain perfect KDP crystals for device application on large scale. Bespalov et al [91] have studied optical properties of KDP and DKDP (deuterated potassium dihydrogen phosphate) crystals grown at high rates much higher (by a factor of 25–30) than usual. They indicates that, in this way crystal suitable for use in quantum electronics.

Yuan et al [92] have reported broadband frequency on DKDP crystals. Hu Guo Hang et al [93] reported on laser damage in KDP and DKDP crystals. Recently, Kondji et al [94] have investigated the nonlinear response of a device consisting of a KDP crystal connected in series in an ac-driven RL circuit.

Frequency converters and Pockels cell fabricated from KDP and DKDP crystals are critical components in fusion class laser system. Due to the high laser power to which the crystals are exposed, their lateral dimensions are kept large (2 X 103 cm^2). To keep fluence below the threshold for laser damage Yoreo et al [95] described the remarkable set of technological and scientific advances that lead to a rapid growth process. The technology was successfully employed to grow KDP crystals for the 192 beams of the National Ignition Facility, USA, the world largest laser system.

KDP crystal also finds some novel applications. KDP based world's largest laser to generate UV beams has been demonstrated [96]. Using cascaded partially deuterated KDP crystals the broad band frequency tripling was demonstrated by Wang et al [97]. Moreover, the third harmonic generation with composite partially deuterated KDP was achieved by Wang et al [98]. Apart from this, a scheme with non-collinear sum frequency generation process of broadband third harmonic generation (THG) with two KDP crystals (one doubler and non mixer) using angular dispersion was proposed by Li and Zhang [99]. Details of physical, optical and nonlinear optical properties of KDP crystals along with the relevant data are well reported [100].

Table (1.4): Parameter and Typical Performance of KDP Crystal [21].

Typical Parameter of KDP	
Transparency range	0.174 - 1.57 µm
Symmetry class	42m
Lattice parameters	a = b = 7.453 Å, c = 6.975 Å
Density	2.338 g/cm^3
Mohs hardness	2.5
Referactive index at 347 nm	n_o = 1.54, n_e = 1.49
at 530 nm	n_o = 1.51, n_e = 1.47
at 694 nm	n_o = 1.51, n_e = 1.47
at 1060 nm	n_o = 1.49, n_e = 1.46
Nonlinear susceptibility at 1060 nm	d_{12} = 0.49, d_{36} = 0.47
Optical damage threshold at 1060 nm	t_{ns} = 0.2, 23.0 GW/cm^2
Linear absorption at 1060 nm	3.0 %/cm
Temperature acceptance	3.5 ^{o}C cm
Angular acceptance	1.0 rad.cm
Typical SHG efficiency	20 %

1.9 Challenges and Advances in NLO

In last one decade, the advances made in semiconductor industry have demanded 193 nm to 157. 6 nm coherent UV light for photolithography, whereas the emerging micromachining and material processing application needed deep UV laser. The barrier 250 nm for obtaining UV coherent light was broken using KBBF ($KBe_2BO_3F_2$) by Chinese group led by Chuangtian Chen. KBBF is the only crystal to achieve deep and even vacuum UV second harmonic generation from 170 nm to 200 nm [101-103]. The KBBF PCT device was used to generate the fifth harmonic (156 to 160 nm) of Ti :

Sapphire laser [104]. The mechanism for linear and nonlinear optical effects in KBBF crystals has been discussed by Lin et al [102].

Another potential NLO crystal developed is organic crystal DAST (Dimethylamino-N-methyl-4-stilbazolium tosylate). DAST was first reported by Marder [27] and still it is recognized as the state of art in organic NLO. DAST is having high second order NLO and electro optic coefficients, being 10 times and twice as large as LiNbO3, respectively. Extraordinary high nonlinearity in combination with low dielectric constant allows DAST for high speed electro-optic applications and broadband THz wave generation. However, DAST is also efficient material for generation and detection of THz waves using the NLO process of optical rectification or difference frequency generation. Moreover, significant progress has been made in terms of integrated EO (Electro-Optic) applications of DAST and organic crystals in general, which have long been hindered due to the difficult growth of their films with a controlled thickness on appropriate substrates as well as due to the special chemically compatible photolithiographic process needed for structuring. Jazbinsek et al [105] have reviewed progress on microstructure techniques developed for DAST, modified photolithography, photo-bleaching, femto-second laser ablation, grapho-epitaxial growth, ion implantation and direct electron beam structuring.

Engineering the domain is a hot topic in condensed matter physics and photoelectronics. The domain engineered ferro-electric crystal in which the ferroelectric domain is modulated artificially according to some sequence, forming so-called Super-lattice structure. The physical properties associated with third-rank tensors, like nonlinear susceptibility tensor, in such a crystal

would be modulated by domains, whereas those associated with even-rank tensor remain constants. This makes the crystal different from a homogeneous single domain one and, specially, suitable for nonlinear photonics applications. In case of wave length of light wave comparable with or smaller than the size of domain, i.e., the reciprocal vector of the modulated structure is comparable or larger than the wave vector of light wave, many novel effects may be created through the interaction of the wave vectors and reciprocal vectors of super-lattice, for instance, the enhancement of optical frequency conversion, the amplification of light scattering signal, the generation of entangled photon pair and polariton excitation etc. The interest in engineering domain structure of ferroelectric crystal also lie in applying to novel devices matched with contemporary nonlinear photonics, laser and quantum dots [106].

One interesting phenomenon of optics is the slow light, which is the propagation of an optical pulse or other modulations of an optical carrier at low group velocity. This term is applied when the velocity is at least 100 times slower than the speed of light in vacuum. Recently, Monat et at [107] reviewed advances related to slow light in periodic structures, where the refractive index varies along one or two directions, i.e., gratings and planar photonic crystals. The recent nonlinear experiment performed in photonic crystal waveguides, which demonstrate the strong reinforcement of nonlinear third order optical phenomenon with slow light. They have discussed the challenges associated with slow light in 2-D structures and their unique advantage in dispersion engineering for creating a broadband nonlinear device for all optical processing. By breaking down the relation between

dispersion and group velocity imposed in gratings, these structures also offer new opportunities for generating soliton like effects over the short length scales at low powers and short pulses.

Nanophotonics is again one prominent developing branch [108,109]. The application of nonlinear optics in photonic nanowires is discussed by Foster et al [110]. Nanowaveguides, fabricated from glasses or semiconductors, provide the maximum confinement of light for index guiding structures enabling large enhancement of nonlinear interactions and group velocity dispersion engineering. The combination of these two properties make photonic nano wires ideally suited for many nonlinear applications such as the generation of single cycle pulse and optical processing with sub-mW powers.

Apart from the growth of organic crystals, the inclusion complexes, mono and multilayered assemblies for example, Langmuir-Blodgett films and poled polymers are considered. In the inclusion complexes, for instance, β-cyclodextric (β-CD), a cyclic polysaccharide that crystallizes with spatial voids in its three dimensional structure and the guest molecules such as N- methyl-4 nitroaniline can be incorporated without destroying the crystal structure of the host β-CD. Due to the polar symmetry of β-CD crystal, a net polar order of the guest molecule is achieved [14]. For creating a polar material, the approach of self-assembled mono and multilayer structures, for example, Langmuir-Blodgett films have been developed. In this method the transfer of monolayer films of an amphiphiles containing β-chromophores from an air-water interface to a solid substrate is carried out. This process can be

repeated to produce multi-layers. Perhaps, the most advantageous approach to the organic second order NLO materials is in the field of polymers. Basically, an NLO active chromophore is incorporated into an optically transparent polymer matrix by either dissolving the compound in the polymer or attaching it to the polymer backbone. The polymer is then heated above the glass transition temperature and placed in a strong external field, which is called poling. This field facilitates to orient the chromophores with its dipole moment parallel to the applied field. The polymer is, thereafter, allowed to cool in the presence of the applied field. Often the polymer is cross linked at this point to further “locked in “the induced polar long order. Recently, the effect of main chains on second order nonlinear optical susceptibility of poled poly (dipropargyloxybenzoates) containing 2-[4-(2-chloro-4-nitrophenylazo)-]-N-ethyl-phenylamino] ethanol is studied. The second order nonlinear coefficient d_{33} were found to be in the range 50-90 pm/V.

The use of optics in computing is a challenge to be met in future. Optical interconnections and optical integrated circuits have several advantages over their electronic counter parts. They are immune to electromagnetic interference and free from electrical short circuits. They have low-loss transmission and provide large band width that is, multiplexing capability, capable of communicating several channels in parallel without interference. The electronic communication along wires or cables requires charging of a capacitor that depends on the length, in contrast the optical signals travel in optical fibers, optical integrated circuits and the free space do not have to charge a capacitor and, therefore, it is faster. In optical method the data processing can be done much easier and less expensive in parallel

fashion than that can be done in electronics. Another advantage is that light being made up of uncharged photos, which do not interact with one another as readily as electrons do. The role of NLO materials have becomes extremely important. Such materials can change the color of light and modulate its properties. Several optical computers require efficient nonlinear optical materials for their operations. Several organic materials have been explored for their use in optical devices, having high nonlinearities, flexibility of molecular design and damage resistance to optical radiation. A novel photo-deposition process for film on to quartz or glass surface has been carried out in NASA which enabled polydiacetylene film deposition having large nonlinearities and fast response time less than 120 fs ($1fs=10^{-15}s$). The optical AND and NAND gates have been demonstrated [111].

Mardar [27], in his well known article on Organic NLO materials. "Where we have been and where we are going", has given details of future developments. It is expected that the electro-optic coefficient value of 500 pm/V would be achieved in poled polymers, which may enable their use for various applications such as, efficient terahertz frequency generation facilitating image process for medical and security purpose. It is expected that all optical signal processing will be possible based on third-order NLO materials. The rapid development of two-photon micro-fabrication will help to push the limits of achievable resolution below 100 nm. The application of organic NLO materials for biomedical application including imaging, sensing, treatment and tissue engineering will be envisaged. The combination of efficient organic NLO materials with nano-structured metal clusters will provide dramatically enhanced NLO effects through surface plasmons.

Moreover, Rao [5] has discussed in details the future prospects of nonlinear optics in his review article. It is indeed practically difficult to cover all major advances and changes within the limited frame

1.10 Global Demand of NLO material

The NLO materials crystals have placed themselves as one of the fore runners at technology front. As per one estimate the total market for NLO materials in the year 2000 was $ 425.3 million and was expected to achieve $11,244 million in 2005 [112]. According to another survey the market for NLO materials would reach to $1.66 Billion in 2009 and out of which KDP, ADP, and other crystals would have a share of $15.6 million [113]**.** A compilation of market demand in the year 2009 is shown in Table (1.5). Other NLO materials include for example KDP, KD*P, BBO, LBO, CLBO, ZGP, tungsten, etc.

Table (1.5): Global Market for Various Types of NLO Materials, Through 2009

Year	2003	2004	2005	2006	2009	AAGR% 2004-2009
$LiNbO_3$	189.7	220.8	249.8	295.0	545.2	19.8
$LiIO_3$, $CuSO_4$, rotators, isolators	380.0	448.0	490.0	563.5	933.2	15.8
KTP	29.5	33.6	46.5	52.3	73.7	17.0
KDP, ADP, other NLO materials	45.2	50.4	69.8	76.5	104.0	15.6
Total	644.4	752.8	856.1	987.3	1,656	17.1

Source: BCC Research Group Global Market for Various Types of Non-linear Optical Materials, 2003-2006 and 2009 ($ Millions).

The business of photonic materials is booming. It was estimated that the photonic device sales worldwide was between $ 12 billion and $ 100 billion in 2000. According to KMI Corporation, the data traffic is growing worldwide at a rate of 100 % per year, whereas, the Phillips Group in London estimated that

the US data traffic would increase by 300 % annually. KMI Corporation also estimated that the sales of dense wave-length division multiplexing equipment will increase by quadruple its growth in the next five years; it was $ 9.4 billion in 2004.

1.11 Literature Available on NLO

A vast spectrum of literature, review articles and books are available on nonlinear optics and nonlinear materials and it is difficult to review and cite them all, humble attempt is made to cite a few of them. Several review and popular articles are written by many authors [114-117]. Review articles are available on advances in parametric amplification and processing [118] and on advances in photorefractive nonlinear optics [119] and on organic nonlinear optical materials [27]. Several well written books are available on NLO optics [3, 4, 12, 13,120,121]. However, there are certain novel features associated with NLO materials explored, for example, the nano-scale nonlinear optics [122], nanophotonic materials [123,124]. New non-linear optical materials have been developed based on ferro fluids [125]. There are certain Handbooks written on various aspects of non-linear optics, for instance, Handbook of non-linear optics [126] and Handbook of Laser Science and Technology of optical materials [127], Handbooks on photonics [11,128,129] Also, books are available on subjects like numerical modeling in nonlinear optics [130], complete study of organic nonlinear optical materials [45] and polymers [114], as well as recent progress [131] and nonlinear optical properties of matter [132] and recent survey of NLO materials [32] .

1.12 Aim of the present study

The advantage of NLO materials in lasers and electro-optics became clear in the early days of lasers, and enabled the expansion of their limited spectral regime. Today, there is a large number of nonlinear optical materials available for specific required wavelengths, with various damage threshold values and with various optical characteristics. The full characterization of NLO materials will involve proper documentation of these parameters. Techniques for measurement of these parameters are numerous and can readily be found in the literature.

Among organic crystals of NLO applications, amino acids exhibit specific features of interest [133] such as:

- Molecular chirality, which secures non-centro (acentric) symmetric crystallographic structure,
- Absence of strongly conjugated bonds, which leads to wide transparency ranges in the visible and UV spectral regions
- Zwitter ionic nature of the molecule, which favors crystal hardness.

Looking at the properties of various amino acids, three amino acids, viz, L-listidine, L-threonine and DL-methionine have been selected for doping in KDP crystals. The aim of the present study is to increase the SHG efficiency and optical transparency of KDP crystals by amino acids doping without giving much sacrifice to other properties. This will help further to develop crystals of better qualities for device applications. In order to investigate that, the present author has focused his attention on of the following aspects.

1. Growth, nucleation studies and nucleation kinetics of pure and amino acid doped KDP crystals.
2. CHN analysis and paper chromatography studies to confirm the amino acids doping.
3. Powder XRD studies to verify the change, if any, in the crystal structure due to amino acids doping along with the assessment of single phase nature.
4. FTIR spectroscopy studies for identification of various functional groups and the presence of amine group due to amino acids doping in KDP.
5. UV-Vis spectroscopy study is intended for the assessing the effect of amino acids doping on the transparency of KDP crystals, which is very important for optical studies.
6. Kurtz powder technique analysis is carried out to measure the SHG efficiency of pure and amino acids doped KDP crystals. This study is capable to indicate the benefit, if any, due to doping of amino acids in KDP.
7. The dielectric measurements are carried out to investigate the effect of amino acids doping on polarization behavior and various dielectric parameters of KDP crystals.
8. The thermal study is carried out to assess the thermal stability of pure and amino acids doped KDP crystals and the effect of doping on crystalline thermal stability.
9. The Vickers micro-indentation hardness is carried out to study the changes brought by amino acids doping in the mechanical behavior of KDP crystals, which is important for machinability and device applications of crystals.

10. The dislocations etching study is carried out to identify the changes taking place in dislocation behavior of KDP crystals due to amino acids doping. The activation energy for the lateral motions of ledges of etch pits is estimated.
11. These studies are expected to reveal whether the amino acids doping in KDP crystals is beneficial or not.

References

1. F. A. Jenkins, H. E. White, "*Fundamentals of Optics"*, McGraw Hill, New York (1957).
2. J. F. Nye, M. V. Berry, *Proc. Roy. Soc*. *London* **A336**(1974) 165.
3. A. C. Newell, J. V. Monoley, "*Non-linear Optics*", Addison, Wesley (1992).
4. G. S. He, S. H. Liu, *"Physics of Non-Linear Optics"*, World- Scientific, Singapore (1999).
5. D. Narayana Rao, *Physics News* **40** (2010) 53.
6. J. W. Goodman, "*Statistical Optics"*, Wiley, New York (1985).
7. J. W. Goodman, "*Introduction to Fourier Optics"*, McGraw-Hill, San Fransisco (1968).
8. P. A. Franken, A. E. Hill, C. W. Peters, G. Weinreich, *Phy. Rev Lett.* **7**(1961)118.
9. J. A. Armstrong, N. Bloemberngen, J. Ducuing, P. S. Pershal, *Phy. Review* **127** (1962) 1918.
10. N. Bloembergen, "*Encounters in the Nonlinear Optics*", World-Scientific, Singapore (1996).
11. V. G. Dimitriev, G.G.Gurzadyan, D. N. Nikogosyan, "*Handbook of Nonlinear Optical Crystals, in Springer Series in Optical Sciences*, Vol. **64**, ed. A. E. Siegman, Springer-Verlag, New York (1991).
12. F. Zernike, J. Midwinter, "*Applied Nonlinear Optics"*, Wiley, New York (1973).
13. Y. R. Shen, "*The Principles of Nonlinear Optics*", Wiley, New York (1984).

14. P. N. Prasad, D. J. Williams, "*Introduction to Nonlinear Optical Effects in*

Molecules and Polymers", Wiley, New York (1990).

15. D. J. Williams*, Angew. Chem. Int. Ed. Engl*. **23**(1984)690.

16. J. Laxmikanth Rao , *Ph.D. Thesis* , Indian Institute of Chemical Technology , Hyderabad (2001).

17. L. V. Tarasov, "*Laser Age in Optics*", Mir Publishers, Moscow (1981).

18. J. A. Giordmaine , R.C. Miller, *Phys. Rev. Lett*. **14** (1965)923.

19. A Yariv, "*Quntum Electronic",* Wiley, Newyork (1989).

20. J. Wilson, J. F. B.Hawkes, "*Optoelectronic An Introduction",* Prentic Hall, New Delhi (1999).

21. R.S. Adhav, "*Application of Non-Linear crystals"*, LIA Hand Book of Laser materials Processing, Magnolia (2001).

22. L. K. Chang, W. Bosenberg, C. L. Tang, *Prog. Cryst. Growth & Charac*, **20** (1990) 9.

23. P. W. Smith, *Bell. Syst. Tech*. *J*. **61** (1982) 54.

24. D. M. Pepper, *Opt. Eng* **21** (1982)156.

25. J. De Yoreo, *Prize lecture in ICCG-16*, Beijing, China, August (2010).

26. G. Szabó, Zs. Bor, *Appl. Phys. B: Lasers & Optics* **58(3)** (1994) 237.

27. S. R. Marder, *Chem. Commun.* **2**(2006) 131**.**

28. D. A. Tharthenopoulos, P. M. Rentzepis, S*cience* **245** (1999) 843.

29. W. Denk, J. H. Streckler, W. W. Web, *Science* **248** (1990) 73.

30. O. Bouevitch, A. Lewis, I. Pinevsky, J. P. Wuskell, L. M. Loew, *Biophysical J.* **65** (1993) 672.

31. W. Blau, *Phys. Technol*. **18** (1987) 250.

32. D. N. Nikogosyan, "*Nonlinear Optical Crystal: A Complete Survey",* Springer, Heidelberg (2005).
33. Y. X. Fan, R. C. Eckardt, R. L. Byer, R. K. Rout, R. S. Feigelson, *Appl. Phys. Lett.* **45**(1984)313.
34. L. Arizmendi, *Phys. Status Solid. A* **201** (2004) 253.
35. P. Yeh, "*Introduction to Photorefractive Nonlinear Optics",* Wiley, New York (1993).
36. P. Gunter, J. P. Huignard, "*Photorefractive Materials and Their Applications",* Springer, Verlag (1989).
37. K. Itoh, F. Marumo, *J. Cryst. Growth* **106** (1990) 728.
38. C. Chen, B. Wu, A. Jiang, G. You, *Sci. Sin, Ser. B (Engl. Ed.)* **28** (1985) 235.
39. J. Lin, *Opt. Quantum Electron* **22**(1990) 305.
40. Z. Liu, J. Lin, Z. Wang, C. Chen, M.H. Lee, *Phys.Rev. B.* **62** (2000)1757.
41. G. C. Bhar, P. Kumbhakar, A. K. Chaudhary, *Quantum Electron* **32**(2002) 341.
42. K. D. singer, J. E. John, L. A. king, H. M. Gordon, H. E. Katz, C.W. Dirk, *J. Opt. Soc. Am. B* **6**(1989) 1339.
43. H. Ma , A. K. Y. Jen , L. R. Dalton , *Adv. Mater.* **14**(2002) 1339.
44. M. Jazbinsek , L. Muthur , P. Gunter , *IEEE J. of selected topic in Quantum Electronics* **14** (2008) 1298.
45. D. S. Chemal, J. Zyss, *"Nonlinear Optical Properties of Organic Molecules and Crystals"*, Vol 1-2, Academic press, Orlando (1987).

46. X. Q. Wang, D. Xu, M. K. Lu, D. R. Yuan, S. X. Xu, S. Y. Guo, G. H. Zhang, J. R. Liu, *J. Cryst. Growth* **245**(2002)126.
47. C. K. L. Perumal, A. Arulehakkaravarthi, P. Santhanaraghavan, P. Ramasamy, *J. Crystal Growth* **241** (2002) 200.
48. K. Jagannathan, S. Kalainathan, T. Gunasekaran, G. Bhagavannarayana, N. Vijayan, *Cryst. Res. & Technol.* **42** (2007) 483.
49. K. Jagannathan, S. Kalainathan, T. Gunasekaran, G. Bhagavannarayana, N. Vijayan, *Cryst. Growth & Design* **7** (2007) 859.
50. T. Taniuchi, H. Adachi, S. Okada, T. Sasaki, H. Nakanishi, *Electronic Lett*. **40** (2004) 549.
51. A. N. Azariah, A. S. Haja Hamid, T. Thenappan, M. Noel, G. Ravi, *Mater. Chem. Phys.* **88** (2004) 90.
52. J. M. Halbout, S. Blit, W. Donaldson, C. L. Tang, *IEEE. J. Quantum Electron* **15**(1979) 1176.
53. A. A. Ballman, R. L. Byer, D. Eimerl, R. S. Feigelson, B. J. Feldman, L. S. Goldberg, N. Menyuk, C.L. Tang, *Appl. Optics* **26** (1987) 224.
54. P. M. Rentzepis, Y. H. Pao, *Appl. Phys. Lett.* **5**(1964)156.
55. G. H. Heilmer, N. Ockman, R. Braunstein, D. A. Karmer, *Apl. Phys. Lett*. **5** (1964) 229 .
56. R. Orlov, *Sov. Phys. Crystallogr*. **11**(1966)410.
57. B. L. Davydov, L. D. Derkacheva, V. V. Dunina, M. E. Zhabotinskil, V. K. Zolin, L. G. Kreneva, M. A. Samokhina, *JEPT Lett.* **12** (1970)16.
58. Y. J. Ding, X. Mu, X. Gu, *J. NLO Phys. & Mater.* **9** (2000) 21.
59. D. Xu, M. Jiang, Z. Tan, *Acta chem. Sinica* **41** (1983) 570.
60. K. Aoki, Kozo Nagano, Y. litaka, *Acta Crystallogr.* **B 27** (1971)11.

61. S. B. Monaco, L. E. Davis, S. P. Velsko, F. T. Wang, D. Eimerl, *J. Cryst. Growth.* **85** (1987)252.
62. A. S. H. Hameed, P. Anandan, R. Jayavel, P. Ramasamy, G. Ravi, *J. Cryst. Growth* **249** (2003) 316.
63. J. P. Julius, S. A. Rajasekar, A. Joseph Pragasam, P. Joseph, P. Sagayaraj, *Mater. Sci. Engg. B* **107** (2004) 259.
64. V. Sivashankar, R. Sankar, R. Siddheswaran, R. Jayavel, P. Murugakoothan, *Mater. Chem. Phy.* **109** (2008) 119.
65. V. Krishnakumar, S. Manohar, R. Nagalakshmi, *Spectrochimica Acta Part A: Molecular & Biomolecular Spectroscopy* **75** (2010) 1394.
66. H. O. Marcy, M. J. Rosker, L. F. Warren, P. H. Cunningham, C. A. Thomas. *Optics Letters* **20** (1995) 252.
67. J. Madhavan, S. Aruna, K. Ambujam, A. Joseph Anil Pragasam, S.M. Ravikumar, M. Gulam Mohamed, P, Sagayaraj, *Cryst. Res. Technol.* **41** (2006) 997.
68. M. Narayan Bhat, S. M. Dharmaprakash, *J. Cryst. Growth* **235** (2002) 511.
69. P. R. Newman, L. F. Warren, P. Cunningham, T. Y. Chang, D. E. Copper, G. L. Burdge, P. P. Dingels, C. K. Lowe-Ma, "*Semi Organics, a new class of NLO Materials, in Advanced Organic Solid State materials"* Ed. C.Y. Chiang, P.M. Chaikan, D.O. Cowan, Materials Research Society Symposium Proceedings (1990) 557.
70. S. P. Velsko, *Laser Program Annual Report,* Lawrence UCRL-JC 105000 Lawrence Livermore National Laboratory, Livermore, California, (1990).
71. G. Xing, M. Jiang, Z Sao, D. Xu, Chin, *J. Lasers* **14** (1987) 302.

72. L. F. Warren, "*New Development in Semi-organic Nonlinear Optical Crystals in Electronic Materials"*, Proc. of the 4th Inter. SAMPE Electronics Conf.,**4** (1990)388.

73. N. Oussaid, P. Beeker, M. Kemiche, N. C, Carabatos, *Phys. Stat. Sol. (b)*. **207** (1998)103.

74. K. Kirubavethi, K. Selvaraju, S. Kumararaman, *Spectrochimica Acta Part A: Mol. & Biomol. Spectro,* **71** (2008) 1.

75. S. Selvakumar, S. M. Ravikumar, K. Rajarajan, A. Joseph Arul Pragasam, S. A. Rajasekar, K. Thamizharasan, P. Sagayaraj, *Cryst. Growth. Design* **6** (2006) 2607.

76. H. Q. Sun, D. R. Yuan, X. Q. Wang, Y. Q. Lu, Z. H. Sun, X. C. Wei, X. I. Duan, C. N. Luan, M. K. Lu, D. Xu, *J. Cryst. Growth* **256** (2003), 183.

77. H. Q. Sun, D. R. Yuan, X. Q. Wang, X. F. Cheng, C. R. Gong, M. Zhou, H.Y. Xu, X.C. Wei, C.N. Luan, D.Y. Pan, Z.F. Li, X.Z. Shi, *Cryst. Res.& Technol*. **40** (2005) 882.

78. K. Nakamoto, "*IR and Raman Spectra of Inorganic and Coordination Compounds",* Wiley, New York (1977).

79. X. L. Duan, D. R. Yuan, Z. W. Zhong, J. G. Zhang, X. Q. Wang, X. N. Jiang, S.Y. Guo, D. Xu, M. K. Lu, *J. of Cryst. Growth* **233**(2001)312**.**

80. S. G. Dong Xu, M. L. Duorong, Y. Z. Yang, G. Zhang, S. Sun, X. Wang, M. Zhou, M. *J. Prog. Cryst. Growth & Charact.* **40** (2000) 111.

81. X. Q. Wang, D. Xu, M. K. Lu, D. R. Yuan, S. X. Xu, *Mater. Res. Bulletin* **36** (2001). 879.

82. A. K. Ghatak, K. Thyagarajan, "*Optical Electronics",* Cambridge Uni. Press, Cambridge (1989) 462.
83. S. S. Jha, "*Perspective of Optoelectronics",* World Scientific, Singapore (1995).
84. V. B. Voloshinov, D. V. Bogomolov, A. Yu. Trokhimovski, *Technical Phy.* **51** (2006) 63.
85. A. Dubietis, G. Tamosauskas, A. Varanavicius, *Opt. Commun.* **186** (2000) 211.
86. J. De Yoreo, A. K. Burnham, P. K. Whiteman, *Inst. Mater. Rev.* **47** (2002) 173
87. M. A. Rhodes, B. Woods, J. J. De Yoreo, D. Roberts, L.J. Atherton, *Appl. Optics* **34** (1995) 5312.
88. J. De Yoreo, J. Britten, K. Montgomery, N. P. Zaitseva, B. W. Wood, L. J. Artherton, C. A. Ebbers, Z.U. Pek, *ICF Quaterly Report 3,Lawrence Livermore National Laboratory*, Livermore **93** (1993) 3.
89. J. Bierlein, H. anherzeele, *J. Opt. Soc. Am*. **B6** (1989) 622.
90. P. Becker, *Adv. Mater.* **10** (1998) 979.
91. V. I. Bespalov, V.I. Bredikhin, V. P. Ershov, V. I. Katsman, N. V. Kiseleva, S. P. Kuznetsov, *J. Quantum Electron.* **12** (1982) 1527.
92. P. Yuan, L. Qian, W. Zheng, H. Luo, H. Zhu, D. Fan, *J. Opt. A: Pure Appl. Opt.* **9** (2007)1082.
93. H. G. Hang, Z. Yuan An, S. S. Tao, L. D. Wei, L. X. Feng, S. Xun, S. J. Da, F. Z. Xiu, *Chinese Phys. Lett.* **26** (2009) 97803
94. Y. S. Kondji, *Phys. Scr.* **81** (2010)15010.

95. J. D. Yoreo, N. Zaitseva, L. Rashkovich, *Scientific and Technological Advances Leading to Rapid Growth of High Quality Meter- scale Crystals for World's Largest Laser Systems, Planery Talk*, ICCG-16, Beijing, 8-13 Aug. (2010).

96. L. Bibeau, P. J. Wegner, R. H. Fedder, *Laser Focus World* (2006).

97. W. Wang, F. Wang, J. Wang, W. Han, B. Feng, K. Li, F. Li, H. Jia, Y. Xiang, L. Wang, W. Zhong, X. Zhang, S. Zhao, *J. Optics* **12** (2010) 75201.

98. W. Wang, J. Wang, F. Wang, B. Feng, K. Li, H. Jia, W. Han, Y. Xiang, F. Li, L. Wang, W. Zhong. X. Zhang, S. Zhao, *Laser Phys*. **20** (2010)1923.

99. K. Li, B. Zhang, *Opti. Commun.* **281** (2008) 2271.

100. R. S. Craxton, S. D. Jacobs, J. E. Rizzo, *IEEE J. Quantum Electron*., **17(9)** (1981) 1782.

101. C. T. Chen, "*Development of New Nonlinear Optical Crystals in Borate Series", Materials for Nonlinear Optics*," Harwood Academics, Switzerland (1993).

102. Z. Lin, Z. Wang, C. Chen, S. K. Chen, M. H Lee, *Chem. Phys. Lett.* **367**(2003) 523.

103. C. Chen, *"Crystal Growth of the KBBF Family and Deep UV-Harmonic Generation", Plenary talk* ,ICCG -16, Beijing, 8-13 Aug.(2010).

104. T. Kanai, T. Kanda, T. Sekikawa, W. Watanabe, T. Togashi, C.T. Chen, C.Q. Zang, Z. Xu and J. Wang. *J. Opt. Soc. Am*. **B 21** (2004), 370.

105. M. Jazbinsek, L. Matter, P.Giinter, *IEEE J.of Selected Topics in Quantum. Elector.* **14**(2008)1077.

106. S. Li, "*Engineering ferroelectric domain for non-linear photonics, laser and quantum optics*", Planeary Talk, ICCG-16, Bejing, 8-13 Aug. (2010).

107. C. Monat, M. de Sterke, B.J. Eaggleton, *J. of optics* **12**(2010) 104003.

108. H. Rigneault, J. M. Laurtioz, C. Delalande, A. Levenson, "*Nanophotonics*", ISTE, London (2006).

109. R. B.Wisherspohn, H. S. Kitzerow , K. Busch, "*Nanophotonic Materials*", Wiley, VCH (2008).

110. M. A. Foster, A.C. Turner, M. Lipson A. L. Gaeta, *Optics Exp.* **16**(2008)1300.

111. H. Abdeldayen, D. Fraizer, M. S. Paley, W. K. Witherew, NASA Marshall Space Flight Centre, Science, NASA.

112. O. Kalisky; *BCC Report*, SMC019B (2000).

113. Electronic Ca. *Research Network Publication* (2005).

114. M. J. Fejer, *Phys. Today* **47** (1994) 25.

115. M. N. Islam, *Phys. Today* (1994) 34.

116. A. Garito, R. F. Shi, M. Wu, *Phys. Today* (1994) 51.

117. D. Arivuoli, *Pramana J. Phys*. **57** (2001) 871.

118. S. Redic, C. Bres, *Proc. of Asia Optical Fiber Communication and Opto-electronic Exposition & Conf.*, Shanghai (2008).

119. P. Yeh, *Laser and Electro-optics*, Pacific Rim Conference (1997).

120. E. G. Sauter, "Non-linear Optics", Wiley, New York (1996).

121. A. J. Stenz, R. W. Boyd, *"Nonlinear optics"*, Academic Press, Boston

(2008).

122. *An International Conference on Advances in Nano-scale Nonlinear Optics,* Roma, Italy (2008).
123. V. Shalaev, ”*Nanophotonics with Surface Plasmons”,* Elsevier, Mexico (2006).
124. P. N. Prasad*, “Nanophotonics”,* Wiley, New York (2004).
125. J. P. Huang, K. W. Yu, *J. of Phys.: Conf. Series* **29** (2006) 69.
126. R. Sutherland, “*Handbook of Nonlinear Optics”*, Dewey (2003).
127. S. Singh, “*CRC Handbook of Laser Science and Technology Optical Materials*,” Ed. M. J. Weber, CRC Press (1986).
128. H. S. Nalwa,” *Handbook of Advanced Electrinic and Photonic Materials and Devices*, “ Academic press, New York (2001).
129. M. C.Gupta , J. Ballato , *“Handbook of Photonic”*, CRC Press, Boca Raton(2008).
130. P. P. Banerjee, *“Nonlinear Optics: Theory Numerical Modeling and Applications”*, Marcel Dekker, New York (2004).
131. M. Takhashi, H. Gotô., *“Progress in Nonlinear Optics Research”*, Nova, New York (2009).
132. M. C. Papadopoulos, A. J. Sadlej, J. Leszczynski, “*Nonlinear Optical Properties of Matter”*, Springer, Heidebarg (2006).
133. J. F. Nicoud, R. J. Twieg, “*Nonlinear Optical Properties of Organic Molecules and Crystals”,* Academic Press, New York (1987).

Chapter II

A Brief Review of Solution Growth Techniques and Study of Nucleation Parameters of Pure and L - histidine, L-threonine and DL-methionine Doped KDP Crystals

2.1 Introduction

Today, the growth of crystals does not remain the phenomenon only occurring in nature, but it has become a well advanced as well as widely used laboratory technique. There is a requirement of good quality crystals for various applications and hence different methods are developed to grow suitable crystals. It has been found that the crystalline property has applications in devices such as: laser resonators, acoustic- optic modulators, phase decay plates, polarizer, pyro-electric detectors, piezo-electric devices, crystal X-ray monochromaters, scintillation detectors, holographic devices, membranes of iron selective electrodes and substrate for thin films.

Single crystal plays a vital role in most of the above applications. Therefore, the growth of single crystals and their characterizations towards device fabrications are important in both basic and applied scientific research. The development and refinement of methods of crystal growth processes to achieve useful products have relied heavily on empirical engineering and on trial and error method. Crystal growth still remains by large an art. The classification schemes for growth techniques are summarized in table (2.1) according to Laudise [1].

Table: 2.1 : The classification schemes for crystal growth techniques.

		Polycomponent	
A	**Solid-solid (solid growth)** 1. Strain annealing 2. Devitrification 3. Polymorphic-phase change	**A**	**Solid-solid (solid growth)** 1. Precipitation from solid solution
B	**Liquid-solid (melt growth)** 1. Conservative (a) Directional solidification *(Bridgman-Stockbarger)* (b) Cooled seed *(Kyropoulos)* (c) Pulling *(Czochralski)* 2. Non conservative (a) Zoning *(horizontal, vertical, float zone, growth on a pedestal)* *(b)* Verneuil *(Flame fusion, plasma, arc image)*	**B**	**Liquid-solid (melt growth)** 1. Growth from solution *(evaporation, slow cooling and temperature differential)* (a) Aqueous solvents (b) Organic solvents (c) Molten-salt solvents (d) Solvents under hydrothermal (e) Other organic solvents *2.* Growth by reaction (a) Chemical reaction (b) Electrochemical reaction
C	**Gas-solid (vapor growth)** 1. Sublimation-condensation 2. Sputtering	**C**	**Gas-solid (vapor growth)** *1.* Growth by reversible reaction *(temperature change, concentration change)* (a) Van Arkel *(hot wire processes)* 2. Growth by irreversible reaction (b) Epitaxial processes

Crystal growth is involved with control of phase change, therefore; one can define three basic categories of crystal growth processes [2].

Solid growth- S $\rightarrow$ S processes involving solid-solid phase transitions.

Melt growth- L $\rightarrow$ S processes involving liquid-solid phase transitions.

Vapor growth- V $\rightarrow$ S processes involving gas-solid phase transitions.

The designing and development of various crystal growth techniques of the present day is a result of continuous and fruitful modifications occurring since last several decades and still today the modification process is continuing. The crystal growth requires emphasis on the following three aspects.

1. Theory of nucleation and growth
2. Experimental crystal growth
3. Characterization of crystals

Schieber [3] has well explained this in a schematic representation, which is shown in figure (2.1).

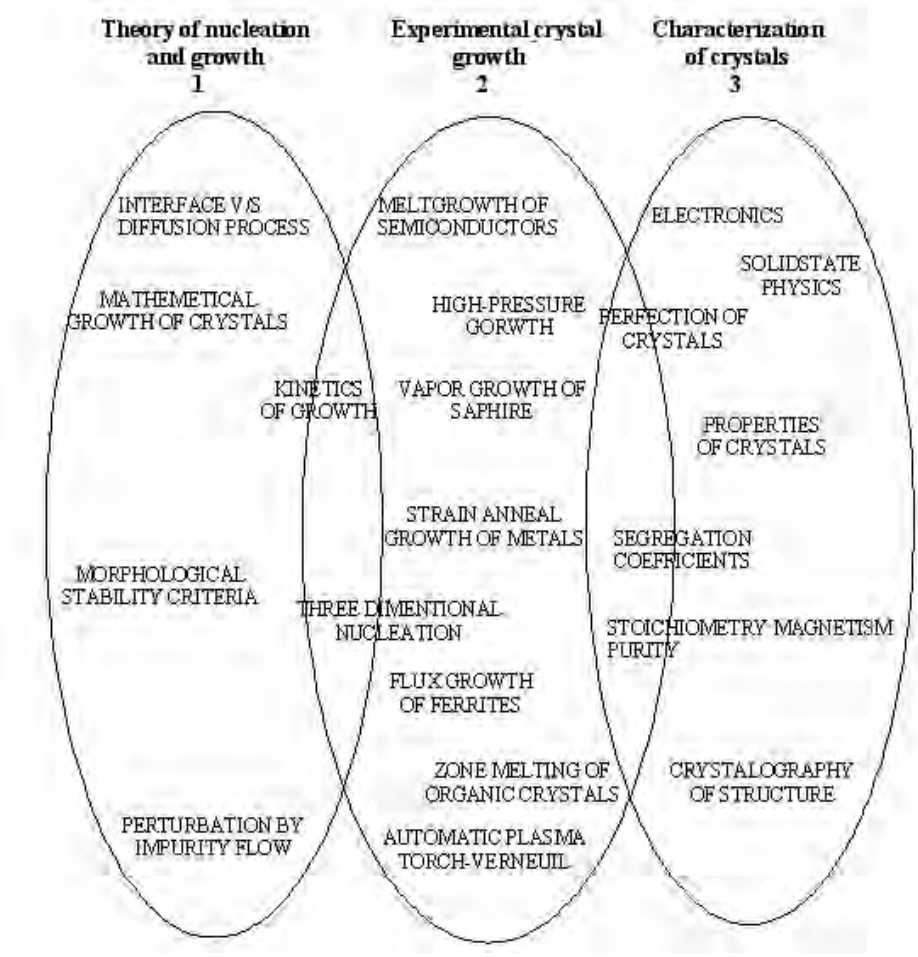

Figure:2.1 Three aspects of crystal growth.

Altogether, the modern as well as the next generation crystal growth requires multi-directional development in various fields and their interconnections, this has been described in a schematic representation by Prasad [4], which is shown in figure (2.2).

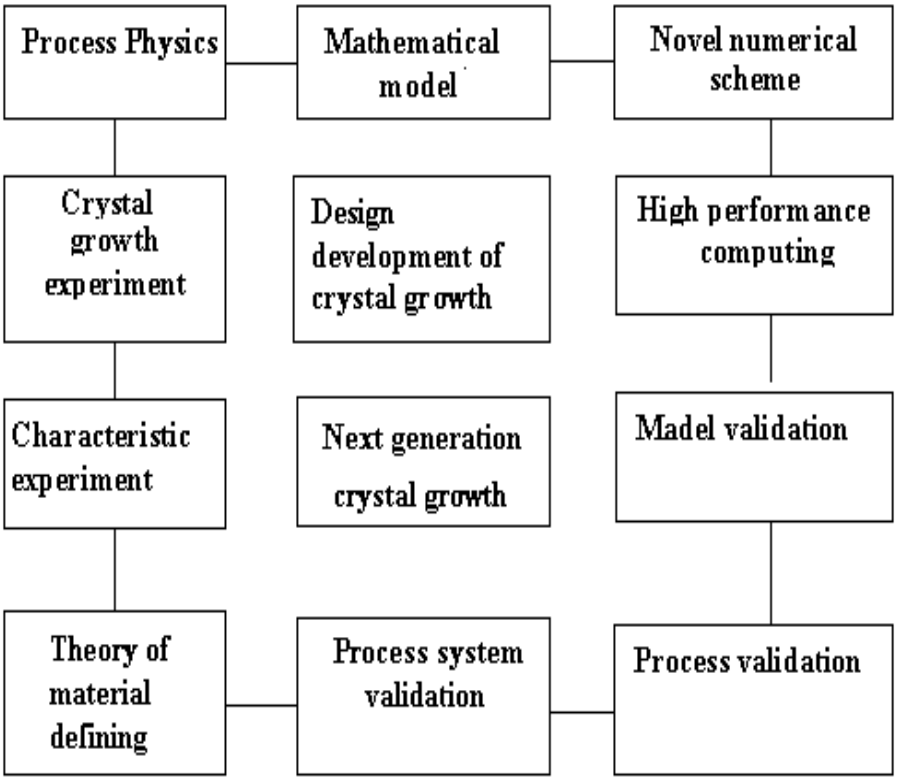

Figure :2.2 Schematic representation of multi-directional development in various fields of crystal growth and their interconnections.

Competitive nucleation in crystal growth is explained by many authors, in detail [5-7]. This has been correctly quoted in a different manner by Gilman [8] in his book “The Arts and Science of Growing Crystals” as, “The systematic production of artificial crystals” might be viewed as a new “agriculture” that has begun flourish. It differs from true agriculture in the manner that its products are mostly inorganic at present, but it has many features common with normal agriculture and promises to have a somewhat comparable effect on society. The new agriculture consists of “growing” solid crystals from a

"nutrient" phase (gas, liquid or solid). To start the growth process, the nutrient is often "seeded" with small crystal to be grown and some workers speak of "repeating the harvest" after a certain length of time.

There are many well written books available on subjects like, fundamentals of crystal growth [9]; different crystal growth techniques, their theories, characterization and applications [10-14] and understanding the growth mechanism [15]. A handbook of crystal growth is also published [16]. Even books are available with wonderful photographs of crystals [17], whereas, the authors Stangl and Stang [18] have considered the growth of a variety of beautiful crystals as the growth of flowers in a garden which one can do, thereby, they have agreed to the concept of Gilman [8].

The basic common principle in all these methods is that a nucleus is first formed and it grows into a single crystal by organizing and assembling ions or molecules with specific interaction and bonding, so that the process is slow and multiple nucleations is minimized. Crystal growth processes and size of grown crystals differ widely and are determined by the characteristics of the material.

Each category of Crystal growth consists of a number of methods. The model for selection of a particular method depends on the properties of materials such as melting point, vapor pressure, decomposition, solubility in solvent, etc. The growth methods are also heavily dependent on growth kinetics involved, crystal size requirement and shape of crystal, purity and nature of application of crystal. However, the present thesis deals with the growth of pure and amino acid doped KDP crystals by the slow solvent

evaporation technique, the details of the other growth techniques are avoided and the focus is made on solution growth techniques.

2.2 Basic Theories and Developments

Crystal growth has been long cherished for the fascinating observations, where the atomic nature of matter clearly shows itself. It has been realized that the subject can be divided into two parts: (1) The study of the equilibrium between the crystal and surrounding medium and (2) The study of the kinetics of growth.

The Kossel model [19] is helpful to understand the basic theories of crystal growth. In figure (2.3 a) a low index face of a perfect (001) face of

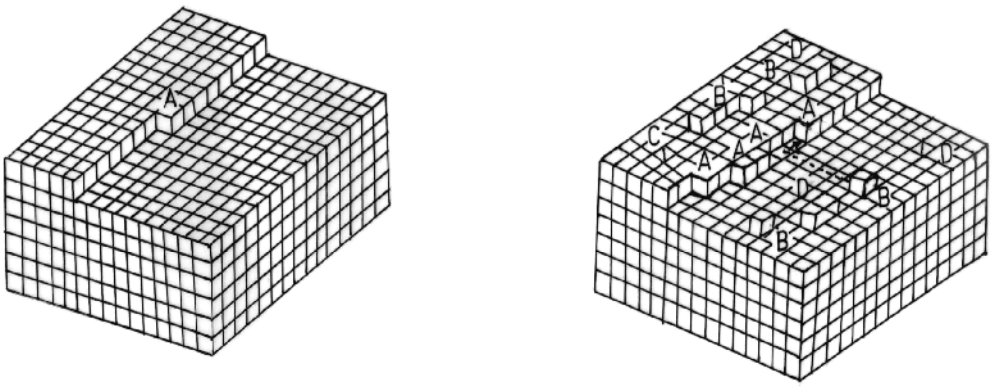

(a) **(b)**

Figure: 2.3 (a) Step on a perfect crystalline surface, (b) Step with kinks and vacancies.

crystal at the absolute zero temperature, at which no thermal vibrations of component molecules are available, is shown. This represents the profile of a completely flat surface partially covered by another layer. The boundary line, where the difference of level equals to an inter-molecular spacing between the two sides of the line, is khown as a step on the crystal surface. If a crystal is in

stable equilibrium with its vapor, which is neither super-saturated nor under-saturated, then a step in equilibrium on the crystal surface will exhibit a constant mean direction h, inclined at an angle θ to the principle direction given by the following expression,

$$\tan \theta = n_+ n_- \qquad (2.1)$$

Where, n_+ and n_- are the numbers of kinks of opposite sign per atom spacing. The potential energy considerations suggest that at absolute zero temperature, a step will tend to remain as straight as possible.

As the temperature increases from absolute zero, the component molecules will start vibrating relative to one another. As the temperature increases the vibrations become progressively stronger. Now the scenario changes, some molecules will be able to overcome the energy that binds them to the crystal and will jump in the space surrounding it. In this manner, a certain vapor concentration, which is the average number of vapor molecules per unit volume, will occur in contact with the crystal surface. With comparison to the other molecules, the molecules positioned at the kink are more prone to depart from the crystal and vaporize. The molecules at the kinks are bound by three molecules. Moreover, the molecules on the straight portions of the step are bound by four molecules and those on the flat portions of the surface by five. The energy required for a molecule to leave the kink position such as *A* in figure (2.3 a) is equal to the evaporation energy *W*. Two different processes will occur simultaneously; in one some molecules will be leaving the crystal and in the other one the molecules will be arriving at the crystal from the

vapor. Equilibrium is reached when the rates of these two processes are equal. Now, the surface will look like as shown in figure (2.3 b).

One can notice the changes in the surface easily by comparing the figures (2.3 a) and (2.3 b). The two main changes are noticeable; which are (1) the step has acquired a number of kinks such as *A* and (2) a small number of molecules have been adsorbed on the crystal surface and on the step, indicated as *B* in the figure (2.3 b), and also a similar number of surface vacancies *C*, a small number of pairs of adsorbed molecules *D* or pairs of vacancies have been created.

The mean distance x_o between the kinks is estimated in terms of the inter-atomic distance, *a*, by

$$x_o = ½ [\exp(\omega / k T)+ 2] \approx ½ a [\exp (\omega / k T)] \quad (2.2)$$

Now, introducing the nearest neighbor interaction as, Φ, which is related to the evaporation energy, *W*, by the expression as follows

$$\Phi = 1/6 (W) \quad (2.3)$$

Therefore, the mean distance x_o can be obtained as

$$x_o = ½ \exp [\Phi / 2kT] \quad (2.4)$$

It was first realized by Volmer [20] in 1922 that the adsorbed molecules diffuse with considerable ease over the crystal surfaces. The process of growth of a crystal surfaces with steps is the result of mainly three processes; (1) a transport of molecules from the vapor to the adsorbed layer, (2) the diffusion of the adsorbed molecules towards the steps and (3) the

diffusion of adsorbed molecules along the edge of the steps towards kinks. This process is shown in figure (2.3 b).

The proportion n_s of the surface sites covered by adsorbed molecules has been given by Burton, Cabrera and Frank [21] approximately as,

$$n_s = \exp [-W_s / kT] \qquad (2.5)$$

Where, W_s is the energy of evaporation from the kinks on to the surface, that is, the energy required to transfer a molecule from a site *A* to site *B* in figure (2.3 b), which was estimated to be about *½ W*.

The mean displacement x_s of adsorbed molecules, which is the average distance a molecule would wander on the crystal surface between the time it hits the surface and the time it evaporates again, is given by Burton et al [21] as,

$$x_s = a \exp \{ (W'_s - U_s)/ 2k T\} \qquad (2.6)$$

Where, U_s is the activation energy for surface diffusion, that is, migration from one surface site to another and this has been estimated to be of the order of *1/20 ;* W'_s is the evaporation energy from the surface to the vapor and is given by, $W_s = 3\Phi$, that is, half the total evaporation energy *W*. One can further neglect U_s and estimate that $x_s \approx a \exp (3\Phi / 2kT)$, which is of the order of 4×10^2 for the typical values of $\Phi / kT \approx 4$. This indicates that $x_s >> a$, therefore, the molecules diffuse considerable distance before evaporating. This leads to conclude that the direct arrival of molecules from vapor at any particular point on a crystal surface is, generally, small as compared with the rate of indirect arrival through the surface migration.

Nevertheless, the concept of minimum total surface free energy is also important in crystal growth. Gibbs [22] in 1878 developed a consistent phenomenological treatment (thermodynamic treatment) of the equilibrium problem, which is still essential as an introduction to the study of crystal growth. Gibbs made use of the analogy of liquid drops and applied it to the conditions governing the growth of water droplets in a mist to the growth of a crystal. The free energy, which resides on the surface separating the two phases, retards the formation of the second phase in the first. The condition for the stability of an isolated drop of a liquid is that its surface free energy and hence its area be minimum. Altogether, in a similar manner for a crystal in equilibrium with its surrounding at constant temperature and pressure, this condition implies that the Gibbs free energy is the minimum for a given volume. Considering the volume free energy per unit volume as constant through out the crystal, one gets the condition,

$$\Sigma\, \sigma_i F_i = minimum, \text{ (Where } i = 1, 2, \ldots n)$$

Where, σ_i is the surface free energy per unit area of the i^{th} face of area F_i on a crystal bounded by n faces. Therefore, those faces will develop which leads to a minimum total surface free energy for a given volume. In a drop of liquid the atoms or molecules are randomly arranged, in contrast to this in a crystal the structural units are arrange in a regular way in three dimensions as per the prevailing symmetries. Curie [23] in 1885 calculated the shapes and end forms of crystals in equilibrium with solution or vapor, which was consistent with the condition that the free energy must be a minimum for a given volume. Later on, Wulff [24] extended this theory and showed that Gibbs equilibrium

shape of crystal was related to the relative surface free energies of the faces in a very simple manner.

It was thought that on perfect crystal faces steps could be created by the thermodynamic fluctuations in much similar way as the kinks are formed on a step. However, in the earlier theoretical considerations the problem was to start the nucleation on the perfect crystal face. Gibbs [22] considered that before a new layer can grow, a two dimensional nucleus or island monolayer, probably of 100 molecular diameters, has to be formed and on the edges of which the growth can proceed. Once such type of layer is formed, it spreads quickly across the whole face and the process of growth is held until a new nucleus is formed. This has been described in Figure (2.4).

`

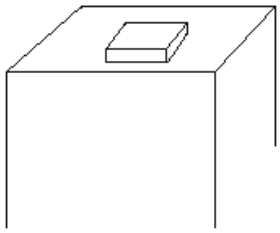

Figure: 2.4 Surface with island monolayer.

The problem of nucleating an island monolayer on a closed-packed crystal surface is analogous to the nucleation of a water droplet as mentioned earlier. For a given degree of super-saturation, there a critical radius ρ_c of the nucleus of circular nature such that a nucleus of radius greater than ρ_c will grow and if less it will evaporate. This is due to the line energy of the step of island monolayer causes a local equilibrium vapor pressure, which is inversely proportional to its radius of curvature. In the case of circular nucleus of radius ρ, the free energy is,

$$F = -\pi \rho^2 \epsilon + 2\pi \sigma \quad (2.7)$$

Where, ϵ is the free energy gained per unit area when an adsorbed molecule becomes attached to the nucleus and σ is the free energy per unit length of the step at boundary of the nucleus. From this expression one finds interesting behavior, initially, as ρ increases from zero, the F also increases until it reaches a maximum value of F_o for $\rho_c = \rho$; thereafter, it decreases with increasing ρ.

Burton et al [21] have re-examined the shape of the nucleus. Their arduous analysis shows that the nucleus is, *ipso-facto,* not circular but varying in the shape and hence the free energy per unit length of the edge changes with the crystallographic directions. In more general manner, the ρ_c can be regarded to be the radius of circumscribing circle to the critical nucleus. The rate of the formation of nuclei is given by,

$$Z = (S / s_o) \exp (- F_o / k T) \quad (2.8)$$

Where, Z gives the rate of arrival of fresh molecules at single surface lattice site**,** S is the surface area of the crystal face under consideration and so is the area per molecule in the layer. Usually, Z cannot exceed 10^{13} sec^{-1} even in a dense environment, however, the pre-exponential factor is about 10^{22}. For the observable growth rate on the time scale of a laboratory experiments, for example, 10^{-3} layers per second or one micron per month, it follows that the logarithm of saturation ratio, $\log \alpha$, must be at least $(\Phi / k T)^2/90$, where, Φ is the binding energy of nearest neighbor, with typical value of $\Phi / k T$ requires a super-saturation of at least 25 to 50%. Therefore, the nucleation rate is very sensitive function of super-saturation. It is worth noting that above this critical

super-saturation, the growth process is not limited by nucleation but below this critical super-saturation, the probability of nucleation would diminish to the negligible value.

The effect of presence of impurities on the nucleation rate has been reported by many researchers. Turnbull [25] proposed that the free energy of formation of a critical nucleus can be catalyzed by a suitable surface in contact with the nucleus.The *Nucleation catalysts* or *nucleates* may be solid particles suspended in liquid, the surface of the container or a solid surface. This process of nucleation is known as *heterogeneous nucleation*. In heterogeneous nucleation, the reaction may be the direct exchange of monomers between the parent phase and embryo, that is, a cluster of molecules, or through the surface, which is normally known as substrate. The theories of heterogeneous nucleation are developed well by many authors and edited by Zettlemoyer [26]. Moreover, in highly polar molecules, the dipole-dipole interaction is expected to play a prominent role in modifying the surface free energy of micro-cluster at the critical stage. In order to determine the effect of dipole-dipole interaction on the surface free energy, a model was proposed by Abraham [27] and discussed for various shapes of nucleation. A nucleation study is discussed in detail in the later sections of this chapter.

One of the major drawbacks of early nucleation theories is that once the kinked ledge receives sufficient ad-atoms to move it to the edge of the crystal, it can no longer work as a low energy nucleation site. Now, the generation of a new ledge requires an adsorption on a flat surface, for which the estimated super-saturation is of the order of 50 %. But in 1931 Volmer and Schultze [28] found astonishing results, while studying the growth rate of

individual iodine crystals at slightly supersaturated vapor at 0 ^{0}C. They found that the growth rate was proportional to the super-saturation down to 1%. Only below this degree of super-saturation it did fall below proportionality and that also not abruptly. New experimental evidences made earlier theory apocryphal; an attempt was made by Frank [29] and Burton [30] to propose a new concept by considering dislocations. A screw dislocation emerging on the face of a crystal provides it with a step. This step, containing kinks, offers a mechanism for growth of crystals at low super-saturations. When the atoms are adsorbed on the crystal surfaces they diffuse to the step and finally to the kinks and thus the step advances. The step provided by the screw dislocation, terminates at the dislocation point, where it remains fixed. Hence, when growth takes place, the step can advance only by rotating around dislocation point. At particular super-saturation, each point on a straight step advance with the same speed; therefore, the section of the step near the dislocation will have higher angular velocity for the same linear velocity and consequently, make a larger number of revolutions in a given time than the section farther away. Actually, for the portion of the step near the centre, having higher curvature, there will be higher equilibrium vapor pressure and, therefore, a lower local super-saturation, hence the rate of advance is bit lower. When steady state has been reached, the whole spiral will rotate uniformly about dislocation. This has been described in figure (2.5). Verma has given a detailed account of the various growth spirals and their significances [31].

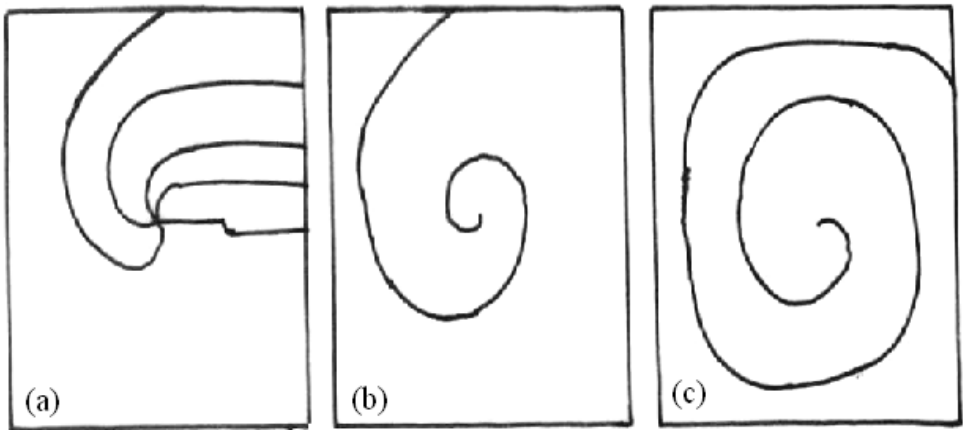

Figure: 2.5 Growth spirals.

A theory of crystal growth, incorporating the mechanism of step generation and transport into the step, was given by Burton, et al [21] in 1951, in their celebrated paper. This theory has gained importance because much of the content will apply to any theory of crystal growth. Verma [5] has elaborated great significances of Kossel- Transki- Volmer theory and BCF (Burton, Cabrera and Frank) theory in his well appreciated book. This BCF theory was originally proposed for growth from the vapor phase but its applicability to solution growth has been strongly advocated by Bennema and Gilmer [31].

Numerous other theories and models have been developed not only for the vapor growth but solution growth and melt growth also which are discuss in details by [2, 8, 32]. Many models are based on Monte Carlo simulations [33]. Derby [34] has given minute details of the present challenges of the crystal growth models. According to him the requirements are that one needs more realistically represent the many important interactions in crystal growth systems; models must be capable of describing detailed system geometry

and design, three dimensional and transient continuum transport, phase change phenomenon, and, ultimately, atomistic events. Altogether, Neugebauer [35] highlighted the challenges in the accurate simulations on crystal growth. According to his views, one naturally gets interested in a problem on a microscopic scale , where the size of typical surface features such as quantum dots, surface roughness, terrace length is in the order of 10 to 1000 nm and the characteristic time-scale to form such features is in the order of seconds, the mechanisms leading to these structures, such as ad-atoms, adsorption, diffusion, de-sorption, island nucleation, require an atomic scale resolution , that is, a resolution in the length scale of 10^{-1} nm and in the time scale of 10^{-13} sec.

2.3 Crystal Growth from Solution

Crystal growth from solution is one of the most widely used techniques for the growth of crystals. This technique is practiced among the crystal growth community next to the melt growth technique. The main advantage of the solution growth is that the crystals are grown at temperatures well below their melting points. A detailed inherent knowledge is required for the melt growth techniques such as, melting point, melting behavior, stability in reduced pressure and atmosphere, however, which is not needed in the solution growth. Myriad technologically important crystals are grown by this technique. Solution growth techniques can broadly be subdivided as follows [11].

(1) Low Temperature Solution Growth

This technique is used for materials having very good solubility at room temperature in water or any other solvents. In the aqueous solution growth technique, water is used as a solvent; while in non-aqueous techniques other than water is used as a solvent. This method hinges on achieving super-saturation without inducing spontaneous nucleation, so that the growth can proceed on the seed material. Super-saturation can be achieved and maintained in a number of ways, depending upon the conditions of the experiment and desired results. Broadly speaking, in the solution growth, the solvent can be evaporated (slow evaporation technique), the solution temperature can be decreased (slow cooling technique) or solution, saturated at a temperature higher than the growth temperature, can be continuously added into the growth vessel (temperature differential method). Many ionic salt crystals as well as organic material crystals have been grown for different applications. Large size KDP (Potassium Dihydrogen Phosphate) single crystals have been grown for LASER applications. The dimensions of KDP crystals are 26 x 21 x 23 inches, and weighing 700 lbs [36].

(2) High Temperature Solution Growth

This technique is also known as flux growth. Molten salts are the only solvents for oxides or solid solutions of oxides, which are having very high melting points and/or decompose before melting. Oxides or fluorides are dissolved in a flux and the growth proceeds at relatively low temperatures, often as much as 1000 ^{0}C below the melting point of the solute. The common

fluxes are KF, PbO, PbF_2, and B_2O_3. Different ferrites and garnets can be grown by this technique.

(3) Hydrothermal Growth

This technique is essentially aqueous solution growth at high temperature and pressure, which is applicable for the materials having limited solubility under ordinary conditions. This technique is used to grow quartz and calcite crystals.

(4) Metallic – Solution Growth

This method is used to grow single crystals of metallic phases and inorganic compounds, which are readily obtained by solidification of saturated metallic solutions. Diamonds are commercially grown from transition-metal solutions under high pressure. Cubic SiC crystals are harvested from iron melts saturated with C and Si. Nowadays, this technique is preferred for semi-conducting material crystals like GaAs for industry.

2.4 Low Temperature Solution Growth

The growth of crystals is a result of addition of new atoms, molecules or more complex aggregates. The addition of a new particle of the same substance is not necessarily the same thing as crystal growth. For example, adsorption on a atomically smooth surface is not sufficient to be regarded as growth, because it may stop once a certain concentration of ad-atoms is achieved; this happens when the chemical potential of the adsorbed atoms or molecules becomes equal to that of the identical atoms or molecules in vapor or solution, as the case may be [37]. The solution growth usually occurs in a

layer wise manner. The crystallizing substance is delivered to the step by either bulk or surface diffusion. However, their relative role is not well established.

Recently, many authors have discussed different crystal growth topics covering mainly the solution growth, which are thermodynamics versus kinetics [15], the terrace-step-kink approach and the capillary wave approach to the fluctuation properties [38] and a comprehensive treatise on crystal growth from solutions [39].

All methods of growing crystals from solutions are based on the dependence of the solubility of a substance on the thermodynamic parameters of the process, temperature, pressure and solvent concentration. In the majority of the cases the temperature dependence of the solubility is employed. The state of super-saturation is very essential for crystallization to occur. One of the convenient ways in which the degree of super-saturation can be expressed by the means of the following expression,

$$S = C / C^{*}$$

Where, C is the concentration of the solution and C^{*} is the equilibrium saturation concentration at the same temperature. Hence different three states of saturations are denoted by the values of S; namely, a saturated solution indicates $S = 1$, under-saturated solution denotes $S < 1$, and supersaturated solution indicates $S > 1$. Other common expressions of super-saturation are the concentration driving force, ΔC, and relative super-saturation, σ, defined by [40]

$$\Delta C = C - C^{*} \text{ and } \sigma = \Delta C / C^{*} = S - 1$$

2.5 Solubility Curve and Its Importance

Depending upon the type of compound to be crystallized, two broad categories of growth are normally used; which are (i) low temperature aqueous solution growth and (ii) high temperature and high pressure hydrothermal growth.

For any solution growth experiment it is required to study the temperature-concentration (*T-C*) diagram or the solubility curve. Figure (2.6) depicts the typical diagram of T-C curve, where the solubility of the test substance increases with temperature. The solubility curve in solid line divides the diagram into two major regions; that of under saturated solutions below the saturation curve and that of supersaturated solutions above the curve. Usually, the region of super saturated solution is divided into a meta-stable and labile zone. The meta-stable region is formed because energy must be spent on the formation of a critical size crystal nucleus. Labile solutions are unstable, strongly supersaturated solutions in which the

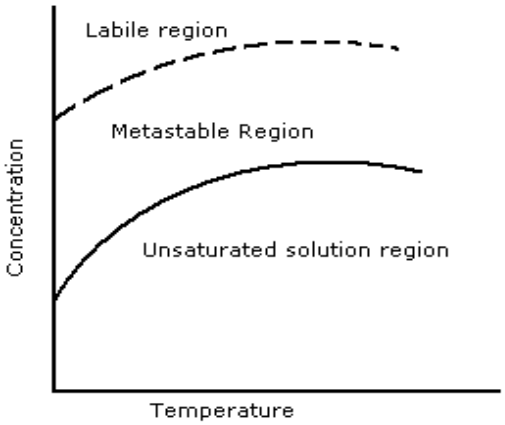

Figure:2.6 Typical T-C curve.

crystal nuclei form readily owing to spontaneous fluctuations in the concentration of the substance. The boundary separating the metastable and labile zones indicates the maximum super-saturation at which excess solute does not crystallize spontaneously. Solutions are relatively stable in the metastable state. This is because of considerable work done for the formation of a critical size crystal nucleus; the energy barrier cannot be overcome by means of natural fluctuations in the concentration of the substance. However, the simple way to initiate growth from supersaturated solutions is to introduce seeds, which provide nucleation centers. The boundary between the labile and meta-stable zones, usually, can not be defined clearly because it depends on the nature of the solution, the processes occurring in them and the degree of the purity of the starting material.

Controlled crystal growth is possible only from metastable solutions. The driving force of the process is the deviation of the system from equilibrium, which can be characterized either by “super-saturation” ΔC or by the value of “super- cooling” ΔT. The super cooling can be defined as the difference between the temperature of saturation of the solution and that of growth. If the possibility of the substance is unknown, the super cooling ΔT serves as a rough estimate of the deviation from equilibrium.

The solubility of KDP in water at temperatures 0, 10, 20, 30, 40, 60, 80 and 90 ^{0}C are 14.8, 18.3, 22.6, 28.0, 33.5, 50.2, 70.4 and 83.5 parts by weight per 100 parts by weight of water, respectively [41].

2.6 Choice of Solvents and Additives

It is important to select proper solvent for the solution growth so that one can yield prismatic growth habits of crystals. A good solvent ideally displays the following characteristics:

(a) Moderate reversible solubility

(b) A reasonable positive temperature coefficient of solubility

(c) A small vapor pressure

(d) Non-corrosiveness

(e) Non-toxicity

(f) Low price in a pure state

(g) Non-flammability

Solvents possessing all these characteristics, altogether, do not exist. However, solvents in practical use include water-both light (H_2O) and heavy (D_2O), ethyl alcohol, acetone, carbon tetrachloride, hexane, xylene and many others. Water is used in about 90% of cases and heavy water, alcohol and acetone each contributes about 1%.

Usually, a solvent is used in which the solute is soluble to the extent of 10 to 60 %. If the solvent is volatile then precautions must be taken to prevent volatilization, which promotes spurious nucleation due to temperature and concentration changes.

The experiments of Bunn and Emmett [42] show that the, electrostatic forces between crystal and solution are involved in crystal growth and, therefore, the polarity of the solvent must be considered. Kohman [43] has

observed that crystals of non-polar organic compounds grow from non- polar organic solvents at rates comparable to the solidification of melts, suggesting that the main difference between two processes is the interaction of solute and solvent molecule. Many additives that influence crystal growth morphology [44] and the crystal growth rates [45] are studied. Many times a change in the growing crystalline habit is desirable. A habit of growing crystal can be altered by changing the temperature of growth, changing the pH of solution, adding a habit modifying agent and changing the solvent.

Moreover, to have a regular and even growth, the level of super-saturation has to be maintained equally around the surface of the growing crystal. An uneven growth leads to localized stresses at the surface generating imperfection in the bulk crystal. The concentration gradients that exist in the growth vessel at different faces of crystal cause fluctuations in super-saturation, which seriously affects the growth rate of individual faces. The gradient at the bottom of the growth vessel exceeds the meta-stable zone width, resulting into spurious nucleation. However, the degree of formation of concentration gradients around the crystal depends on the efficiency of agitation of the solution. For these reasons, the agitation of saturated solution in either direction at an optimized speed of stirrer motor is advisable.

2.7 Selection of Seeds

Gilman [8] compared the artificial growth of crystals with agriculture. Alike in agriculture, good crystal growth needs good quality seeds, uninterrupted supply of nutrients and allowing the fittest to grow. Getting a proper quality of seed crystals is a prime factor in crystal growth. The classical

method is either evaporating or slow cooling saturated solution. But it is frequently more practical to use a piece from a natural or a previously grown crystal or to produce oriented

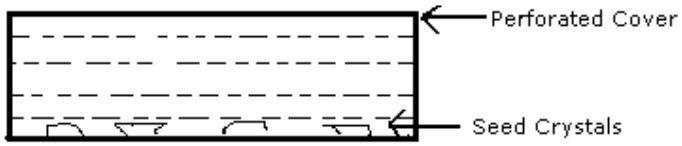

Figure: 2.7 Grown Seed crystals.

over growth on a seed of similar material. Any fragment of the desired crystal can serve as a seed. A piece bounded by the natural faces is not always the most preferable one. The most efficient seed is a plate whose faces are normal to the most rapid growth direction [46].

2.8 Preparation of the Solution for Crystal Growth

For solution preparation it is necessary to have an accurate solubility temperature data of the material. The saturated solution is prepared in accordance with the solubility curve. It is tested for saturation by suspending a small seed crystal in the solution. The temperature of the solution is slightly raised above the saturated temperature to dissolve any unwanted nuclei or any surface damage of seed. The temperature then lowered to the equilibrium temperature in order to commence the crystal growth. Sintered glass filter of different pore size are used for solution purification. The clear solution saturated at the desired temperature is taken in growth vessel is perfectly or partially closed during crystallization.

2.9 Agitation or Stirring

In a motionless solution the delivery of the substance is carried out by diffusion and the growing crystals exhibit all the defects of growth in the diffusion regime. In a pure diffusion regime the super saturation changes over different areas of the faces. In order to reduce this non-uniformity of the super saturation and nutrition of different areas of the faces, motion of the crystal and solution relative to one another must be required. This is usually achieved in two ways; (i) by free convection of the solution as a result of temperature difference in different zones of the crystallizer and (ii) by stirring the solution. Even in the case of free convection of solution the improvement in nutrition supply to the growing crystal is observed. Notwithstanding, it is often insufficient because in the steady state of free convection the flow of the solution near the crystal may be non -uniform. Moreover, the solution velocity here can only be increased by increasing the temperature difference between the zone where the growing crystals is placed and the remaining volume of the solution and this changes the super saturation.

There are several methods adopted for stirring and crystal motion, which are elaborately discussed by Chernov [37]. The simplest method is unidirectional central rotation of the crystal on the holder. It is, however, avoided because the solution flow leads to the formation of cavities in the crystal and as a result promotes the trapping of inclusions. The faces receiving more nutrition grow more rapidly, whereas, the others suffering from malnutrition grow slowly and acquire various defects. In the case of recessive rotation the reversal period may last several minutes. The assigned rotation speed depends on the length and shape of the crystal support, the viscosity

and amount of solution, and the crystal size. For the supply of uniform nutrition supply to all growing faces of a crystal, spiral motion of the crystal has been advocated. There are several other types of crystal motion, mechanisms are proposed, for example, eccentric unidirectional, eccentric reversive, planatory rotation, reciprocating, circular motion, magnetic agitator, etc. More recently, accelerated seed rotations based on microprocessor controlled or programmable seed crystal movements have been proposed. A set up designed and fabricated having bi-directional accelerated seed rotation controller for solution growth has been employed for the growth of KDP crystals [47], which is useful for forced convection configurations to maintain a higher homogeneity of the solution. Using 5 liter capacity crystallizer with accelerated crucible rotation technique (ACRT) and simulated platform geometry to control the hydrodynamic conditions, Dixit et al [48] reported rapid growth of KDP crystals along (100) and (001) directions.

2.10 Crystal Habit

The shape or habit, which a crystal achieves in the process of its growth, is highly sensitive to growth conditions and reflects the growth mechanism [37, 49]. Therefore, growth shapes make it possible to judge the conditions prevailing during growth and growth parameters affecting. The following conditions and parameters have been discussed [33, 37].

Kinematics

Polyhedral shapes are obtained when each face remains parallel to itself in growing, i.e., when the growth rate depends exclusively on the surface orientation and is equal on the average for all points: $V = V(n)$. It has been

demonstrated by Chernov [50] that under the described conditions the steady state growth shape can be determined by Wulff's rule with help of function *V(**n**)* alike the equilibrium shape is determined with help of specific surface energy *α(**n**).* Analytically, the steady state growth shape is described by the envelope of the families of planes given by equation,

$$n\, r = V(n)\, t$$

Where, *t* is the time for nucleation and ***n*** is the vector normal to envelope, i.e., to the surface of the crystal of equilibrium shape, at a point defined by the radius vector ***r***.

Determination of Crystal Habit by PBC Method

During growth from the gas phase and solution most crystals atomically achieve smooth surfaces and hence exhibit faceted growth shapes. To describe such forms, it is necessary to establish the crystallographic indices of the faces and their relative sizes, i.e., *the crystal habit***.** However, the sequences of sizes of the most probable faces are possible qualitatively during growth from gas phase is and with less certainty during the growth from solutions and melts.

The faces with lowest growth rates will be the most developed on the crystal surface. The lowest rates should be expected for faces parallel to the maximum number of the strongest bonds, i.e., for atomically smooth F (Flat) faces [51- 53].

By applying the Periodic Bond Chain (PBC) theory developed by Hartman and Perdock, one can find that the growth rate of a face is lower when the fewer chains of strong bonds cross this face.

The growth of flat faces requires either a potential barrier for the formation of two-dimensional nuclei be overcome or dislocation or other defects for step generation be present. Both of the indicated generation processes are slower, the higher the specific linear energy of the step is. This energy is higher, the stronger are the PBC and crossing and give rises of various oriented steps on a given face, i.e., parallel to the face. Moreover, during growth, due to the arrival of particles from the adsorption layer to the steps, the growth rate is higher and also the greater is the density of this layer. The layer density reduces exponentially with increasing energy of the bond between the adsorbed building-block particle and the surface, i.e., it must again be least for the faces crossed by the least number of the most energetic PBCs.

This correlation of surface energy and the growth rate results from the crystal structure, which determines both quantities for any orientation. In short the angular dependence of the growth rate is minimum for the same faces as does the angular dependence of the surface energy.

In accordance to the postulates of PBC theory, the “specific weight” of a face in the habit decreases in order F,S,K, (Flat, Stepped, Kinked) faces.

The growth forms of KDP shows tetragonal (100) prisms and on both ends tetragonal (101) pyramids. This is in agreement with the morphological theory of Hartman and Perdock which predicts for ADP and KDP as F faces

growing by layer by layer mechanism [54, 55]. Moreover, the growth spiral morphology on (100) KDP face related to impurity effect is analyzed on basis of PBC theory by Noor and Dam [56].

The Bravais –Donnay- Harker Rule

According the Bravais rule, the minimum growth rates are characteristic of the faces with the (h, k. l) orientation, that are parallel to those atomic nets of the lattice between which the distance $d_{h\,k\,i}$ is the largest, in other words, between which the bond strength is the least. As it is known that $d_{h\,k\,l}$ **α** $(h^2 + k^2 + l^2)^{-1/2,}$ i.e., the largest $d_{h\,k\,l}$ corresponds to planes with simplest indices, which often form crystal habit. The faces with simplest indices are usually those of closest- packed atomic nets.

To find the growth shape one has to use the distance between the nearest planes in which the atoms are situated, instead of $d_{h\,k\,l.}$ In determining these distances, it is necessary to consider the space-symmetry elements in the crystal structure. This is the modification suggested by Donnay and Harker in Bravais rule. This has been discussed by Chernov [37] in detail.

Effect of Growth Conditions

The structure of the surface and the mechanism of growth depend on super-saturation, temperature and composition of the environment, therefore, the habit of the crystal depends not only on its structure but also on these factors. For instance, at super-saturations of ≤ 1 % octahedron, cube, rhombo-dodecahedron morphologies are obtained. The reason is that singular faces have clearly defined non-linear dependence of the growth rate on the

super saturation and different kinetic coefficients and also on nonlinear dependence of growth rate on super saturation *V(σ).* The rates of layer generation by homogeneous and heterogeneous nucleation and due to dislocations depend on the linear energies of the steps, which differ significantly for various faces. Therefore, at small deviations from equilibrium and at low growth rates, the face velocities differ widely on non-linear part of *V(σ).* At large deviations from equilibrium, the acts of incorporating particles at kinks and steps as well as transport over the surface and the bulk, increasingly become the limiting stages of the process [37]. The growth of crystal at approximately equivalent rate along all the directions is a prerequisite for its accurate characterization. This will result in a large bulk crystal from which samples of any desired orientation can be cut. Further, such large crystal should also be devoid of dislocation and other defects. These imperfections are isolated into defective region surrounded by large volume of high perfection, when the crystals grow with a bulk habit. In the crystal, which grows as needle or plates, the growth dislocation propagates along the principle growth direction of the crystal [2]. Needle like crystals have very limited application and plate like crystals are needed to be favorably oriented. Change of habit in such crystals, which naturally grow as needles or plates, can be achieved by any one of following ways

(1) Changing the temperature of growth

(2) Changing the pH of solution

(3) Adding a habit modifying agent

(4) Changing the solvent

2.11 Inclusion

Inclusions are very important in crystal growth. The aim is always there to grow inclusion free perfect crystal. Trapping of mother liquor into crystalline imperfection is also a common problem in crystal growth, which results in loss of stability by crystal growth form. In dendritic growth, parts of the mother medium remains between the dendritic branches and communicate with the bulk of the mother medium only through a network of narrow channels.

Inclusions are also trapped when the growth front as a whole remains stable. In the case of this front is a singular face growing in layer wise manner, the inclusions arise when growth takes place by deposition of macroscopic rather than elementary steps. During the growth from solution, the nutrition of the step rise is better in the vicinity of the outer edge than it is in the vicinity of the inner edge forming the reentrant angle. The rise of macro-step, therefore, cannot remain flat while propagating at high super-saturation and a layer overhanging the growing face appears.

Macro-steps often have rounded shapes in the plane of the face along which they propagate. In experiments the appearance of macro-steps, then inclusions and finally ending into crystal cracking was noted [57]; Chernov [37] has discussed inclusion of mother liquor and impurities at length.

2.12 Solution Growth Methods

A variety of crystals are grown by the solution growth techniques for industrial applications. The size of the crystallizer vessels varies depending upon the requirements, whether it is for the research or industry. A

large number of ionic salt crystals, organic crystals and semi-organic crystals are grown by these methods. Various authors [2, 8, 37, 58-60] have given elaborative discussions on various solution growth techniques and hence a brief review is presented here.

Usually, slow cooling method is employed to achieve the required degree of super-saturation. The simplest illustration of the method is crystallization in a closed vessel, which is depicted in figure (2.8).

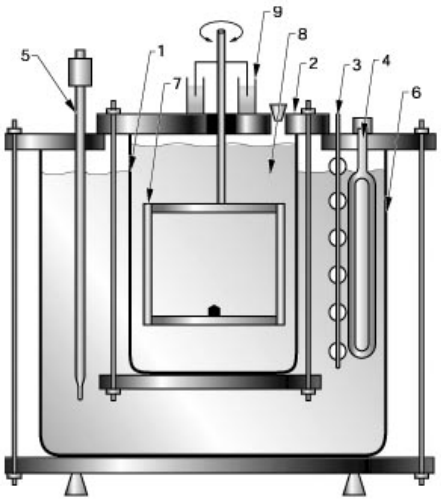

Figure:2.8 Schematic diagram of a crystallizer used for rapid crystal growth: (1) growth tank; (2) air-sealed lead; (3) stirrer; (4) heater; (5) thermo-controller; (6) water bath; (7) platform with the seed; (8) growth solution; (9) water cup seal.

A solution saturated at and above room temperature is poured into a crystallizer, which is then hermetically sealed. Prior to this, the solution is heated to a temperature slightly above the saturation point in order to avoid spontaneous crystallization at the moment it is filled into the crystallizer. A seeding crystal is suspended in the solution and the crystallizer is placed in a water thermostate whose temperature is reduced according to a pre-assigned plan. Super-saturation is maintained by slow cooling and the rates required can be as low as 0.1 ^{0}C to 1 ^{0}C per day. This requires appropriate

temperature controllers and also made easier to achieve solution temperature near the room temperature. The solution is agitated either by mechanical stirrer or by rotating seed holder. The fluid flow thus provided breaks up the boundary layer of rejected solvent and leads to more perfect and faster growth. This method often produces sufficiently large crystals. A very large size, in terms of several kilograms of weight, KDP crystals have been grown for LASER applications by this method [36].

Temperature difference methods are based on the formation of two regions with different temperatures in the crystallizer. In one of them, the substance which is always in excess in the form of the solid phase is dissolved and in the other, crystal growth takes place. In this case two vessels connected by tubes are usually prefered. The substance is dissolved in the vessel with the higher temperature and the crystal is grown in the other. The exchange between the vessel is achieved both by natural convection of the solution and by stirring with a mechanical agitator. Due to natural convection, the solution from the dissolution chamber moves along the upper tube into the growth chamber and along the water tube in the reverse direction. The large size crystals of various compounds can be grown successfully by this method. Figure (2.9) shows the schematic diagram of this method.

\

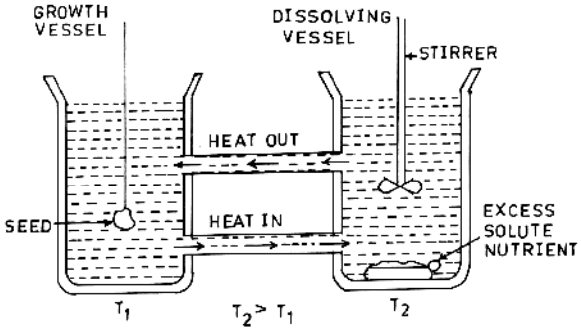

Figure: 2.9 Temperature difference method.

In slow solvent evaporation method the super-saturation is achieved by evaporating the solvent and as it evaporates the solute concentration increases to above equilibrium value. The process is carried out at a constant temperature under strictly isothermal conditions. Preferential evaporation of the solvent occurs “spontaneously” if contact is provided between the solution and the atmosphere, for non-toxic solvents. The rate of evaporation can readily be controlled by changing the solution temperature or controlling the passage using a screw-capped jar. The details of this technique are given by Chernov [37].

2.12.1 Advantages of growth from solution

There are several advantages of crystal growth from solution. This technique makes it possible to grow crystals that are unstable at their melting points or those exist in several crystalline forms depending on the temperature and provide control over temperature of growth [61]. Many times an advantage in control of viscosity in solution growth methods which permits crystals that tends to form glasses when cooled from their melts to be grown. Low viscosity solvents such as water greatly accelerate diversification of silica glass [44]. Generally, the rates of growth from melts are very large than those from solution. Crystals grown from solution usually have well defined faces as compared with those grown from melts. Solution growth methods are comparatively inexpensive. In addition, the growth from solution can be visually inspected; in fact it has been extensively used for studying the growth parameters, including convection and transport, by means of photography. However, the solution growth techniques are comparatively slower, requires

high purity solvents and a good deal of designing and parameter settings for good quality crystal growth [62].

2.13 Recent Work on KDP Crystals

KDP and its analogous systems such as Dueaterated KDP (DKDP) and ADP crystals are one of the most widely studied crystals. These crystals are studied for their different applications, but also for their morphologies, habits, effect of various growth parameters, effect of impurities, etc. The amount of literature reported for growth and characterization of these crystals is enormous, notwithstanding, some important studies on growth, morphology and habit modifications carried out over the period of more than a decade is attempted to cover in this section.

One of the aims of the researchers all over the world is to grow high quality KDP crystals rapidly. For this purpose various authors have made various modifications in the growth techniques as well as designed the new set ups. In 1987, a splicing technique was reported by Sui et al [63] to speed up the enlargement of the cross- section of KDP crystals. An n^2 (n = 1, 2, 3, 4…) array of (001) oriented seed crystals were applied to grow KDP crystals up to 72 cm^2 in cross-section. The authors reported the results of a research program concerning the seed splicing technique to grow large KDP crystal. They mounted several seed crystals together in a frame in such a manner that the seeds had the same crystallographic orientation. This composite seed was then placed into a super saturated solution. It would be possible, despite the unavoidable mutual mis-orientation of the separate seed crystals in reference to each other of about 1 Å, to grow a single crystal of a large

diameter and high perfection. Because of the highly stressed areas disappeared in the non-growing prism faces, this technique was unique for KDP. It can also be applied, the authors pointed out, to similar crystals with a needle-like habit where pyramidal faces do grow but prism faces do not.

For high power laser application quite large size KDP and DKDP crystals are needed and attempts have been made to grow them in large dimensions by various authors. In 1983 an attempt was made to grow 40 x 40 cm^2 cross-section and 100 cm length KDP crystals by Newkirk et al [64]. KDP and DKDP crystals have been grown with the sizes up to 57 x 57 cm^2 in cross section and about 55 cm in height by Zaitseva et al [65]. It is also important to control habit during the growth of KDP crystals to achieve the large size crystal with specific habit for desired applications. Zaitseva et al [66] proposed certain measures for the habit control. The ratio of dimensions along the crystallographic axis was controlled by (i) creation of special dislocation structure during the seed regeneration process and (ii) change in the orientation of the seed. The authors applied these techniques to grow KDP and DKDP crystals of various habits at 100-20 mm/day to the linear sizes of 90 cm.

The effect of bacteria in KDP solution on the growth habits of KDP crystals has been explored by Sasaki et al [67]. They found hillocks only on the tapered prismatic surfaces of KDP crystals grown by solution containing live bacteria. The possible interpretation was proposed as biochemical reaction between bacteria and KDP crystals.

Rapid growth of KDP crystals has been obtained by various workers. Linear high speed growth of 80 mm/day was obtained by computer controlled mechanism by Minagawa et al [68] and earlier than this a rapid growth of over 50 mm/day was reported by Nakatsuka et al [69] for KDP crystals. Recently, a movie of KDP crystal growth weighing 800 pounds is put on internet in Youtube [70], which uses six feet high tank containing one ton supersaturated solution of KDP. By using the turntable tank to rotate the crystal it was possible to grow the crystal in two months, otherwise, it would have taken two years in the conventional technique.

Two modifications have been proposed to avoid spurious nucleations and seed isolations. Karnal et al [71] suggested modification in the growth set up against spurious nucleation. Stability of the solution against spurious nucleation plays a dominant role in the growth of crystals at high growth rates requiring high levels of super saturations. If any spurious nucleation takes place during the growth, it becomes practically impossible grow very large size crystals. An indigenous nucleation-trap crystallizer was developed by the authors to trap any unwanted nuclei and particles that appeared and settled at the bottom of the crystallizer. Any particles and nuclei nucleating during the growth were forced into the nucleation trap (or well) and, subsequently, by manipulating the temperature of the well, those could be arrested. This was successfully demonstrated for DKDP crystal growth. Moreover, a novel seed isolation technique was proposed by Karnal et al [72]. In this method a mercury seal was developed that facilitated the processing of the solutions with immersed seed. This technique allowed a seed crystal to be introduced into the crystallizer prior to the processing of the solution and hence allowed

the seed to be present in the growth chamber during the filtration and overheating operations, while at the same time it prevented the seed from getting dissolved by under- saturated solution. When the solution process was over and the solution had been cooled to the near saturation temperature, the mercury seal was removed and the seed was exposed. This technique was tested on DKDP crystal growth.

The effect of pH of KDP solution on the crystal growth has been studied widely in order to grow good quality KDP crystals. KDP crystals at low pH value (~ 1.5 pH) were grown by Gau et al [73]. In situ measurement of pH and super- saturation dependent growth kinetics of prismatic and pyramidal faces of KDP crystals were reported by Sharma et al [74]. The pH of solution of KDP can be adjusted by using phosphoric acid.

The effect of different additives and impurities on the growth habit of KDP crystals has been studied by large number of researchers. The effect of meta phosphate, boric acid and quaternary ammonium cations of different concentration on habit of KDP crystals was reported by Sun Xun et al [75]. Different impurities affect growth habit in different manner due to their varying impurity adsorption mechanism. Maeda et al [76] used organic dyes (sunset yellow FCF, brilliant blue FCF and sky blue) to study the growth rate and morphology of (100) and (101) faces of KDP crystals. Dhanaraj et al [77] added different molar ratio of K_2CO_3 in KDP and meta-stable zone widths of KDP solutions were measured. The effects on meta-stable zone widths of KDP by anions doping [78,79] and by trivalent transition metal ions (Mn^{+3}, Cr^{+3}) have been reported by Lai et al [80].

From crystal chemistry point of view the growth units and forming mechanism of KDP crystals is discussed by Weizhuo Zhong et al [81]. The thickness of the boundary layers is changing with lattice faces as it has been studied by the authors with Raman spectra, where the solution structure during the crystal growth can be observed. It has been found that the solution structure at the boundary layer is similar to that of the crystal, so that the growth unit proposed as $[H_2PO_4]^-$. The difference of growth rates of lattice faces is determined by the combination of growth units, which is mainly dominated by the angular orientation of K-O and H-O bonds. As a result, the reason about the difference of growth rates of lattice faces and the influence of pH values on the crystal morphology can be well elucidated.

In a quest to grow the long crystals of KDP, the Sankarnarayana – Ramasamy (S-R) method has been employed by Balamurugan and Balamurugan et al [82, 83]. A KDP crystal of 15 mm diameter and 65 mm length has been reported. Furthermore, the feasibility of melt growth methods for KDP crystals was checked by Pastor and Pastor [84]. Also, the gel grown KDP [85] is reported.

The surface topography of KDP crystals has been studied by AFM (Atomic Force Microscopy) by Yoreo et al [86]. Apart from this, Akasuma et al [87] studied the topography characteristics of (100) and (101) faces of KDP using AFM. Fractal dimensions of the surface patterns were measured by them, including the step height and the terrace distance of KDP.

In the following section the growth of various amino acids (L - histidine L- threonine and DL - methionine) doped KDP crystals will be discussed.

2.14 Solubility Curves of Pure and Amino Acid Doped KDP

The solubility data of pure KDP is available in the literature [32]: In the present study, the author has measured the solubility of various amino acids added KDP crystals. The representative solubility curves for pure KDP, 0.3 wt % L-histidine doped KDP, 0.3 wt% L- threonine doped KDP and 0.3 wt % DL-methionine doped KDP crystals are drown and presented in figure (2.10). It is found that the solubility of doped KDP increases very marginally with respect to pure KDP.

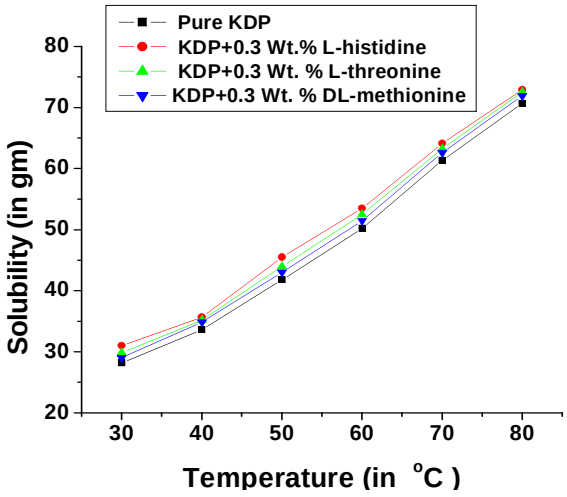

Figure: 2.10 Solubility curves for pure and 0.3 wt% various amino acids (L-histidine, L-threonine and DL-methionine) doped KDP.

2.15 Growth of Pure and Amino Acids Doped KDP Crystals

For the growth of pure and amino acids doped KDP crystals AR grade, chemicals were used. All the solutions were made in double distilled water. Three amino acids were selected for doping, viz, L- histidine, L-threonine and DL-methionine. Various weight percent concentrations of amino acids were selected for doping, viz, 0.3 wt %, 0.4 wt% and 0.5 wt %, which were obtained by dissolving 0.3, 0.4 and 0.5 mg selected amino acid into 100 ml solution of one molar KDP, respectively. The mixture was stirred well by using magnetic stirrer

for 8 hours to achieve homogenization. The solutions were then transferred into the crystallization vessels having selected seed crystals and placed in a water bath with temperature controlling accuracy of ± 0.1 ^{0}C. Glass beakers of 250 ml were selected as crtstallizers. The solution containing crystallizer was kept at 35 ^{0}C for crystal growth under controlled evaporation. The crystallizer was covered with clean lead and the controlled evaporation was allowed. Figure (2.11) shows the photograph of water bath with temperature controller used for crystal growth.

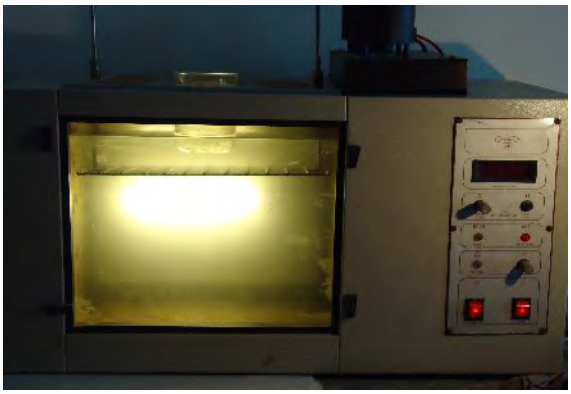

Figure: 2.11 Constant temperature water bath with crystal.

Figures 2.12 (a-d), show the photographs of pure KDP, 0.3 wt % L- histidine doped KDP, 0.3 wt % L-threonine doped KDP and 0.3 wt %, DL- methionine doped KDP crystals, respectively.

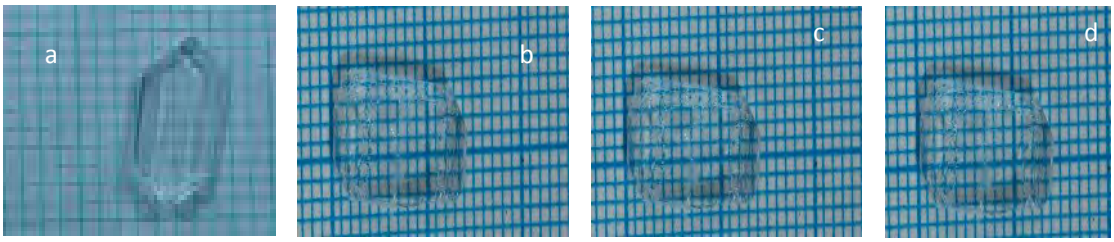

Figure: 2.12 (a) Pure KDP, 0.3 wt % (b) L – histidine (c) L – threonine (d) DL – methionine doped KDP crystals.

The growth habits of pure KDP crystals are platelet type with both prismatic and pyramidal face type and doping of amino acids does not change habits of KDP crystals. For example 0.3 wt % amino acid doped KDP crystals palate type habits are shown in figure 2.12 (a-d). Figure (2.13) shows the schematic diagram of observed habit of KDP crystals with indications of Millar indices of major faces.

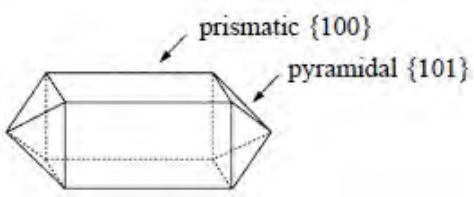

Figure :2.13 Schematic diagram of observed habit of KDP crystal.

2.16 Nucleation Study

As it has been discussed in section 2.2 that the nucleation is very important in crystal growth process and hence it is briefly reviewed hrerby. Nucleation is an early phenomenon in the growth of crystals irrespective of the starting materials from which the crystals grow and its study is very important to control the growth of crystals. A knowledge of the nucleation process leads to an understanding of many natural and industrial processes. Nucleation plays important role in different engineering processes where condensation, boiling, crystallization, sublimation and catalytic processes occur.

Nucleation is the process of generating a meta-stable mother phase, the initial fragments of a new and more stable phase capable of developing spontaneously into gross fragments of the stable phase. Nucleation is

consequently a study of initial stage of the kinetics of such transformations. There are four different stages in the phase transformation:

(1) The development of the supersaturated state which may arise due to chemical or photochemical reaction or the consequence of a change in temperature, pressure, tension or other chemical or physical condition.

(2) The generation of minute specks of nuclei.

(3) The growth of nuclei to form particles of microscopic dimensions or domains of the new phase.

(4) The relaxation process such as agglomeration by which the texture of a new phase changes.

In a supersaturated or super-cooled system when few atoms or molecules join together, a change in the energy takes place in the process of formation of a cluster. The cluster having such atoms or molecules is generally known as an embryo. The embryo may grow or disintegrate and disappear completely. If it grows up to a particular size then it is known as critical nucleus and there is a greater possibility for the nucleus to grow.

2.17 Types of Nucleation

Nucleation may occur spontaneously or it may be induced artificially. These two cases are frequently referred to homogeneous and heterogeneous nucleation, respectively. At the present state of knowledge, there is no general agreement on nucleation nomenclature. The term primary will be reserved for both cases of nucleation; homogeneous or heterogeneous, in systems that do not contain crystalline matter. On the other hand, nuclei are often generated in the vicinity of crystals present in the supersaturated

system. This phenomenon is referred to secondary nucleation. This classification can be represented as follows:

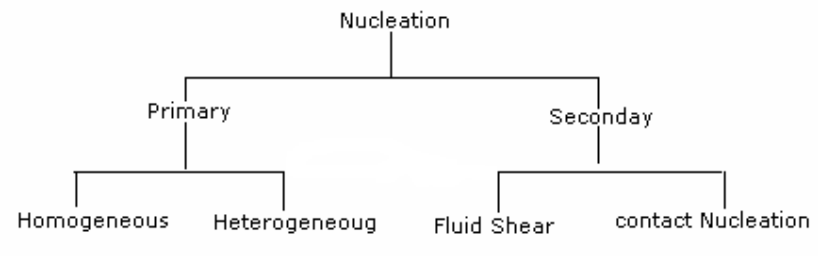

Nucleation can often be induced by external influences like agitation, mechanical shock, friction, extreme pressures, electric and magnetic fields, spark discharge ultraviolet, X-rays, γ - rays irradation, sonic and ultrasonic shaking etc. Stirred water can be super-cooled by about 0.5 ^{0}C, whereas, undisturbed distilled water can be super-cooled to as much as -4 ^{0}C. Similarly, water in a capillary tube can be super-cooled to lower temperatures than in larger vessels.

2.18 Nucleation Thermodynamics

In the first order phase transition there is a discontinuous change in some order parameters between the two phases. Such a change is driven by the change in the free energy as the new phase is formed. The condition for stable equilibrium between two large phases is the equality of their chemical potentials. By chance if the chemical potential of one of them is higher than that of the other, a mass transport occurs until the chemical potentials become equal again throughout the system. The driving force of this transport is the difference between the chemical potentials *($\Delta \mu$)* of the two phases is called super-saturation and the product of this quantity and the number of transported molecules will contribute for the bulk energy change of the new phase.

The transformation can be divided into two discrete steps that occur one after the other.

(1) The formation of tiny particles of new phase, which is known as nucleation, and

(2) The increased in size of the stable particle, which is called growth.

A distinction between the nucleation and growth stages of transformation is important. When a particle in a new phase is formed a new interface is created between the particle and the liquid. Like all surfaces this interface has a positive energy which must be supplied during the transformation process. The tiny particles have large surface area to volume ratio and can therefore be unstable. For a spherical particle of radius *r*,

$$\frac{Surface\quad Area}{Volume} = \frac{4\pi r^2}{\frac{4}{3}\pi r^3} = \frac{3}{r} \qquad (2.9)$$

As *r* tends to zero, this ratio becomes very large and the energy of the surface can effectively prevent the initial formation of tiny particles. A particle is said to be nucleated, when it becomes stable and will not disappear because of thermal fluctuations. Once a particle achieves this stage, it grows further with continuous decrease in energy. The surface energy is no longer a dominant factor in the growth process.

2.19 Kinetic of Nucleation

The nucleation process is explained after considering the under-cooled and supersaturated phases which refers to unstable conditions. When the pressure of a vapor P is less than, equal to, or greater than the vapor

pressure of the liquid phase at the same temperature known as equilibrium pressure P*, the vapor is described as under-saturated, saturated or supersaturated, respectively with respect to the liquid phase. The under-saturated state and saturated state are thermodynamically stable. The supersaturated vapor in contact with the bulk liquid phase will condense into the liquid until saturation is obtained.

In a supersaturated vapor, not only monomers A_1 are present but also embryos, which are clusters of molecules bound together by their intermolecular interactions. The mechanisms of formation of such embryos is the simple collision process consisting of a single molecules A_1 with a cluster A_{i-1} consisting of *(i-1)* molecules and hence giving rise to a cluster A_i as follows

$$A_1 + A_{i-1} \rightarrow A_i$$

The cluster A_i may also form by the evaporation of a molecule from some cluster A_{i+1} as follows,

$$A_{i+1} \rightarrow A_i + A_1$$

The phase change takes place by single molecule attached to embryos of various sizes, this process predominant slightly over the reverse process in which the different embryos lose single molecules. The size distribution of embryos changes with time, the numbers of the larger ones increasing. There is a critical size which is unstable equilibrium with the supersaturated vapor and this critical nucleus forms the bottleneck of the phase change. Once embryos achieve this critical size, there is a high probability that they will grow, relatively unhindered, to microscopic size.

Details of kinetics and thermodynamics of nucleation are discussed by many authors [26,88-91].

2.20 Induction Period

When a supersaturated condition is achieved, the embryos are formed by single molecular addition starting from the monomer at the beginning. Thus it takes sometime for the formation of critical nucleus from the monomers. The time taken between the achievement of super-saturation or super-cooling and the appearance of crystal nucleus in a supersaturated system is known as the induction period.

The methods of induction period measurements are:

(1) Conductivity method

(2) Turbidity method

(3) Dilatometer method

(4) Visual observation method

Depending upon solubility of material one can choose appropriate technique available for determination of induction period. For example, if materials have low solubility, the conductivity and turbidity methods are suitable; on the other hand, for materials having high solubility, dilatometer and direct vision methods are used. These have been discussed extensively by several authors [92-96].

As the present author has used visual observation method, a detailed discussion of other methods has been avoided.

2.20.1 Visual observation method

Figure :2.14 Constant temperature bath.

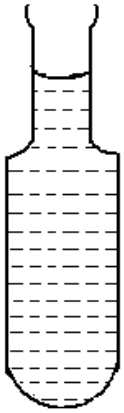

Figure :2.15 Specially designed container for induction period measurement.

In the present study, the experimental technique used to measure induction period is the modification of technique used by Mullin [97] and Joshi and Antony [98]. The solution supersaturated at 35 ºC of both pure and amino acids doped KDP were prepared in accordance with available data of solubility of KDP. To ensure that any unwanted metallic or non-metallic impurity do not affect the nucleation process, recrystallized samples of Analar Grade KDP powder and double distilled water were used. To minimize the evaporation from the surface,the saturated solution was kept in the specially designed glass vessel, which is shown in figure (2.15). Small drop of oil was also kept on the solution. The volume of solution taken for each experiment was 100 ml and it was preheated up to 40 ºC with stirring to achieve homogeneous concentration and temperature through out the volume of solution. To measure the temperature of solution exactly similar dummy vessel was used in which solution of same volume was kept. Normally, the time required for the growth of critical nucleus to a detectable size is negligibly small compare to time needed between the achievements of super-saturation

and appearance critical nucleus of detectable size and this time can be measured as induction period [99]. The appearance of first visible speck of nucleus at the bottom of the vessel was observed, the experiment was repeated for different level of super-saturation and for each super-saturation level average value of three trials of reading were taken to ensure the accuracy. Studies on the induction period are important not only from the point of view of practical information on the crystallization process but also they can yield information about the crystallization mechanism; the nature of the various stages of crystallization process and some of the physical properties of the crystalline substance.

2.21 Classical Theory of Nucleation

The formation of crystal nuclei is the difficult and complex process. Not only have the constituent atoms or molecules to coagulate, resisting the tendency to redissolve, but also they have to become oriented into a fixed lattice. The number of atoms or molecules in a crystal nucleus can vary from about ten to several thousand. The formation of such a nucleus cannot result from the simultaneous collision of a large number of atoms or molecules. It can be understood that a number of atoms or molecules may come together, as a result of statistical incidents, to form an ordinary clusters of molecules known as embryo. Simple energetic considerations show that this embryo is likely to dissolve again unless it reaches a certain critical minimum size. This does not necessarily mean that a macroscopic crystal will grow, since it depends on the availability of sufficient solute. It does mean that the assembly is stable under the prevailing conditions. The classical theory with necessary formulations is discussed in the following sections.

2.22 Steady State Nucleation Rate

Non- steady state nucleation and steady state nucleation processes are related by the induction period. The induction period is related in some way to the size and complexity of the critical nucleus and it can be affected by external influences. Even then, the induction period has been frequently used as a measure of the nucleation rate. Toschev et al [100] have shown that the steady state nucleation rate is inversely related to the non-steady state time lag, the induction period. Several authors [101-103] have made the assumption that the induction period is devoted to nucleus formation and considered to be inversely proportional to the steady state nucleation rate.

$$T \alpha J^{-1} \tag{2.10}$$

From the classical nucleation theory

$$\log\left[\frac{1}{\tau}\right] \alpha \frac{\gamma}{T^3 \log\left[\frac{C}{C^*}\right]^2} \tag{2.11}$$

$$S = \frac{C}{C^*}$$

Where,

C = Mole fraction of solute in the supersaturated salt solution at temperature T

C^* = Mole fraction of solute in the salt solution saturated at temperature T

γ = Interfacial tension of crystal

T = Temperature (K)

2.23 Critical Theory of Homogeneous Crystal Nucleation

The classical homogeneous nucleation theory has been successfully tested for the nucleation of liquid droplets from vapor and from liquid solutions and for crystal formation in melts [104 - 108]. Experimentally observed induction period can be used to evaluate the interfacial tension γ, energy of formation ΔG and radius of the critical nuclei *r*. With the help of the following theoretical consideration the basic relation of the equilibrium between solid and its solution which links the solubility expressed as the chemical potential to the particle size in the Thomson equation as suggested by Volmer [109].

$$\mu_r - \mu_\infty = \frac{2\gamma}{r}\nu \tag{2.12}$$

Where, μ_r =Chemical potential of nuclei of radius *r*

μ_∞ = Chemical potential of nuclei of infinite radius

ν =Volume per molecule in solid phase

γ =Interfacial tension of crystal

When the crystal attains a radius *r*, it will be in equilibrium with the solution and under these conditions the chemical potential of two coexisting phases are equal. While, equation (2.12) is written for the equilibrium between macroscopic particles and a particle of radius *r* with their respective solutions, the energy of formation of the nucleus of the new phase of radius *r* in equilibrium with in solution is expressed as,

$$\Delta G = \frac{16\pi\gamma^3\nu^2}{3\left(\mu_r - \mu_\infty\right)^2} \tag{2.13}$$

The frequency of formation of these crystals nuclei from their respective supersaturated solution has been given [110] as,

$$\tau = K \exp\left(\frac{-U_1}{kT}\right) \times \exp\left(\frac{-\Delta G}{kT}\right) \qquad (2.14)$$

Where, K = Constant

U_1 = Energy of activation for the molar phase transition from solution to crystal.

k = Boltzmann constant

T = Temperature in Kelvin

For a given volume of solution, the rate of nucleation is inversely proportional to the induction time. After taking logarithms on both sides,

$$1n\,\tau = 1n\,K - 1 + \frac{U_1}{kT} + \frac{\Delta G}{kT} \qquad (2.15)$$

For an isotherm, the term U_1/kT is a constant and so equation (2.15) is written as,

$$1n\,\tau = B + \frac{\Delta G}{kT} \qquad (2.16)$$

To evaluate the energy of formation ΔG, simplification in the form of first approximation is taken for the change in chemical potential [110] as,

$$\mu_r - \mu_{10} = \mu_r - \mu_\infty = -kT\,1n\,S \qquad (2.17)$$

μ_1 = Chemical potential of supersaturated solution.

μ_{10} = Chemical potential of saturated solution.

Applying equations (2.13) and (2.16) in (2.17)

$$1n\tau = B + \frac{16\pi\gamma^3 v^2}{3K^3T^3\,1n\,S^2} \qquad (2.18)$$

$$\ln\tau = B + \frac{16\pi\gamma^3 v^2 N}{3R^3T^3 \ln S^2} \tag{2.19}$$

Where, *v* is the molar volume of the crystal, *N* is the Avagadro's number and *R* is the gas constant. Equation (2.19) suggests a straight line for a plot of $1/\ln S^2$ against $\ln\tau$ can be drawn with a slope given by,

$$m = \frac{16\pi\gamma^3 v^2 N}{3R^3T^3} \tag{2.20}$$

Since *B* weakly depends on temperature. All the quantities in equation (2.20) are known except the interfacial tension γ. The interfacial tension of the solid relative to its solution can be calculated from the slope of the line *1/lnS*^{2} as,

$$\Delta G = \frac{RTm}{\ln S^2} \tag{2.21}$$

The energy of formation of a critical nucleus can be calculated from the experimental using following relation,

$$\gamma = RT\left[\frac{3m}{16\pi v^2 N}\right]^{\frac{1}{3}} \tag{2.22}$$

The radius of the nucleus in equilibrium with its solution has been computed as,

$$r = \frac{2\gamma v}{RT \ln S} \tag{2.23}$$

2.24 Effect of Soluble Impurities on Nucleation

The nucleation rate of a solution or melt can be affected appreciably by the presence of mere traces of impurities in the system. Crystallization from solutions always proceeds in multi component systems, because even in the purest form there are some impurities. Impurities may be both in

dissolved state and in the form of solids. If the crystallizing substance is an electrolyte, an excess of composite ions of any sign may serve as impurities. In crystallization from solution, the solvent itself represents a massive impurity in the system [111]. It is not merely a separate phase through which the solute must diffuse towards the growing crystal face; but it can also interact with the solute. It can be involved in the salvation of ions or molecules in solution, in the adsorbed layer and at the active growth sites. The solvent, therefore, can have an important influence on the crystallization process.

Crystal nucleation can occur either homogeneously or heterogeneously or by secondary nucleation. Homogeneous nucleation occurs either spontaneously or as induced. On careful examination, many reports of spontaneous nucleation are found to have been induced in some way. It is generally accepted that true examples of spontaneous nucleations are rarely encountered. A super-cooled system can be seeded unknowingly by the presence of atmospheric dust. Aqueous solutions prepared in the laboratory normally may contain 10^6 to 10^8 solid particles per cm^3 acting as heteronuclei. Large volumes of a given system nucleate spontaneously at smaller degrees of super-cooling than small volumes and, therefore, the larger samples stand a greater chance of being contaminated with active heteronuclei. The size of the solid foreign bodies is important and there is an evidence to suggest that the most active heteronuclei in liquid solution lie in the rage 0.1 to $1\,\mu m$. Heterogeneous nucleation occurs due to materials in contact with the solution. Minute cracks and crevice in the surface of the nucleation cell may act as a catalyst for nucleation.

2.25 Nucleation Studies of KDP and Related Systems

The reliability of homogenous nucleation studies is difficult to judge. Melia and Moffit [112], while studying the nucleation of ammonium chloride and ammonium bromide in aqueous solution have reported that the value of pre-exponential factor lies in the range 10^3 to 10^5 $cm^{-3}S^{-1}$, which is well outside the range predicted from Gibbs-Volmer theory $\cong 10^{25}$. Because of the experimental difficulty of preparing solutions completely free from foreign bodies, most of the crystallization and nucleation experiments reported in the literature have been concerned with heterogeneous nucleation.

The nucleation behavior of a solute can be affected considerably by the presence of impurities. The presence of small amounts of impurities can suppress nucleation in aqueous solution and certain surface active agents also exert strong inhibiting effect. The presence of insoluble foreign crystals reduces the super-saturation required to form crystals from their solutions.

It would be unwise to attempt a general explanation of the phenomenon of nucleation suppression by added impurities. Some impurities can suppress the nucleation entirely; some may enhance nucleation while others may exert a highly selective effort. The effect of soluble impurities on the nucleation of supersaturated KDP solution has been studied by the several authors and presented here by briefly.

The classical homogeneous nucleation theory has been successfully verified for different crystal systems. In 1976, Paul and Joshi [113] studied the effect of super-saturation on the induction period of KDP crystal. They calculated the surface energy at the phase boundary separating the growing

crystals from the solution and found to be 546 ergcm^{-2}. Shanmugham et al [114] studied nucleation of KDP. The nucleation rates, as indicated by induction period, were studied for supersaturated solution of potassium dihydrogen orthophosphate with and without addition of soluble impurities in the temperature range from 20 ^{0} to 40 ^{0} C. The effects of temperature, super-saturation and impurity content were discussed by them. The interfacial tension, energy of formation and critical radius of nuclei were calculated on basis of classical nucleation theory. It was found that the selected soluble impurities (K_2CO_3, K_2 PO_4, $K_2C_2O_4$, $Na_2B_4O_7$, and K_2CrO_4) enhanced the nucleation rate of KDP crystals. Apart from this, Shanmugham et al [115] also reported non-steady state nucleation process in KDP solution in the presence of XO_4 type impurities. Based on the probabilistic approach to the nucleation process, the steady state nucleation rate being inversely related to the induction period of the non-steady state time lag, the time of formation of first nucleation, they calculated different nucleation parameters for CrO_4, SO_4, IO_4, MnO_4, VO_4 and ClO_4 impurities.

The nucleation studies of KDP doped by KBr and $K_2Cr_2O_7$ were presented by Mahadevan et al [116]. They measured induction period by direct vision method and calculated different parameters by classical theory of homogeneous crystal nucleation. They found that the critical nucleation parameters increased with increase in doping concentration for both dopants.

Altogether, the nucleation study of KDP crystals added by L-arginine mono hydrochloride (LA HCl) was reported by Dhanaraj et al [117].The dopant concentration was varied from 1 to 10 M % and it was found that the meta-stable zone width of KDP was enhanced by addition of LAHCl.

The effect of stirring solution on induction period for precipitation of KDP was studied by Barata and Serrano [118]. They measured induction period as a function of super-saturation in the agitation range from 50 to 500 rpm by visual method. The induction periods were constant between 50 to 400 rpm and decreased later on due to decrease in the Kolmogoroff turbulence micro scale. The micro-mixing process did not interfere with formation of the new solid phase, since the micro-mixing time contribution to the induction period was negligible. The authors concluded that the precipitation mechanism was primarily nucleation followed by the normal growth in the all agitation intensity range studied. The interfacial surface tension also did not depend on agitation intensity.

Qu. et al [119] studied the effect of ethylene diamine tetra acetic acid (dipotassium salt -EDTA) and potassium pyrophosphate (KPY) on the batch crystallization of KDP. The crystal growth rates of certain crystal faces were determined by in-line images taken with MTS particle image analyzer (PIA) video camera. Nucleation kinetics was studied by measurement of meta-stable zone width and induction period. A significant promotion effect was found for nucleation and growth for EDTA, notwithstanding, the KPY exhibited the inhibitive effect. This was studied by two dimensional nucleation model. It was concluded by them that the presence of EDTA increased the density of adsorbed molecules of the crystallizing solute on the surface of crystal.

Apart from this, the advantage of Atomic Force Microscopy (AFM) is used for 2D nucleation studied on the (100) face of KDP crystal [120]. One of the most popular and similar system to KDP is the ammonium dihydrogen phosphate (ADP). The effect of urea on meta-stable zone width, induction

period and nucleation parameters of ADP crystals were reported by Rajesh et al [121]. They evaluated the critical parameters based on classical theory and concluded that the parameters increased on increasing doping concentration. Altogether, Rajesh et al [122] reported the nucleation studies of ADP doped with thiourea. They also found, as in their earlier studies, by urea doping in ADP the increase in the values of induction period and critical nucleation parameters on increasing the concentration of doping.

Moreorless, the similar results were obtained for $MgSO_4 \cdot 7H_2O$ crystals doped with KCl, KNO_3, urea and thio-urea [123]. The critical parameters increased as the concentration of dopants increased.

2.26 Nucleation Studies of Pure and Amino Acids Doped KDP

From the solubility curves of figure (2.10), pure KDP, 0.3 wt % L-histidine, 0.3 wt % L – threonine and 0.3 wt % DL – methionine doped KDP crystals; it is observed that the solubility of both pure and amino acids doped KDP increase with increase in temperature, which is in accordance with previously reported results for KDP [46]. It has also been observed that the solubility of KDP increases with doping of different amino acids. To study the effect of super-saturation on induction period, experiments were conducted for various level of super-saturations (S = 1.2 to 1.5) at a 35 ^{0} C temperature. The data are presented in table (2.2).

Table 2.2: Induction period and kinetic parameters of nucleation for pure and doped KDP

Sample	Supersaturation Concentration	Induction period (S)	Interfacial Tension (mJm^{-2})	Energy of formation ($Jmol^{-1}$)	Radius of Critical nucleus (nm)
Pure KDP	1.2	5410	16.83	934.75	4.26
	1.3	3060		1935.66	2.96
	1.4	1650		3183.61	2.30
	1.5	685		4623.04	1.91
KDP + 0.3 wt.% L-histidine	1.2	5510	17.40	1032.48	4.41
	1.3	3120		2138.03	3.06
	1.4	1688		3516.44	2.39
	1.5	701		5106.37	1.98
KDP + 0.4 wt.% L-histidine	1.2	5540	17.77	1100.46	4.49
	1.3	3155		2278.80	3.12
	1.4	1700		3747.97	2.43
	1.5	709		5442.58	2.02
KDP + 0.5 wt.% L-histidine	1.2	5554	18.00	1142.95	4.57
	1.3	3185		2366.79	3.17
	1.4	1715		3892.69	2.47
	1.5	714		5652.73	2.05
KDP + 0.3 wt.%L-threonine	1.2	5498	17.49	1049.47	4.42
	1.3	3125		2173.23	3.07
	1.4	1695		3574.33	2.39
	1.5	705		5190.43	1.98
KDP + 0.4 wt. % L-threonine	1.2	5510	17.72	1091.96	4.49
	1.3	3165		2261.21	3.12
	1.4	1709		3719.03	2.43
	1.5	712		5400.56	2.02
KDP + 0.5 wt. % L-threonine	1.2	5525	17.91	1125.95	4.53
	1.3	3198		2331.60	3.15
	1.4	1724		3834.80	2.45
	1.5	725		5568.67	2.03
KDP + 0.3 wt. %DL-methionine	1.2	5510	17.37	1028.23	4.38
	1.3	3140		2129.23	3.04
	1.4	1718		3501.97	2.37
	1.5	705		5085.35	1.97
KDP + 0.4 wt. % DL-methionine	1.2	5525	17.69	1086.01	4.45
	1.3	3165		2248.89	3.09
	1.4	1735		3698.78	2.41
	1.5	708		5371.14	2.00
KDP + 0.5 wt. % DL-methionine	1.2	5545	17.98	1139.55	4.53
	1.3	3180		2359.75	3.15
	1.4	1765		3881.11	2.45
	1.5	720		5635.91	2.03

From which it is clear that the induction period increases with increase in super-saturation level. The values of different critical parameters of nucleation, such as, the interfacial tension (*γ)* , the energy of formation (*ΔG*) and the radius of critical nucleus (*r)* are calculated using equations (2.21), (2.22) and (2.23), respectively. Equation (2.18) of the section 2.23 suggests a linear nature and a plot of *ln τ* versus $1/lnS^2$ can be drawn.

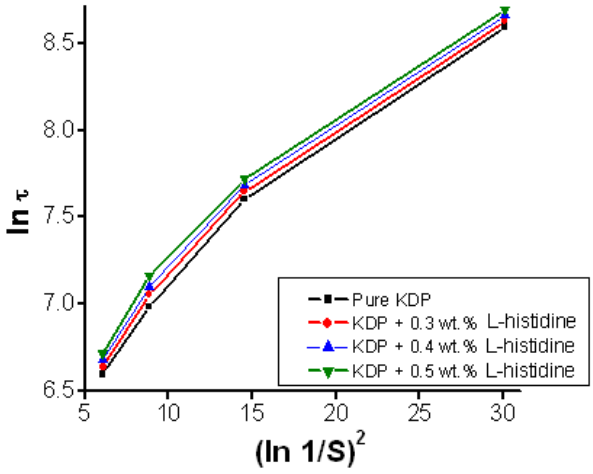

Figure: 2.16 Plots of *ln τ* versus $1/lnS^2$ for pure and L-histidine doped KDP.

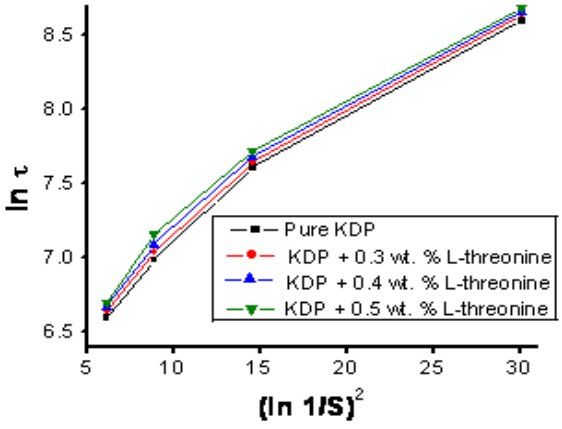

Figure:17 Plots of *ln τ* versus $1/lnS^2$ for pure and L-threonine doped KDP.

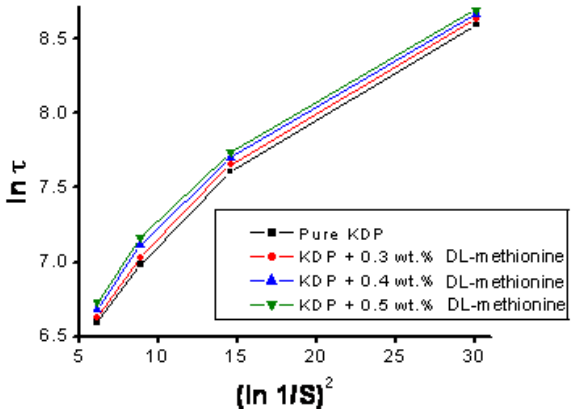

Figure: 2.18 Plots of *ln τ* versus *1/lnS²* for pure and DL-methionine doped KDP.

Figure (2.16),(2.17), (2.18) are plots of *ln τ* versus $1/lnS^2$, for pure KDP and L-histidine doped KDP, threonine doped KDP and DL- methionine doped KDP, respectively. However, the plots of figure (2.16-2.18) are not linear as observed by Shanmugham et al [114]. However, the linear nature is observed above 1.4 supersaturation, which is used for calculation of various nucleation parameters. The similar nature was observed by Shanmugham et al [115].

The values of different nucleation parameters indicates that the induction period, the interfacial tension, the energy of formation and radius of critical nucleus decrease as the super-saturation increase. The similar results were obtained by Shanmugham [114,115]. Moreover, the condensation of water nuclei from vapor in presence of soluble salts like ammonium sulphate and sodium chloride exhibited similar results [124].

Considering principles of homogeneous and heterogeneous nucleation theories, the free energy of formation of a nucleus under heterogeneous nucleation is less than homogeneous mediation [125]. Considering here the addition of amino acids and their different solubility in water may be the probable reason for the earlier precipitation of specks of doped amino acids to further induce heterogeneous nucleation.

Conclusion

1. Some limited effect of amino acids doping was observed on the morphology of KDP crystals.

2. The solubility of pure and amino acids doped KDP crystals increased with increase in temperature. The solubility at given temperature was more for amino acids doped KDP crystals than for pure KDP crystal.

3. As the doping level of amino acids increased the induction period increased marginally for particular dopant. Therefore, the doping of amino acids affected the nucleation process.

4. The values of interfacial tension, energy of formation of critical nucleus and radius of critical nucleus were calculated at various super-saturation levels for both pure and doped KDP crystals from classical nucleation theory, and it was found that the nucleation parameters decreased as the super-saturation level increased.

5. The values of different nucleation parameters were comparatively larger for amino acids doped KDP crystals than the pure KDP crystals. The difference in solubility of amino acids and KDP might have resulted in the formation of specks of amino acids earlier than KDP , which might have accelerated the nucleation , probably , in a heterogeneous manner.

References:

1. R. A. Laudise, "*Crystal Growth", in "Techniques of Crystal Growth*", Proc. of Int. Conf. on Crystal Growth, Boston (1966).

2. B. R. Pamplin, "*Crystal Growth*", Oxford Press, New York (1975).

3. M. Schieber, "*Introductory Remarks" in "Techniques of Crystal Growth*", Proc. of Int. Conference on Crystal Growth, Boston (1966).

4. V. Prasad, "*Role of Modeling in Process and System Development for Crystal Growth*", Invited Talk, P.C.S. C., N.P.L., New Delhi, 26-28, February, India (2001).

5. A. R. Verma, "*Crystal Growth and Dislocations*", Butterworths, London, (1953).

6. K. A. Jackson, "*Growth and Perfection of Crystals*", Eds. R. H. Doremus, B. W. Roberts, D. Turnbull, Wiley, New York (1958).

7. W. A. Tiller, *Acta. Met*. **5**(1957) 565.

8. J. J. Gilman, "*The Arts and Science of Growing Crystals*", John Wiley, New York, (1963).

9. J. P. van-der Eerden, "*Fundamentals of Crystal Growth*", World Scientific Publishing, Singapore (1993).

10. B. Chalmers, "*Principles of Solidification*", John Wiley, New York (1964).

11. N. Bardsley, D. T. J. Hurle, J. B. Mullin, "*Crystal Growth*: *A Tutorial Approach*", North- Holland Series in Crystal Growth, Vol-2, Amsterdam (1979).

12. A. V. Shubnikov, A. A. Chernov, N. N. Sheftal; "*Growth of Crystals*", Kluwar Academic (1979).

13. A. Majchrowski, "*Single Crystal Growth, Characterization and Applications*", Ed. J. Zielinski, SPIE-International Society for Optical Engineering (1999).

14. K. Byrappa, T. Ohachi, Eds.; *Crystal Growth Technology: Characterization and Applications,* Noyes Publication (2001).

15. K. Nishioka, J. Harda, A. Sasaki, H. Teiki; "*Advaces in Understanding of Crystal Growth Mechanism*", Elsevier Science, Amsterdam (1997).

16. D. T. J. Hurle, *"Handbook of Crystal Growth"*, Vols.-1 to 3, Elsevier Science, (1999-2000).

17. A. Holden, P. S. Morison, "*Crystal and Crystals Growing"*, MIT Press, Amazon (1982).

18. J. Stangl, J. Stang, "*Crystals and Crystal Gardens You Can Grow"*, Horn Book (1990).

19. W. Kossel, *Nachr. Ges. Wiss.,* Göttingen (1927) 135.

20. M. Volmer, *Z. Phys. Chem*. **102** (1922) 267.

21. W. K. Burton, N. Cabrera, F. C. Frank*, Phil*. *Trans.* **A243** (1951) 299.

22. J. W. Gibbs, *Collected Works*, Longman & Green, London (1928).

23. P. Curie, *Bull. Soc. Franc. Miner*. **8** (1885) 145.

24. G. Wulff, *Z. Kristallogr*. **34** (1901) 449.

25. D. Turnbull, *J. Chem. Phys*. **20** (1952) 411.

26. A. C. Zettlemoyer, "*Nucleation"*, Decker, New York (1969).

27. A. A. Abraham,"*Homogeneous Nucleation Theory"*, Academic Press, New York (1974).

28. M. Volmer, W. Shultze, *Z. Phys.Chem.,* **A156** (1931)1.

29. F. C. Frank, *Phil. Mag. Supply* **1** (1952) 91.

30. W. K. Burton, *Penguin Sci. News* **21** (1951) 286.

31. P. Bennema, G. H. Gilmer, "*Kinetics of Crystal Growth*, in "Crystal *Growth: An Introduction"* Ed. P. Hartman, Amsterdam, North Holland (1973).

32. P. Ramasamy, P. Santhana Raghvan; "*Fundamentals of Crystal Growth*", KRU Publications, Kumbakonam (2001).

33. W. Miller, J. Neugebauer, *Modeling of Crystal Growth Processes*, ISSCG-12, Aug 1-7, Berlin (2004).

34. J. J. Derby, *Modeling of Crystal Growth Processes*, ISSCG-12, Aug 1-7, Berlin (2004).

35. J. Neugebauer, *Multi-scale Growth Simulations*, Abstract, ICCG-14, , Grenoble, France, 9-13 August (2004).

36. N. Zaitseva; Lawrence Livermore National Laboratory, U.S.A.(2002).

37. A. A. Chernov; *"Modern Crystallography*", Vol. III: Crystal Growth", Springer Verlag, Berlin (1984).

38. T. Yamamoto, N. Akutsu, Y. Akutsu, "*Advances in the Understanding of Crystal Growth Mechanisms",* Eds. T. Nishinaga, K. Nishioka, J. Harda, and A. Sasaki, Book News, Portland (1999).

39. T. Ogawa, *"Advances in the Understanding of Crystal Growth Mechanisms*", Eds. T. Nishinaga, K. Nishioka, J. Harda & A. Sasaki, Book News, Portland (1999).

40. J. W. Mullin, "*Bulk Crystallization",* in "*Crystal Growth"*, Ed. B. Pamplin, Peragamon Press, Oxford (1975).

41. J. A. Dean,"*Handbook of Chemistry*", McGraw Hill, New York (1979).

42. C. W. Bunn, H. Emmett; *Discussion Faraday Soc.* **5** (1949) 119.

43. G. T. Kohmann, *"Precipitation of Crystals from Solution",* in the*" Arts and Science of Crystal Growth",* Ed. J. J. Gillman, John Wiley, New York, (1963).

44. A. C. Walker, *J. Franklin Inst.* **250** (1950) 481.

45. G. W. Sears, *J. Chem. Phys.* **27** (1957) 1308.

46. P. H. Egli, L. R. Johnson., "*Ionic Salts" in "Arts and Science of Crystal Growth"* Ed. J. J. Gilman., John Wiley, New York (1964).

47. M. Jayaprakasan, *Ph.D. thesis*, Anna University, Chennai (2006).

48. V. K. Dixit, B. V. Rodrigues, H. L. Bhatt, *Bull. Mater. Sci.* **24** (2001)455

49. I. Sunagawa, P. Bennema, "*Morphology of Growth Spirals, Theoretical & Experimental, in Preparation & Properties of Solid State Materials*", Marcel Dekker Inc. New York (1982).

50. A. A. Chernov, *Sov. Phys. Crystallogr* **7** (1963) 728

51. J. S.Langer, H. Muller - Krumbhaar, *J. Cryst. Growth* **42**(1977)11.

52. J. S. Langer, *Rev.Mod.Phys*.**52** (1980)1.

53. H. Muller-Krumbhaar*, "Theory of crystal Growth*", *Ser. E. Appl. Sci.*, N69, Ed.L.D.Lande, Nijhoff, The Hague, 1983, 197.

54. J. W. Mullin, A. Amatavivadhana, M.Chakroborty, *J. Appl. Chem*. **20**(1970) 153.

55. P.Hartman, P.Bennema, *J. Cryst .Growth* **49**(1980) 145.

56. W. Noor, B.Dam, *J.Cryst, Growth* **76** (1986)243.

57. A. V. Shabni kov, N. N. Sheftal, "*Growth of Crystal"*, Izd-vo Akad, Nauk, USSR, Moscow (1957).

58. J. C. Brice, "*The Growth of Crystals from Liquids"*, Wiley, New York (1972).

59. J. C. Brice, "*Crystal Growth Processes"*, John Wiley, New York (1986).

60. H. E. Buckley,"*Crystal Growth",* John Wiley, New York (1951).

61. M. Tanenbaum, "*Methods of Experimental Physics",* Vol.6, Academic Press, New York (1961).

62. H. C. Gatos, "*On the Selection of Methods for Crystal Growth. The Methods in Crystal Growth: A Tutorial Approach",* Eds. W. Bradsley, D. T. J. Hurle and J. B. Mullin, Amsterdam, North Holland (1979).

63. W. Y. Sui, P. Bennema, W. H. van der Linden, J. Boshaar, J. W. M. van Kessel, *J.Cryst. Growth*. **83**(1987)471.

64. H. Newkrik, J. Swain, S. Stokawski, D. Milam, D. Smith, H. Klapper, *J.Cryst. Growth*.**65**(1983) 651

65. N. P. Zaitseva, J. J. De Yereo, M. R. Dehaven, *J. Cryst Growth*.**180** (1977) 255.

66. N. Zaitseva, L. Carman, I. Smolsky, *J. Cryst.Growth*., **241** (2002)363.

67. T. Sasaki, A. Yokotani, K. Fujioka, Y. Nishida, T.Yamada, C. Yamanaka, *Japanese J. Appl. Phys*. **26**(1987) L1767.

68. H. Minagawa, T. Mizota, U. Shimomura, *J. of Japanese Asso. Cryst. Growth* **26** (1999) 134.

69. M. Nakatsuka, K. Fujioka, T, Kanabe, H. Fujita, *J. Cryst. Growth* **171** (1997)531.

70. www.Youtube. Com / watch? v = l U S Yab 3djy

71. A. K. Karnal, A. Saxena, S. Ganesamoorthy, I. Bhaumik, V. K. Wadhawan, H. L. Bhat, P. K. Gupta *J. Cryst. Growth* **297** (2006) 152.

72. A. K. Karnal, A. Saxena, H. L. Bhat, V. K. Wadhawan, T.P.S Nathan, *J Cryst. Growth* **289**(2006) 617.

73. Z. D. Gau, Z. Bing, D. Sheng-Ming, W. Qing – Guo, Z. Yan-Shuai, H. Wan-Xia, Y. Tao, *Cryst. Res. & Technol* **44** (2009)500.

74. S. K. Sharma, S. Verma, B. B. Srivastava, U. K. Wadhawan, *J. Cryst. Growth* **244** (2002)342.

75. S. Xun, F. Youjun, G. Zhangshou, W. Shenglai, Z. Hong, L. Yiping, *Chinese Sci.Bull* **46**(2006) 1142.

76. K. Maeda, A. Sokada, H. Miki, Y. Akasuma, K. Fukui, *Cryst. Res. & Technol*. **39** (2004) 1006.

77. P. V. Dhanaraj , C. K. Mahadevan, G.Bhagavannarayana , P. Ramasamy, N.P. Rajesh, *J. Cryst. Growth* **310** (2008) 5341.

78. Y. J. Fu, Z. S. Gao, X. Sun, S. L. Wang, Y. Li, H. Zeng, J. P. Luo, A. D. Duan, Y. Wang, *Prog. In Cryst. Growth & Charact. Of Materials* **49**(2000) 211.

79. J. Zhang, S. Wang, C. S. Fang, X. Sun, G. Gu, Y. Li, B. Wang, B. Liu, X. Mu, *Mater. Lett.* **61**(2007) 2703.

80. X. Lai, K. J. Roberts, *Chem.Mater*.**17** (2005) 4053.

81. W. Zhong, X. Yu, H. Luo, Z. Cheng, S. Hua*, Sci. in China Series E : Technol. Sci.* **41**(1998) 586.

82. S. Balamurugan, G. Bhagavannarayana, P.Ramasamy, *Mater Lett*. **62**(2008) 3963.

83. S. Balamurugan, P.Ramasamy, S.K. Sharma, Y. Inkong, P. Manyam, *Mater Chem. Phys*.**117**(2009) 465.

84. A. C. Pastor, R. C. Pastor, *Ferroelectric* **71** (1967) 61.

85. M. Priya, C. M. Padma, T. H. Freeda, C. Mahadevan, C.Balasingh, *Bull.Mater.Sci*. **24**(2001) 511.

86. J. J. De Yoreo, T. A. Land, B.J. Dair, *Phys. Rev. Lett.* **73 6** (1994)838.

87. Y. Akasuma, E. Ukita, K.Maeda, K.Fukai, K. Iimura, M. Sujuki M. Hirota, *Cryst. Growth & Design*. **7**(2007)420.

88. D. Turnbull, *J. Chem. Phys*. **18** (1950) 198.

89. J. L. Schmitt, G. W. Adams, R.A. Zalabsky, *J. Chem. Phys*., **77**(1982)2089.

90. M. R. Appleby, G. L. Leedon, S. V. Babu, *J. Cryst. Growth* **64** (1983) 229.

91. H. Reiss, *"Methods of Thermodynamics",* Blasdell, New York (1965).

92. O. Söhnel,,*J. Cryst. Growth* **57**(1982)101

93. S. Chenthamarai, *Ph. D. Thesis*, University of Madras (2000).

94. S. Abraham Rajsekar, *Ph. D Thesis*, University of Madras (2004).

95. O. Söhnel, J. W. Mullin, *J. Cryst. Growth* **44**(1978) 377.

96. A. E. Nielson, O.Söhnel, *J. Cryst. Growth* **11**(1971)233.

97. J. W. Mullin, M. M. Osman , *Kristal & Technik* **8** (1973) 471.

98. M. S. Joshi, A. V. Antony, *J.Cryst. Growth* **46** (1979) 7.

99. R. Kanagadurai, R. Durairajan, R. Sankar, G. Sivanesan, S. P. Elangovan, R. Jayavel, *E-J.l of Chemistry*, **7(1)** (2010)137.

100. S. Toschev, A. Milchev, S. Stoyanov *J. Cryst. Growth* **14** (1972) 123.

101. W. J. Dunning, A.J.Shipman, *Proc. of Agriculture Industry's 10th International Congress*, Madrid (1954).

102. A. Van Hook, A.J.Bruno, *Discussion. Faraday Soc*. **5** (1949) 112.

103. A. Felbinger, H. Neels , *Kristal & Technik* 1 (1966)136

104. A. E. Nielsen, *"Kinetics of Precipitation"*, Pergamon Press, Oxford (1964).

105. A. G. Walton, "*The Formation and Properties of Precipitates"*, Inter Science, New York (1957).

106. A.E. Nielsen,"Crystal Growth "Ed. H.S. Peiser, Pergamon Press, Oxford(1967).

107. A. E. Nielsen, Kristall & Technik **4** (1969) 17.

108. A. E. Nielsen, S.Sarig, *J. Cryst. Growth,* **8** (1971)1.

109. M. Volmer " *Thremodynamic der phasenbildung* " Dresden and Leipzig , Theodor Steinkopffo (1939).

110. K. Neuman, A. Miess, *Ann. Physik* **41**(1942) 319.

111. J. W. Mullin "*Industrial Crystallization 78*" , Plenum Press, New York (1978)

112. T. P. Melia, W. P. Moffitt, *J. of Colloid Sci*. **19(5)** (1965) 433.

113. B. K. Paul, M.S, Joshi, *J. Phys. D : Appl. Phys*. **9** (1976) 1253.

114. M. Shanmugham, F. D. Gnanam, P. Ramasamy, *J. Mater.Sci*., **19** (1984) 2837.

115. M. Shanmugham, F. D. Gnanam, P. Ramasamy, *J. Mater. Sci. Lett*. **4** (1985) 746.

116. C. Mahadevan, G. Janiland Angel, U. Anton Sophana, V.Unayorubhagan, *Bull. Mater.Sci*. **22** (1999) 817.

117. P. V. Dhanaraj, S. K. Mathew, N. P. Rajesh, *J. Cryst. Growth*., **310** (2008) 2532.

118. P. A. Barata, M.C.Serrano, *J. Cryst. Growth* **163** (1996) 426.

119. H. Qu, M. Louhi – Kultanen, J. Kalls, *J.Cryst.Growth* **289** (2006) 280.

120. C. Min, L. M. Wei, C. Yachao, W. Xiaoding, G. Jinli, *Cryst. Res. & Technol.* **44** (2009) 1215.

121. N. P. Rajesh, C. K. L. Perumal, P.Santhana Raghavan, P. Ramasamy, *Cryst. Res. & Technol*. **36** (2001) 55.

122. N. P. Rajesh, V. Konnan, P. Santhana Raghavan, P. Ramasamy, C. W. Lan, *Mater.Chem.Phys*. **76**(2002) 181.

123. C. K. Mahadevan, R. S. S. Sarvanan, *Mater. & Manufact. Process* **22** (2007) 357.

124. E.A. Boucher, " *Nucleation* ", Marce Dekker , New York (1969)

125. K.Srinivasan, K. Meera, P.Ramasamy, *J.Cryst. Growth* **205** (1999) 457.

Chapter - III

CHN Analysis, Paper Chromatography, FTIR and Powder X – Ray Diffraction Studies of Pure and L-histidine, L-threonine and DL-methionine Doped KDP crystals

3.1 Introduction

It is important to confirm the doping in KDP crystals, because the doping affects various properties of grown crystals. In the present study, attempts have been made to confirm the amino acids doping in KDP crystals by employing CHN analysis, FT-IR spectroscopy and paper chromatography. This chapter is dedicated to the studies related to the confirmation of doping and its effects on crystal structure.

The powder XRD study has been carried out for pure and amino acids doped KDP crystals in order to identify the single phase or multi phase nature of the compound, the distortion in the unit cell of KDP crystal due to doping and effect on the powder XRD pattern due to progressive increase in doping concentration.

3.2 CHN Analysis

All dopants, viz, L-histidine, L-threonine and DL-methionine (amino acids) contain carbon, hydrogen and nitrogen, while in KDP carbon and nitrogen are absent, therefore, the confirmation of successful achievement of doping of various amino acids in KDP crystals can be carried out by detecting the presence of carbon and nitrogen in the doped samples and their different proportions for different levels of various doping. Elemental analysis of carbon, hydrogen and nitrogen is the most essential and in many cases investigation performed to characterize and/or to prove the elemental composition of an organic sample.

In this method the sample weighing 2 -3 mg is placed in a tin capsule. After folding the capsule the sample is placed in the auto sampler. The tin capsule enclosing the sample falls into the ignition chamber where excess oxygen is introduced before. At about 990 °C the material is mineralized. Formation of carbon monoxide is probable at this temperature even under these conditions of excess oxygen. The complete oxidation is reached at a tungsten trioxide catalyst which is passed by the gaseous reaction products. The resulting mixture should thus consist of CO_2, H_2O and NO_2. The product gas mixture flows through a silica tube packed with copper granules. In the zone held at about 500 °C remaining oxygen is bound and nitric/nitrous oxides are reduced. The leaving gas stream includes the analytically important species CO_2, H_2O and NO_2. Eventually, included SO_2 or hydro-halogenides are absorbed at appropriate traps. High purity helium is used as carrier gas. Finally, the gas mixture is brought to a defined pressure/volume state and is passed to gas chromatographic system. Separation of the species is done by so called zone chromatography. In this technique a staircase type signal is registrated. Step height is proportional to the substance amount in the mixture. The schematic diagram of CHN element analyzer is shown in figure (3.1).

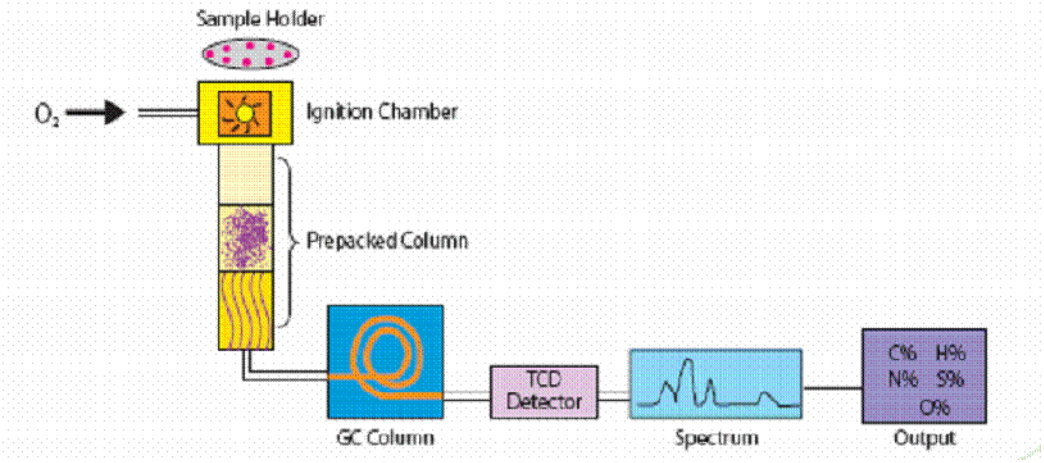

Figure: 3.1 Schematic diagram of CHN elemental analyzer.

Percentile analysis of C and N for various amounts of different amino-acids doped KDP crystals is compiled in Table (3.1).

Table: 3.1 C and N % in different doped sample.

Sample	C %	N %
Pure KDP	_	_
KDP + 0.3 L - histidine	0.17	0.58
KDP + 0.4 L - histidine	0.42	0.87
KDP + 0.5 L - histidine	0.71	0.93
KDP + 0.3 L - threonine	0.13	0.51
KDP + 0.4 L - threonine	0.29	0.78
KDP + 0.5 L - threonine	0.55	0.89
KDP + 0.3DL - methionine	0.20	0.61
KDP + 0.4DL - methionine	0.40	0.85
KDP + 0.5DL - methionine	0.57	1.06

3.3 Paper Chromatography

The paper chromatography of dissolved samples of pure and amino acids doped KDP crystals in water was carried out using nin-hydrin. Paper chromatograph of doped samples exhibited the characteristic purple color spot which confirmed the presence of amino acid in the doped sample.

3.4 Infrared Spectroscopy

Infrared spectroscopy is one of the most powerful analytical techniques, which indicates the possibility of chemical identifications [1]. Till the early 1980s, instruments for the mid-infrared region were mostly of

dispersive type based on diffraction gratings. Due to the advent of Fourier Transform technology, the scenario is completely changed. Photometers based on interference filters also find applications in measuring the composition of gases and atmospheric contaminants. Before the appearance of these new instruments, the mid-infrared frequency region of the spectra were largely used for organic qualitative analysis and structural determination based on absorption spectrum. Nowadays, the mid-infrared spectroscopy is used for quantitative analysis for complex samples by both absorption and emission spectrometry. In addition to this the mid-infrared spectral regions find applications in microscopic studies of surfaces, analysis of solids by attenuated total reflectance and diffuse reflectance, photo-acoustic instruments and others [2].

The infrared region of the electromagnetic spectrum extends from the red end of the visible spectrum to the microwave region. Infrared spectral region can be divided into three regions; near-infrared, mid-infrared and far-infrared. Table (3.2) gives the details of different infrared spectral regions. Molecular vibrations are falling into basic categories of stretching and bending. A stretching vibration involves a continuous change in the inter-atomic distance along the axis of bond between two atoms. However, the bending vibrations are characterized by a change in the angle between two bonds, which are of four types, scissoring, rocking, wagging and twisting in the figure (3.2).

Because of the interaction with infrared radiation, portions of the incident radiation are absorbed at particular wavelengths. The multiplicity of vibrations occurring simultaneously produces a highly complex absorption spectrum, which is a unique characteristic of the overall configuration of the atoms as well.

Details of assignments of different frequencies with different vibrations of bonds, such as H-O, N-H, C=O, C-C, C-H etc are given in detail by many authors [1-5].

Table 3.2 Different infrared spectral regions and its applications.

Spectral regions	**Wave numbers (cm^{-1})**	**Type of Measurement**	**Analysis**	**Type sample**
Near-infrared	12,800 - 4000	Diffuse reflectance	Quantitative	Solid or liquid materials
		Absorption	Quantitative	Gaseous mixtures
Mid-infrared	4000 - 200	Absorption	Qualitative	Gaseous, liquid or solid organic compounds. Complex gaseous, liquid or solid mixtures.
		Reflectance	Qualitative	Pure solid or liquid compounds
		Emission	Quantitative	Atmospheric samples
Far-infrared	200 - 10	Adsorption	Qualitative	Pure inorganic or metal-organic species

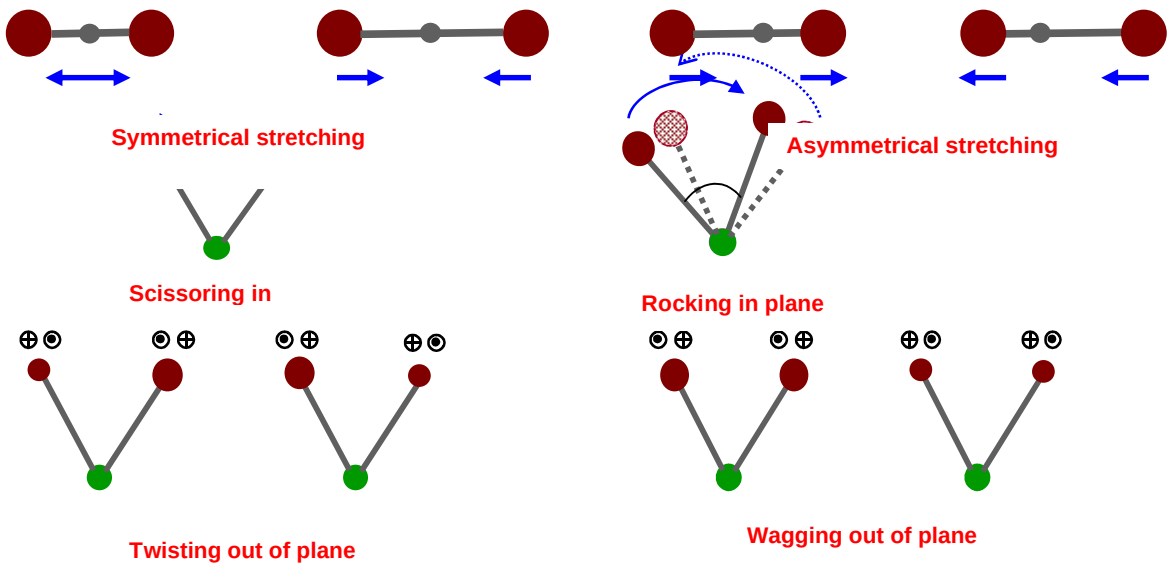

Figure: 3.2 Various stretching and bending modes of vibrations in molecule.

Many times it is given in the chart and tabular form to facilitate the user to identify the specific bond vibrations from the frequency in wave numbers, represented in the figure (3.3).

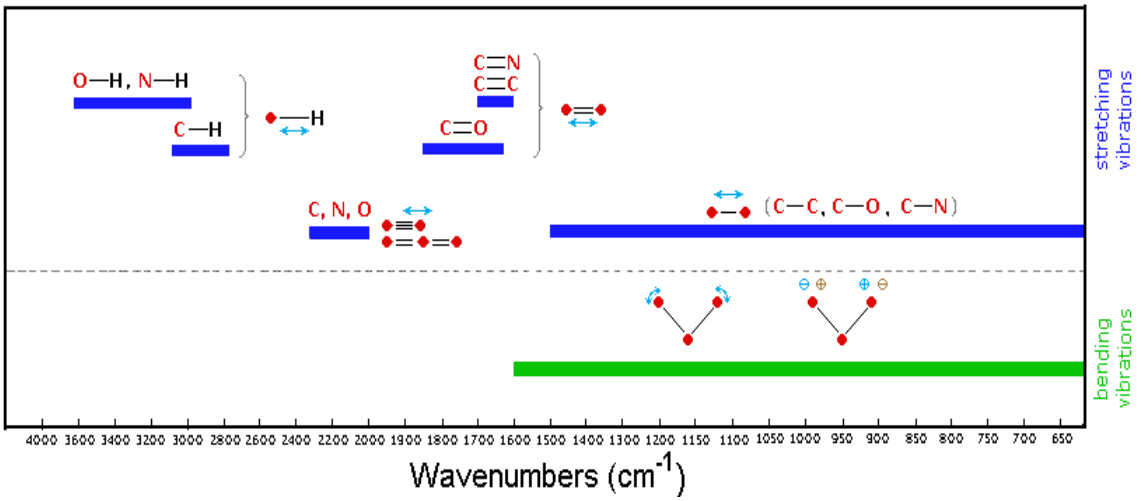

Figure: 3.3 A chart to identify specific bond vibrations in wave numbers.

There are mainly three types of instruments available, which are (1) dispersive grating type, (2) multiplex type and (3) non-dispersive type. Variety of infrared sources are developed depending upon requirements, which include the Nernst glow-bar, incandescent wire sources, mercury arc, tungsten filament lamp, etc. Good transducers such as, thermal, pyro-electric and photo-conducting are also important in the detection and measurement of infrared radiation. For different regions, different type of radiation sources, optical systems and detectors are needed. The standard infrared spectrometer is a filter-grating or prism-grating instrument covering range from 4000-650 cm^{-1} (2.5-15.4 μm). However, the grating instruments offer high resolution that permits separation of closely spaced absorption bands, accurate measurements of band position and intensities and high scanning speeds for a given resolution and noise level. Modern spectrometers generally have attachments that permit speed suppression, scale expansion, repetitive

scanning and automatic control of slit, period and gain. These are very often under the control of a microprocessor. Accessories such as beam condensers, reflectance units, polarizers and micro-cells can usually be added to extend versatility or accuracy [5].

3.5 Fourier Transform Infrared Spectroscopy

Multiplex type of instruments employs the mathematical tool of Fourier Transform [6]. The apparatus of Fourier Transform Infrared (FTIR) spectrometer is derived from Michelson interferometer, which is shown in figure (3.4). The main components of the FTIR spectrometers are (1) drive mechanism, (2) beam splitters and (3) sources and transducers. In figure (3.5) a parallel beam of radiation is directed from the source to the interferometer, consisting of a beam splitter (B) and two mirrors (M1 and M2). It is well known that for coherent and monochromatic radiation the interference patterns can be obtained.

The constructive or destructive interference is produced depending on the relative path lengths B to M_1 and B to M_2. When mirror M_2 moves smoothly towards or away from B, a detector sees radiation of changing intensity. If white radiation is used, the interference patterns are obtained which can be transferred back to the original frequency distribution. This can be achieved by a mathematical process known as Fourier Transform, nowadays; this process is carried out by a computer or microprocessor of the spectrometer. Under these conditions, the detector response fluctuates at a rate, which depends upon the rate of movement of mirror and the wavelength of radiation. In general, any combination of frequencies with corresponding amplitudes will produce an interferogram containing all the

spectral information of the original radiation. The interferogram is the Fourier Transform of the spectrum and the task of the computer is to apply the inverse Fourier Transform.

Interferometric or Fourier Transform spectroscopy makes use of all the frequencies from the source simultaneously, rather than sequentially as in scanning instrument. This was first proposed by Fellgett and hence also called as Fellgett advantage FTS. The Fellgett advantage is an improvement in signal to noise ratio of $(M)^{1/2}$, where M is the number of resolution elements desired in the particular spectrum. It is worth noting that the resolving power of Fourier Transform instrument is constant over the entire spectrum, whereas, it varies with frequency in the conventional technique [7]. Fourier transform spectroscopy is providing simultaneous and almost instantaneous recording of whole spectrum in the magnetic resonance, microwave and infrared regions. Fourier Transform (FT) spectroscopy is equally applicable to both emission and absorption spectroscopy.

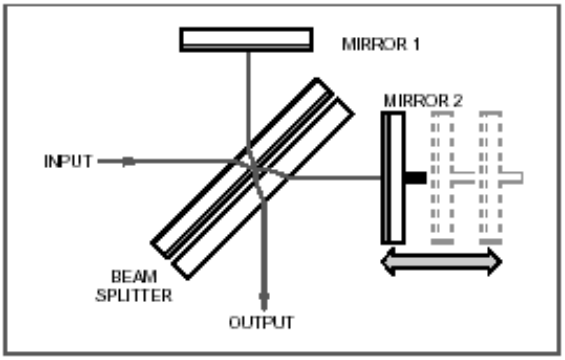

Figure: 3.4 Schematic diagram of Michelson interferometer.

The FTIR set up has, as noted earlier, design based on Michelson interferometer, which is having mainly three important components:

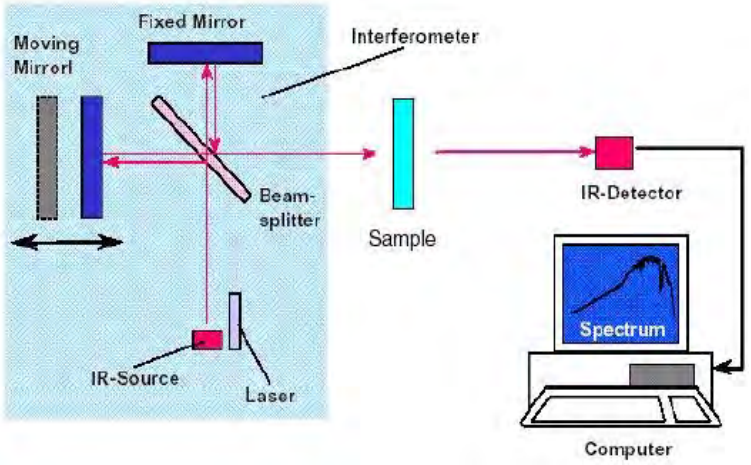

Figure: 3.5 Schematic diagram of FTIR spectrometer.

(1) A drive mechanism is important for satisfactory interferograms, which needs that the speed of the moving mirror should be constant and its position be known exactly at any instant. The planarity of the mirror must remain constant during the entire sweep of 10 cm or more.

(2) Beam splitters are constructed of transparent materials with refractive indices such that approximately 50% of the radiation is transmitted and 50% is reflected. A thin film of germanium or silicon coated on cesium iodide or bromide, sodium chloride or potassium bromide is employed for mid infrared region.

(3) The sources of FTIR are usually the same as IR ones. Because of processing the slow response times, the thermal transducers are not generally preferred in FTIR; the Triglycine Sulphate transducers are widely preferred in the mid-frequency range.

The FTIR instrument has many advantages. It has better signal to noise ratio than other good quality dispersive type instrument. Another important advantage is that its optics provides a much larger energy throughput (one or two orders of magnitude) than the dispersive type, where it is limited by the

necessity of having the narrow slit widths. The prime advantage of FTIR is that the interferometer is free from the problem of stray radiation because each infrared radiation is chopped at a different frequency.

There are many applications of FTIR spectroscopy, which are, spectroscopic investigations of gaseous mixtures having complex spectra resulting from superposition of vibrational and rotational bands as found in atmosphere; study of samples with high absorbance; study of the substances with weak absorption bands; collecting data from very small samples; investigations requiring fast scanning such as kinetic studies or detection of chromatographic effluents and infrared emission studies.

There are different versions, modifications and attachments available with FTIR. Diffuse Reflectance Infrared Fourier Transform Spectroscopy (DRIFTS) uses an effective way of obtaining infrared spectra directly on powdered samples with a minimum sample preparation efforts and time [8-10]. The advantage is that it permits conventional infrared spectral data to be obtained on the samples that are not altered much from their original state. Apart from this, the Photo-acoustic Infrared Spectroscopy is another popular technique. This technique was introduced in 1970s, which provides a mean for obtaining ultraviolet, visible and infrared absorption spectra of solids, semisolids or turbid liquids. This is based on the effect first investigated by Alexander Graham Bell in 1880. When a gas in a closed cell is irradiated with a chopped beam of radiation of a wavelength that is absorbed by a gas, the absorbed radiation causes periodic heating of the gas, which, consequently, gives in regular pressure fluctuations in the chamber. This method has been used for detecting the components of mixtures separated by thin- layer and

high-performance liquid chromatography. Most manufacturers offer photo-acoustic cell along with FTIR as the accessories.

In the present study, the FTIR spectra of pure and L-histidine, L-threonine and DL-methionine doped KDP crystals were recorded on BRUKER IFS 66V FT-IR spectrometer, which is shown in Photograph of figure-(3.6). The spectra of powdered samples in KBr medium were recorded in the range from 400-4000 cm^{-1}.

Figure: 3.6 Photograph of BRUKER IFS 66V FT-IR spectrometer.

3. 6 Experimental Study of FTIR Spectroscopy

Infrared spectroscopy is an excellent technique for both qualitative and quantitative analysis [11-13]. As it has been already noted earlier in this Chapter, FTIR spectroscopy is the further advancement of IR spectroscopy by using the mathematical concept of Fourier Transform through proper electronic circuit and computer interfacing. From the earliest days of infrared spectroscopy it was observed that functional groups of atoms could be associated with definite characteristic absorption bands, i.e., the absorption of infrared radiation over certain frequency intervals. The infrared spectrum of any given substance is interpreted by the use of the known group frequencies and thus it will be easy to characterize the substance as one containing a

given type of group or groups. Although group frequencies occur within narrow limits, interference or perturbation may cause a shift of the characteristic bands due to (a) the electro negativity of neighboring groups or atoms, (b) the spatial geometry of the molecule or (c) the mechanical mixing of vibrational modes.

Functional groups sometimes have more than one characteristic absorption band associated with them. On the other hand, two or more functional groups may absorb in the same region and hence, in general, can only be distinguished from each other by means of other characteristic infrared bands, which occur in non-over lapping regions.

Absorption bands may be considered as having two origins, these being the fundamental vibrations of (a) functional groups, e.g. C=O, C=C, C≡N, CH_2, CH_3 and (b) skeletal groups, i.e. the molecular backbone or skeleton of the molecule e.g., C-C-C-C. Absorption bands may also arise from stretching vibrations, i.e., vibrations involving bond-length changes or deformation vibration, i.e., vibrations involving bond-angle changes of the group. Each of these, in some cases, may be considered as arising from symmetric or asymmetric vibrations. For a given functional group, the vibration bands due to stretching occur at higher frequencies than those due to deformation. This is because more energy requires to stretch the group than to deform it due to the bonding force directly opposing the change.

3.7 FTIR Studies of Pure and Amino Acids Doped KDP Crystals

Many researchers have studied the FT-IR spectra of pure and doped KDP crystals. FTIR spectra of the pure KDP and doped with CH_3COOK (5 mol%) and $K_3C_6H_5O_7$ (5 mol%) studied by Dhanaraj et al [14] . They observed broad

envelope between 3700 cm^{-1} and 2500 cm^{-1} due to O-H stretching vibrations of KDP. Hydrogen bonding within the crystal is suggested to be the cause for the broadening of the peak. The C-H vibrations of CH_3 group in Potassium acetate are seen to provide its characteristics peaks just below 3000 cm^{-1}, which is absent in pure KDP crystal and confirmed the successful achievement of doping. Gunasekaran and Ramkumar [15] have studied the FT-IR spectra of pure and α- histidine doped KDP crystals and confirmed the presence of α - histidine. In another study, Suresh Kumar and Rajendra Babu [16] have studied the FT-IR spectra of pure and amino acids doped KDP crystal and observed that some bands of $[H_2PO_4]^-$ overlap with amino acid vibrations and some of the frequencies are slightly shifted. The symmetric deformation of NH_3^+ ion appears at around 1500 cm^{-1} with medium intensity which revealed the incorporation of impurities in the crystals. The FTIR spectra of pure and glycine doped KDP crystals have been studied by Hussaini et al [17]. They concluded that the 3703.29 cm^{-1} and 3318 cm^{-1} may represent the O-H stretching of unchanged COOH group of the amino acid. The involvement of NH_3^+ in hydrogen bonding is evident by the fine structure of the band at lower energy region. Recently, Parikh et al [18] have studied the FTIR spectra of pure and L-alanine doped KDP crystals and confirmed the presence of NH^{3+} stretching vibration, O–H stretching, symmetrical bending vibration and torsion oscillation of the NH_3^+ group. They confirmed L-alanine doping by the absorption due to N-H, C=O, C-H remained present in doped crystals and absent in pure KDP crystals. Rahman and Podder [19] have studied the FTIR spectra of the pure and EDTA-added KDP crystal. Broad envelope between 3700 cm^{-1} and 2500 cm^{-1} includes O–H stretching vibrations of KDP. Hydrogen bonding within the

crystal is suggested to be the cause for the broadening of the peak. The peaks below 1200 cm^{-1} are due to PO_4 vibrations. The broad envelopes observed between 2300 and 3600 cm^{-1} are mainly due to P–OH stretching of H_2PO_4. Govani et al [20] have studied the interaction of L-arginine with KDP crystal by FTIR and Raman spectroscopy. They have confirmed the interaction by additional vibrational line originating from the distributed N-H, C-H and C-N bonds of L-arginine. They also suggest the possibility of Hydrogen bonding primarily between the nucleophilic-O of phosphate unit of KDP with amino group of arginine. It has been found that the weak interaction of the dopants with one of the O-H groups of KDP and possible entry of dopants into the lattice sites of the crystal leads to the decrease in the frequency and confirms the nonlinear optical nature in pure and doped crystals [21]. The FT – IR spectra for both pure and various amino acids doped KDP crystals are presented in figure (3.7 to 3.10) and assignments are given in table (3.3). Some additional absorption peaks are observed in spectra of amino acids doped KDP crystals, which is, a clear indication of successful doping of different amino acids in KDP crystals. Nevertheless, from the assignments of various absorption peaks in FTIR spectra, the general natural of spectra can be deduced. The absorption peaks at 3580 cm^{-1} for pure KDP crystal and the absorptions within 3445 cm^{-1} to 3481.7 cm^{-1} for amino acids doped KDP crystals are due to O-H stretching vibration and N-H stretching vibration. However, there is a possibility of overlap of O-H and N-H asymmetric stretching vibrations in case of amino acids doped KDP crystals. The reduction absorption peak values may be due to either the overlap or the hydrogen bond interaction with amino group.

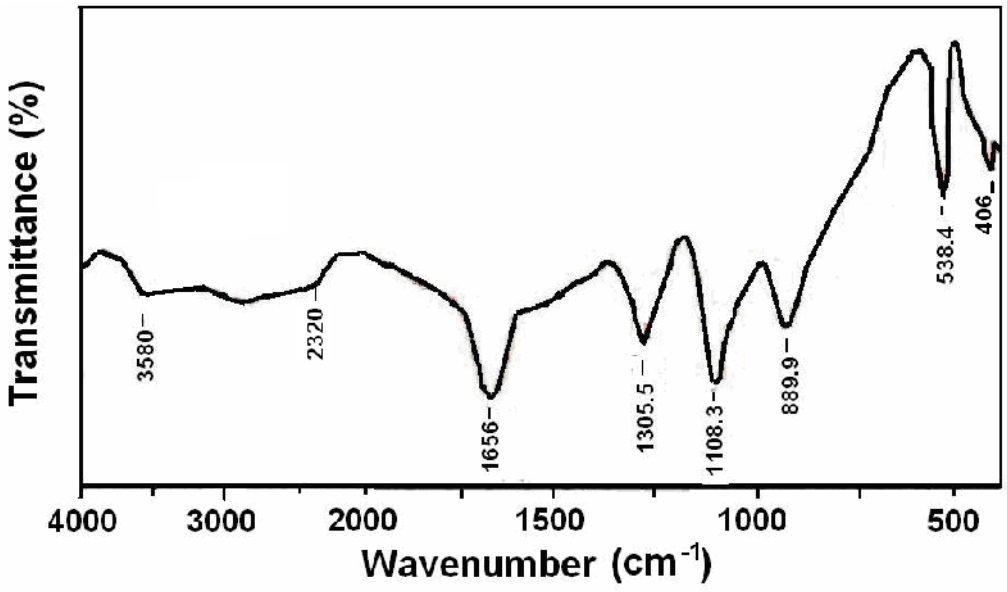

Figure:3.7 FTIR spectra of pure KDP crystal.

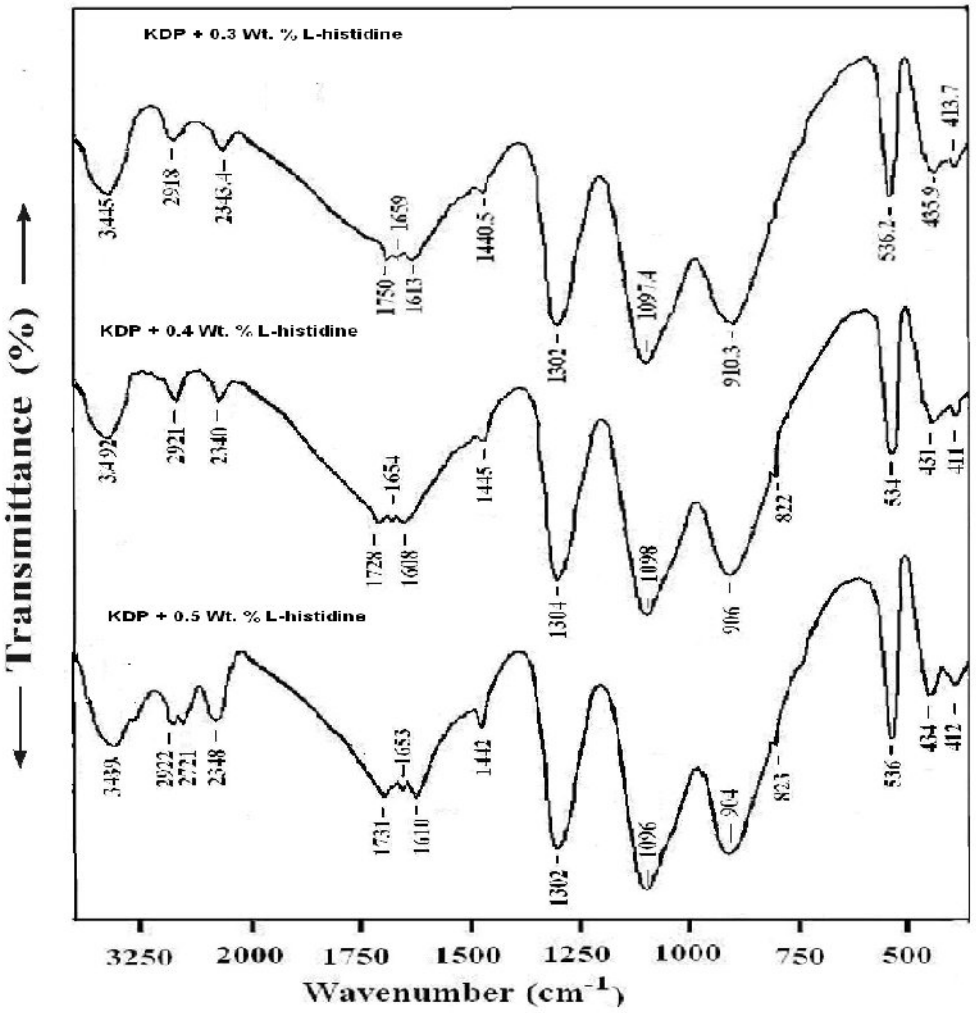

Figure:3.8 FTIR spectra of different amount of L-histidine doped KDP crystals.

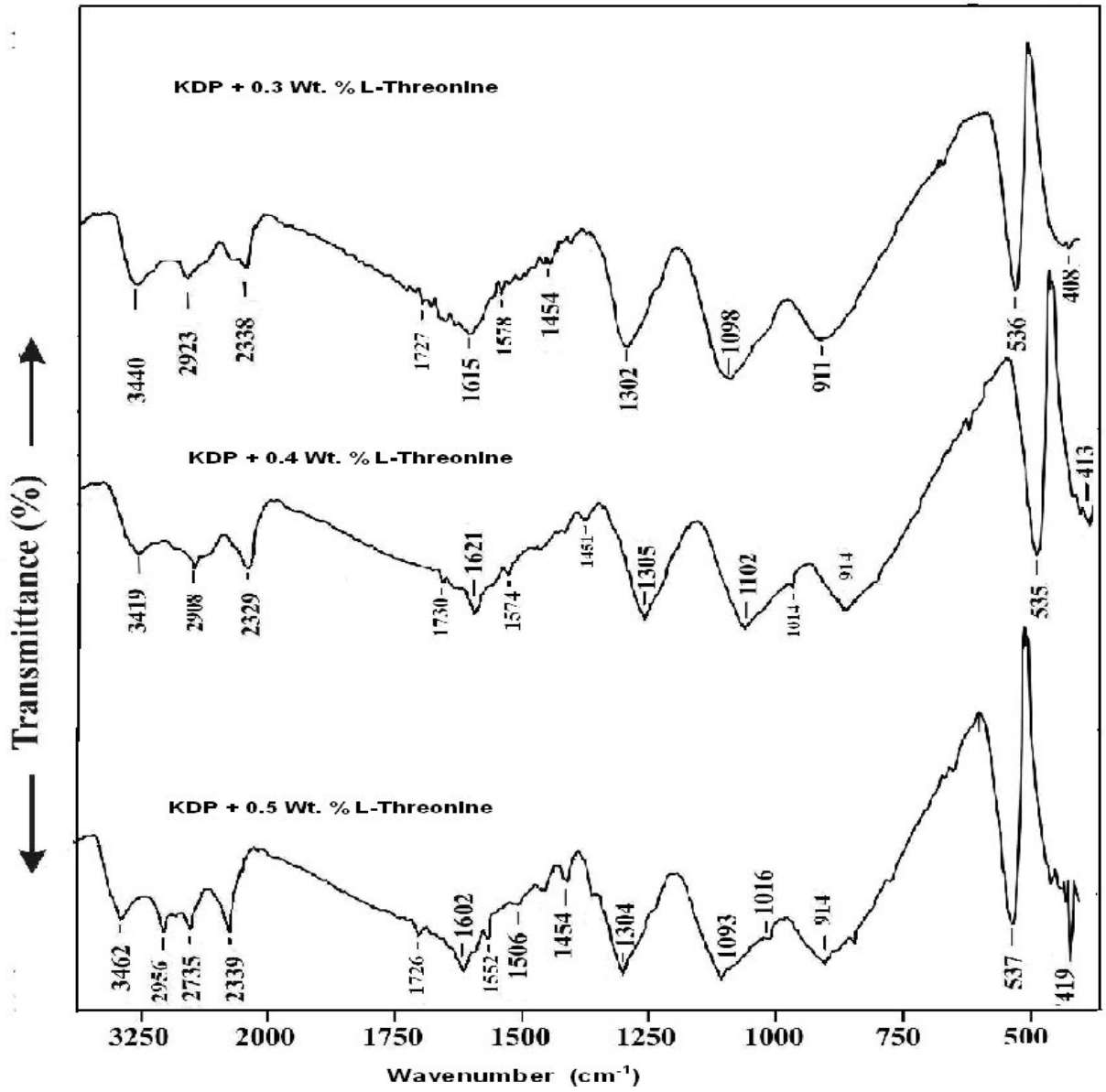

Figure: 3.9 FTIR spectra of different amount of L-threonine doped KDP crystals.

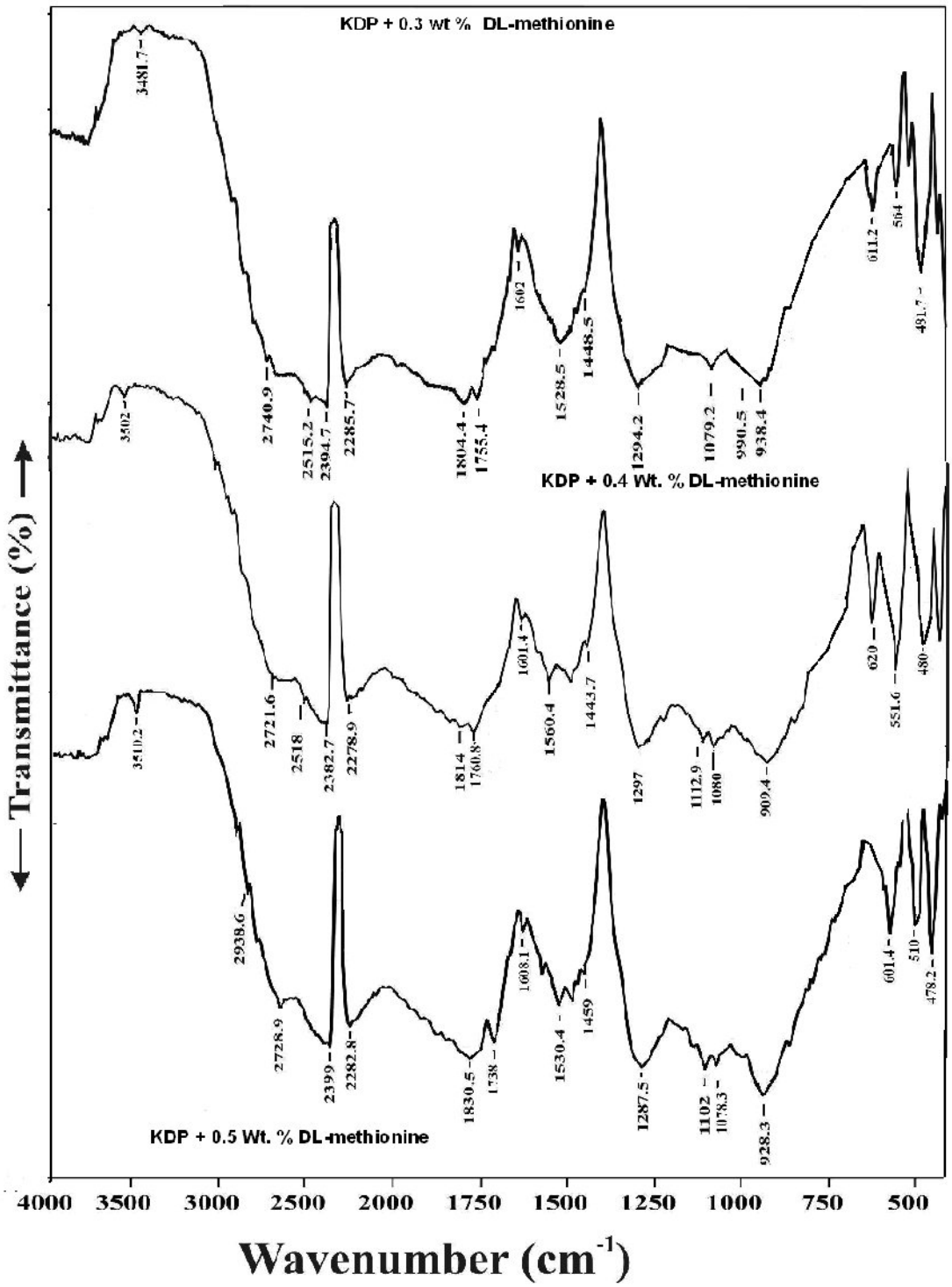

Figure: 3.10 FTIR spectra of different amount of DL-methionine doped KDP crystals.

Table: 3.3 FT-IR assignments of pure and 0.3 wt % various amino acids doped KDP

crystals.

Frequency (cm^{-1})	Absorptions in wave numbers				Assignments
	Pure	KDP + L-histidine	KDP+ L-threonine	KDP+ DL-methionine	
3615	3580	3445	3440	3481.7	Free O – H Stretching
3350					N – H asymmetric stretching
2380		2343.4	2338	2394.7	N – H symmetric stretching
2250	2320			2285.7	P – O – H asymmetric stretching
1715		1750	1727	1755.4	C = O stretching
1600	1656	1659	1615	1602	O = P – OH symmetric stretching
1350	1305.5	1302	1302	1294.2	P = O symmetric stretching
1100	1108.3	1097.4	1098	1079.2	O - P – OH symmetric stretching/
975	889.3	910.3	911	990.5,938.4	O = P – OH bending
530	538.4	536.2	536	564	P–OH deformation

The absorption around 2380 cm^{-1} due to N-H symmetric stretching vibration is absent in Pure KDP crystals. Similarly, the absorptions around 1715 cm^{-1} due to C=O stretching is not present in pure KDP crystals. These two assignments are exclusively related to presence of amino acids in KDP crystals. While, the absorptions around 1600 cm^{-1}, 1350 cm^{-1}, 1100 cm^{-1}, 975 cm^{-1} and 530 cm^{-1} are due to O=P-OH symmetric stretching, P=O, O-P-OH symmetric stretching, O=P-OH bending and P-OH deformation vibrations.

Obviously, these are present in pure and amino acids doped KDP crystals. It is also interesting to note that P=O stretching vibration frequency practically remains unaltered for all crystals; notwithstanding , the frequencies of O=P-OH symmetric stretching and O-P-OH symmetric stretching vibrations of doped KDP crystals decrease with respect to pure KDP , which indicates the interaction of amino acids with KDP through hydrogen bonds of the particular groups. At the same time, the absorptions due O=P-OH bending exhibit larger values for amino acids doped crystals and the pure KDP crystals , which also further hints the interaction of amino acids with KDO through hydrogen bond.

The force constant of particular diatomic atoms can be calculated from the particular absorption peak in FTIR spectrum. Considering a molecular model, where the nuclei are presented by point masses and the inter-atomic bonds as mass less spring which follows the Hooke's law, the vibrations changes the inter atomic distance sinusoidally but the center of gravity remains the same. Therefore, at any time during the vibrations the atomic displacements are inversely proportional to the masses. If masses are expressed in the unified atomic masses (u) and the force constant is m-dyne/Å [1].

$$\nu = 1303 \sqrt{F\left(\frac{1}{M_1} + \frac{1}{M_2}\right)} \qquad (3.1)$$

Where, 1303 is equal to $(N_A \times 10^5)^{1/2} / (2\pi C)$

N_A - Avogadro's number, F - force constant.

By taking into account this simple model, the force constant for O-H vibrations at 3600 cm^{-1} was found to be 7.2 is m-dyne /Å [1]. In the present study, the force constants for O-H bond are calculated for pure and various

amino acid doped KDP crystals. As the doped amino acid is expected to form a bond with hydrogen atom of KDP, which is resulted in to altered fundamental vibrations and the values of force constants are lower for doped crystals in comparison to pure KDP crystals as that can be seen from table (3.4).

Table: 3.4 Values of force constant for pure and different amino acids doped KDP crystals.

Samples	Force Constant for O-H Vibrations (Nm^{-1})	Absorption (frequency in cm^{-1})
Pure KDP Crystal	710	3580
KDP + 0.3% L-histidine	640	3445
KDP + 0.4% L- histidine	639	3492
KDP + 0.5% L- histidine	639	3439
KDP + 0.3% L-threonine	670	3440
KDP + 0.4% L- threonine	680	3419
KDP + 0.5% L- threonine	685	3462
KDP + 0.3% DL-methionine	657	3481.7
KDP + 0.4% DL-methionine	650	3500
KDP + 0.5% DL-methionine	667	3510.0

3.5.1 X-ray Diffraction by Powder Method

The powder X-ray diffraction (XRD) was devised independently in 1916 by Peter Joseph William Debye, a Nobel Laureate and P. Scherrer in Germany and in1917 by A. W. Hull in United States [22,23]. The powder XRD is a non-destructive technique widely used for the characterization of a variety of crystalline materials. This method has been conventionally used for phase

identification, quantitative analysis and the determination of structure imperfections. However, in recent years the applications have been extended to new areas, such as the determination of crystal structures and the extraction of three-dimensional micro-structural properties. In the pharmaceutical industries the powder-XRD is popular for identification of drug molecule and its polymorphs. The physical states of the materials can be loose powders, thin films, poly-crystalline and bulk materials. By properly using this technique one can yield a great deal of structural information about the material under investigation. For most applications, the amount of information which is possible to extract depends on the nature of the sample microstructure (crystalline, structure imperfections, crystallite size and texture) the complexity of the crystal structure(number of atoms in the asymmetric unit cell and unit cell volume), the quality of the experimental data (instrument performances and counting statistics) [24].The powder method can be used as a tool to identify crystals, since the powder XRD patterns produced by a crystalline substance is a characteristic of that particular substance. One of the most important uses of the powder method is in the identification of an unknown material. If a set of standard diagrams of known substances or tabular representations of them, available, then it is possible to identify a pure substance with the aid of a set of rules for finding an unknown diagram. The ASTM data cards as well as JCPDS data files are available for large number of substances for identifications and comparison. Statistical study of the relative orientations of the individual crystals of an aggregate is one of the important secondary uses of the powder method [25,26]. Identification of phases can be done by powder technique without solving crystal structure or

assigning indices to the reflections. Apart from these, cold work, recovery and re-crystallization are readily recognized by their effect on the powder patterns. Basically, this method involves the diffraction of monochromatic X-ray by a powdered specimen. Usually 'monochromatic' means the strong characteristic K component of the filtered radiation from an X-ray tube operated above the K excitation potential of the target material. The "Powder" can mean either an actual, physical powder held together with suitable binder or any specimen in polycrystalline form. Since single crystals are not always available, this method is more suitable for structural determination of various substances. The powder method is also known as the Debye-Scherrer method.

When X-ray is incident on the crystalline powdered sample, it gets diffracted in form of cones, which is exhibited in figure (3.11 b). The broad applications of powder XRD are summarized in the following points:

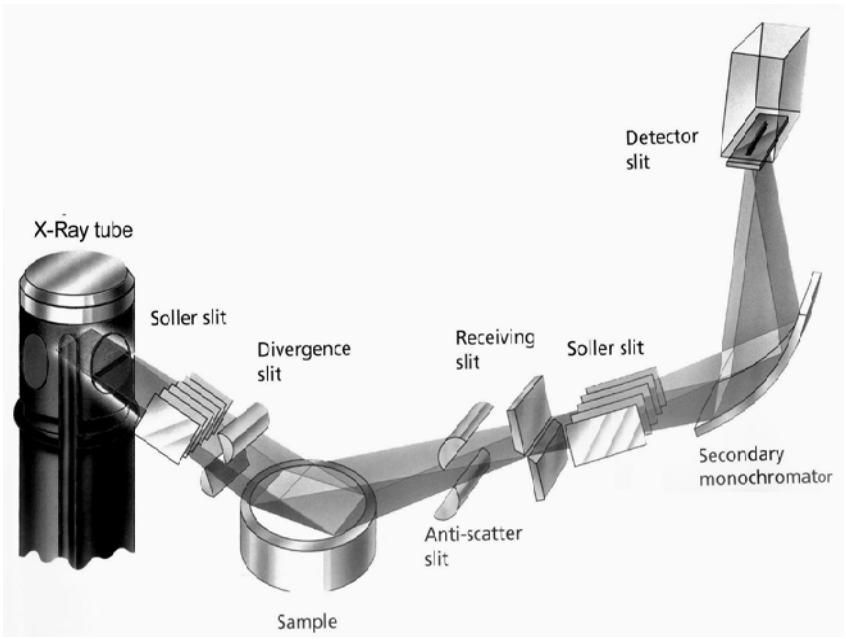

Figure:3.11a Set up for powder XRD.

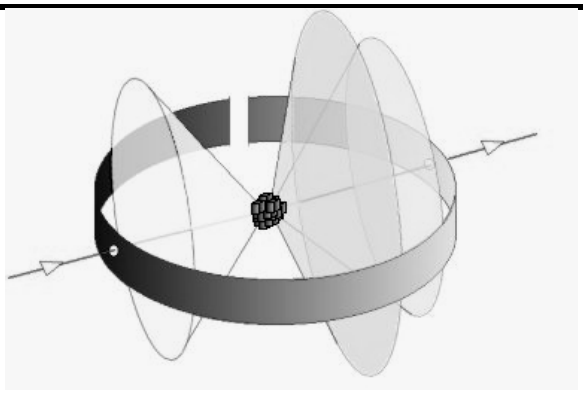

Figure: 3.11b Powder sample diffract x-ray beam in cones.

Diffraction Line	**Parameter of Applications**
Peak position	Unit-cell parameter refinement
	Pattern indexing
	Space group determination
	Anisotropic thermal expansion
	Macrostress: sin2ψ method
	Phase identification (*d*/*I*)
Intensity	Phase abundance
	Reaction kinetics
	Crystal structure analysis (whole pattern)
	Rietveld refinement (whole pattern)
	Search/match, phase identification
	Preferred orientation, texture analysis
Width/breadth and shape	Instrumental resolution function
	Microstructure: line profile analysis
	Microstructure (crystallite size, size
	distribution, lattice distortion, structure
	mistakes, dislocations, composition
	gradient), crystallite growth kinetics
	Three-dimensional microstructure
	in situ diffraction under external dynamic
Non-ambient and	diffraction constraints reaction kinetics

There are three types of powder methods, differentiated by the relative position of the specimen and the film.

Debye-Scherrer Method:

The film is placed on the surface of a cylinder and specimen on the axis of the cylinder.

Focusing Method:

The film, specimen and X-ray source are all placed on the surface of a cylinder.

Pinhole Method:

The film is flat, perpendicular to the incident X-ray beam and located at any convenient distance from the specimen.

For the purpose of simultaneous and quick measurement of the positions and intensities of diffraction lines the diffracto-meters are advantageous; on the other hand, the diffraction cameras are preferred when a very small amount of specimen is available, if an entire diffraction ring is required to be recorded in order to do the rapid estimation of grain size and preferred orientation and in case of large immovable specimen. The powder photographic methods are well described by Klug and Alexander [27] as well as Azaroff and Buerger [25]. The simplest and most inexpensive way of practicing the powder method is to record the X-ray diffraction on photographic film, using a powder camera. A more elaborate way is to detect the diffracted radiation by means of a quantum counter, like Geiger counter. The use of counter diffracto-meter and recorder equipment is justified chiefly when one wants to examine different samples rapidly. Such methods also have a real advantage whenever accurately measured intensities are

necessary. Nowadays, many types of soft-wares are available in market for powder XRD data analysis. In the present work crystals were analyzed by PHILIPS X'PERT MPD System at CSMCRI at Bhavnagar and SICART at Vallabh Vidyanagar. The data were analyzed by the software powder-X.

3.5.2 Structural study Of KDP

The structure of KDP at room temperature was determined by West [28] as early as 1930 and later on it was confirmed by Frazer and Pepinsky with the help of X-ray diffraction studies [29] and Becon and Pease [30] by using neutron diffraction techniques.

KDP possesses ferroelectric properties above T = 123 K in tetragonal symmetry with four formula of KDP per unit cell having space group 14d2 and lattice parameters as a=b=7.453 Å. This has been discussed by Santos et al [31], monoclinic form of KDP crystal has been reported [32]. Figure (3.12) crystal structure of KDP is reported by Dolin et al [33].

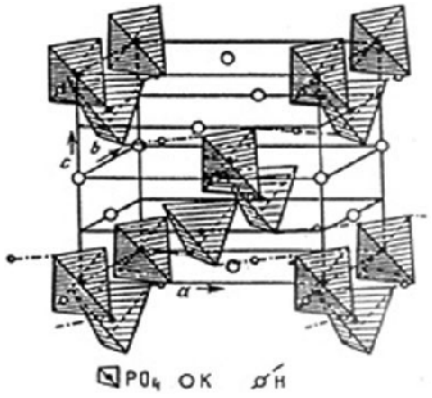

Figure 3.12 Crystal structure of KDP.

This structure includes the potassium ions and the PO^{-1}_4 tetrahedra, turned around their local *z*-axes and connected over the vertices by symmetric strong

short H bonds with two equivalent minima on the potential profile of proton. Thus, in KDP, H atom connects two PO^{-1}_4 tetrahedra. At the same time, each PO^{-1}_4 tetrahedron is surrounded by four H atoms that connect it with four neighboring PO^{-1}_4 tetrahedra.

The H- bonded system in KDP and its analogues like ADP and DKDP posses continuous three-dimensional H –bond network is recently studied for proton transfer along H bonds and to effective air coupling of proton that play the key role on the ferroelectric behavior of crystals and discussed by the tunneling parameter (Ω) and the Ising parameter (J_{ij}) by .Dolin et al [47] and same is represented in figure (3.13)

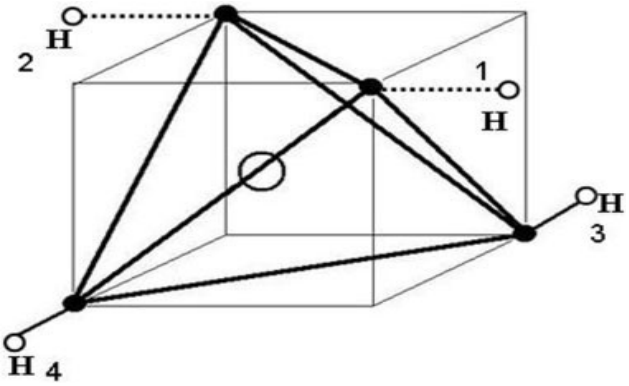

Figure : 3.13 H surroundings of PO_4 tetrahedron in KDP.

The polymorphism of KDP was reported by Subramony et al [34]. The structural ordering below T_c in KDP has been studied by using high resolution neutron diffraction by Nelmes et al [35].The nature of hydrogen bond the electron density distribution in tetragonal KDP at room temperature was obtained by Maximum Entropy Method (MEM) using the synchrotron radiation X-ray powder diffraction data by Yamamura et al [36] .Moreover, the synchrotron radiation X – ray multiple diffraction study of KDP phase transition induced by electric field has been reported by Santosh et al [31].The effect of doping on crystal structure of KDP and the presence of KDP and the

presence of extra phase can be detected by powder XRD. Podder et al [37] have investigated lattice distortion in urea and KCl doped KDP crystals, and found that the structures of the doped crystals were slightly distorted compared to pure KDP crystal. This might be attributed to strains on the lattice by the absorption of urea and KCl. Pritula et al [38] studied the effect of urea doping concentration on unit cell parameters of KDP by powder XRD. To determine the lattice parameters of KDP crystals more precisely, the parameter c depending on the concentration of urea in solution has been measured by the Bond method. The lattice parameter *c* (Δc = 1.4 X 10^3) essentially increased with the concentration of 0.2M/2.0M of urea to the solution. At urea concentration exceeding 0.2M, the observed lattice parameter variation was insignificant. The author have also pointed out that the behavior of the lattice parameter *a* was less sensitive to the change in urea concentration in the solution. Kumaresan et al [39] studied the powder XRD patterns of various organic dye (Amaranth, Rhodamine B and Methyl Orange) doped KDP crystals. Dyes distorted the crystal structure of doped KDP slightly. This might be due to the strain on the lattice by absorption or substitution of dyes. Peaks observed in the doped KDP crystals were correlated well with those observed in individual parent compound with slight shift in the Bragg angle.

Recently, several authors [15,18,40-42] have reported powder XRD studies of amino acid doped KDP crystals. All the workers have reported the single phase nature after doping and shift in the peak positions with change in unit cell parameters. Gunasekaran and Ramkumar [15] obtained the unit cell

parameters of α - histidine doped KDP crystals and also found less value of axial ratios for doped crystals than the pure KDP crystal. Kushwaha et al [40] have recently reported the powder XRD pattern of L- threonine doped KDP crystals and observed a systematic variation in the intensity of diffraction peaks with varying L-threonine concentration. They did not report any extra peak due to doping of L-threonine. Also, recently Parikh et al [18] have reported that the single phase nature of L-alanine doped KDP crystals. Altogether, L-arginine and L-histidine doped KDP crystals [41] and L-arginine doped KDP crystals [42] were reported. They reported the single phase nature and slight change in the unit cell parameters on doping.

3.5.2 Powder XRD of Pure and Amino Acids Doped KDP Crystals

In the present study, the powdered samples were analyzed by employing Cu K_α radiation of X-ray. The data were analyzed by using computer software *powder X*. The standard unit cell parameters of KDP were given as reference and the unit cell parameters for each sample were calculated by the software with assignment of different planes to Bragg reflections. Figures (3.14 -3.16) represent the powder XRD patterns of pure and the different amount of various amino acids doped KDP crystals and unit cell parameters of different samples are listed in table (3.5).

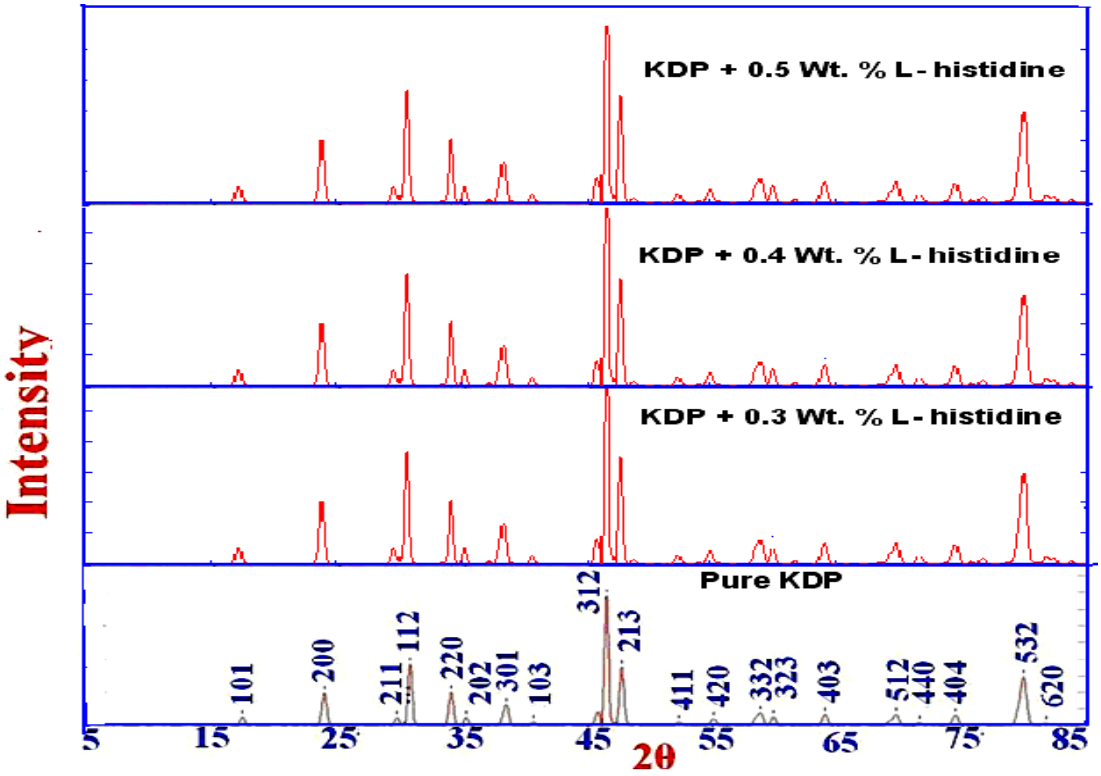

Figure: 3.14 Powder x– ray diffraction pattern for L – histidine doped KDP crystals.

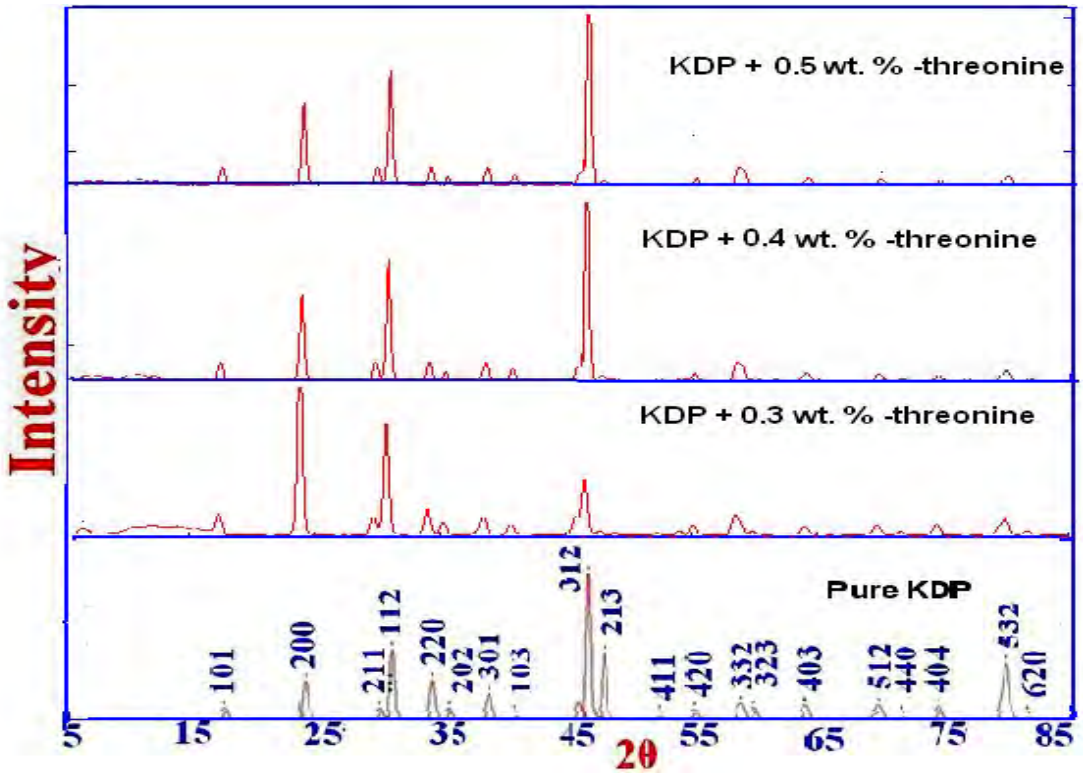

Figure 3.15 Powder x– ray diffraction pattern for L – threonine doped KDP crystals.

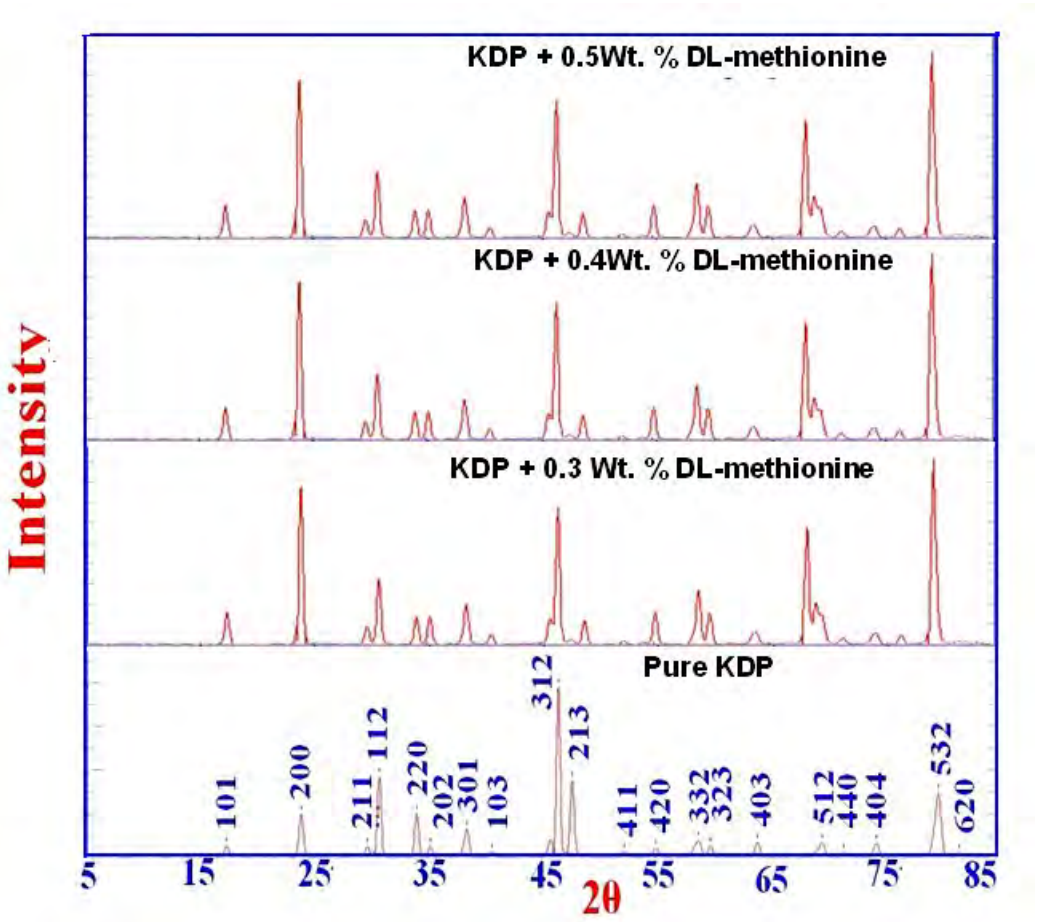

Figure: 3.16 Powder x – ray diffraction pattern for DL – methionine doped KDP crystals.

From figures (3.14 to 3.16) one can notice that all the figures exhibit almost the single phase nature. The doping of amino acids does not bring large distortion in KDP crystal and it allows retaining almost the single phase nature. In all doped samples, very little variation in the unit cell parameters is observed compare to pure KDP crystal, this may be due to larger amino acid molecules have adjusted inside interstitial voids instead of replacement of KDP molecule at any lattice point, the small variation in cell parameters can also be attributed to small strain on lattice.

Table 3.4 Unit cell parameters for pure and different amount of various amino acids doped KDP crystals.

Sample	Lattice Parameter (Å)	
	a = b	**c**
Pure KDP	7.457	6.976
KDP + 0.3 Wt. % L - histidine	7.454	6.971
KDP + 0.4 Wt. % L - histidine	7.451	6.972
KDP + 0.5 Wt. % L - histidine	7.452	6.973
KDP + 0.3 Wt. % L - threonine	7.455	6.974
KDP + 0.4 Wt. % L - threonine	7.457	6.972
KDP + 0.5 Wt. % L - threonine	7.453	6.971
KDP + 0.3 Wt. % DL- methionine	7.457	6.976
KDP + 0. Wt. % DL- methionine	7.454	6.972
KDP + 0.5 Wt. % DL- methionine	7.452	6.974

Conclusion

1. Data of CHN analysis indicated the presence of carbon and nitrogen in doped sample and it was found to be increased as doping concentration increased and remained absent in the pure KDP sample. The paper chromatographs of doped samples gave the characteristic purple spot for the presence of amino acids.
2. The presence of absorption peaks corresponding to various functional groups like C=O stretching, N-H symmetric and asymmetric stretching in the FT–IR spectra confirmed the presence of amino acids in KDP crystals. The change in the absorption frequency of O-H vibrations in doped samples with respect to pure KDP towards lower wave-number indicated the interaction of dopants to hydrogen bond of KDP crystals. The force constant values of O-H vibration decreased on doping of various amino acids in KDP crystals further suggested the interaction of dopants to hydrogen bond of KDP crystals. The frequency of absorption of O=P-OH and O-P-OH symmetric decreased in doped samples with comparison to pure KDP and opposite thing happened for O=P-OH bending, which indicated the interaction of dopant through hydrogen bond of KDP.
3. Powder XRD patterns of both pure and various amino acids doped KDP crystals confirmed the single phase nature. Very marginal change in the unit cell parameters was observed, which also indicated that the doping did not alter the crystal structure of KDP.

References

1. B. Colthup, L. H. Daly, S. E. Wiberley, "*Introduction to Infrared and Raman Spectroscopy"*, Academic Press, London (1975).
2. D. A. Skoog, F. J. Holler, T. A. Nieman; "*Principles of Instrumental Analysis",* Saunders College Publishing, Philadelphia (1998).
3. S. M. Khopkar, "Basic *Concepts of Analytical Chemistry*", Wiley Eastern, New Delhi (1984).
4. G. Socrates, "*Infrared Characteristic Group Frequencies*", John Wiley, Chichester (1980).
5. M. J. D. Lon, *Anal. Chem* . **97A** (1969) 41.
6. E. G. Brame (Jr.), J. G. Grasselli, "*Infrared and Raman Spectroscopy" Vol. 1, Parts A, B and C, in Practical Spectroscopy Series*, Marcell Decker, New York (1977).
7. B. C. Smith, "*Fourier Transform Infrared Spectroscopy*", CRC Press, Boca Raton (1996).
8. B. K. Sharma, "*Spectroscopy*", Goel Publ., Meerut (1997).
9. M. P. Fuller, P. R. Griffiths, *Anal. Chem*. **50** (1978) 1906.
10. M. P. Fuller, P.R, Griffiths, *Appl. Spectrosc*.**34** (1980) 533.
11. V. P. Tolstoy, I. V. Chernyshova, V. A. Skryshevsky, "*Handbook of Infrared Spectroscopy of ultrathin film",* Wiley Interscience, New Jersey (2003).
12. R. R. Griffiths; "*Chemical Infrared Fourier Transform Spectroscopy*", Academic Press, New York (1972.)
13. K. Nakamoto, *"Infrared and Raman Spectra of Inorganic and Coordination Compounds"*, John Wiley 5th Ed. (1997).

14. P. V. Dhanaraj, N. P. Rajesh, P. Ramasamy, M. Jeyaprakasan, C. K. Mahadevan, G. Bhagavannarayana, *Cryst. Res. Technol*. **44** (2009)54.
15. S. Gunasekaran, G. R. Ramkumar, *Indian J. of Phys.* **83(11)**(2009)1549.
16. B. S. Kumar, K. R. Babu, *Indian J. of Pure & Appl. Phys.***46** (2008)123.
17. S.S. Hussaini, K. Datta, P. Ghosh, S. B. Kadam, M. D. Shirsat, *International Conf. on Optics and Photonics,* Chandigarh, India, 30 Oct- 1 Nov(2009)
18. K. D. Parikh, D. J. Dave, B. B. Parekh, M. J. Joshi, *Cryst. Res. & Technol*., **10**(2010)1.
19. A. Rahman, J. Podder, *International J. of Optics*, **2010** (2010)978763.
20. J. R. Govani, W. G. Durrer, M. Manciu, C. Botez, F. S. Manciu, *J. Mater. Res.* **24** (2009)2316.
21. A. A. Chernov, *J. Cryst. Growth* **102** (1990)793.
22. P. Debye ,P. Scherrer; *Physik. Z*.**27** (1917) 277.
23. A. W. Hull, *Phys. Rev.* **(2)10** (1917) 84.
24. J. I. Langford, D. Louër, P. Scardi, *J. Appl. Cryst.* **33**(2000)964.
25. L. V. Azaroff, M. J. Buerger, "*The Power Method in X-ray Crystallography"*, Mc Graw-Hill, New York (1958).
26. H. Lipson, H. Steeple "Interpretation *of X-ray Powder Diffraction Patterns"* MacMillan, New York (1970).
27. H. P. Klug, L. E. Alexander, "*X-ray Diffraction Procedures*" 2nd ed. Wiley, New York (1974).
28. J. West, Zeist*. Krist.* **74** (1930) 306.
29. B.C.Frazer, R. Pepinsky , *Acta Crystallographica* **6** (1953) 273.
30. G. E. Bacon, R. S. Pease, *Proc. Roy. Soc. A* **220** (1953) 397.

31. A. O. do Santosh, R. V. Gelamo, B. B. Li , L. P. Cardoso , M. A. R. Miranda, M A M Nogueria , C M R Remedios , A E A Melo , J M Sasaki , L H Avanci , S L Morelhaa , *Mater. Res*. **4 (**2001) 43.
32. T. Fukami , R. H. Chen, *J. Phys. Soc. Jpn* **75** (2006) 074602
33. S. P. Dolin, T. Y. Mikhailova, M. V. Solin, N. N. Breslavskaya, A. A. Levin , *Int. J. of Quantum Chm.***110** (2010) 77.
34. A. Subramony, S. Lovell, B. Kahar, *Chem. Mater.* **10** (1998) 2053.
35. R. J. Nelmes, W. F. Kuhs, C.J. Howard, J. E. Tibballs, T. W. Ryan, *J. Phys. C Solid State Phys.* **18** (1985) L711
36. S. Yamamura, M. Takata, M. Sakata, Y. Sugawara, *J. Phys. Soc. Jpn.* **67** (1998) 4124.
37. J. Podder, S. Ramalingum, S.N. Kalkura, *Cryst. Res. & Technnol.* **36** (2001) 551.
38. I. Pritula, A. Kosinova, M Kolybayeva, V. Puzikov, S. Bondernko, *Materials.***14** (2007) 295.
39. P. Kumaresan, S Moorthy Babu , P.M. Anabarasan *J. Cryst. Growth* **310** (2008) 1999
40. S. K. Kushwaha, M. Sakir, K. K. Maurya, A. L. Shah, M. A. Wahab, G Bhagavannarayana, *J. Appl Phys*. **108** (2010) 33506.
41. G. G. Mulley, M. N. Rode, B. H. Pawar, *Acta Physica Polonica,* **A 116** (2009) 1033.
42. K. D. Parikh, D. J. Dave, B. B. Parekh, M. J. Joshi, *Bull. Mater. Sci*. **30** (2007)105.

Chapter IV

Thermal Studies of Pure, L-histidine, L-threonine and DL-methionine Doped KDP Crystals

4.1 Introduction

According to widely accepted definition of thermal analysis (Thermo analytical), it is a group of techniques in which physical properties of a substance and/or its reaction products are measured as a function of temperature whilst the substance is subjected to a controlled temperature program [1]. Nearly over a dozen thermal methods can be identified, which differ in the properties measured and temperature programs [2-4]. These methods find widespread use for both quality control and research applications of various substances, such as, polymers, pharmaceuticals, crystals, clays, minerals, metals and alloys. Various thermal techniques are categorized in figure (4.1).

Thermo analytical methods involve the measurement of various properties of materials subjected to dynamically changing environments under predetermined condition of heating rate, temperature range and gaseous atmosphere or vacuum. Among all the thermal methods, the most widely used techniques are TGA, DTA and DSC which find extensive use in all fields of inorganic and organic chemistry, metallurgy, mineralogy and many other areas.

In many cases, the use of a single thermoanalytical technique may not provide sufficient information to solve the problem on hand and hence the use of other thermal techniques, either independently or simultaneously

for complementary information becomes necessary. For example, both differential thermal analysis (DTA) and thermo gravimetric analysis (TGA) are widely used in studies involving physicochemical changes accompanied by variation in the heat content and the weight of the material.

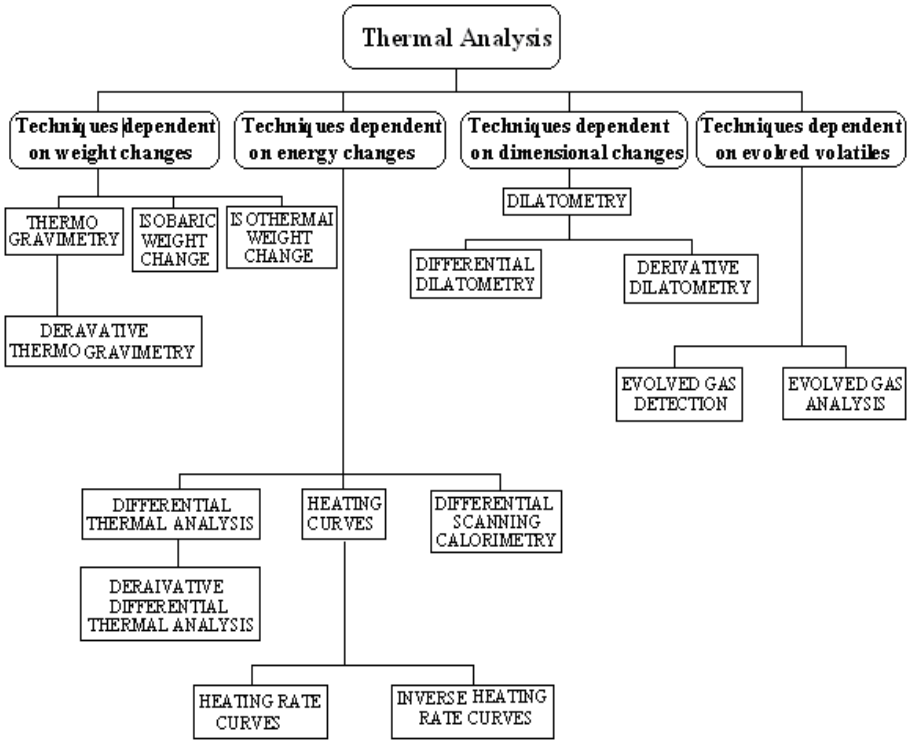

Figure: 4.1 Various thermo analytical techniques.

In the present investigation pure and amino acid doped (L-histidine, L-threonine and DL-methionine) KDP crystals have been studied by employing thermo-gravimetric analysis (TGA) in order to study the effect of doping on thermal stability of KDP crystals and evaluate the kinetic and thermodynamic parameters for the initial stage of dehydration.

4.2 Thermo Gravimetric Analysis

Thermo gravimetric analysis is a technique in which the mass of a substance is measured as a function of temperature or time while the

substance is subjected to a controlled temperature program. The curve obtained in a thermo gravimetric analysis is called thermogram (TG) and its first derivative is called a derivative thermogram (DTG).

Modern commercial TG instrument consists of following main parts:

- A sensitive analytical balance
- A temperature programmable furnace
- A purge gas system for providing suitable gas atmosphere
- A microprocessor for instrument control, data acquisition and display

The null-point weighing mechanism is employed since the sample remains in the same zone of furnace irrespective of changes in mass. The furnace is normally an electrical resistive heater and the temperature range for most of the furnace is from ambient to 1000-2000 ^{o}C. The rate of heat exchange between the furnace and the sample depends on the heating rate which influences the TG curve in a number of ways. A slower rate gives a better resolution of the closely lying steps, while the faster heating rate merges such steps.

One of the objectives of TG and DTA is to delineate as accurately as possible the various temperatures associated with the thermal behavior of a given substance, i.e. temperature of decomposition, stability range of an intermediate compound and the temperature at which the reaction get completed. The TGA involves change in weight with respect to temperature. The acquired data obtained as a plot of mass or loss of mass in percentage as a function of temperature is considered as a thermal spectrum, or a thermogram, or a thermal decomposition curve.These thermograms characterize a system in terms of temperature dependence of its

thermodynamic properties and physical-chemical kinetics. The TGA involves measurement of a change in weight of a system as the temperature is increased at pre-determined rate. Changes in weight are a result of the rupture and/or formation of various physical and chemical bonds at elevated temperatures that lead to the evaluation of volatile products or the formation of heavier reaction products. From such curves, parameters concerning the thermodynamics and kinetics of the various chemical reactions can be evaluated, reaction mechanism, the intermediate and final reaction products. Usually, the temperature range is from ambient to 1200 °C with inert or reactive atmospheres. The derivative in TG is often used to pinpoint completion of weight- loss steps or to increase resolution of overlapping weight-loss occurrences.

Modern commercial variety of instruments for TGA usually consists of, (1) a sensitive analytical balance, (2) a furnace, (3) a pure gas system (for providing an inert or sometimes reactive gas atmosphere) and (4) a microcomputer or microprocessor for instrumental control and data acquisition and display. A block diagram of TGA is shown in figure (4.2).

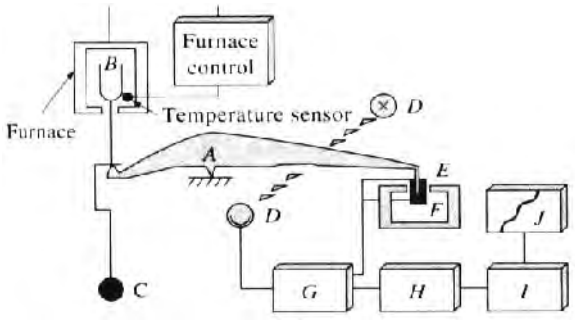

Figure: 4.2 Components of a thermal balance. *(Courtesy: Mmatter instrument corp. Hightston)*

A- beam, *B*- sample cup and holder, *C*- counterweight, *D*- lamp and photodiodes, *E*- coil, *F*- magnet, *G*- control amplifier, *H*- tare calculator, *I*- amplifier, *J*- recorder.

There are mainly two types of thermo-gravimetry available, one is a dynamic thermo-gravimetry and the other is a static or endothermic thermo-gravimetry. In the dynamic thermo-gravimetry the sample is subjected at continuous and linearly increasing temperature, whereas, in the static or endothermic thermogravimetry, the sample is maintained at constant temperature for a certain period of time during which any change in weight is recorded. The basic requirements for the analysis are a precision balance and a recorder. At present, in market the availability of automatic recording thermo-balances is, usually, ranging from 1 mg to 100 g. In general a furnace should have a linear rise of temperature with time and should be capable to work in inert, oxidizing or reducing atmosphere from ambient to 1500 ^{o}C. Often the heating and cooling rate of the furnace can be selected from slightly higher than zero to as high as 200 ^{o}C/min. Because of the continuous record of weight and temperature no features of thermograms are overlooked. The shape of thermogravimetric curve of a particular compound is influenced by the heating rate of the sample and the atmosphere surrounding it [2, 5, 6].

Figure: 4.3 A typical TGA set up.

The thermo grams of pure and L-histidine, L-threonine and DL-methionine doped KDP crystals were recorded on PerkinElmer, Pyris1 TGA,

setup from room temperature to 800 ^{o}C at a heating of 15 °C/min in nitrogen atmosphere at SICART, Vallabh Vidyanagar, Gujarat. Powdered samples were used for this study. A typical TGA set up used is shown figure (4.3).

4.3 TGA Study of Pure and Amino Acids Doped KDP Crystals:

Many workers have reported thermal studies of pure and doped KDP crystals and also identified phase changes at higher temperatures. The techniques like TGA, DTA, DTG and DSC have been employed for these studies. Abdel-Kader et al [7] employed simultaneous TGA, DTA and DTG in the temperature range from 25 ^{o}C to 600 ^{o}C and showed that KDP crystal decomposed into potassium pyrophosphate and then to metaphosphate as an end product. DTA studies at higher heating rates of 50 ^{o}C/min to100 ^{o}C/min showed clear resolution of the first peak into two peaks; the first was attributed to the phase transition at 200 ^{o}C and the second due to decomposition of the sample. It is worth noting that the high temperature phase transition (HTPT) of KDP was also obtained at 175 ^{o}C by DSC studies at 2^{o}C/min. The activation energies for the thermal process of KDP crystals occurring at 230 ^{o}C, 267 ^{o}C, 310 ^{o}C were estimated as 155.56 kJ mol^{-1}, 286.56 kJ mol^{-1} and 81.46 kJ mol^{-1}, respectively, by Kissinger method, however, the values of activation energies were 164.01 kJ mol^{-1}, 294.97 kJ mol^{-1} and 91.34 kJ mol^{-1} for Ozawa method, respectively. The authors also confirmed the high temperature phase transitions by X-ray diffraction and IR spectra.

In another study the HTPT was reported by Ortiz et al [8] and argued strongly for partial polymerization instead of a structural phase transitions. These authors employed X-ray diffraction and TGA to study the kinetic

process of dehydration and HTPT at T_p = 453 ±10 K in KDP. The authors obtained strong evidence that the earlier reported phase transition at T_p was not the structural transition from tetragonal phase to monoclinic phase in high temperature modification of KDP, but the transition occurred due to the formation of various polymeric intermediates, such as $K_nH_2P_nO_{2n+1}$, during the course of the sample. These results supported the earlier study [9] that the term HTPT should be replaced by onset of partial polymerization at reaction sites distributed on the surface.

Moreover, the HTPT were also observed in several systems similar to KDP. Park et al [10] reported HTPT in KH_2PO_4 and RbH_2PO_4 (RbDP) by using DTA, TGA and thermo polarizing microscopy. They estimated T_p = 196 ^oC for KDP and T_p = 96 ^oC for RbDP crystals. On heating beyond T_p, the thermal transformations showed several endothermic peaks and weight losses. The thermo polarizing microscopy showed that until the T_p was exceeded, the uniaxial interference figures were exhibited by KDP and RbDP crystals.

With cracks and chemical changes at the surface of KDP nearly at $T_p \approx 192$ ^oC and RbDP nearly at $T_p \approx 92$ ^oC. However, the high temperature phenomenon exhibited by KDP and RbDP near T_p could indicate no changes from tetragonal to monoclinic structure but chemical decomposition at the surface of the crystals such that exhibited by the type of reaction.

$$nMH_2PO_4 \rightarrow M_nH_2P_nO_{3n+1} + (n\text{-}1)\ H_2O \quad \textit{(where, M = K or Rb)}$$

Similarly, HTPT in ADP crystals were reported by the Torijano et al [11] particularly focused on TGA in the range 300 K to 500 K and DSC of 430 K to 483 K. The powder XRD indicated that when ADP sample was heated above 430 K additional peak appeared beside those corresponding to tetragonal

structure at room temperature. The observed change of symmetry of the crystal suggested a phase transition like phenomenon called HTPT at characteristic temperature T_p = 430 K. The observed weight loss from TG curve suggested that T_p marked the onset of partial polymerization taking place on the surface of the sample such that the phase above 430 K was a mixed phase consisting of tetragonal ADP in the bulk of the sample and ammonium polyphosphates $(NH_4)_2H_2P_2O_7$ at the surface of the crystal.

Several other authors studied thermogravimetry of pure KDP crystals [12, 13] and various doped KDP crystals [14-17]. It has been found that glycine doped KDP crystals starts decomposing at 204.93 ^oC and KDP crystal at 207.91 ^oC [16] this also further supports that amino acid doping slightly increases thermal destability and reduces the phase transition temperature.

Moreover, thermal studies on amino acids (L-glutamic acid, L-histidine and L-valine) doped KDP crystals are reported by Kumaresan [17] using TGA and DTA. The author [17] observed that L-glutamic acid doped KDP melted at a 125 ^oC and undergone irreversible endothermic transition around 210 ^oC followed by another endothermic transition around 290-675 ^oC. The TGA exhibited a weight loss of about 13 % in the temperature range 190-350 ^oC due to liberation of volatile substances. However, the prolonged heating up to 900 ^oC did not produce any endothermic peaks in the DTA curve and TGA exhibited a total weight loss of nearly 13 % at 900 ^oC. Interestingly, the DTA curve of L-histidine doped KDP revealed two more events at 560 ^oC and 798 ^oC reported which did not accompany by weight loss. It has been argued that this might be due to high temperature phase transition of KDP. Apart from

this, a significant splitting of DTA trace appeared at 92 ^{o}C might be due to decomposition of KDP into KPO_3 and water as,

$$2KH_2PO_4 \rightarrow 2KPO_3 + 2H_2O$$

Further, for L-histidine doped KDP crystals, the dopant was actually substituted into the lattice and the KDP phase stability improved in the presence of L-histidine. The DTA results of L-histidine doped KDP were comparable to the pure KDP except the small deviations in the peaks. Another major observation was made that the intensity of the major peak at 272.6 ^{o}C, which splitted into two peaks when compared to pure samples.

In the present investigation, thermal stability of pure and different amounts of (0.3, 0.4 and 0.5 wt. %) various amino acids such as, L-histidine, L-threonine and DL-methionine doped KDP crystals were studied by employing the Thermo-Gravimetric Analysis (TGA). The crystals were grown by slow solvent evaporation method and the details are already described in chapter II.

Figures (4.4 – 4.7) are the thermo-grams for pure and various amounts of (0.3, 0.4 and 0.5 wt. %) L-histidine, L-threonine and DL-methionine doped KDP crystals, respectively.

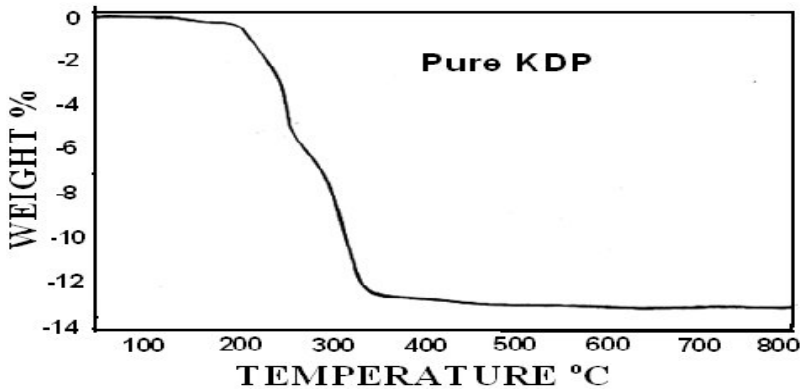

Figure: 4.4 Thermo-gram of pure KDP Crystal.

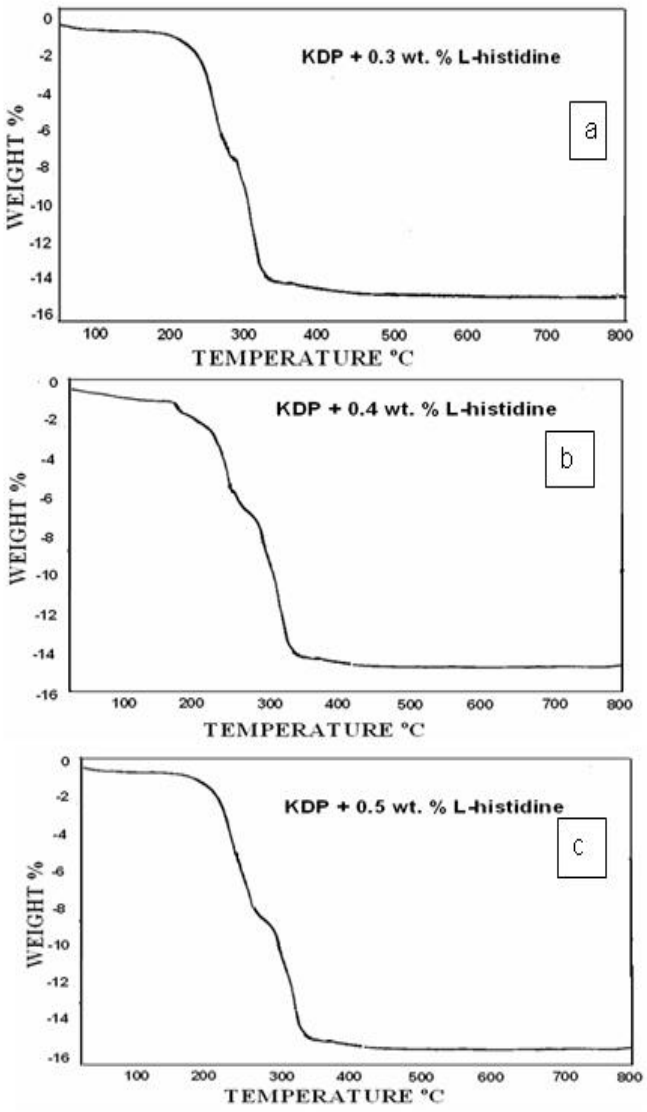

Figure: 4.5, a,b,c Thermo-grams of different amount of L-histidine doped KDP crystals.

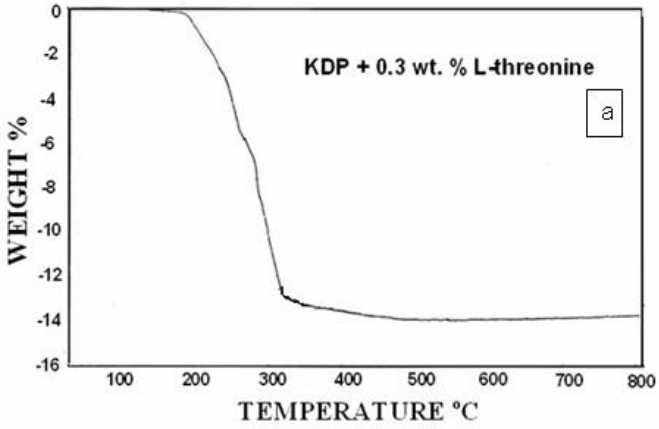

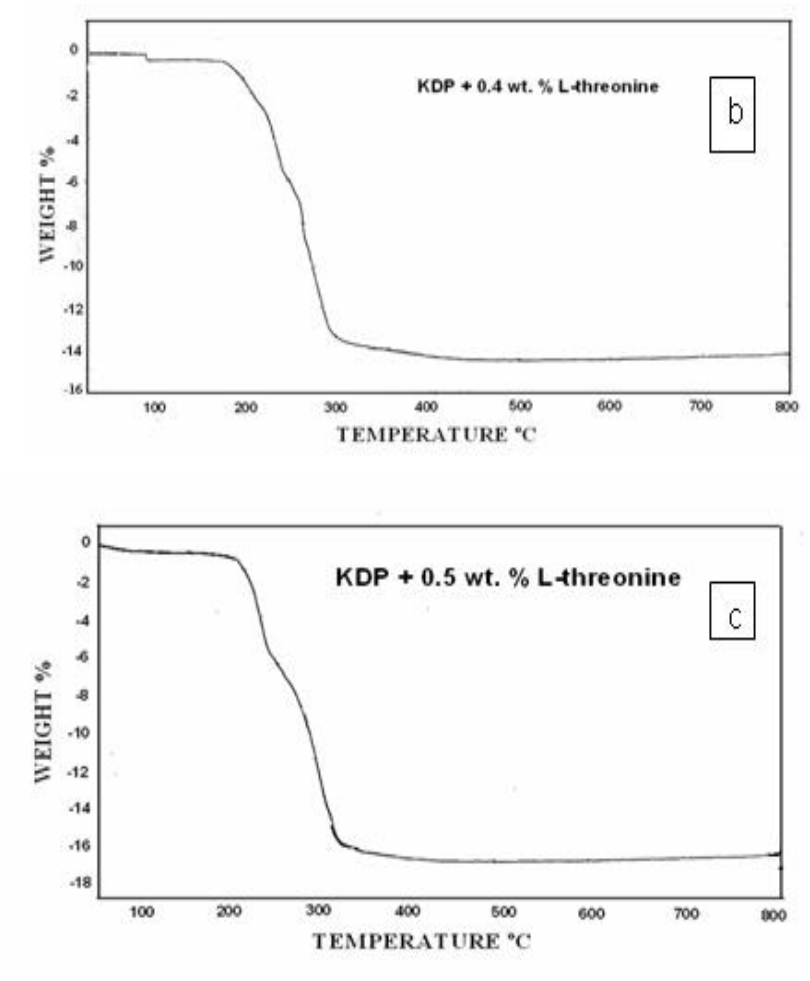

Figure: 4.6,a,b,c Thermo-grams of different amount of L-threonine doped KDP crystals

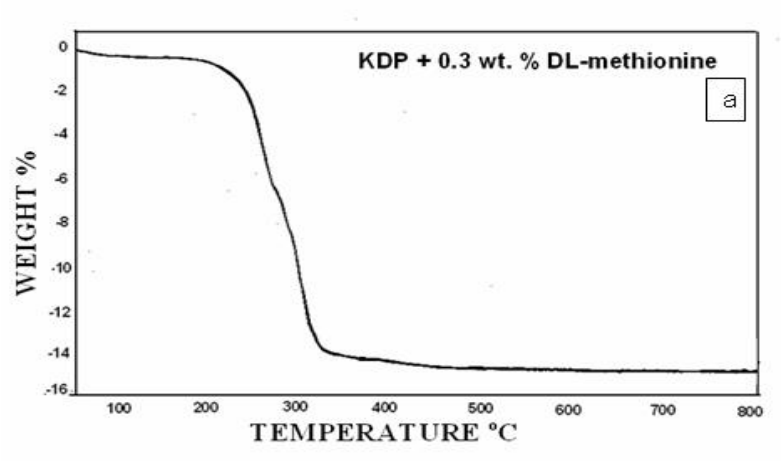

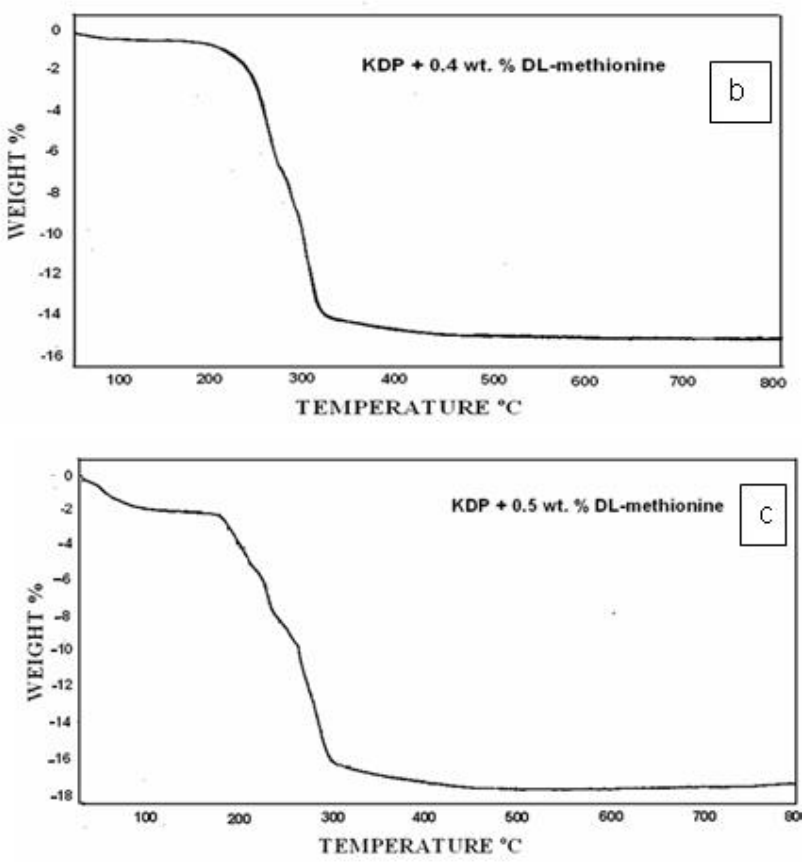

Figure: 4.7 a,b,c Thermo-grams of different amount of DL-methionine doped KDP crystals

It has been observed that initially the crystal gives up the water of hydration and remains in that form up to end of the analysis. One can see from the thermo- grams that on increasing amount of doping the dehydration as well as the phase transition process starts early and the crystals becomes anhydrous faster than the pure KDP. Since amino acid becomes unstable at lower temperatures, it weakens KDP crystals and as a result the dehydration process takes place earlier and faster with comparison to pure KDP crystal. This also proves that the amino acid has entered the KDP crystal in a doped form. The similar nature was observed for L-arginine [18], L-alanine [19] and L-lysine [20] doped KDP crystals.

From the thermo-grams the number of water molecules associated with pure and amino acids doped crystals was estimated, which is shown in table (4.1). It can be observed that as the doping of amino acid increases the bulk values of water molecules attached with the crystals increases.

Table: 4.1 Number of water molecules for pure and amino acids doped KDP crystals.

Sample	No. of water molecule
Pure KDP Crystal	0.43
KDP + 0.3% wt. L-histidine	0.59
KDP + 0.4% wt. L-histidine	0.76
KDP + 0.5% wt. L-histidine	0.82
KDP + 0.3% wt. L-threonine	0.45
KDP + 0.4% wt. L-threonine	0.49
KDP + 0.5% wt. L-threonine	0.51
KDP + 0.3% wt. DL-methionine	0.74
KDP + 0.4% wt. DL-methionine	0.83
KDP + 0.5% wt. DL-methionine	0.86

4.4 Kinetic and Thermodynamic Parameters:

The use of thermo-gravimetric data to evaluate the kinetic parameters of solid-state reactions involving weight loss has been investigated by many workers [21-24]. If the pyrolysis occurs through a many-stepped mechanism, usually, the shape of the curve can be determined by the kinetic parameters of pyrolysis, such as order of reaction, frequency factor and energy of activation. Kotru et al [25] reported the kinetics of solid-state decomposition of

neodymium tartrate. They also calculated various kinetic parameters and suggested that the decomposition process took place according to cylindrical kinetic model. The kinetics of dehydration of gypsum [26], lithium sulphate monohydrate single crystals [27] as well as the kinetic and thermodynamic parameters of decomposition of chromate in different gas atmosphere [28] has been evaluated.

Usually, the kinetic parameters can be evaluated from the TG curves by applying several equations [21-23], which are proposed by different authors on the basis of different assumptions to the kinetics of the reaction and the Arrhenius law. These equations are as follows:

(1) Coats and Redfern Relation

(2) Horowitz and Metzger Relation

(3) Freeman and Carroll Relation

However, in the present investigation, the Coats and Redfern relation is discussed in detail because it facilitates not only to evaluate the activation energy and order of reaction but also the frequency factor. Thus, it helps to evaluate the thermodynamic parameters further.

The use of thermogravimetry data to evaluate the kinetic parameters of solid state reaction involving weight loss has been investigated by many workers [29-31]. The kinetic parameters of dehydration process of pure and different amount of (0.3, 0.4 and 0.5 wt. %) amino acids (L-histidine, L-threonine and DL-methionine) doped KDP crystals were evaluated by using the Coats and Redfern relation [21], which is as follows,

$$\log_{10}\left(\frac{1-(1-\alpha)^{1-n}}{T^2(1-n)}\right)=\left\{\log_{10}\left(\frac{AR}{aE}\right)\left(1-\frac{2RT}{E}\right)\right\}-\left\{\frac{E}{2.3RT}\right\} \qquad (4.1)$$

Where, $\alpha = (W_0 - W) / (W_0 - W_f)$, W_0 = Initial weight, W = Weight at time t, W_f = Final weight, n = Order of the reaction, A = Frequency factor, E = Activation energy of the reaction, R = Gas constant, a = Heating rate in deg.min^{-1}

To determine the value of activation energy and order of reaction, a plot of $log_{10}[\{1 - (1- \alpha)^{1-n}\} / \{T^2 (1- n)\}]$ versus $1/T$ is drawn for different values of n. The best linear fit gives the correct value of n. The value of activation energy can be calculated from the slope of a linear plot. The value of frequency factor can be obtained from equation (4.1). Equation (4.1) is applied for all values of n, except n = 1. For n =1, the modified equation has been proposed [21].

$$-\log_{10}\left[\frac{-\log(1-\alpha)^{1-n}}{T^2}\right] = \left\{\log_{10}\left(\frac{AR}{aE}\right).\left(1-\frac{2RT}{E}\right)\right\} - \left\{\frac{E}{2.3RT}\right\} \qquad (4.2)$$

Figures (4.8 - 4.11) show the best linear fitted plots drawn for Coats and Redfern relation for pure and different amount of (0.3, 0.4 and 0.5 wt. %) L-histidine, L-threonine and DL-methionine doped KDP crystals for dehydration process.

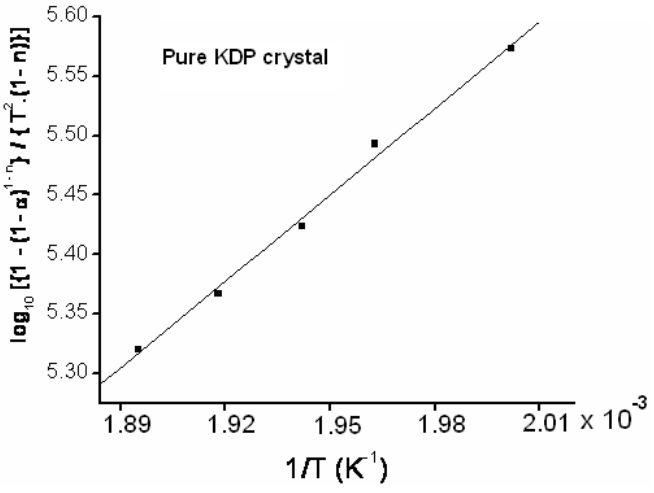

Figure: 4.8 The plot of C-R relation for Pure KDP crystal.

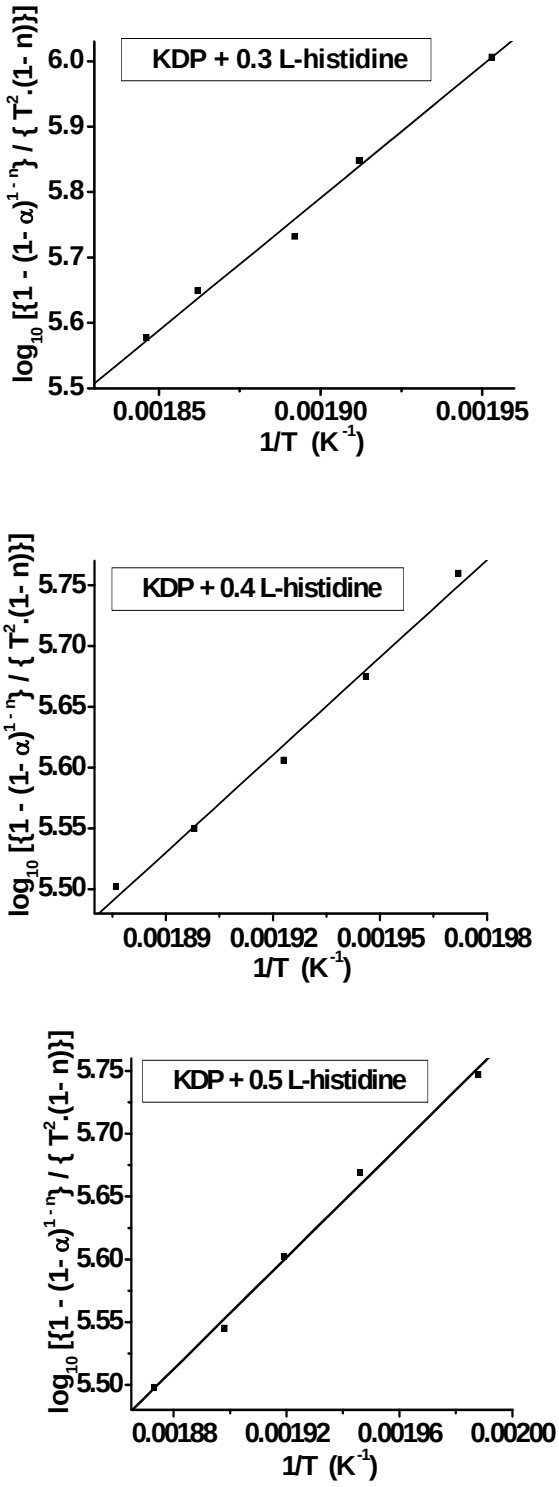

Figure: 4.9 The plots for C-R relation for different amount of L-histidine doped KDP crystals.

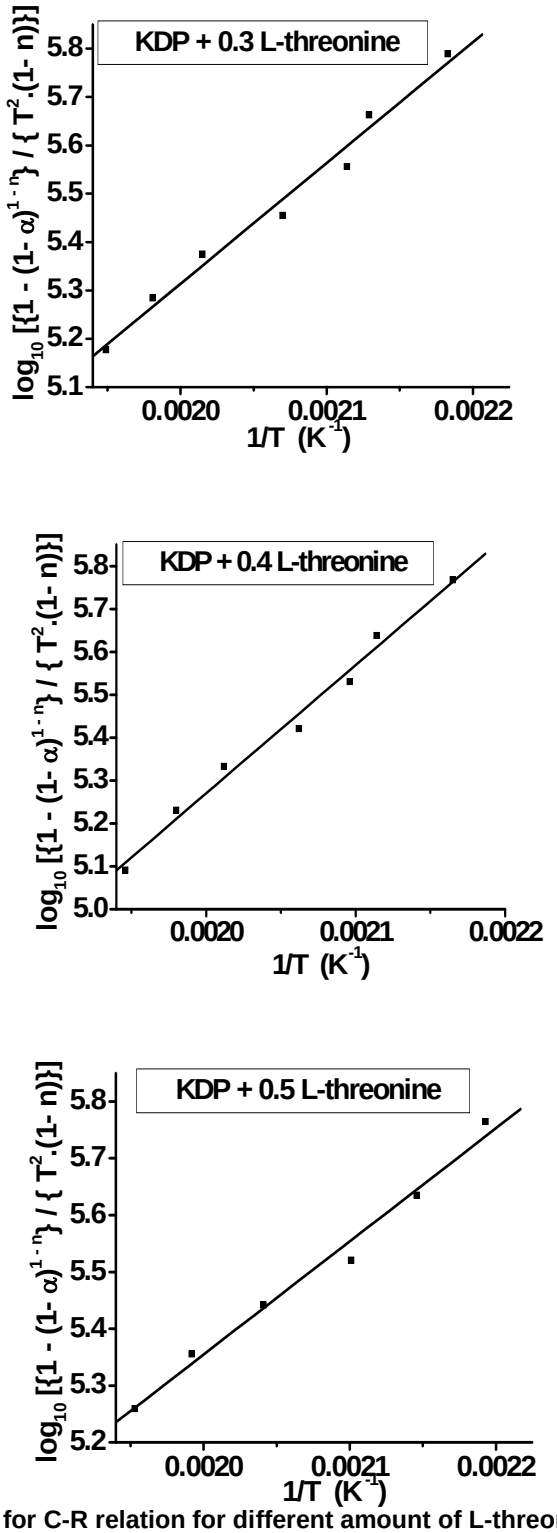

Figure:4.10 The plots for C-R relation for different amount of L-threonine doped KDP crystals.

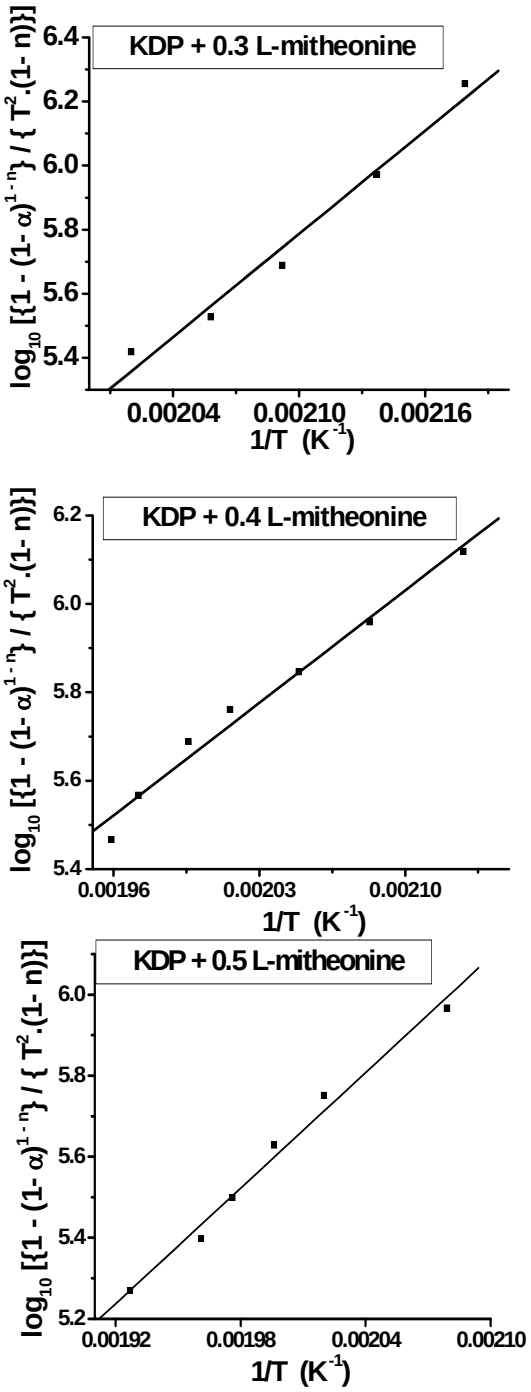

Figure: 4.11 The plots for C-R relation for different amount of DL-methionine doped KDP crystals.

Table (4.2) compiles the values of activation energy, frequency factor and order of reaction. The values of activation energy and frequency factor decrease as the amount of amino acid doping increases. The activation energy is considered as a barrier to be surmounted for reactant to combine to

form product. Higher the value of activation energy slower is the rate of reaction. Hence the higher value of activation energy for pure KDP crystal indicates more stable nature.

Table (4.2): Values of kinetic and thermodynamic parameters

Sample	Order of Reaction n	Activation Energy kJ mol^{-1}	Frequency Factor A	Standard Entropy $JK^{-1}mol^{-1}$	Standard Activation Enthalpy kJ mol^{-1}	Standard Gibbs free Energy kJ mol^{-1}
Pure KDP Crystal	$^{1}/_{2}$	103.82	3.24×10^{21}	162.25	95.25	11.59
KDP + 0.3Wt. %L-histidine	$^{9}/_{10}$	64.66	1.3×10^{17}	78.32	56.25	16.62
KDP + + 0.4Wt. % L-histidine	$^{9}/_{10}$	52.28	5.0×10^{15}	51.18	43.89	18.06
KDP + + 0.5Wt. %L-histidine	$^{2}/_{3}$	42.96	3.55×10^{14}	29.2	34.52	19.68
KDP + 0.3Wt. %L-threonine	$^{9}/_{10}$	101.18	1.07×10^{21}	153.41	92.83	15.82
KDP + 0.4Wt. %L-threonine	0	73.57	1.61×10^{18}	99.25	65.08	14.47
KDP + 0.5Wt. %L-threonine	0	66.29	3.62×10^{17}	86.86	57.88	13.93
KDP + 0.3Wt% DL-methionine	$^{1}/_{4}$	98.16	$2.07X10^{20}$	139.38	89.46	16.56
KDP + 0.4Wt% DL-methionine	$^{1}/_{4}$	95.84	$8.26X10^{19}$	131.75	87.14	18.28
KDP + 0.5Wt%DL-methionine	$1_{/4}$	86.32	$8.12X10^{17}$	128.5	83.26	17.25

Thermodynamic parameters have been evaluated for the dehydration process of pure and amino acids doped KDP crystals. Thermodynamic parameters are evaluated by following well known expressions [32]. The standard entropy of activation $\Delta^{\#}S^{o}$ can be calculated by the relation of

$$\Delta^{\#}S^{o} = 2.303 \times R \times \log_{10}[Ah/kT_m] \quad (4.3)$$

Where, k = Boltzmann constant, h = Planck's constant,

T_m = Temperature, A = Frequency factor.

The standard enthalpy of activation $\Delta^{\#}H^{o}$ can be calculated by using the following relation,

$$\Delta^{\#}H^{o} = E - 2RT \quad (4.4)$$

The standard Gibbs energy of activation $\Delta^{\#}G^{o}$ is possible to estimate from the equation.

$$\Delta^{\#}G^{o} = \Delta^{\#}H^{o} - T\Delta^{\#}S^{o} \quad (4.5)$$

Enthalpy is a state function whose absolute value cannot be known. $\Delta^{\#}H^{o}$ can be ascertained, either by direct method or indirectly. An increase in the enthalpy of a system, for which $\Delta^{\#}H^{o}$ is positive, is referred to as an endothermic process. Conversely, loss of heat from a system, for which $\Delta^{\#}H^{o}$ has a negative value, is referred to as an exothermic process.

Entropy is a thermodynamic property of a system. It is a state function and it is defined in terms of change rather than its absolute value. A spontaneous process has a natural tendency to occur, without the need for input work into the system. In contrast to this, the non-spontaneous process does not have a natural tendency to occur.

However, $\Delta^{\#}G^{o}$ is negative for a spontaneous process. An exothermic reaction ($\Delta^{\#}H^{o} > 0$) with positive ($\Delta^{\#}S^{o} > 0$) is always spontaneous. A reaction for which $\Delta^{\#}H^{o} < 0$ and $\Delta^{\#}S^{o} < 0$ is spontaneous only at low temperatures, whilst a reaction for which $\Delta^{\#}H^{o} > 0$ and $\Delta^{\#}S^{o} > 0$ is spontaneous only at high temperatures. The temperature at which the reaction becomes spontaneous in each case is given by $T = \Delta^{\#}H^{o}/\Delta^{\#}S^{o}$.

The standard free energy $\Delta^{\#}G^{o}$, is the change in the Gibbs free energy, which accompanies the conversion of reactants in their standard states into products in their standard states. It can be calculated from the standard enthalpy and standard entropy using $\Delta^{\#}G^{o} = \Delta^{\#}H^{o} - T\Delta^{\#}S^{o}$ or from tabulated value for the standard free energy of formation $\Delta^{\#}G^{o}$.

For spontaneous process, $\Delta^{\#}S^{o}$ is positive and $\Delta^{\#}G^{o}$ is negative. The relationship $\Delta^{\#}G^{o} = \Delta^{\#}H^{o} - T\Delta^{\#}S^{o}$ allows predictions of the conditions under which a reaction is spontaneous. Temperature has a major effect on spontaneity of reactions. For the reactions where $\Delta^{\#}H^{o} < 0$ and $\Delta^{\#}S^{o} < 0$, $|T\Delta^{\#}S^{o}|$ will be less than $|\Delta^{\#}H^{o}|$ provided that T is small, and such a reaction will be spontaneous at lower temperatures. Conversely, when $\Delta^{\#}H^{o} > 0$ and $\Delta^{\#}S^{o} > 0$, $|T\Delta^{\#}S^{o}|$ will be greater than $|\Delta^{\#}H^{o}|$ provided that T is large, and such a reaction will become spontaneous at higher temperatures. In both cases, the temperature at which the reaction becomes spontaneous (when $\Delta^{\#}G^{o} = 0$) is simply given by $T = \Delta^{\#}H^{o}/\Delta^{\#}S^{o}$ [33]. The prediction for the processes is given in table (4.3).

Table (4.3): The conditions for the prediction of processes

$\Delta^{\#}H^{o}$	$\Delta^{\#}S^{o}$	**Spontaneous or not**	**Spontaneity favored by**
-ive	+ive	Under all conditions	All conditions
-ive	-ive	If $\lvert T\Delta^{\#}S^{o}\rvert < \lvert\Delta^{\#}H^{o}\rvert$	Low temperature
+ive	+ive	If $\lvert T\Delta^{\#}S^{o}\rvert > \lvert\Delta^{\#}H^{o}\rvert$	High temperature
+ive	-ive	Never	No condition

The thermodynamic parameters for dehydration of iron tartrate have been estimated by Joseph and Joshi [34]. Dabhi and Joshi [30, 31] have also reported the thermodynamic parameters for dehydration of various gel grown

metal tartrate crystals. Hajiyani et al [35] reported the study of kinetic and thermodynamic parameters for decomposition bis thiourea strontium chloride crystals.

The estimated thermodynamic parameters are given in table (4.1). It can be noticed that on increasing the doping of amino acids in KDP, the value of standard entropy and standard enthalpy decrease, whereas the value of standard Gibbs energy increases. In an isolated system a process being considered is attended by an increase in entropy $(\Delta^{\#}S^{o})$ is known as the spontaneous process, which occurs itself [32]. The single crystalline nature of the sample is the most order form of the sample and the dehydration of the sample brings the disorder in the sample, obviously the large value of $\Delta^{\#}S^{o}$ in the case of pure KDP crystals is obtained than the doped crystals.

Comparing the nature of the thermodynamic parameters listed in Table (4.3) with table (4.2), one can suggest easily from the positive values of $\Delta^{\#}H^{o}$ and $\Delta^{\#}S^{o}$ that the reaction is spontaneous at comparitively high temperature.

Conclusion

1. Thermo-grams of pure and amino acids doped KDP crystals suggested that as the doping increased the crystals became thermally less stable and dehydrated faster at comparatively lower temperature.
2. The values of kinetic and thermodynamic parameters decreased with The increase in the level of doping.
3. The higher values of activation energy and standard entropy of activation suggested more stable condition for pure KDP crystal than amino acids doped KDP crystals.
4. The positive value of $\Delta^{\#}H^{o}$ and $\Delta^{\#}S^{o}$ suggested spontaneous nature of reaction or phase transition at higher temperature.
5. By doping amino acids in KDP crystals, one faces slight sacrifice in the thermal stability of crystals.

References

1. D. A. Skoog, F. J. Holler, T. A. Nieman, "*Principles of Instrumental Analysis",* Saundrs College Publishing, Philadelphia (1998).
2. W. W. Wendlandt, "*Thermal Analysis"*, Wiley, New York (1985).
3. M. E. Brown, "*Introduction to Thermal Analysis*: *Techniques and Applications"*, Chapman and Hall, New York(1988).
4. P. J. Haines, "*Thermal Methods of Analysis",* Blackie, London(1995).
5. L. Erdey, "*Gravimetric Analysis",* Pergamon Press Ltd. (1963).
6. S. M. Khopkar, "*Basic Concept of Analytical Chemistry"*, Wiley Eastern, New Delhi (1984).
7. A. Abdel-Kader, A.A. Ammar, S.I. Salch, *Thermochim*. *Acta* **176** (1991) 293.
8. E.Ortiz, A. Vargas, B.E. Mellander, *J.Phys. Chem of solids* **59** (1998) 305.
9. K. S. Lee. *J .Phy. Chem. Solids* **57** (1996) 333.
10. J. H. Park, K. S. Lee, B. C. Choi, *J. Phys. Condensed Mat.* **13** (2001) 9411.
11. E. Torijano, R.A. Vargas, J.E. Diosa, B.E. Mellander, *Phys. Status Solidi (b)* **220** (2000) 659.
12. S. Balamuragan, P. Ramasamy, *Spectrochem. Acta. A.Mol Biomal. Spectr.* **71** (2009) 1979.
13. S. Chandra, A. Kumar, *J. Phys. Condensed Mat.* 3 (1991) 5271.
14. M. D. Shirsat, S. S.Hussaini, N. R. Dhumane, V.G. Dongre, *Cryst. Res. & Technol.* **43** (2008) 756.

15. S. S. Hussaini, N. R. Dhumane, V. G. Dongre, M. D. Shirsat, *Cryst. Res. & Technol.* **42** (2007) 111.

16. S. S. Hussaini, K. Datta, P. Ghosh, S. B. Kadam, M. D. Shirsat, ICOP-2009, *Int Conf on optics & photnics*, CSIO, Chandigarh, India, 30th Oct to 1st Nov, 2009.

17. P. Kumaresan, *Ph.D Thesis*, Anna University, Chennai (2008).

18. K. D. Parikh, D. J. Dave, B. B. Parekh, M. J. Joshi, *Bull. Mater. Sci*. **30** (2007) 105.

19. K. D. Parikh, D. J. Dave, B. B. Parekh, M. J. Joshi, *Cryst. Res. Technol.* **19** (2010)1.

20. K. D. Parikh, D. J. Dave, M. J. Joshi, *Mod. Phys. Lett. B*. **23** (2009)15892.

21. A. W. Coats, J. P. Redfern, *Nature* **201** (1964) 68.

22. H. H. Horowitz, G. Metzger, *Anal. Chem.* **35** (1963) 1464.

23. E. S. Freeman, B. Carroll, *J. Phys. Chem*.**62** (1958) 394.

24. D. Van Krevelan, C. Van Hardeen, F. J. Huntlens, *Fuel* **30** (1951) 253.

25. P. N. Kotru, K. K. Raina, M. L.Koul, *Indian J. Pure & Appl. Phys*. **25** (1987) 220.

26. D. Fatu, *J. Thermal Analysis & Calorimetry* **65(1)** (2001) 205.

27. A. N. Modestov, P. V. Poplankhin, N. Z. Lyakhov, *J. Thermal Analysis & Calorimetry* **65(1)** (2001) 103.

28. S. A. Halawy, N. E. Fouad, M. A. Mohamed, M. I. Zaki; *J. Thermal Analysis & Calorimetry* **65(1)** (2001) 153.

29. V. S. Joshi, M. J. Joshi, *Cryst. Res. & Technol*. **38**(2003) 817.

30. R. M. Dabhi, M. J. Joshi, *Indian J. Phys*. **76A** (2003) 481.

31. R. M. Dabhi, M. J. Joshi, *Indian J. Phys.* **76A (2)** (2002) 211.

32. K. J. Laidler, "*Chemical Kinetics"*, 3rd Ed, Harper and Row Pub. New York(1987).

33. A. G. Whittaker, A. R. Mount, M. R. Hill, "*Physical Chemistry"*, Viva, New Delhi (2001).

34. S. Joseph, M. J. Joshi, *Indian J. Phys*. **71A** (1997) 183.

35. R. R. Hajiyani, D. J. Dave, C. K. Chauhan, P. M. Vyas, M. J. Joshi, *Mod. Phy. Lett. B* **24** (2010) 735.

Chapter V

Dielectric Study of Pure and L-histidine, L-threonine and DL-methionine Doped KDP Crystals

5.1 Introduction

Dielectric study is important part of materials characterizations, because it does not only throw light on the materials behavior under the influence of applied electric field but also its applications. In general, for any molecules will have two possibilities when influenced by an external field,

1. Molecules may have permanent dipole moments which may be aligned in an external field.
2. The distances between ions or atoms may be influenced by external field.

However, the polarization in atoms or molecules is induced by an external field by displacing electrons with respect to the corresponding nuclei. The electric properties of molecules are generally characterized by three quantities,

(i) Polarizability due to electronic displacement within atoms or ions.

(ii) Polarizability due to atomic or ionic displacement within the molecules. (changes in bond angles and inter-atomic distances)

(iii) A permanent dipole moment.

Notwithstanding, the discussion becomes more interesting when solid material is considered for dielectric study for both static and alternating fields. This may lead to some interesting phenomena like piezoelectric effect, pyroelectric effect and ferroelectric effect in certain crystals. This has brought novel applications of various materials in science and technology.

5.2 Fundamentals of Dielectric Studies

Materials, which are electric insulators or in which an electric field can be sustained with a minimum dissipation power are known as dielectric materials. The dielectric includes all materials except condensed states of metals. A dielectric is characterized by its dielectric constant ε_r, which relates the charge density to the electric field by the following relation,

$$D = \varepsilon E = \varepsilon_0 . \varepsilon_r E \quad (5.1)$$

Where, $\varepsilon = \varepsilon_0 . \varepsilon_r$, ε_0 is the permittivity of free space and ε_r is the relative permittivity or dielectric constant of the material ($\varepsilon_r = \varepsilon / \varepsilon_0$).

In the earlier experiments Faraday found that by inserting a dielectric material between the capacitor plates, the capacitance was increased by a factor of ε_r. The reason is the appearance of charges on the surface of the dielectric necessitating the arrival of fresh charges from the battery in order to keep the voltage constant. This is described in a schematic diagram of figure (5.1).

In vacuum the surface charge density (D_0) on the condenser plate is represented as

$$D_0 = \frac{\varepsilon_0 V_0}{d} = \varepsilon_0 E \quad (5.2)$$

Where, d is the distance between the plates.

In the presence of dielectric, the surface charge density (D) of dielectrics increase to

$$D = \frac{\varepsilon_0 \varepsilon_r V_0}{d} = \varepsilon_0 . \varepsilon_r E \quad (5.3)$$

The dipole moment per unit volume of dielectric (polarization- P) is equal to the surface charge density of dielectrics, therefore,

$$P = \varepsilon_0 . \varepsilon_r E \quad (5.4)$$

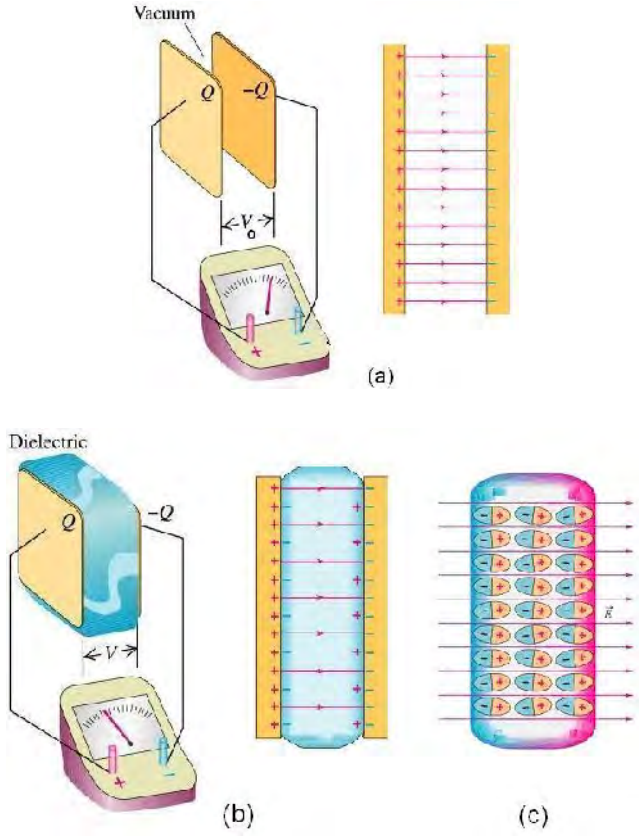

Figure: 5.1 (a) Charge stored on capacitor plates in a vacuum, (b) Charge stored on capacitor plates in a dielectric, (c) The dipole arrangement in a dielectric.

If field is not very strong, the electric susceptibility (χ) is define as the ratio of polarization to electric field,

$$\chi = \frac{P}{E} \tag{5.5}$$

The electric susceptibility is also expressed by this relation; $\chi = \varepsilon_r - 1$

From equation (5.3) and (5.4) the following relationship can be obtained,

$$P = \varepsilon_0 \chi E \tag{5.6}$$

In most cases (linear dielectrics) the magnitude of polarization is directly proportional to the electric field. In the cases of non linear dielectrics, including ferroelectrics, there is no proportionality between polarization and

electric field. For anisotropic dielectrics the relationship between *P* and *E* is tensorical.

Usually, the dielectric constant for a given material is defined as the ratio of a capacitance of capacitor containing a given dielectric (*C*) to a capacitance of vacuum capacitor (C_0) of identical dimensions. This can be represented by the following relationship,

$$\varepsilon_r = \frac{C}{C_0} \tag{5.7}$$

For a given charge distribution, the dielectric constant expresses the ratio of electric field strength in vacuum to that in a dielectric, the later field being reduced by the polarization of the dielectric medium.

5.2.1 Polar and Non-polar Dielectrics

Dielectrics can be divided into two classes

(i) Polar dielectrics

(ii) Non-polar dielectrics

This classification is extremely important when electrical, general physical and chemical properties of materials are considered.

A molecule of any material consists of atoms or ions having definite positive or negative electric charges. Even in the absence of external electric field if the molecule exhibits electric dipole (figure: 5.1-c) with dipole moment different from zero, it is referred to as a permanent dipole and the molecule is called as polar dielectric. The magnitude of the electric dipole moment of a molecule is,

$$\mu = q.l \tag{5.8}$$

Where, *q* is the magnitude of positive or negative electric charge of a molecule and *l* is the length of the dipole. Here, μ is the intrinsic electric

dipole moment of a molecule exhibited in the absence of external electric field.

Irrespective of the results obtained in the study of electrical properties of materials, its polarity can be judged from the chemical structure of its molecules. An experimental definition of the dipole moment μ leads to very important conclusions regarding the structure of the molecules of materials. The atom has a positively charged nucleus surrounded by an electron cloud. Due to symmetry in non-polar dielectric substance, in the absence of electric field, the centers of positive and negative charges coincide. As a result of this $l = 0$ in the molecules of non-polar dielectric material and hence $\mu = 0$. Conversely, the asymmetric molecules are always polar dielectric.

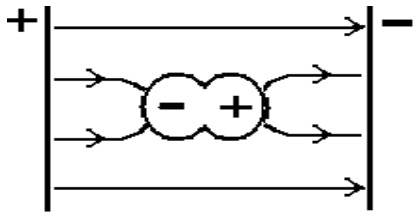

Figure: 5.2 Formation of dipole in non-polar dielectric in electric field.

Figure (5.2) shows formation of dipole in non-polar dielectric material when placed in electric field. When an electric field is applied, the centers of positive and negative charges are separated from each other due to the influence of electric force acting on them in mutually opposite directions. This induces an electric dipole.

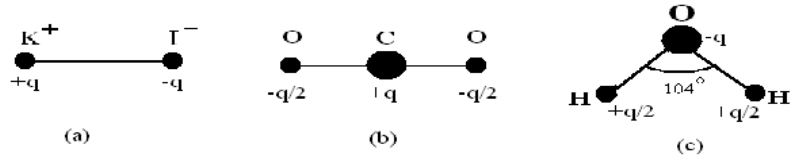

Figure: 5.3 Molecules structure of (a) KI, (b) CO_2 and (c) H_2O.

The mono-atomic molecules (He, Ne, Ar, Kr, Xe) and molecules consisting of two identical atoms linked by a homo-polar bond (H_2, N_2, Cl_2) are

non-polar, while the molecules of a typical ionic compound such as KI with a hetro-polar bond have a very high dielectric moment $\mu = 23 \times 10^{-30}$ Cm [1]. This moment is directed from the negatively charged ion I^- to the positively charged ion K^+, to which is shown in figure (5.3-a).

It is quite obvious that the polarity of a molecule is judged by its geometrical picture and actual arrangements of charges in space. A molecule of carbon dioxide exhibits symmetric structure with a centre of symmetry as shown in figure (5.3-b), and for this reason carbon dioxide is not polar; whereas a molecule of water has the form of isosceles triangle as shown in figure (5.3-c), therefore, water displays sharply pronounced polar properties with $\mu = 6.1 \times 10^{-30}$ Cm [1].

All hydrocarbons are non-polar or weakly polar substances. However in hydrocarbons, if hydrogen atoms are substituted by the atoms of halogens (F, Cl, Br or I) or by the groups (**-**OH, **-**NH_2, **-**NO_2, etc), the asymmetric molecules are formed in which $\mu > 0$.

Considering simplest hydrocarbon methane CH_4 and the products of substitution of hydrogen by chlorine are methyl chloride CH_3Cl, methylene chloride CH_2Cl_2, chloroform $CHCl_3$ and carbon tetrachloride CCl_4, whose structural formulae are as shown in figure (5.4).

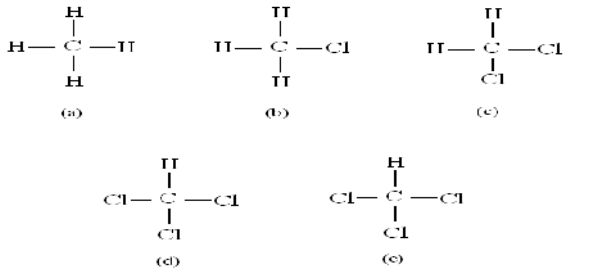

Figure 5.4: (a) methane, (b) methyl chloride, (c) methylene chloride, (d) Chloroform, (e) Carbon tetrachloride.

It is quite obvious that for methane $\mu = 0$. The molecules of CH_3Cl, CH_2Cl_2 and $CHCl_3$ are asymmetric and their values of μ are equal to 6.2×10^{-30} Cm, 5.17×10^{-30} Cm and 3.8×10^{-30} Cm ,respectively, but the molecule of CCl_4 is symmetric and its $\mu = 0$ [1].

The polarization is some ordering in space of the electrically charged particles with their displacement in a dielectric under the dipole moment in the entire volume of the dielectric and in each separate polarizing constituent (atoms, ions and molecules).

5.3 Polarization of Dielectrics

Linear dielectric show a direct proportionality between the induced dipole moment μ, acquired by the molecule during the process of polarization, and the electric field *E* acting on the molecule in dielectric material.

$$\mu = \alpha E \qquad (5.8)$$

The proportionality constant (α) is known as polarizability.

The polarizability reflects the properties of individual molecule of dielectric material and not of very large volume. Also it is the most important microscopic electrical parameter of a dielectric material.

There are four different types of polarizations operational, viz, electronic, ionic, orientational and space charge polarizations [1-2].

(i) Electronic Polarization

The electronic polarization occurs in all atoms or ions, which can be observed in all dielectrics irrespective of the presence of other types of polarizations. All materials consist of ions surrounded by electron clouds. As electrons are very light they have a rapid response to the external field. The electronic exchange of the number of ions in the crystals gives local

displacement of the electrons in the direction of applied field, which in turn gives rise to polarization. It is the displacement of electrons with respect to the atomic nuclei. To be more precise the displacement of electrons, under the action of external electric field, the electronic orbits occurs around the atomic nuclei. When the external electric field is superposed, this type of polarization occurs during a very brief interval of time (order of 10^{-15} sec) *i.e.* the time of the period of oscillations of ultraviolet rays [1].

(ii) Ionic Polarization

It is the mutual displacement of ions forming hetro-polar (ionic) molecule. A short time is required for the process of ionic polarization to set in but longer than for electronic polarization *i.e*. 10^{-12} to10^{-13} sec.

The bonds between atoms are stretched by applied electric fields when the lattice ions are charged. This is easily visualized with an alkali halide crystal in figure (5.5), where small deformation of the ionic bond will occur when a field is applied, increasing the dipole moment of the lattice.

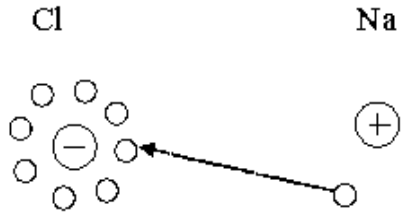

Figure: 5.5 Stretching of Alkalihallide bonds when ion is charged.

Altogether, the processes of electronic and ionic polarizations have much in common. Both phenomena may be regarded as the varieties of polarizations caused by the deformation which is displacement.

(iii) Orientational Polarization

The polar dielectrics exhibit tendency towards orientational polarization. According to Debye [3], this type of polarization is due to the rotation or

orientation of the molecules of a polar dielectric having a constant dipole moment in the direction of an electric field. In the original theory, the model of an orienting polar molecule was a sphere rotating in a viscous medium and overcoming a friction. If orientational polarization is considered more strictly it must be understood as the introduction by an electric field of certain orderliness in the position of polar molecules being in uninterrupted chaotic thermal motion and not as a direct rotation of polar molecules under the action of an electric field. For this reason, orientational polarization is connected by its nature with the thermal motion of molecules and temperature must exert an appreciable effect on the phenomenon of orientational polarization.

Orientational polarization can appear in a pure form only in gases, liquids and amorphous viscous bodies. In crystals at a temperature below the melting point the dipoles are said to be "frozen", *i.e.,* secured in their places so tightly that they can not be oriented and hence the orientational polarization can not occur in them. The orientational polarization sometimes, manifests itself in some crystals with loose packing of molecules, for example, water ice. In some cases for example in cellulose and its derivatives there may be rotations of not complete molecules but of their separate parts.

After a dielectric is energized or de-energized, the process of establishing a orientational polarization requires a relatively long time as compared with that of deformated orientational polarization.

This type of polarization occurs in liquids or gases when molecules having a permanent or induced dipole moment aligned along the applied field.

Physically, one may consider the dipole moments as trying to line up, but jostled by their thermal motion and not all of them are successful. Since the energy of dipole in an electric field *E* is given by

$$U = -\mu E \cos\theta \qquad (5.9)$$

According to statistical mechanics, the number of dipoles in a solid angle ($d\Omega$) is

$$= 2\pi \sin\theta \exp(\mu E \cos\theta / kT) \qquad (5.10)$$

Hence the average dipole moment is given as

$\langle \mu \rangle$ = Net number of the assembly / Total number of dipoles

Integrating in the interval of 0 to π, one yields

$$\frac{\langle \mu \rangle}{\mu_0} = L(a) = \coth a - 1/a \qquad (5.11)$$

Where, *L(a)* is called the Langevin function [4] and

$$a = \frac{\mu E}{kT} \qquad (5.12)$$

If *a* is small, which is true under the quite wide conditions, equation (5.12) may be approximated by, $\langle \mu \rangle = \frac{\mu^2 E}{kT}$ (5.13)

i.e., the polarizability is inversely proportional to the absolute temperature.

(iv) Space charge Polarization:

Space charge polarization is important in dielectric materials, which contain charge carriers that can migrate for some distance through the bulk of the material (via, e.g., diffusion, fast ionic conduction, or intercalation) thus creating a microscopic field distortion. Such a distortion appears to an outside observer as increase in capacitance of the sample and may be distinguishable from real rise of the dielectric permittivity. Space charge polarization is the only type of electrical polarization that is accompanied by a

macroscopic charge transport and in the case when the migrating charge carriers are ions, a macroscopic mass transport as well.

The electric response of a normal dielectric can be explained by its dielectric strength (breakdown strength), conductivity, dielectric loss, and dielectric constant. The behavior of nonlinear dielectric depends on the amplitude and time variation of the electric field.

Dielectric strength is defined as the maximum electric field, which can be applied to a dielectric without causing breakdown, the abrupt irreversible drop in resistively at high fields often accompanied by destruction of the material. Dielectric strength of most insulating materials is in the range from 10^4 to 10^7 V/m. at room temperature and low frequencies and it decreases at higher temperatures.

5.4 Permittivity in the Medium

In the general case of isotropic media, D and E are parallel vectors and ε is a scalar, but in anisotropic media it is rank-2 tensor (causing birefringence). The permittivity ε and magnetic permeability μ of a medium together determine the phase velocity v of the electromagnetic radiation through that medium, $\varepsilon \mu = \frac{1}{v^2}$

When an electric field is applied to a medium, a current flows and the current flowing in real medium is made up of two parts; such as conduction and displacement current. The displacement current can be considered as the elastic response of the material to the applied electric field. As the magnitude of the electric field increases, the displacement current is stored in the material when the electric field decreases the material releases the

displacement current. The electric displacement can be separated into the vacuum contribution and the contribution from the material as,

$$D = \varepsilon_0 E + P = \varepsilon_0 E + \varepsilon_0 \chi E = \varepsilon_0 E (1 + \chi) \quad (5.14)$$

Where, *P* is the polarization of the medium and χ is its susceptibility. The relative permittivity and susceptibility of a sample are related $\varepsilon_r = \chi + 1$.

5.4.1 Complex permittivity

In figure (5.6), the dielectric permittivity spectrum over wide range of frequencies is presented. Various processes such as ionic and dipolar relaxation, atomic and electronic resonance at higher energies are labeled.

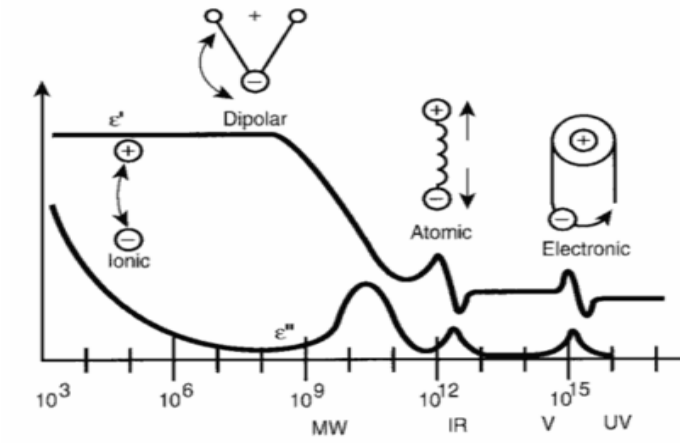

Figure: 5.6 Dielectric permittivity spectrum (www.wikipedia.org).

Unlike in vacuum, the response of normal materials to external fields depends on the frequency of the applied field. In fact, a polarization of material does not respond instantaneously to an applied field. For this reason the permittivity is often treated as a complex function of the frequency of the applied field [2, 5]. The definition of complex permittivity is

$$D_0 e^{i\omega t} = \varepsilon^*(\omega) E_0 e^{i\omega t} \quad (5.15)$$

Here, D_0 and E_0 are amplitudes of the displacement and electrical fields, respectively. The response of a medium to static electric fields is described by the low frequency limit of permittivity (also called the static permittivity) or dielectric constant ε_r or ε_s.

$$\varepsilon_S = \lim_{\omega \to 0} \varepsilon^*(\omega) \tag{5.16}$$

At high frequency limit, the complex permittivity is commonly preferred to as ε_∞. At plasma frequency and above, dielectric behave as ideal metals, with electron gas behavior. The static permittivity is a good approximation for the low frequency altering fields but as the frequency increases a measurable phase difference δ comes in to the picture between D and E. The frequency at which the phase shift becomes noticeable depends on the temperature and the details of the medium. For the moderate field strength (E_0), D and E remain proportional, therefore,

$$\varepsilon^* = \frac{D_0}{E_0} e^{i\delta} = |\varepsilon| . e^{i\delta} \tag{5.17}$$

As the response of the materials to alternating fields is characterized by a complex permittivity, it is needed to isolate the real and imaginary parts, and hence

$$\varepsilon^*(\omega) = \varepsilon'(\omega) - i\varepsilon''(\omega) = \frac{D_0}{E_0}(\cos\delta - i\sin\delta) \tag{5.18}$$

Where, ε' is the real part of the permittivity and ε'' is the imaginary part of the permittivity. The ε'' is related to the rate at which energy is absorbed by the medium and converted into thermal energy [5].

The complex permittivity is generally a complicated function of frequency, because it is a superimposed description of dispersion phenomena

occurring at multiple frequencies. The dielectric function $\varepsilon(\omega)$ must have poles for frequencies with positive imaginary parts and, therefore, satisfies the Kramers- Kronig relations. At a given frequency, the imaginary part (ε'') of the permittivity leads to absorption loss or gain depending on its sign; leads to absorption loss, if its value is positive and leads to gain, if its value is negative. More commonly, the imaginary part of the eigen values of the anisotropic dielectric tensor should be considered.

5.4.2 Classification of Materials

Materials can be classified as per their permittivity.

(1) Materials with negative real part of permittivity.

Metals are usually having negative real part of permittivity and propagation of electromagnetic waves exists.

(2) Materials with positive real part of permittivity

Dielectric materials exhibit this nature.

Distinction is often made for semiconductors and dielectrics. A non-polar material is having no permanent dipoles, for example, silicon, germanium and carbon (diamond). The III-V compounds such as GaAs, InSb and GaP share their valance electrons in such a manner that the ions forming the lattice tend to be positive (group-V) or negative (group- III). Hence, the lattice is a mass of permanent dipoles whose moment can be changed by applied field. There are compounds, such as hydrocarbons (C_6H_6 and paraffin) having permanent dipole arrangements but surprisingly zero net dipole moment. There are molecules like water and many transformer oils that have permanent dipole moments and the total dipole moment is determined by their orientational polarizability.

Depending upon the frequency range under investigation the experimental method of measuring dielectric constant varies. For frequencies below 10^9 Hz the permittivity or impedance of a dielectric sample, inserted in a parallel plate capacitor, can be measured by suitable circuits. A Schering bridge arrangement is used up to 10^7 Hz and a resonance circuit is employed in the range of 10^4 to 10^9 Hz. In the case of frequencies above 10^8Hz, the dielectric constant may be determined by measuring the interaction of electromagnetic waves with the medium. From 10^8 to 10^{11} Hz the material is generally inserted in wave-guides or co-axial lines and the standing wave patterns are measured. However at still higher frequencies, optical techniques involving reflections and transmission measurements are employed.

The applicability of dielectric materials not only requires the knowledge of their electric properties, but also their general physical and chemical properties, such as, mechanical strength, elasticity, resistance to heat and cold, thermal conductivity, hygroscopic, stability, crystalline structure and other parameters.

There are many applications of dielectric materials. Because the dielectric constant is related to the chemical structure, it can be used for both qualitative and quantitative analysis. If the dielectric constants for all constituents except one constituent, in a multi-component system, are similar and there is little interaction between them in solution, then the unique component can often be determined. Interestingly, in the analysis for toluene in the presence of complex mixtures of aliphatic hydrocarbons in petroleum refining as well as determining moisture in cereal grains and other solids uses

this type of dielectric measurement techniques. When the nominally electric insulating material is placed in a varying electrostatic field, the heating effect of a material due to its own electric (dielectric) losses is known as dielectric heating. The material to be heated is placed between two metallic electrodes and high frequency signals of 2 to 90 MHz are applied by high frequency oscillator. The resultant heat is generated within the material and in the homogeneous materials it is through out uniform.

Solid dielectrics are employed for the vast majority of commercial applications. Important solid dielectrics include many ceramics and glasses; plastics and rubber; minerals such as quartz, mica, magnesia, and asbestos; and paper and fibrous products. The mechanical and thermal properties as well as the electrical response are important in the choice of dielectric for a particular product. For high mechanical strength and temperature resistance, ceramic and mineral insulators are preferred, while plastic and rubber are employed where flexibility is desired. Low-loss non-polar dielectrics, such as polyethylene or polystyrene, are necessary for many ultra high frequency applications.

The material requirements for dielectric devices are usually determined by the specific electrical characteristics desired for the operating frequencies selected. Semiconductors, such as silicon and germanium, and piezo-electric or ferroelectric ceramics, including heavy metal titanates, zirconates, and niobates, have found considerable application. Many authors have discussed various dielectric properties, dielectric applications and dielectric theories in details [6-11]. Classical theory of dielectric constant was also been given by Kachhava and Saxena [12].

5.5 Dependence of Permittivity on Various Factors

The permittivity ε depends on the external factors such as frequency of applied voltage to the dielectric material, temperature, pressure, humidity etc [7]. This has been summarized hereby briefly.

The permittivity of nonpolar dielectrics does not depend on frequency, when it is changed within very broad range. On the other hand, in the case of polar dielectrics when the frequency of alternating voltage increase the value of ε remains invariable, initially, but beginning with certain frequency f_0 the polarization fails to settle itself completely during one half cycles and ε begins to drop at very high frequencies. The value of f_0 can approximately be obtained if relaxation time (τ) is equated to half period $1/2f_0$ of voltage, when

$$f_0 = \frac{kT}{8\pi\eta r^3} \qquad (5.19)$$

Where, η - Dynamic viscosity, r – Radius of the molecule, T - Absolute temperature and k - Boltzmann constant.

In the case of water τ is estimated to be the order of 10^{-11} sec, hence the value of f_0 should be of order of 10^{11} Hz. A phenomenon of migrational polarization is observed in inhomogeneous trielectrics, particularly in dielectrics with water inclusions. The phenomenon of so called resonance polarization may cause maxima in ε at very high frequencies.

Temperature is not expected to affect the process of electronic polarization in non-polar dielectrics. A relative sharp change in ε of non-polar dielectric is observed for temperature variation when crystalline material goes

into transition to liquid. The nature of dependence of permittivity on temperature may be different in solid ionic linear dielectrics. In most cases, an ionic mechanism of polarization permittivity increases when temperature grows. Generally, the molecules can not orient themselves in polar dielectrics in the low temperature region. When the temperature is raised the orientation of dipoles is facilitated, and this increases permittivity.

As temperature grows the chaotic thermal oscillation of molecules are intensified and the degree of orderliness of their orientation diminishes. This causes the curve of ε *Versus Temperature to pass through the maximum end then drop. Also, in case of chemically individual polar material jump like change in* ε observed at the melting point.

In the dielectrics, which obey the Clausius- Mosotti law, the magnitude of permittivity increases when pressure rises because the density of substance increases.

Moreover, the permittivity of hygroscopic dielectrics is smaller than the permittivity of water. The permittivity is expected to increase with moistening.

A strong dependence of permittivity on the applied voltage to dielectrics is typical in ferroelectrics. As regards in linear dielectrics the permittivity can be assumed practically independent of voltage, however, a saturation effect can be expected in polar liquid and gases.

5.6 Dielectric Losses

Dielectric study has been carried out by various workers. In this brief survey an overview is given on dielectric study carried out on different materials, however, a focus is made on the NLO type KDP and ADP crystals and their different doped systems. When an electric field acts on any material

the latter dissipates a certain quantity of electrical energy that transforms into heat energy. This phenomenon is commonly known as "the expense" or "loss of power", meaning an average electric power dissipated in material during a certain interval of time. As a rule the loss of power in a specimen of material, all other conditions being equal, is directly proportional to the square of the voltage applied to the specimen ($P = V^2/R$). The amount of power loss in a dielectric under the action of the voltage applied to it is commonly known as "dielectric loss". This is general term determining the loss of power in an electrical insulation both at a direct and an alternating voltage.

The process can be represented by simple position of in phase and out of phase components of dielectric constant. For alternating voltage the permittivity can therefore be written by equation (5.18) as,

$$\frac{\varepsilon''}{\varepsilon'} = \tan\delta = \text{dielectric loss} \qquad (5.20)$$

In practice, ε' is independent of the frequency of applied field but ε'' is associated with power absorption. For static fields $\varepsilon'' = 0$.

5.7 Dielectric Study of Different Materials

Dielectric study has been carried out on different materials by various workers. In this brief survey an overview is given on dielectric study carried out on different materials, however, a focus is made on the NLO type KDP and ADP crystals and their different doped systems. Dielectric studies on single crystalline materials [13], ceramics [14-15], glasses [16-18], acrylic acid doped ethyl cellulose films [19], poly (N- Methyl Pyrrole) thin films [20], copper ferrite- barium titanate composites [21] and Zn- substituted cobalt ferialuminates [22] have been reported.

In the present author's laboratory, the dielectric property of many crystals were studied earlier, for example, organic molecular crystals 4-(2-hydroxyphenylamino)–pent–3-en-2-one [23], calcium pyrophosphate crystals [24], Mn^{+2} [25] and Cu^{+2} [26] doped calcium tartrate crystals, pure and mixed iron manganese levo tartrate crystals [27] and zinc tartrate crystals [28].

It is important to study the effect of irradiation on dielectric properties. The dielectric properties of barium strontium borate, a NLO crystal, was investigated by Ishwar Bhat et al [29], before and after irradiation by 8 MeV electrons as well as silver ions of 120 MeV. It was found that there was an increase in the dielectric constant due to swift heavy ion irradiation as well as due to electron irradiation. The effect of swift heavy ions on the dielectric properties of doped and undoped ammonium dihydrogen phosphate (ADP) crystals was also investigated by Ishwar Bhat et al [30]. The increase in dielectric constant was found to be dependent on dopants in the crystals and electronic energy loss in the crystals. The effect of swift heavy ion (SHI) irradiation of doped and undoped ADP crystals has been studied by Bhat et al [31]. The change in the dielectric constant was noted after the irradiation and the increase in dielectric constant was found to be dependent on dopants in the crystals and electronic energy losses in crystals.

Ananda Kumari and Chandramani [32] have studied dielectric properties of Au^{+} doped/undoped KDP crystals containing KI/NaI with varying frequency at room temperature. They have found that the dielectric constant decreases with increase in frequency of applied field. Ambujam et al [33] have measured the dielectric properties of γ-glycine single crystals (an organic NLO material).

Dielectric studies on L-threonine monohydrochloride dihydrate single crystal have reported by Ramesh Babu et al [34].

Various parameters affect the dielectric properties. Doping of various impurity ions changes the dielectric and optical properties. The presences of aqueous solution of 5-10% $(NH_4)_2Cr_2O_7$ causes decrease in dielectric constant D_{11} and D_{33} and asymmetry of the electro-optic coefficient r_{63} of ADP crystals [35]. Studies on the dielectric properties of potassium hydrogen phthalate single crystals have shown that the dielectric constant and dielectric loss increase rapidly in the vicinity of the decomposition temperature [36].

The dielectric properties of ADP type crystals were investigated using the antiferroelectric version of extended pseudo-spin model [37]. This model was also applied to KDP. In this model the transverse polarization induced by proton displacement along the hydrogen bond is considered. The Hamiltonian is based on four-sublattice version of Slater-Takagi protonic configurations around PO_4 groups, which also includes long range antiferroelectric interaction energy.

In one study, the impedance data were obtained as a function of frequency and temperature between 40-150^oC for ADP crystals [38]. The frequency dependent conductivity followed Jonscher's dynamical law with relaxation, $\sigma(\omega) = \sigma(0) + B\omega^n$

Where, ω is the frequency of applied ac field and *B* is the constant.The obtained value of *n* decreased from 1.0 to 0.25 as the temperature raised. The electrical conductivity at low temperatures below 70 ^oC was attributed to the hopping of protons m O-H-O hydrogen bonds among the vacancies. The activation energy of migration was 0.12 eV in this extrinsic region. However,

at temperature from 70 to 79 ^{o}C, additional defects were created by breaking the stronger hydrogen bond in ammonium groups. At temperature above 97 ^{o}C, ammonium ions in the crystal were proposed to have contributed for the electrical conduction.

Recently, Ambujan [39] studied the effect of cation doping (Mg^{+2}, Cu^{+2}, Ni^{+2} and Ca^{+2}) in KDP crystals on their dielectric properties. The variation of dielectric constant with frequency suggested that as the frequency increased the dielectric constant decreased and at high frequency the leveling of the plot to the X-axis was observed. The pure KDP crystals exhibited the least values of dielectric constant. It was observed that due to change in the sizes of the metal dopant ions, there was change in the value of dielectric constant at any particular frequency. The polarizability was expected to increase as the ions were smaller and highly charged. Ambujan [39] could observe the increase in the value of dielectric constant of doped sample in accordance with the ionic radii of the metallic dopant.

KDP crystallizes in tetragonal crystal system with space group 14 2d. The crystal structure consists of PO_4 tetrahedral joined by four hydrogen bonds to neighboring PO_4 tetrahedral in such a way that each PO_4 tetrahedral has two hydrogen atoms associated with it giving $(H_2PO_4)^-$ ion. The PO_4 group and K^+ ions are built up in such a way that K and P atoms alternate each other at a distance of $c/2$ along the c-axis. During the metal ion substitution the hydrogen bond in the structure break down giving rise to the loosening of the hydrogen and the creation of additional charged defects. These lattice defects cause the increased space charge contribution.

Dielectric study of NLO material is very important because the operation of electro-optic devices is based on the Pockel's effect in which the change in the dielectric constant is a linear function of applied field [40]. Microelectronics industry requires replacement of dielectric materials in multi-level inter connect structures with new low dielectric constant materials as an interlayer dielectric (ILD), which surrounds and insulates interconnecting wirings. Lowering the dielectric constants of the ILD decreases the RC delay, lowers the power consumptions and reduces the "crosstalk" between the nearby interconnects [41]. Therefore, many attempts were made to study the reduction dielectric constant values of the doped systems.

The electrical characterizations of L-histidine doped KDP and ADP has been reported by Meena and Mahadevan [42]. It has been found that the σ_{dc} (d.c conductivity), ε_r (dielectric constant), σ_{ac} (a.c conductivity) and $tan\delta$(dielectric loss) values increase with temperature and decrease with impurity concentration in KDP and ADP crystals along both *a*- and *c*-directions. The values have been found more for ADP crystals than that for KDP crystals. The electrical conductivity of KDP type crystals can be determined by the proton transport within the framework of hydrogen bonds [43]. Two mechanisms can be proposed, which are, (1) considering similarity to the conductivity mechanism in ice having hydrogen bonds [43] and (2) considering conductivity associated with the incorporation into the crystal lattice of impurities having different valences and the formation of corresponding defects in the ionic crystals [44]. It has been assumed that the conductivity of ice is obtained by the simultaneous presence of positive and negative ions and orientational defects – vacant hydrogen bonds (L-defects)

and doubly occupied hydrogen bonds (D-defects). Other possible defects are vacancies and defect associates [43]. The temperature dependence of conductivity has lead Meena and Mahadevan [42] to consider that the conductivity of KDP crystals can be determined by both thermally generated L-defects and the foreign impurities incorporated into the lattice and generating the L-defects there Lokshin [45] assumed that $(HPO_4)^{-2}$ ions are also responsible for the formation of vacant hydrogen bonds (L-defects). Therefore, it is easy to understand from this discussion that the proton transport depends on the generation of L-defects. The increase of conductivity with increase in temperature for L-histidine doped KDP and ADP crystals [42] can be due to the interstices which are expected to be occupied by L-histidine molecules in KDP. This induces bulk defect states due to competition in getting the sites for the L-histidine molecules to occupy. The L-histidine molecules can be added to some extent in addition to the replacement of ions in the KDP and ADP lattice and creating additional hydrogen bonds. As the conduction in KDP and ADP occurs through protons and mainly due to the anions $(H_2PO_4)^-$ ions and not due to the cations (K^+, NH_4^+), the additional hydrogen bonds created may reduce the L-defects and consequently obstruct the movement of protons. This is the possible explanation given by Meena and Mahadevan [42] for the decrease in the conductivity value with increase in impurity concentration. The addition of L-histidine leads to decrease electrical parameters such as σ_{dc}, $\sigma_{ac,}$ ε_r and $tan\delta$ for both KDP and ADP crystals, which has lead Meena and Mahadevan [42] to conclude that L-histidine addition makes possible for the KDP and ADP crystals to become low ε_r value dielectrics. Moreover, the dielectric study of amino acids (L-

glutamic acid, L-histidine and L-valine) doped KDP crystals was carried out by Kumaresan and Kumaresan [46, 47]. The authors found that on doping of amino acids the value of dielectric constant of KDP crystals decreased and also decreased with increase in the frequency of applied field. Moreover, L-arginine, L-histidine and glycine doped KDP crystals were grown by Kumar and Babu [48]. They have studied the dielectric behavior and found the dielectric constant and dielectric loss less in doped crystals in compare to pure KDP crystals.

Udupa et al [49] have found for KDP crystals that the dielectric constant decreases with the increase of temperature at all frequencies studied. The same authors also have observed the appreciable increase in the value of dielectric constant after impurity (MgO) addition and decrease in its value with increase in frequency.

An anomalous dielectric behavior in ferroelectric KDP was noticed by Gilchrist [50]. The dielectric permittivity $\varepsilon = \varepsilon' - \varepsilon''$ of KDP pressed powder was measured between temperature from 1.4 K to 25 K in the presence of d.c. electric field bias. Usually, if the bias was switched at time t = 0, the ε' and ε'' would jump to new values and then decrease approximately as $\log t$ ($6 < t < 20000$ *S*). This well-know effect, which is also found in single crystals, can be attributed to the switchable micro-domains present accidentally in crystals but present more in powders. A very different type of after effect was observed in a narrow temperature range from 7 K to 8 K. The ε' jumped to lower value, thereafter increased with t according to a stretched exponential with a temperature dependent time constant. This is similar to the extrapolation of the Arrhenius law of known but unassigned weak-field

dispersion i.e. a property of poly-domain single crystals as well as powders. The weak field dispersion is due to the elementary movement of a jog on a lateral step displacement of a domain wall, consisting of a single H-bond reversal. This is anomalous effect results from the interaction between these point defects and the micro domain systems.

Moreover, the high frequency dielectric measurements were carried on Lithium ion added KDP crystals in X-band region (8 to 12 GHz) of microwave frequencies at room temperature by Shirsat et al [51]. The authors selected three different lengths of crystals. Initially the standing wave pattern was obtained for with and without sample and the wavelength was determined and then the dielectric constant was calculated by using the suitable formula [52]. Also, in another study the dielectric constant values were obtained comparatively low for Li^+ ion added KDP crystals than the pure KDP crystals within the frequency range 8 GHz to 12 GHz. This suggested that the Li^+ ion added KDP crystals were more suitable for high speed electro-optic modulation than pure KDP crystals [53]. Similarly high frequency dielectric study of thiourea doped KDP crystals was carried out in X-band region of micro-wave frequency by Hussain et al [54]. They also found that the dielectric constant of thiourea doped KDP was less than the pure KDP crystals.

In the present chapter, the dielectric properties of different amount of (0.3, 0.4 and 0.5 weight percentage) L-histidine, L-threonine and DL-methionine doped KDP crystals are reported. The single crystals of pure and amino acid doped KDP crystals were grown by the slow aqueous solution evaporation technique, which is described in Chapter-II.

5.8 Dielectric Measurments

.**Figure (5.7-a): LCR meter**

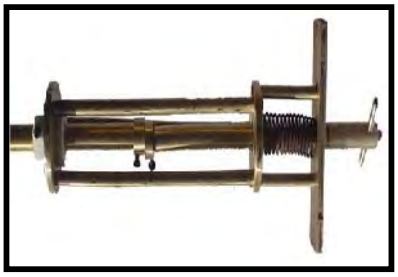

Figure (5.7-b): The sample holder

Suitably made pellet (sample) are subjected to dielectric studies using Agilent 4274A LCR meter in the frequency range from 100 Hz to 1 MHz. Agilent 4274A LCR meter available in Physics Department of Saurashtra University, is capable of measuring different parameters such as capacitance and dielectric loss for various applied frequencies. Figure (5.7-a) shows the photograph of the set up and the figure (5.7-b) shows the design of spring-loaded sample holder. By placing a pellet form of sample between the two copper electrodes, a parallel plate capacitor was formed. The capacitance (*C*) of the sample was noted for the applied frequency that varied from 100 Hz to 1 MHz at room temperature. The dielectric constant ε_r was calculated using the relation,

$$\varepsilon_r = \frac{Cd}{\varepsilon_0 A} \qquad (5.21)$$

Where, *d* is the thickness of the pellet, ε_0 is the vacuum dielectric constant (permittivity of free space) and *A* is the area of the pellet.

The dielectric loss is a measure of the energy absorbed by dielectric. It is known that in a capacitor, the dielectric material usually has a resistance *R* and reactance $1/\omega C$. Which are related to the phase angle $\tan\delta = 1/\omega CR$.

Here, the *tan δ* is referred to as the dielectric loss. The dissipation factor is measured along with the capacitance at room temperature using the LCR meter. The dielectric loss *tan δ* is obtained by using the following relation,

Dielectric loss (tan δ) = Dissipation factor

The high value of dielectric constant at low frequencies may be due to the contributions from all the four polarizations, namely, electronic, ionic, orientational and space charge polarizations. The space charge depends on the purity and perfection of the material. Its influence is noticeable in the low frequency region [55]. The orientational effect can some times be seen in some materials even up to 10^{10} Hz. Ionic and electronic polarization always exist below 10^{13} Hz [56].

5.9 Dielectric Study of Pure and Amino Acid Doped KDP Crystals

Figure (5.8) shows the plots of dielectric constant versus frequency of applied field for pure and L-histidine doped KDP crystals. It can be observed that as the frequency of applied field increases the dielectric constant decreases and for high frequency region it remains almost constant. This can be explained on the basis of polarization. The electronic exchange of the number of ions in the crystals gives local displacement of electrons in the direction of the applied field, which in turn is expected to give rise to the polarization. As the frequency of the applied field increases, a point will be reached where the space charge cannot sustain and comply with variation of the external field and hence the polarization decreases. This further gives the diminishing values of dielectric constant with increase in frequency. The dielectric constant of pure KDP crystal is higher than the doped KDP crystals.

It has also been found that the value of dielectric constant decreases as the amount of doping of L-histidine increases.

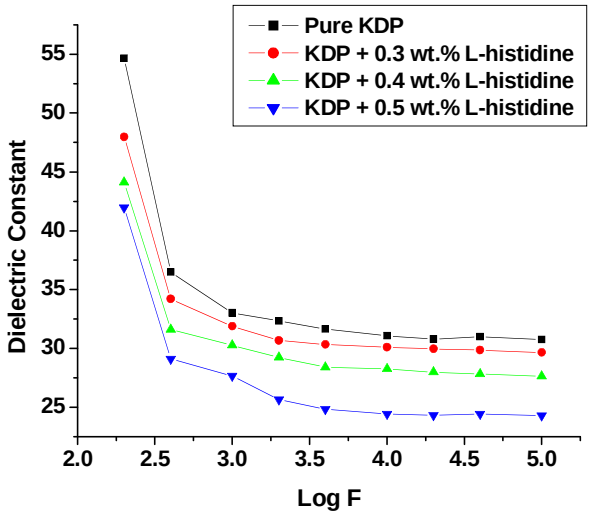

Figure: 5.8 Plots of Dielectric constant versus frequency of applied field for pure and L-histidine doped KDP crystals.

Figure (5.9) and (5.10) show the plots of variation of dielectric constant with frequency for L-threonine doped KDP crystals and DL-methionine doped KDP crystals, respectively. These figures show the similar nature as depicted by figure (5.8) for pure and L-histidine doped KDP crystals.

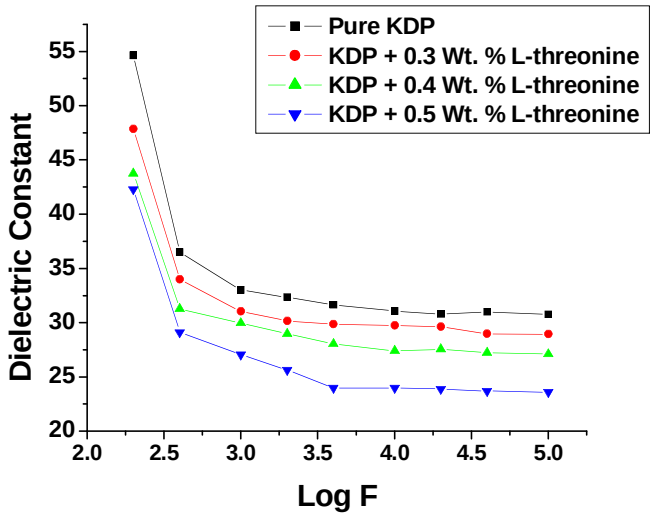

Figure: 5.9 Plots of Dielectric constant versus frequency of applied field for pure and L-threonine doped KDP crystals.

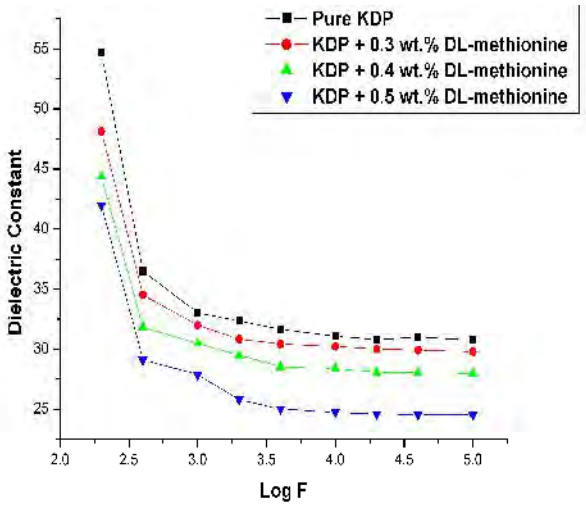

Figure: 5.10 Plots of Dielectric constant versus frequency of applied field for pure and DL-methionine doped KDP crystals.

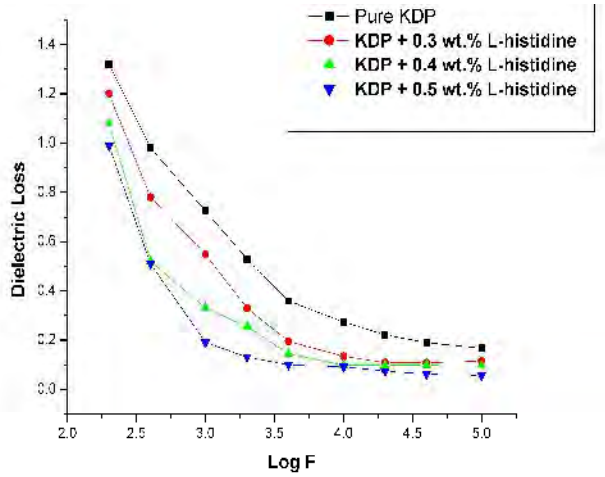

Figure :5.11 Plots of dielectric loss versus frequency for pure and L-histidine doped KDP crystals.

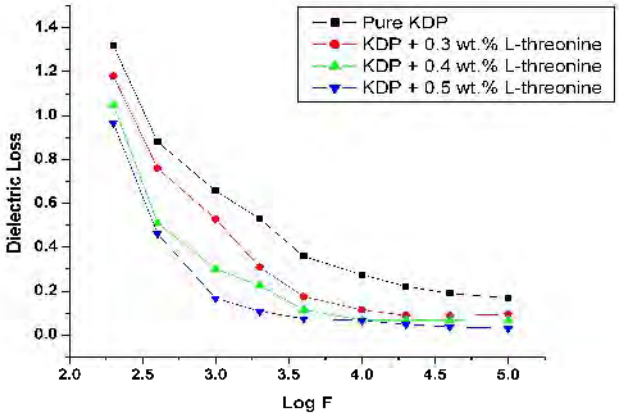

Figure:5.12 Plots of dielectric loss versus frequency for pure and L-threonine doped KDP crystals.

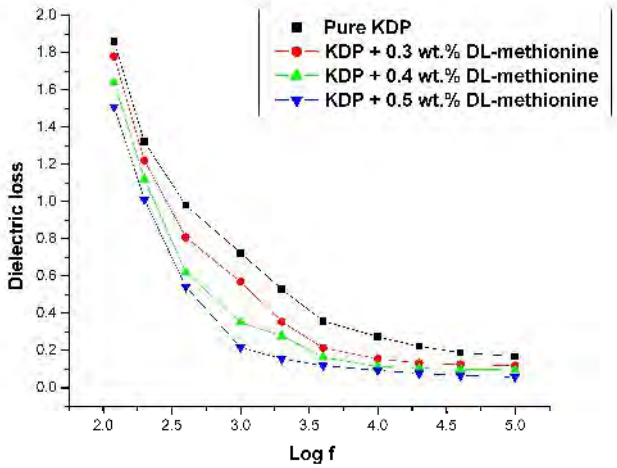

Figure: 5.13 Plots of dielectric loss versus frequency for pure and DL-methionine doped KDP crystals.

Figure (5.11) exhibits the variation dielectric loss (*tan* δ) with frequency for L-histidine doped KDP crystals. From the figure one can notice that as the frequency increases the dielectric loss decreases. Also, the dielectric loss decreases as the amount of doping increases in the crystals. The high amount of doping makes the crystals less lossy. The similar nature was observed for L-threonine and DL-methionine doped KDP crystals, which has been shown in figures (5.12) and (5.13), respectively.

The value a.c. resistivity is calculated by using the expression,

$$\rho_{ac} = \frac{A}{2\pi fCd} \tag{5.22}$$

Where, *d* is the thickness of the pellet, *C* is the capacitance, *f* is the frequency and *A* is the area of the pellet.

Figure (5.14) shows the plots of a.c. resistivity versus frequency of applied field for pure and L-histidine doped KDP crystals. It can be noticed that as the frequency increases the a.c. resistivity decreases. It can also be noticed that the value of a.c. resistivity is the least for pure KDP crystals and progressively increases on increasing the doping concentration. The similar

nature has been found for L-threonine and DL-methionine doped KDP crystals, in figures (5.15) and (5.16), respectively.

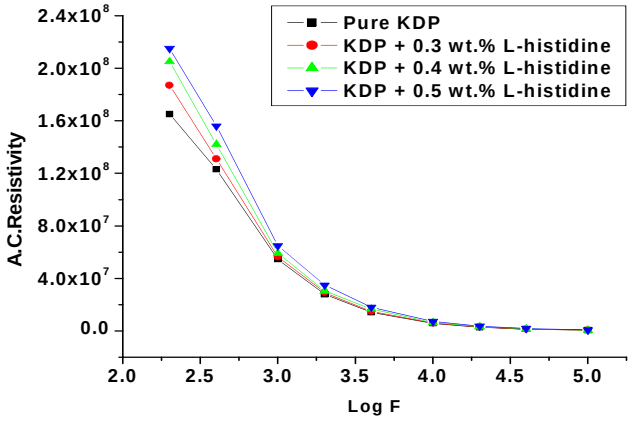

Figure: 5.14 Plots of a.c. resistivity versus frequency for pure and L-histidine doped KDP crystals.

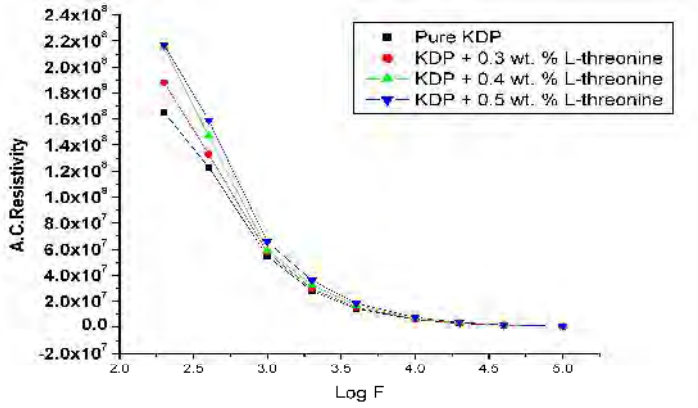

Figure: 5.15 Plots of a.c. resistivity versus frequency for pure and L-threonine doped KDP crystals.

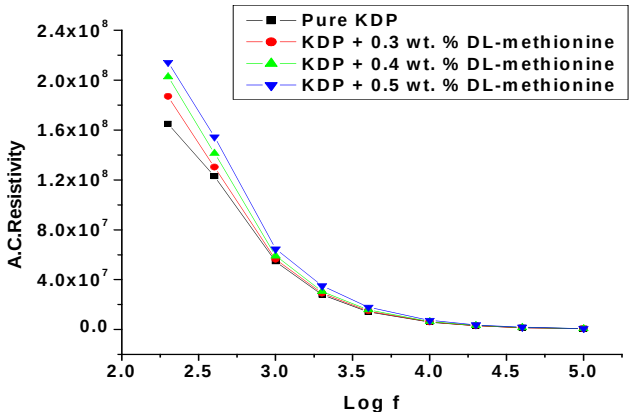

Figure:5.16 Plots of a.c. resistivity versus frequency for pure and DL-methionine doped KDP crystals.

The conduction in KDP occurs through protons and mainly due to anions; the additional hydrogen bonds created may reduce the L-defects and as a result obstruct the movement of protons. This corresponds to the observation of Meena and Mahadevan [42] that the a.c. resistivity values increases on increasing amino acid doping concentration. The addition of amino acid decreases *tan* δ and dielectric constant values of KDP crystals in comparison to pure KDP crystals, this also corresponds to the earlier reported observation [42]. The significant lowering of dielectric constant on increasing the amino acid can make the doped KDP crystals good candidates for electro-optic applications.

Conclusion

1. The dielectric constant of pure and amino acids doped KDP crystals decreased as the frequency of applied field increased and ultimately became constant at high frequency. This might be due to the dipoles could not comply with the rapid changes in the alternating electric field.
2. At any range of frequency the dielectric constant of the doped KDP crystals was found to be lower than those for pure KDP crystals, which might be due to generation of L-defects on addition of amino acids.
3. As the doping of amino acids increased the dielectric loss of KDP crystals decreased. The nature of the variation of dielectric loss with frequency was similar to that of the dielectric constant with frequency. The low values of dielectric loss in doped crystals indicated that the doping of amino acids did not bring major defects.
4. The variation of a.c. resistivity with frequency of applied field suggested that the resistivity decreased with increasing the frequency and its value increased on increasing the amount of amino acids doping.

References:

1. B.S. Saxena, R.G. Gupta, P.N. Saxena, "*Fundamental of Solid State Physics,"* Pragati Prakashan, Meerut, India, 12th Eds. (2008).
2. A. J. Dekker; *"Solid State Physics"* Mac Millan India Ltd. (1998).
3. P. Debye, *Phys. Z.* **13** (1912) 97.
4. P. Langevin, *J. Physque* **4** (1905) 678.
5. http://en.*wikipedia.org*/wiki/Dielectric.
6. L. Solymar, D. Walsh, *"Lectures on the Electrical Properties of Materials"* Oxford University Press, New York (1984).
7. B. Tareev, "*Physics of Dielectric Materials"* Mir Publishers, Moscow (1975).
8. N. E. Hill, W. E. Vaughan, A. H. Price, M. Davies, *"Dielectric Properties and Molecular Behavior",* Van Nostrand Reinhold, Landon (1969).
9. J. C. Anderson, *"DielectrIcs",* Chapman and Hall, London, (1963).
10. J.B. Birks, J. Hart, "*Progress in Dielectrics"* Vol. I-V, Heywood, London (1959-1963).
11. F. Barsoukov, J.R. Mac Donald, *"Impedance spectroscopy: Theory, Experiment and Application"* Wielly, (2005), New York.
12. C. M. Kachhava, S. C. Saxena, *Indian J. Phys.* **41** (1967) 440.
13. L. Sirdeshmukh, K. Krishna Kumar, S. Bal Laxman, A. Ram Krishna, G. Sathain, *Bull. Mater. Sci.* **21** (1998) 219.
14. P. S. Ram Shastry, G. S. Kumar, T. Bhimasankaran, G. Prasad, *Bull. Mater. Sci*. **22** (1999) 59.
15. J. Koshy, J. Kurian, R. Jose, A. M. John, P. K. Sajita, J. James, S.P. Pai, R. Pinto, *Bull. Mater. Sci*. **22** (1999) 243.

16. A. V. Ravi Kumar, B. A. Rao, N. Veeraiah, *Bull. Mater. Sci.* **21** (1998) 341.

17. M. K. Murthy, K. S. N. Murthy, N. Veeraiah, *Bull. Mater. Sci.* **23** (2000) 285.

18. D. K. Durga and N. Veeraiah, *Bull. Mater. Sci.* **24** (2001) 421.

19. P. K. Khare, S. K. Jain, *Bull. Mater. Sci.* **23** (2000) 17.

20. A. K. Narula, R. Singh, S. Chandra, *Bull. Mater. Sci.* **23** (2000) 227.

21. R. P. Mahajan, K. K. Patankar, M. B. Kothale, S. A. Patil, *Bull. Mater. Sci.* **23** (2000) 273.

22. N.H. Vasoya, V.K. Lakhani, P.U. Sharma, K.B. Modi, R. Kumar, H. H. Joshi, *J. Phys: Condens. Matter.* **18** (2006) 1.

23. B. B. Parekh, D.H. Purohit, P. Sagayaraj, H.S. Joshi , M.J. Joshi, *Cryst. Res. Technol.* **42** (2007) 407.

24. B. B. Parekh, M.J. Joshi, *Cryst. Res. Technol,* **42** (2007) 127.

25. S. R. Suthar, M.J. Joshi, *Cryst. Res. & Technol,* **41** (2006) 664.

26. S. R. Suthar, S.J. Joshi, B.B. Parekh , M.J.Joshi, *Indian J. Pure & Appl. Phys.* 45 (2007) 52.

27. S. J. Joshi, B. B. Parekh, K. D. Vohra, M. J. Joshi, *Bull. Mater. Sci.* **29** (2006) 307.

28. R. M. Dabhi, B. B. Parekh, M.J. Joshi, *Indian J. Phys.* **79** (2005) 503.

29. S. I. Bhat, P. M. Rao, V. Upadhyaya, H.S. Nagaraja, *J. Cryst. Growth* **236** (2002) 318.

30. S. I. Bhat, N. G. Nayak, V. Rao, V. Ganesan, H.S. Nagaraja, D. K. Avasthi, *J. Cryst. Growth* **36** (2003) 695.

31. A. P. Bhat, P.S. Aithal, P. Mohan Rao, D. K. Avasthi*, Nuclear Instr & Methods in Phys. Res Sect. B.* **964** (2000) 166.
32. R. Ananda Kumari, R. Chandramani, *Bull. Mater. Sci.* **26** (2003) 255.
33. K. Ambujam, S. Selvakumar, D. Prem Anand, G. Mohamed, P. Sagayaraj, *Cryst. Res. Technol.* **41** (2006) 671.
34. R. Ramesh Babu, K. Sethuraman, N. Vijayan, G. Bhagavannarayana, R. Gopalkrishnan, P. Ramasamy, *Cryst. Res. Technol.* **41** (2006) 906.
35. J. Eisner, *Phys.Lett.* **A 47** (1974) 375.
36. K. B. R. Verma, A.K. Raychaudhury, *J. Phys. D: Appl. Phy*. **22** (1989) 809.
37. S. Havlin, E. Litov, H. Sompolinsky, *Phy.Rev.* **B14** (1976) 1297.
38. R. H. Chen, Chen-Chien Yen, C.S. Shem, T. Fukami, *J. Appl. Phys.* **98** (2005) 044104.
39. K. Ambujan, *Ph.D. Thesis, University of Madras*, India, 2005.
40. G. T. Boyd, *J. Opt. Soc. Am.* **B6** (1989) 685.
41. B. T. Hatton, K. Landskron, W.J. Hunks, M.R. Benett, D. Shukarias, D.D. Perovic, G.A. Ozinn, *Mater Today* **9** (2006) 22.
42. M. Meena, C.K. Mahadevan, *Cryst. Res. Technol.* **43** (2008) 166.
43. L. B. Harris and G.J. Vella, *J.Chem. Phys.* **58** (1973) 4550.
44. A. Holden, *"The Nature of Solids",* Columbia Press, New York, 1968.
45. E. P. Lakshin, *Crystallogr. Rep*. **41** (1996) 1070.
46. P. Kumaresan, S. Moorthy Babu, P.M. Anbarasan, *Optical Materials* **30** (2008) 1361.
47. P. Kumaresan, *Ph. D Thesis, Anna University*, India, 2008.
48. B. S. Kumar, K.R. Babu, *Indian J. Pure & Appl Phys*. **40** (2008) 123.

49. K. S. Udupa, P. M. Rao, S. Aithal, A.P. Bhatt, D.K. Avasthi, *Bull Mater.Sci.* **20** (1997) 1069.

50. J. Gilchrist, *Phys. Rev.* **B6** (2000) 6547.

51. M. D. Shirsat, S.S. Hussaini, N.R. Dhumane, V.G. Dongre, *Cryst. Res. Technol.* **43** (2008) 756.

52. R. R. Babu, N. Vijaynan, R. Gopalkrishnan, P. Ramasamy, *Cryst. Res. Technol.* **41** (2006) 405.

53. R. Mohankumar, RajanBabu, D. Jayaraman, R. Jayavel, K. Kitmura, *J. Cryst. Growth* **275** (2005) 1935.

54. S. S. Hussaini, N. R. Dhumane, G. Rabbani, P. Karmuse, V. G. Dongre, M. D. Shirsat, *Cryst. Res. Technol.* **42** (2007) 1110.

55. K. V. Rao, A. Smakula, *Mater. Res. Bull.* **6** (1965) 2031.

56. B. Narsimha, R. N. Choudhary, K. V. Rao, *J. Mater. Sci*. **23** (1988) 1416.

Chapter VI

UV-Vis Spectroscopic and SHG Efficiency Studies of Pure and L-histidine, L-threonine and DL-methionine Doped KDP Crystals

6.1 Introduction

Nonlinear optical (NLO) materials play a vital role in the fabrication of optoelectronic devices. Recent interest is focused on the development of materials which have suitable NLO properties for use as the active media in efficient second harmonic generators, tunable parametric oscillators and broadband electro-optic modulators. In this regard, a large number of compounds are needed to be screened for NLO applications. The Kurtz powder technique represents the first real means of screening experimentally large numbers of unknown materials for non linear activity without the need of growing good quality crystals of each material. In 1968 Kurtz and Perry [1, 2] showed that it is possible, by measurements on powders, to ascertain whether a crystal has large or small nonlinearity as well as it can be phase matched or not. From this information and the commonly known data of crystal properties, the probability of selecting a particular material for crystal growth to achieve NLO application is drastically increased. Kurtz and Perry [2] also proposed a powder SHG method for comprehensive analysis of the second order nonlinearity. Employing this technique, Kurtz surveyed a very large number of compounds.

A good NLO crystal should also possess good transmission in ultra-violet and visible region. It is also important to find the UV cut-off limit for particular crystal. For this purpose UV-Vis spectroscopy is usually employed.

In the present chapter the SHG efficiency of pure and amino acids doped KDP crystals are reported by using the Kurtz powder technique. The optical transparency and UV cut off limit for pure and amino acids doped KDP crystals are studied by UV-Vis spectroscopy.

6.2 Brief Theory of Kurtz and Perry Method

To determine the essential features of second harmonic generation (SHG) in thin powder layers, the dependence of second harmonic intensity on, (1) angle between detector and direction of incident light beam (θ), (2) powder layer thickness (L) and (3) average particle size ($\hat{r}$) and laser beam diameter (D) are studied [2].

Within certain ranges of layer thickness and particle size, it was found that a fairly simple and reproducible result could be obtained for above parameters. This region is $\hat{r} << L << D$, which ensures that the fundamental beam strikes a large number of particles of random orientation and thereby gives a significant statistical average.

6.2.1 Angular Distribution

When the average particle size, layer thickness and beam diameter follow $\hat{r} << L << D$ order, the angular distribution of second harmonic intensity for the powder in air nearly depends on $Cos\ \theta$ for both forward and backward scattering directions. Thus, the sample can be considered as a source of second harmonic radiation with isotropic planar radiator.

$$I(\theta, \Phi) = I_o Cos\theta \qquad (6.1)$$

Where, θ and Φ are spherical polar angles and the photometric intensity I_o is defined as,

$$I_o = \int B.\, ds \qquad (6.2)$$

Where, *B* is the photometric brightness and *dS* is a surface element.

However, the photometric intensity I_o of the front and back surfaces of the powder layer is not equal for powders in air. As the particle size decreases, the second-harmonic lobe in the backward direction grows, whereas, reduces in the forward direction. Moreover, when the same powder is contained in a liquid of matching refractive index, the uniaxial distribution is observed. The advantage of the index matching of the powder is that the second harmonic is not significantly scattered due to reflection and refraction at particle interfaces and hence all the harmonic flux is contained in a narrow cone in the forward direction. This has been demonstrated for ADP powders by Kurtz and Perry [2], which is schematically depicted in figure (6.1).

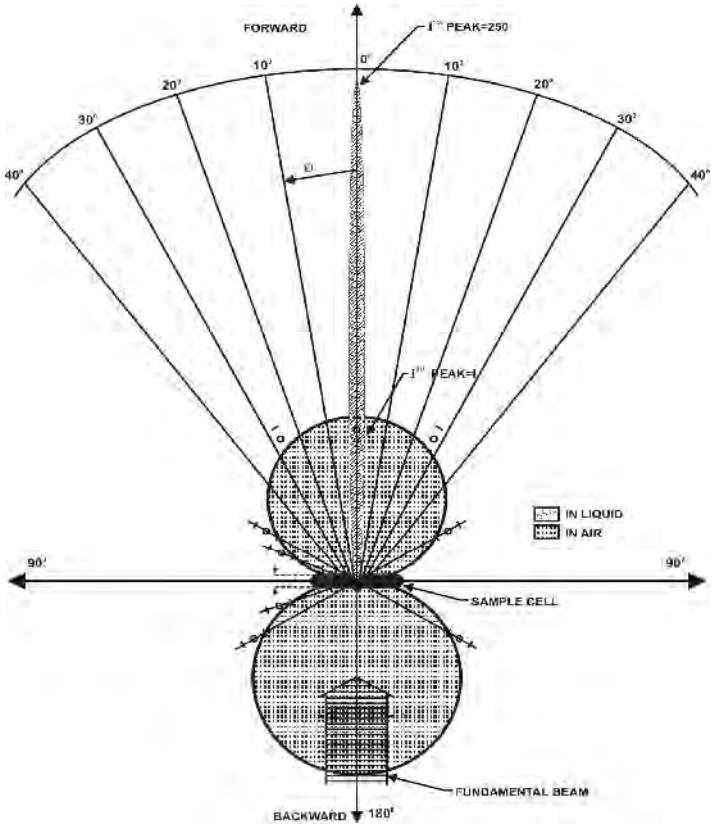

Figure: 6.1 Angular distribution of second harmonic generated in ADP powders.

6.2.2 Dependence on Layer Thickness

The second harmonic signal varies linearly with layer thickness *L* for fixed particle size *r* after integrating over the 4π solid angle. This indicates that the second harmonic intensity $I^{2\omega}$ is proportional to the total number of particles present. A linear dependence on *L* was also found in the case of immersion of the powder in the refractive index-matching liquid.

Considering that the fundamental beam strikes each particle at normal incidence. After traversing each particle the beam moves further in the forward directions and encounters nearly $L/\hat{r}$ particles, where, $\hat{r}$ is average particle size. This can be discussed for phase matchable and non-phase matchable materials.

For the non-phase matchable materials, $n_{2\omega} - n_{\omega} \to 0$ for certain directions of propagations, the average coherence length is

$$\hat{l}_c \equiv \left\langle \lambda / 4\left(n_{2\omega} - n_{\omega}\right)\right\rangle_{av} \qquad (6.3)$$

The total second harmonic intensity for the powder $\hat{r} >> l_c$ is

$$I_{total}^{2\omega} \cong \frac{32\pi}{c}\left\langle \left(d^{2\omega}\right)^2\right\rangle \left[\frac{64\pi I_{ext}^{\omega}}{\lambda\left(n_{\omega}+1\right)^2\left(n_{2\omega}+1\right)}\right]^2 \times L\frac{\hat{l}_c^{\,2}}{\hat{r}} sin^2\left(\frac{\pi}{2}.\frac{\hat{r}}{\ell_c}\right) \qquad (6.4)$$

Where, $d^{2\omega}$ is non linear optical coefficient

l_c= Coherence length

It is very difficult to obtain powder having an exact particle size *r*, in fact, a distribution about some mean value $\hat{r}$. If the r.m.s. deviation of *r* form $\hat{r}$

$$\sin^2\left(\frac{\pi}{2}.\frac{\hat{r}}{\ell_c}\right) \approx \frac{1}{2} \qquad (6.5)$$

For $\hat{r} << l_c$ the $sin^2\left(\frac{\pi}{2}.\frac{\hat{r}}{\ell_c}\right)$ is replaced by $\left(\frac{\pi}{2}.\frac{\hat{r}}{\ell_c}\right)^2$ and gives $I^{2\omega} \propto \hat{r}L$.

Considering that the second-harmonic fields from different particles are correlated provided that the particles are separated by a distance less than coherence length. Dividing the cell thickness up to *N* regions $\left(N \equiv L/\hat{l}_c\right)$ and each contains $N' = \hat{l}_c/\hat{r}$ particles and treating the non-linear polarization P^{NLS} within each of the *N* regions by a one-dimensional random walk model having step length proportional to $d^{2\omega}$, the net contribution of each region to second-harmonic intensity is,

$$I_{total}{}^{2\omega} \propto N\left[\left\langle\left(d^{2\omega}\right)^2\right\rangle\Big/N'\right] = L\frac{\hat{r}}{\hat{l}_c}\left\langle\left(d^{2\omega}\right)^2\right\rangle \tag{6.6}$$

Now considering the phase matching condition, for certain directions of light propagation in uniaxial and biaxial crystals, the phase matching can occur between the polarizing wave, traveling with velocity $c/n_o(\omega)$, and the transmitted second harmonic wave, traveling with velocity $c/n_e(2\omega)$.

For these certain directions the coherence length becomes very large. However, the angular width over which phase matching takes place is usually very small and only a small fraction of the particles will have the correct orientation.

In the vicinity of the phase-matched direction the coherence length is

$$lc = \pi/2\beta\left(\theta - \theta_m\right) \tag{6.7}$$

$$\text{Where, } \beta \equiv \left(\omega n_\omega^o/c\right) sin\ \rho \tag{6.8}$$

Here, θ_m = angle between phase-matching direction and optic axis,

θ = angle between direction of fundamental wave and optic axis, n^{o}_{ω} = ordinary refractive index at fundamental frequency, ω = angular frequency of fundamental, ρ = angle between ellipse and sphere index surfaces at matching.

For small birefringence, $\left(n^{e}_{2\omega} - n^{o}_{2\omega}\right) \Big/ n_{2\omega} << 1$ and small dispersion, $\left(n_{2\omega} - n_{\omega}\right) \Big/ n_{2\omega} << 1$. Where, n^{e}= extra-ordinary refractive index,

$$\tan \rho \cong \rho \cong \left(n^{o}_{2\omega} - n^{e}_{\omega}\right) \Big/ n_{2\omega} \qquad (6.9)$$

and

$$l_c \cong \frac{\lambda}{4}\left(n^{e}_{2\omega} - n^{o}_{\omega}\right)\left(\sin 2\theta_m\right)\left(\theta - \theta_m\right) \qquad (6.10)$$

The intensity is obtained for phase matchable is

$$I_{ext}{}^{2\omega} \cong \frac{32\pi}{c}\left[\frac{64\pi\, I_{ext}{}^{\omega}}{\lambda\left(n_\omega + 1\right)^2\left(n_{2\omega} + 1\right)}\right]^2 \times \left(d^{2\omega}_{PM}\right)^2 \times \left[\frac{\pi^2}{4} L\, \Gamma_{PM}\right] \qquad (6.11)$$

Where, $\Gamma_{PM} \equiv \pi \sin\theta_m / \beta$ and $d^{2\omega}_{PM}$ is that $d^{2\omega}_{ijk}$ for which the phase matching occurs, d_{ijk} is the second order polarizability tenser.

When the non linear co-efficients $d^{2\omega}_{ijk}$, k and coherence length l_c are known, it is possible to evaluate the ratio of second harmonic intensities of any two materials using above equation.

The schematic representation of different particle size dependences for phase-matchable and non-phase matchable materials are given in figure (6.2).

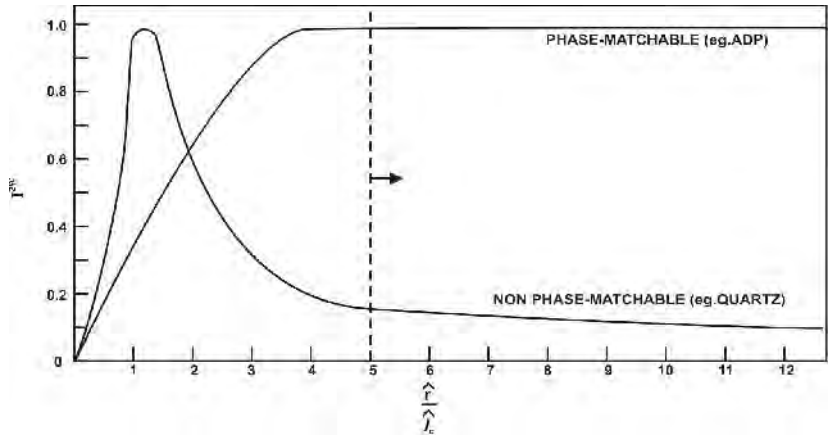

Figure: 6.2 Schematic representation of different particle size dependences for phase-matchable and non-phase matchable materials.

By omitting all parameters, which are identical due to using the same experimental set up, powder size etc., the equations are simplified as [2],

$$I_{ext}^{2\omega} \propto \left\langle \left(d_{ijk}^{2\omega}\right)^2 \right\rangle \left[(l_c)^2 / 2\hat{r} \right], \text{ for not phase matchable } \hat{r} >> l \quad (6.11)$$

$$\text{and } I_{ext}^{2\omega} \propto \left(d_{PM}^{2\omega}\right)^2 \left[(\pi^2/4)\Gamma_{PM} \right], \text{ for phase matchable } \hat{r} >> \Gamma_{PM}/\sin\theta \quad (6.12)$$

6.3 Some Prominent NLO Crystals

Traditionally, the materials used to measure second order nonlinear optical behavior are inorganic crystals, such as, lithium niobate ($LiNbO_3$) [3, 4], potassium dihydrogen phosphate (KDP) [5], ammonium dihydrogen phosphate (ADP) [6, 7], potassium titanyl phosphate (KTP) [8].

The NLO family is expanding very rapidly; however, it is difficult to cover all different types of NLO materials crystals reported in the literature. However, different types of NLO materials in terms of their NLO properties are described in detail in chapter-1.

As already discussed earlier potassium dihydrogen phosphate (KH_2PO_4 or KDP) single crystals have a high laser damage threshold, a large non-linear optical coefficient, good structural quality and mechanical properties,

KDP crystals find several device applications. The electro-optic effect in KDP is used to obtain phase and amplitude modulations [9, 10]. The acousto-optic tunable filters have been developed using KDP [11].

Organic materials also have been shown better nonlinear optical properties. All the compounds in this class contain an optically active carbon atom and, therefore, all of them form acentric crystals. All the crystals were optically biaxial and among them several gave second harmonic signals greater than quartz. The popular organic NLO material crystals are 4-dimethylamino-4-methyl-4-stilbazoliumtosylate [12], p-hydroxyacetophenone [13], methyl-p-hydroxybenonate [14], 3-methyl 4-nitropyridine 1-oxide [15]. Urea L-Malic acid (ULMA) crystals have been grown from aqueous solution employing the techniques of solvent evaporation and slow cooling [16]. De Matos Gomes et al [17] have reported that ULMA crystal has SHG efficiency three times greater than that of KDP.

Another interesting class of crystals receiving wider attention in recent past is the semi organic crystals. L-arginine phosphate monohydrate (LAP) is a popular semi-organic NLO material first introduced by Chinese material scientists in 1983 [18]. LAP crystals caught the attention of many researchers because of their high nonlinearity, wide transmission range, high conversion efficiency and high damage threshold [19, 20]. Yokotani et al [21] have reported the synthesis and growth of deuterated LAP (DLAP) crystals for experiments of higher harmonic generation.

As already discussed in chapter-I, amino acid exhibits specific features of interest [22] such as, (i) molecular chirality, which secures non-centro symmetric crystallographic structure, (ii) absence of strongly conjugated

bonds, which leads to wide transparency ranges in the visible and UV spectral regions and (iii) zwitter ionic nature of the molecule, which favors crystal hardness for application in devices. Therefore, in many semi-organic materials crystals different amino acids were used, for example, L-alaninium-oxalate [23], tetra L-lysine alanine monohydrochloride dihydrate [24] L-arginine hydrochloride monohydrate [25], L-histidine hydrochloride monohydrate [26], L-proline cadmium chloride monohydrate [27], etc. Moreover, pure amino acid crystals have been grown for NLO applications, for example, L-alanine crystals exhibited higher damage threshold than KDP [28]. L-threonine exhibited the second and third order optical non-linearities and the phase matching curves for second harmonic generation were obtained [29].

To investigate the effect of different amino acids doping on the SHG efficiency of KDP crystals, the Kurtz powder technique has been employed and the results are given in the following section. The single crystals of pure and L-histidine, L-threonine and DL-methionine doped KDP crystals were grown by the slow aqueous solution evaporation technique, which is described in Chapter-II.

6.4 Experimental Setup

Kurtz and Perry powder technique was employed to obtain the second harmonic generation (SHG) efficiency. The schematic representation of the experimental set-up of Kurtz powder method used for the comprehensive analysis of the second order nonlinearity is shown in figure (6.3).

In the present study, Q-switched Nd:YAG laser emitting 1064 nm, 10 ns laser pulses having repetition rate 10 Hz with spot radius of 1 mm was used as a source for illuminating the powder sample.

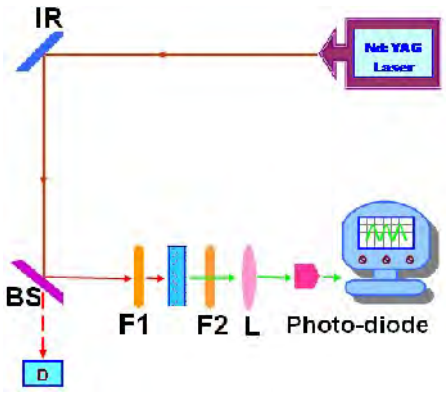

Figure: 6.3 Experimental set-up of Kurtz powder method.

This experimental setup used a mirror and a 50/50 beam splitter (BS) to generate a beam with pulse energies about 4.0 mJ. The input laser beam was passed through an IR reflector, beam splitter (50/50) and then directed on the micro-crystalline powdered sample. The sample was prepared by sandwiching the graded crystalline powder with average particle size of about 90 µm between two glass slides, using copper spacers of 0.4 mm thickness. Since typical values of the coherence length are in the range of 1-10 µm, this value of average particle size yields maximum second harmonic signal independent of particle size in phase matchable crystalline powder.

The energy meter D_1 served as a reference to monitor the fluctuation in the input pulse, Filter F_1, which transmits the fundamental laser emission, is used to filter out any visible radiation present in the fundamental laser emission by flash lamps. Filter F_2 is used to cut off the fundamental laser radiation and to pass the generated second harmonic. The second harmonic signal emitted in the sample is collected by the lens (*L*) and detected by photo diode detector then measured by oscilloscope assembly. The out put power and frequency of the pulse is thus determined and compared with the standard KDP crystal.

6.5 Study of Pure and Amino acids Doped KDP Crystals

Various techniques have been employed to study the non linear optical behavior of KDP crystals. Ganeev et al [30] studied the third order susceptibilities $\chi^{(3)}$ and the non linear refractive indices (n_2) of KDP at wave lengths 1064 nm and 532 nm by Z-scan technique. The measurements were carried out at different pulse energies, focusing conditions and crystal lengths. It was shown by the authors that the increase of phase matching angle leads to decreasing of $\chi^{(3)}$ of KDP crystals. Also, the self and gross-phase-modulation coefficients in KDP crystals were measured by the Z-scan technique by Zheng and Meyerhofer [31]. However, in the present investigation the author has employed Kurtz powder technique to evaluate the SHG efficiency, as this technique is quite rapid and does not need large single crystal specifically cut and oriented in the proper direction. The effect of doping of amino acids such as, L-glutamic acid, L-valine, L-histidine [32], L-arginine, L-histidine and glycine [33] in KDP crystals have been reported earlier.

Amino acids contain both a carboxyl group (COOH) and an amino group (NH_2). The general formula for an amino acid is given below in figure (6.4).

Figure:6.4 General formula for an amino acid.

Although the neutrally-charged structure is commonly written, it is inaccurate because the acidic COOH and basic NH_2 groups react with one another to

form an internal salt called a zwitterion. The zwitterion has no net charge; there is one positive (COO^-) and one negative (NH_3^+) charge. On the basis of the nature of their side chains amino acids can be characterized as follows:

(i) Non-polar side chains (ii) Polar side chains (iii) Charged side chains

Out of three selected amino acids, viz., L-histidine, L-threonine and DL-methionine; L-histidine (NH-CH=N-CH=C-CH_2-CH (NH_2)-COOH) and L-threonine (CH_3-CH (OH)-CH (NH_2)-COOH) have polar and uncharged side chains. L-histidine has heterocyclic aromatic amine group and also its imidazole group shows some degree of pH-dependent ionization, whereas, L-threonine has hydroxyl groups. DL- methionine (CH_3-S-(CH_2)$_2$-CH (NH_2)-COOH) has non-polar larger side chains and strongly hydrophobic [34]. Figure (6.5) shows the molecular structure of these selected amino-acids.

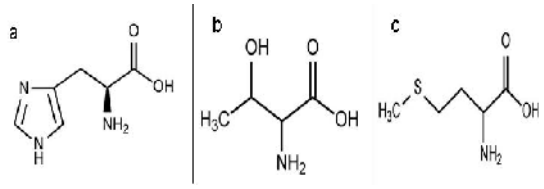

Figure:6.5 Molecular structure of L-histidine (a), L-threonine (b) and DL-methionine (c).

In the present investigation, non linear optical property of pure and various Wt % doped different amino acids (L-histidine, L-threonine and DL-methionine) in KDP crystals was studied by Kurtz powder method using the fundamental beam of 1064 nm from Nd:YAG laser.

An intense green radiation of 532 nm was observed from the pure and different amino acids doped KDP crystals confirming the second harmonic generation (SHG).

The SHG efficiency is estimated with respect to standard KDP and listed in table (6.1) for different samples. It can be noticed from table (6.1) that as the doping of L-histidine, L-threonine and DL-methionine increases in KDP crystals, the SHG efficiency increases. The amino acid doping is beneficial for SHG efficiency. The SHG of the doped crystals is found to be more than the pure one.

Table: 6.1 SHG efficiency of pure, L-histidine, L-threonine and DL-methionine doped KDP crystals.

Samples	SHG Efficiency
Pure KDP Crystal	1
KDP + 0.3% L-histidine	1.33
KDP + 0.4% L-histidine	1.61
KDP + 0.5% L-histidine	1.80
KDP + 0.3% L-threonine	1.11
KDP + 0.4% L-threonine	1.24
KDP + 0.5% L-threonine	1.46
KDP + 0.3% DL-methionine	1.17
KDP + 0.4% DL-methionine	1.26
KDP + 0.5% DL-methionine	1.71

Attempts have been made to explain the origin of optical non-linearity in terms various chemical bond contributions. Lin et al [35] studied the mechanism of the optical behavior of KDP crystals theoretically by using the plane wave pseudo-potential total energy software package. The origin of non-linear effects has been explained through the real space atom cutting analysis of KDP. The contribution of PO_4 group to the SHG effects is dominant. And the hydrogen bonds contribute much for birefringence. In another study, Xue and Zhang [36] have studied the hydrogen bonds such as O-H---O, N-H---O in KDP and ADP. The second order NLO behavior of crystals studied and it is found that hydrogen bonds play very important roles in NLO contributions to the total nonlinearity. Moreover, Xue and Ratajczak

[37] studied the effects of hydrogen bonds in ADP crystallographic frame on its optical properties, such as, static polarizabilities and first hyperpolarizabilities by quantum chemical calculations.

As it has been discussed in Chapter-III that amino acids are expected to interact through hydrogen bonds with KDP, which is reflected in FTIR spectra of amino acids doped KDP crystals with respect to pure KDP crystals. The increase in SHG efficiency of amino acids doped KDP crystals may be due to interaction of amino acids with KDP through hydrogen bonds. This favorable condition may be responsible for the increase in SHG efficiency on doping of amino acids.

6.6 UV-Vis Spectroscopic Study

Ultraviolet-visible (UV-Vis) spectroscopy involves electro-magnetic radiation in the UV-visible region (UV region 200-400 nm and visible region 400-800 nm). The absorption in the visible ranges directly affects the color of the compound or sample involved. In this region of the electromagnetic spectrum, molecules undergo electronic transitions. UV-Vis spectroscopy is routinely used in the quantitative determination of solutions of transition metal ions and highly conjugated organic compounds. Organic compounds, especially those with a high degree of conjugation, also absorb electromagnetic radiation in the UV or visible regions of the electromagnetic spectrum [38].

Different molecules absorb radiation of different wavelengths. An absorption spectrum will show a number of absorption bands corresponding to structural groups within the molecule. For example, the absorption that is observed in the UV region for the carbonyl group in acetone is of the same

wavelength as the absorption from the carbonyl group in diethyl ketone [39-40].

The instrument used in ultraviolet-visible spectroscopy is called a UV-vis spectrophotometer. It measures the intensity of light passing through a sample (I), and compares it to the intensity of light before it passes through the sample (I_o). The ratio I/I_o is called the transmittance and usually express in percentage (%).

The basic parts of a spectrophotometer are a light source, a holder for the sample, a diffraction grating or monochromator to separate the different wavelengths of light, and a detector. The radiation source is often a tungsten filament (400-2500 nm), a deuterium arc lamp which is continuous over the ultraviolet region (200-400 nm), and more recently light emitting diodes (LED) and xenon arc lamps for the visible wavelengths. The detector is typically a photodiode or a CCD. Photodiodes are used with monochromators, which filter the light so that only light of a single wavelength reaches the detector.

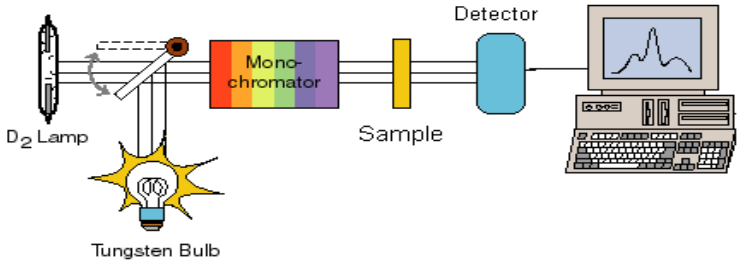

Figure: 6.6 Schematic diagram of single-beam UV-Vis spectrophotometer.

A spectrophotometer can be either single beam or double beam. In a single beam instrument, all of the light passes through the sample. I_o must be measured by removing the sample. This was the earliest design, but is still in common use in both teaching and industrial labs. In a double-beam instrument, the light is split into two beams before it reaches the sample. One beam is used as the reference and other beam passes through the sample.

Some double-beam instruments have two detectors (photodiodes), and the sample and reference beam are measured at the same time. In other instruments, the two beams pass through a beam chopper, which blocks one beam at a time. The detector alternates between measuring the sample beam and the reference beam. An ultraviolet-visible spectrum is essentially a plot of light absorbance or transmittance versus wavelength in a range of ultraviolet or visible regions. Such a spectrum can often be produced directly by a more sophisticated spectrophotometer. The wavelengths of absorption peaks can be correlated with the types of bonds in a given molecule and are valuable in determining the functional groups within a molecule.

Many researchers are interested in optical characterization of single crystal. Some of these crystals are transparent to UV-Vis radiation while others are not. For transparent crystals that have a negligible reflectance and absorption, measurement of the transmittance is necessary for complete optical characterization.

In the present study, single crystalline as grown crystals were used for UV-Vis study without cutting and polishing them. The samples were prepared for UV-Vis study in a standard manner by exposing equal area of sample and blocking the other portion. A photograph of typical set up of UV-Vis spectrophotometer is shown in figure (6.7).

Figure :6.7 A photograph of typical set up of UV-Vis spectrophotometer.

The UV-Vis spectrophotometer of “Perkin Elmer Lambda 19”; range: 185-3200 nm having photomultiplier tube as a detector with double beam, double monochromator, ratio recording was used. Deuterium lamp for UV radiation and tungsten-halogen lamp for visible radiation were used. The measurements were taken at SICART, Vallabh Vidyanagar, Gujarat, India.

6.6.1 UV-Vis Spectroscopy Study of Pure and Amino Acids Doped KDP Crystals

Transparency is one of the important parameters that a good NLO material should posses for second harmonic generation (SHG). The wider transparency range, the greater will be the practical applicability of that material. The UV-Vis transmission spectra of single crystals of pure and L-histidine, L-threonine and DL-methionine doped KDP crystals were recorded in the region 200-1400 nm by using a UV-Vis spectrometer described in the previous section of this chapter. The UV-Vis optical transmission spectra of pure and different amount of (0.3, 0.4 and 0.5 wt %) L-histidine, L-threonine and DL-methionine doped KDP crystals are shown in figures (6.8, 6.9 and 6.10), respectively.

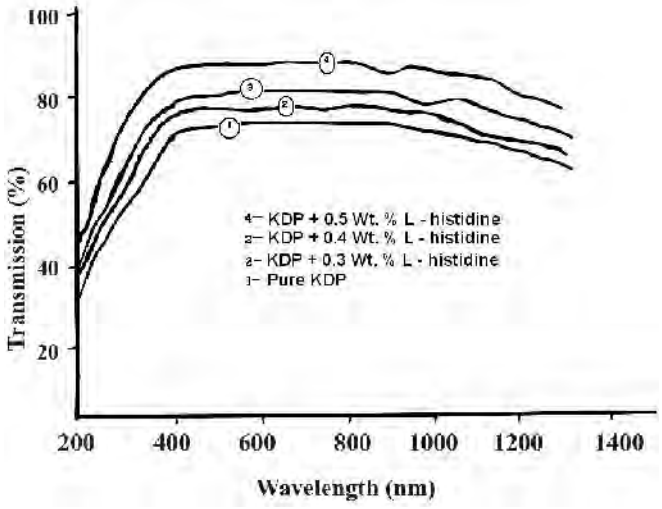

Figure:6.8 UV-Vis Spectra of pure and L-histidine doped KDP crystals.

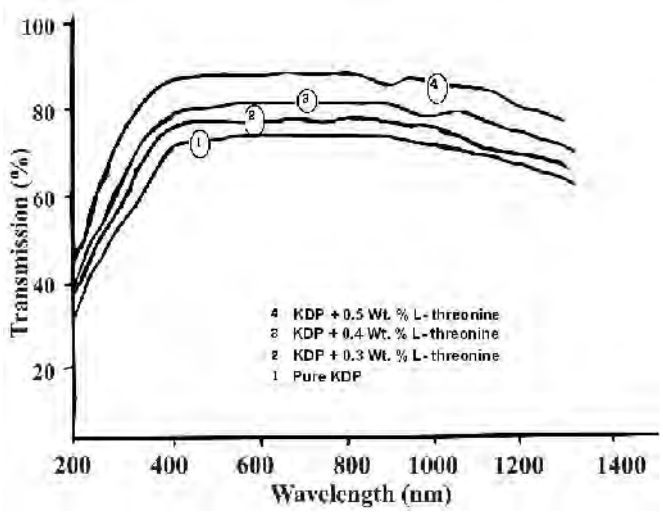

Figure:6.9 UV-Vis Spectra of pure and L-threonine doped KDP crystals.

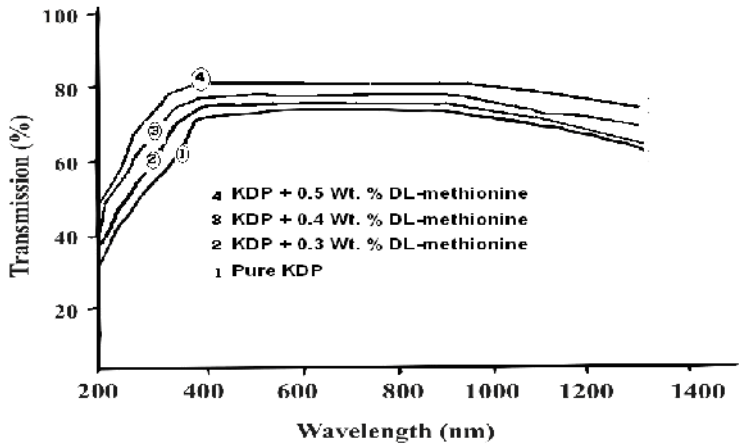

Figure:6.10 UV-Vis Spectra of pure and DL-methionine doped KDP crystals.

It is inferred from the spectra that both pure and doped KDP crystals have large transmission window in the entire visible region. The UV transparency cut-off limit and percentage optical transmission data are compiled in table (6.2). The lower cut off wavelength for pure KDP, L-histidine, L-threonine and DL-methionine doped KDP crystals are around 350 nm, 375 nm, 350 nm, and 385 nm, respectively.

Table: 6.2 Optical transmission data of pure and different Amino acids doped KDP crystals.

Samples	Optical Transmission	Transparency Cut-off
Pure KDP Crystal	72 %	≈ 350 nm
KDP + 0.3% L-histidine	74 %	≈ 375 nm
KDP + 0.4% L- histidine	76 %	≈ 375 nm
KDP + 0.5% L- histidine	80 %	≈ 370 nm
KDP + 0.3% L-threonine	78 %	≈ 350 nm
KDP + 0.4% L- threonine	81 %	≈ 350 nm
KDP + 0.5% L- threonine	86 %	≈ 350 nm
KDP + 0.3% DL-methionine	74 %	≈ 385 nm
KDP + 0.4% DL-methionine	77 %	≈ 385 nm
KDP + 0.5% DL-methionine	81 %	≈ 380 nm

Therefore, L-histidine and DL-methionine doping in the KDP crystals narrows down the window and decreases the cut off limit, while L-threonine doping in KDP keeps the cut off limit unaltered. The UV transparency cut-off frequency increases marginally on doping L-histidine in KDP crystals from 350 nm to 375 nm, for DL-methionine in KDP crystals from 350 nm to 385 nm and for L-threonine doped KDP crystals almost remaining the same around 350 nm. Altogether, the percentage optical transmission increases on increasing the doping of L-histidine, L-threonine and DL-methionine in KDP crystals. On sacrifying slightly the UV-transparency cut-off limit, the L-histidine and DL-methionine doping increase the transparency of grown crystals, whereas, for L-threonine the UV- cut off limit remains almost unaltered and greater transparency is obtained.

Conclusion

1. As the doping level of amino acids increased the SHG efficiency increased.

   The effect of doping on SHG efficiency is roughly the same for all three dopant Viz. L-histidine, L-threonine and DL-methionine. The interaction of amino acids through hydrogen bond with KDP crystal may be responsible for enhanced SHG efficiency.

2. The UV cut-off frequency increased and the UV cut off limits except for L-

   threonine doped crystal decreased slightly as the doping increased. For obtaining higher percentage optical transmission in KDP crystals by doping L-histidine and DL-methionine, There was slight sacrifice in the UV cut-off limits. The percentage optical transmission for L-threonine doped KDP crystals was higher than pure and L-histidine and DL-methionine doped KDP crystals, but the UV cut-off limit remained almost constant without any deteoration.

3. Looking at SHG efficiency data, UV cut-off limit and percentage transmission data, it could be concluded that L-threonine doping in KDP was a better option compared to other two amino acids.

References:

1. S. K. Krutz, T. T. Perry, *J. Quantum Electron.* **4** (1968) 578.
2. S. K. Krutz, T. T. Perry, *J. Appl. Phys.* **39** (1968) 3798.
3. G. D. Boyd, R. C. Miller, K. Nassau, W. L. Bond, A. Savage., *Appl. Phys. Lett*, **5** (1964) 234
4. R. C. Miller, G. D. Boyd, A. Savage, *Appl. Phys. Lett*. **6** (1965) 77.
5. F. Zernike, J. E. Midwinter, "*Applied Non-linear optics",* Wiley, New York (1973).
6. P. D. Maker, R. W. Terhune, M. Nynenoff, C. M. Savage, *Phy. Rev. Lett.* **8** (1962) 21.
7. F. B. Dunning, E. D. Stokes, R. F. Stebbings, *Opt. Commun.* **6** (1972) 63.
8. J. D. Bierlein, H. Vanherzeele, *J. Opt. Soc. Am.* **6** (1989) 622.
9. A. K. Ghatak, K. Thyagarajan, "*Optical Electronics"*, Cambridge University Press, Cambridge (1989).
10. S. S. Jha, "*Perspective of Optoelectronics"*, World Scientific, Singapore (1995).
11. V. B. Voloshinov, D. V. Bogomolov, A. Yu. Trokhimovskii, *Technical Phys.* **51** (2006) 63.
12. A. Nixon, A. S. H. Hameed, L. Thenappan, M. Noel, G. Ravi, *Mater. Chem. Phys.* **88** (2004) 90.
13. N. Vijayan, R. R. Babu, M. Gunsekaran, K. Gopalakrishnan, R. Kumaresan, P. Ramasmy, C. W. Lan, *J. Cryst. Growth* **249** (2004) 309.
14. C. K. L. Perumal, A. A. Chakkaravarthi, N. P. Rajesh, P. Santhana Raghavan, Y. C. Huang, M. Ichimura, P. Ramasamy, *J. Crystal Growth* **240** (2002) 212.

15. S. Boomadevi, H. P. Mittal, R. Dhanasekaran. *J. Cryst. Growth* **261** (2004) 55.

16. V. K. Dixit, S. Vanishri, H. L. Bhat, E. De Matos Gomes, M. Belsley, C. Santinha, G. Arunmozhi, V. Venkataramanan, F. Proena, A. Criado, *J. Cryst. Growth* **253** (2003) 460.

17. E. De Matos Gomes, V. Venkataramanan, E. Nogueira, M. Belsley, F. Proenca, A. Criado, M. J. Dianez, M. D. Estrada, S. Perez-Garrido *Synthetic Metals,* **115** (2000)225.

18. D. Xu, M. Jiang, Z. Tan, *Acta chem. Sinica* **41** (1983)570.

19. K. Aoki, N. Kozo Nagano, I. Yiochi litaka, *Acta Crystallogr B* **27** (1971) 11.

20. S. B. Monaco, L. E. Davis, S. P. Velsko, F. T. Wang, D. Eimerl, *J. Cryst. Growth* **85** (1987) 252.

21. A. Yokotani, T. Sasaki, K. Fujioka, S. Nakai, C. Yamanaka, *J. Cryst. Growth* **99** (1990) 815.

22. J. F. Nicoud, R. J Twieng, "*In Non-linear Optical Properties of Organic Molecules and Crystals",* vol 1, Academic Press, London (1987).

23. S. Dhanuskodi, K. Vasantha, *Cryst. Res. & Technol.* **39** (2004) 256.

24. V. Sivashankar, R. Sankar, R. Siddheswaram, R. Jayavel, P. Murugakortham, *Mater. Chem. Phys.* **109** (2008) 119.

25. T. Pal, T. Kar, G. Bocelli, L. Rigi, *Cryst. Growth & Design* **4** (2004) 743.

26. J. Madhvan, S. Aruna, P. C. Thomas, M. Vimalan, S. A. Rajsekar, P. Sagayaraj, *Cryst. Res. & Technol.* **42** (2007) 59.

27. A. Kandasamy, R. Mohan, M.L. Caroline, S. Vasudevan, *Cryst. Res. & Technol.* **43** (2008) 186.

28. N. Vijayan, S. Rajasekaran, G. Bhagavannarayan, R. R. Babu, R. Gopalakrishnan, M. Palanichamy, P. Ramasamy, *Cryst. Growth & Design* **6** (2006) 2441.

29. J. J. Rodrigues, L. Misoguti, K. D. Nunes, C. R. Mendonca, S. C. Zilio, *Optical Mater* **22** (2003) 235.

30. R. A. Ganeev, I. A. Kalagin, A. I. Ryasnyansky, R. I. Tugashev, *Optics Comm*. **229** (2008) 403.

31. L. Zheng, D. D. Meyerhofer, *LLE Rev*. **74** (1998) 125.

32. P. Kumaresan, *Ph.D Thesis*, Anna University, Chennai, India (2008).

33. B. S. Kumar, K.R. Babu, *Indian J. Pure & Appl Phys.* **46** (2008) 123.

34. D. M. Vasudevan, S. Sreekumari, "*Text Book of Biochemistry"*, Jaypee, New Delhi (2007).

35. Z. Lin, Z. Wang, C. Chen, M. H. Lee, *J. Chem. Phys.* **118** (2003) 2349.

36. D. Xue, S. Zhang, *Chem Phys Lett.* **30** (1999) 449.

37. D. Xue, H. Ratajczak, *J. Mol. Structure* **716** (2005) 207.

38. H. H Jaffe and M. Orchin, "*Theory and Applications of Ultraviolet Spectroscopy"*, Wiley, New York (1962).

39. C. N. R. Rao, "*Ultraviolet and Visible spectroscopy: Chemical Applications"*, 3rd Ed, Butterworth, London(1975).

40. D.A. Skoog, F.J. Holler and T.A. Nieman, "*Principles of Instrument Analysis"*, Saunders College, Philadelphia (1998).

Chapter VII

Reactivity at Dislocation in Pure and Amino acids Doped KDP Crystals

7.1 Introduction

Reactivity of solids is of practical and fundamental importance. In some cases like propellants, heterogeneous catalysis, etc., high reactivity is required; whereas, the low reactivity is a need in oxidation and corrosion of materials. The study of reactivity of crystals is mainly carried out by preferential etching and gross dissolution. The preferential etching is subjected to the qualitative analysis of the defects sites of a crystalline solid and, thereby, indicates the quality or perfection of the crystal.

Etching though a simple and widely adopted technique for the study of imperfections in a large variety of crystalline materials, the process is still not very well understood. An etching technique in association with optical microscopy can be used alternatively to X-ray method for the detection as well as quantitative analysis of defects in crystalline solids [1-5]. The high-resolution imaging a capability achievable with Atomic Force Microscopy (AFM), has enabled the initial stages of the process of etch pit nucleation to be monitored on a scale previously unattainable [6-7]. The segregation of foreign solute particles during crystal growth leads to the introduction of defect into the crystals [8-9].

In the present study pure and amino acids (L-histidine, L-threonine and DL-methionine) doped KDP crystals were subjected to chemical etching on their (100) as grown faces. The kinetic as well as thermodynamic parameters are reported in the present chapter for the motion of ledges of the etch pits.

7.2 Etching Methods

Etching is a process that has been used extensively in a variety of trades. They range from the ancient craft of the jeweler to the application of photolithography in the production of printed electrical circuits. With recent advances in crystal growth and purification, more rigorous demands are put forwarded on crystal perfection, orientation and special surface treatments. Etching plays an important role in the perfection and characterization of the crystals. Reasons for performing etching are grouped as follows [10].

1. Cleaning

Any surface for its macroscopic or microscopic study requires to be cleaned up because cutting and other mechanical treatments leave a damaged layer that must be removed before certain surface studies can be made.

2. Revealing Dislocations

Dislocations and other lattice imperfections affect the strength, surface potential, electrical properties and other properties of crystals. Etchants that reveal imperfections give direct measure of crystal perfection.

3. Orientation of crystals

Many studies such as dissolution, oxidation and electrical effects require single crystals whose faces are of a specific crystallographic orientation.

The main etching techniques are listed as under with their brief outlines [11].

(a) Chemical Etching

When a crystal is etched in a proper etchant, its surface atoms undergo a chemical reaction. The reactions at defect sites form products and is removed

from the surface during etching. This is known as preferential etching. This technique is very simple and gives plenty of information, if it is used properly.

(b) Electrolytic Etching

Current flow is employed to cause dissolution of the material in a suitable electrolytic. When a metal dissolves it forms positive ions, thereby each atom should lose one or more electrons, i.e., it must be oxidized. This oxidation process can be achieved either by an oxidizing substance in the solution or by selecting the metal as an anode in the electrolytic cell; in that case the electrons are removed by the battery or generator in the circuit. The rate of reaction in electrolytic method is directly measured by the current flowing in the circuit.

(c) Thermal Etching

The material is removed from the surface by vaporization in a vacuum or in an inert atmosphere. Thermal etching depends upon the conditions of atmosphere, pressure and temperature of the media in which it is carried out. The temperature is required sufficiently high for the surface atoms to become mobile so that the thermal etching takes place. The conditions of temperature and pressure for thermal etching, are such that either the reaction product is removed by evaporation or it becomes chemically unstable.

(d) Ionic Etching

The material is removed by sputtering of ions. If the metal is placed as cathode in a gas discharge tube, the current in the tube is carried out by positive ions of the gas, which bombard the cathode and remove atoms from its surface. This process is known as “sputtering”. Depending upon the tube conditions, such as

current, voltage, time, nature and pressure of the gas and the arrangement of anode and cathode, the individual crystals of the sputtered surface may become smooth, showing only the grain boundaries, or they may be etched, showing structure within the crystals.

7.3 Etching process

When the rate of dissolution of a solid is rapid, the process is controlled by the rates of chemical and thermal diffusion in the solvent. As the dissolution rate or the under saturation of solvent becomes smaller, the surface imperfections of the solid play prominent role [12].

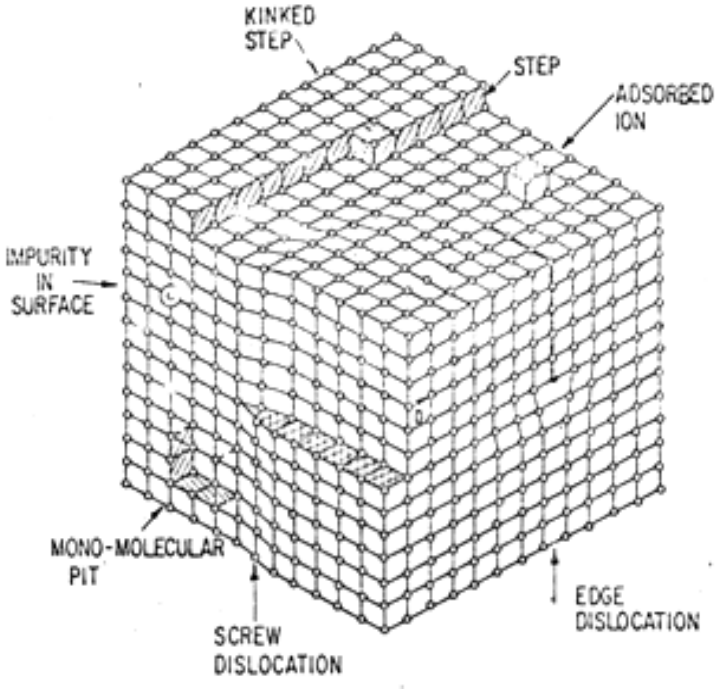

Figure:7.1 Surface imperfection on a crystal.

The unit process in dissolution can be considered as a removal of a molecule from the corner of a kink in a surface step; however, the process occurs only if: (a) a step exists on the surface, (b) the step contains kinks and (c) the solvent is

under saturated at a particular kink under consideration. Any one or combination of these factors controls the dissolution. This has been shown in figure (7.1).

The edges of a crystal are considered to be good source of steps and kinks during dissolution; therefore, in practical cases the rate of dissolution is not limited by the requirement of these defects. The first step in dissolution at the centre of a crystalline face is the generation of a mono-molecular pit, as shown in figure (7.1). If the bond energy in simple cubic structure is Φ, then 5Φ energy is required to remove first atom from a perfect surface. However, this energy is 3Φ for an atom at a kink, and 4Φ for an atom on a step edge. One can consider an atom at center of an edge dislocation is also having energy nearly 4Φ, which is less than the energy for the perfect surface.

Single lattice vacancies situated at the surface also form small monomolecular pits and may influence dissolution under certain conditions. However, the steps produced by them are difficult to observe. On the other hand, the clusters of lattice vacancies or impurity atoms can some times be detected [13]. It is important to note that the dislocation lines are quite effective in acting as nucleation centers for dissolution steps. The effect of dislocation lines on dissolution nucleation is due to their elastic energies or the chemical potential of the material near by [14].

The surface layer around a screw dislocation that lies normal to a free surface is stress free except at the core of the dislocation. However, for an edge dislocation that intersects a free surface, the most of the strain energy remains with the edge. The surface steps associated with screw dislocations are thought

to be important; the dissolution takes place at moderate under-saturations. However, both the edge and the screw dislocations are etched in nearly the same manner and nearly the same rate in many crystals. Different theories of dissolution, thermodynamic and topo-chemical adsorption are of interest since they deal with the formation of dislocation etch pits on a crystal surface [15, 16].

The topo-chemical theories suggest the dissolution rate in terms of chemical reactions on the crystal surface [16, 17]. It is considered that etch pits at the sites of dislocations are formed as a result of enhanced dissolution caused by the preferred adsorption of a reactant at that site because of the strain associated with the dislocation. If the reactants are absorbed more strongly at the site of dislocation it produces good contrast etch pits.

Topo-chemical theories are attractive for crystalline substances. The dissolution of crystals involves the formation of reaction products, however, they poses certain limitations. One limitation is that each etching system has to be treated independently. Whereas, the thermodynamic theories are based on the postulate that the energy localized in the vicinity of a dislocation lowers the free energy needed for the nucleation of unit depth in the surface at the site of the dislocation.

This decrease in the free energy is the cause of preferred dissolution of the surface at the emergence points of dislocations. The free energy change associated with the formation of a mono-molecular pit at dislocation site, ΔG is given by the following expression,

$$\Delta G = 2\pi r a\gamma - \frac{\pi r^2 a \Delta \mu}{\Omega} - aE_d \qquad (7.1)$$

Where, *r* is radius of cavity, *a* is its height, $\Delta\mu$ the change in free energy during dissolution (chemical potential), Ω the molecular volume of the crystal, and γ the specific surface free energy of an atom or molecule going from the solid surface into solution. The chemical potential is shown as,

$$\Delta\mu = - kT \ln(C/C_0) \tag{7.2}$$

Where, C_0 is the saturation concentration of the material in an etching medium and *C* is the actual concentration at the dislocation site. The localized energy per unit length at a dislocation, E_d is shown as,

$$E_d = A \ln(r_1/r_0) \tag{7.3}$$

Here, $A = \frac{Gb^2}{4\pi(1-\mu)}$ (for edge dislocations) and $A = \frac{Gb^2}{4\pi}$ (for screw dislocations)

$$E_d = \frac{\alpha G b^2}{4\pi} \cdot \frac{r_1}{r_o} \tag{7.4}$$

Equations (7.3 and 7.4) represent the elastic strain energy and dislocation core energy, respectively, where, *G* is the shear modulus, *b* is the modulus of Burgers vector of dislocation and μ is the Poisson's ratio, r_0 is the radius of the dislocation core beyond which elasticity theory holds, *r* is the outer radius of the strained region of the crystal and α is a constant equal to 1.5 and 2.0 for screw and edge dislocations, respectively. In the Cabrera's theory [18-19] the free energy change involved in the formation of a dislocation etch pit, ΔG^*, is given as,

$$\Delta G_n^* = (1-\xi)^{\frac{1}{2}} \tag{7.5}$$

Here, $$\xi = \frac{2A\Delta\mu}{\pi\Omega\gamma^2} \quad (7.6)$$

On the other hand, the maximum free energy change associated with the formation of unit etch pit on a perfect surface is given as,

$$\Delta G_S^* = \frac{\pi\gamma^2 a\Omega}{\Delta\mu} \quad (7.7)$$

Whereas, in the Schaarwachter's theory [20], the maximum free energy change is

$$\Delta G_n^* = p\Delta G_S^* \quad (7.8)$$

Where, (7.9)

The value of $p = \left(\frac{1-\alpha qGb}{4\pi\gamma}\right)^2$ constant q is ≈ 0.1

Cabrera's treatment yields similar conclusion as Schaarwachter's theory, but Schaarwachter's theory connects the dependence of etch pit slope on different parameters more clearly. The etch-pits are kinetic phenomenon immediately following nucleation of the appropriate "hole" at the crystal defect. The two aspects of the kinetics, viz., the nucleation of mono-molecular steps at the defect and the motion of the steps away from this source, have been outlined by Gilman

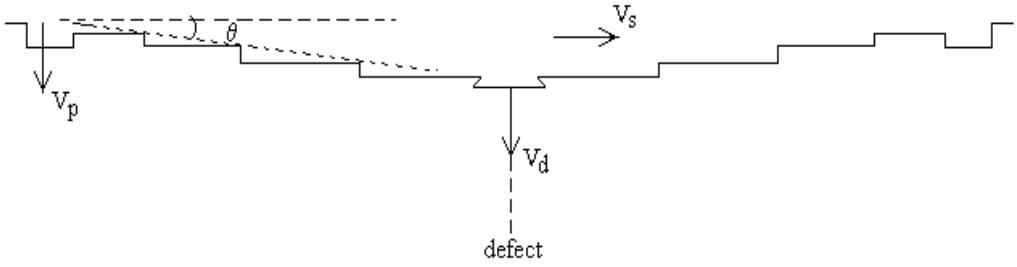

Figure: 7.2 Various dissolution rates at etch pits.

et al [9] and Cabrera [21] and the same model is used by Ives and Mc Ausland [22] to explain the etch pit slopes. Successive nucleation of steps at the defect (assumed a straight line defect perpendicular to the surface) gives rise to a

dissolution rate V_d at the defect. If the height of these steps is h, then V_d/h steps are produced in unit time. The model takes no account of the square shape of the steps and hence that of the pit they comprise, and it is thought to be a two-dimensional model. Following nucleation, the steps move out by removal of atoms [23] and can have velocity V_s. The V_s may be influenced by the superimposed diffusion field, particularly close to the defect source. It has been predicted that a series of steps emanating from a source will, after sufficient distance travel, achieve a uniform velocity V_s^{∞} [12, 24]. This suggests that the velocity, V_s at a sufficient distance from the source, is independent of the rate of production of steps and hence is independent of V_d. If the steady state is achieved well inside the pit, its slope and rate of widening will be independent of the type of defect. Ives and Hirth [25] applied this analysis to etch pits in lithium fluoride, but no definitive verification of the parametric dependence of V_s^{∞} was possible.

The possibility of certain special situations arises when a pit is formed at the intersection of a dislocation which has a component of its Burgers vector perpendicular to the surface [26]. No nucleation event is necessary in this case because this type of dislocation produces a step, which commences at the point of intersection with the surface. Various authors have given account of this situation and proposed spiral step in growth [12] and in evaporation [19], which at sufficient radius can achieve steady state spacing between successive turns. Ives and Hirth [25] have assumed that V_s is independent of the distance from the source, then, since V_d is a measure of the rate of production of steps and V_s

represents their uniform speed away from the source, by simple geometry the resulting pit will have slope,

$$\tan\theta = \frac{V_d}{V_s} \tag{7.10}$$

The slope *tan* θ can be measured experimentally, but more attention is required to measure V_d.

There are many other heterogeneities at which surface "holes" may be nucleated [27] giving rise to a finite value of surface dissolution or the polishing rate V_p; that describes the dissolution of the surface area free from dislocation and is directed normal to the surface.

The rate of pit deepening is given by, $dD/dt = V_d - V_p$, using this in the earlier equation,

$$\tan\theta = \frac{1}{V_s}\frac{dD}{dt} + \frac{V_d}{V_s} \tag{7.11}$$

For etch pits formed at a constant rate, this expression can be transferred into a linear expression,

$$\tan\theta = \frac{1}{V_s}\frac{D}{t} + \frac{V_d}{V_s} \tag{7.12}$$

Where, *d* is the measured depth of a pit after time *t*.

It is well-known that inorganic salts in solutions exist in the form of complexes whose chemical constitution depends on the concentration of the salt in solutions as well as on the concentration of another substance having an anion common with the additive salt [28, 29]. The instability constant of a series of complexes of salt, in general, regularly decreases, i.e., each successive complex is more stable [30]. The enhanced nucleation rate along the dislocation line, due to the

presence of the localized energy, and the lateral growth of pits may depend on the formation of successive complexes as a result of the availability of the common, or chemically similar-behaving, ions. Denoting the additive impurity as MX_n and an alkali halide by AX, the formation of successive complexes on the surface at the dissolution site is as,

$$[M(H_2O)_6]^{n+} + mAX \rightarrow [M(H_2O)_5]^{(n+1)+} + (m-1)AX + A^+$$

The dissolution is more along the dislocation line and this type of mechanism explains not only the change in the lateral growth of pits but also the change in pit morphology [15-17], which has been studied by the application of activated complex theory in conjunction with the adsorption of reacting species and complexes on MgO crystals [17]. The role of dislocations in etching created a great interest amongst many workers and many significant experiments were conducted. It was the first time, the quantitative proofs regarding the reliability of etch pit technique and the correctness of Burgers model was given by Vogel et al [31]. Subsequently, the etch pit technique has been successfully applied to study dislocations in plastically deformed crystals. Vogel [32] has studied the dislocations in bent germanium crystals. Evidences of decoration of dislocations by the etch pit techniques have been reported, as early as in 1952-53, by Gevers et al and Gevers [33, 34]. During their study of etching on silicon carbide crystals in fused forax at 900 ^oC, they observed that at the center of growth spirals, the etch pits were developed. However, some of the pits were not located at the center of the spirals. It was concluded that these other types of pits correspond to edge dislocations.

The nature of the etch pits depends on the character of the dislocation and on exact composition of the etchant. Edge and screw dislocations etch slightly different, the former produce deeper pits. The etching is inhibited by some segregated impurities at dislocations, therefore, aged and fresh dislocation etch differently. Gilman et al [9] have studied etch pits on the lithium fluoride crystals formed by etching in dilute aqueous solution of FeF_3. They have suggested that the faster nucleation rate at edge dislocations is due to their higher energy, whereas the low nucleation rate at dislocations with segregated impurities is because of lowering in the dislocation energy.

By proper choice of slip traces one can chose emergence points of screw and edge dislocations separately and check whether both types of dislocations are etched. For cleaved specimen of alkali halide, the 45^o traces are due to edge dislocations while the bands parallel to the crystal edges contain screws inclined 45^o with respect to the surface. These circumstances then permit investigation of the effect of the inclination of the dislocations with respect to the etched face. It is not certain that all pits corresponds to dislocations, for instance, precipitates may cause etching. It has been shown that precipitates in LiF crystals cause the formation of terraced pits [35]. Fission tracks can also be etched [36]. There are certain review papers [15, 37, 38] and books [39-41] available on etching study. The book written by Heimann describes the intricasies of art of etching study and science [42].

7.4 Tests for Dislocation Etch Pits

If one could make a crystal with a predetermined dislocation density, the easiest check of the one-to-one correspondence of etch pits and dislocations would consist in comparing calculated and observed dislocation densities. The easiest method to introduce a known number of dislocations into the crystal consist in bending it to given a radius of curvature. It is found that, usually, after bending more etch pits are present than predicted, however, after a slight annealing polygonization takes place and the density of pits corresponds to that predicted one. These pits are arranged in a way such that they reveal the polygonized structure of the crystal; they are on lines perpendicular to the active glide planes [43-45].

Whether the etch pits are formed at dislocation sites or not, that can be decided by conducting certain tests. When annealed and slowly cooled specimens are successfully etched, it can be demonstrated that dislocations with an atmosphere or with precipitates can be revealed. If the same etchant is also able to reveal dislocations in freshly formed slip traces, it is reasonable to say that impurities in the crystals do not take active part. This was shown for NaCl etched with anhydrous methyl alcohol [43] and for lithium fluoride etched with ferric chloride [46].

When cleaved specimens are used, the easiest check on reproducibility and reliability consists in comparing the two counter parts of cleaved faces, the etch patterns should be mirror images, a small deviation may occur, for example, due to branching of the dislocations in the cleavage plane [47]. Gilman et al [9] have

studied two counterparts of LiF cleavages and observed mirror images of etch pits. When metal specimens are used, successive attacks, alternated with electro polishing, should reveal consistently of the same pattern.

Tests were conducted to check the dislocation sites of etch pits by verification of the relation; $n_a \approx n_b + n_c$, where n_a, n_b and n_c are the density of etch pits along the intersecting grain boundaries. Also, the densities of etch pits remained unchanged with the time suggesting the occurrence of pits at dislocation sites [40].

7.5 Etching Studies of KDP Crystals

There are numerous researchers who have carried out chemical etching studies on KDP crystals with different aims. In this section an attempt is made to summarize the information available in the literature. Usually, the water-soluble crystals find water as a good etchant. Water easily produce etch pits on these crystals. The etching capability decreases along the series of homologous alcohols and acids with addition of a $–CH_2$ group. The change in the solvent not only changes the etching capability but also the pit morphology and the different surfaces behave differently to the same series of solvents. This has been discussed elaborately by Sangwal [39].

Balamurugan et al [48] have reported etching study of KDP crystals on (100) faces with water as an etchant at room temperature. They observed elongated rectangular etch pits with dislocation density of the order of $10^2/cm^2$**,** further Balamurugan and Ramasamy [49] have carried out chemical etching on the (110) faces of KDP crystals grown by Sankaranarayanan–Ramasamy (S-R)

method. They used water as an etchant and obtained triangular etch pits for 10 second etching time. They also found that as the etching time increased from 10 to 30 sec, the morphology of triangular etch pits changed. Also, they found from chemical etching that the dislocation density was less in S-R method grown KDP crystals than for the conventional crystals. Moreover, Ravi et al [50] have reported rectangular etch pits on (100) planes of deuterated KDP crystals by unsaturated solution as an etchant and obtained the dislocation density of about $5x10^3/cm^2$.

Chemical etching technique was used to investigate the dislocation behaviors on various sectors of KDP crystals grown with low pH values recently [51]. Chemical etching revealed that pyramid sector of the crystal displayed more growth defects. A (100) slice with thickness of 5 mm was cut and polished and subsequently etched by HAC: H_2SO_4: H_2O = 240:1:25, rectangular etch pits were observed. A Large number of dislocations and etch pits at the trapezi-form section showed a serious mismatch in the crystals. Earlier, the growth character of splicing mis-oriented KDP seeds of both single seed and the special growth of splicing parallel seeds were investigated [52]. The author used chemical etching to determine the prismatic and z-plate surfaces of the crystals grown by splicing bulk KDP crystals.

Chemical etching technique has also been used to reveal certain surface features, for instance, hillocks and etch spirals. When dissolution of the crystalline surface takes place on wide spread and leaving a few undissolved specific parts, it forms hillocks having just opposite nature to the etch pits. Gupta

et al [53] chemically etched prismatic (100) faces of gel grown KDP crystals and observed the presence of hillocks and etch spirals. Both screw and edge dislocations were clearly identified by selecting suitable etchants. The authors also studied the influence of different alcohols and acid concentrations on the morphology of etch pits. Altogether, in another attempt of etching on (100) faces of mixed KDP-ADP crystals Sen Gupta and Sen Gupta [54] observed growth hillocks, pyramids, trisection boundaries, branching of dislocations etc.

Javidi et al [55] used water as an etchant and selected 3 second etching time for etching slice of (101) face of KDP. They observed concentrated triangular etch pits. Another etchant they selected was acetic acid saturated with KI salt and etched for 90 sec, which produced rectangular shaped etch pits. However, the orientation of the etch pits on (100) face was different for each etch pits. The etching experiments showed the appearance of etch pits on the (100) and (101) faces by different etchants with the same morphology. They concluded that the etch pits were due to surface dislocations.

The effect of environment has also been studied on the crystalline face of KDP crystals. Wheeler et al [56] have investigated the etch pits formation on KDP crystals with sol-gel based anti reflection coatings. They found that the etch pits were produced beneath the sol-gel coating after the exposure to ambient humidity. The etch pits were uniformly distributed and their sizes were found to be governed by relative humidity and the thickness of the coating. Water absorbed from the environment in to the porous sol-gel coating came to the contact of crystalline surface, causing the etch pit nucleation at high under

saturation with their facets correspond to the low energy planes of KDP crystal. The growth of etch pit was found continuous until the reservoir of water in the sol-gel was saturated with KDP crystal. Moreover, in another study of surface dynamics during environmental degradation of KDP crystal surfaces, Whitman et al [57] have studied the occurrence of etch pits as a function of humidity and under saturation. The pit formation was characterized by nucleation and growth process. The introduction of water created a condition of under saturation at the crystal surface. The equilibrium step directions could define the orientations of the edges of the pits. The internal surfaces of the pits were the low index facets of KDP crystal.

It would have been an incomplete discussion, if the present author had not mentioned the efforts made by Sangwal and his colleagues to understand chemical etching of crystalline faces,particularly, on KDP crystals [15,58,59].

Nelson et al [60] have studied the X-ray photoemission spectroscopic aspects of etch pits on KDP crystals. They argued that the solution grown KDP was a stable phase in the $K_2O - P_2O_5 - (H,D)_2O$ ternary phase. If there was residual P_2O_5 on the surface following the growth and knowing the hydroscopic nature of P_2O_5 forming phosphoric acid (H_3PO_4), it can be surmised that the holes/etch pits were due to the chemical etching.

In the case of dislocations, the formation of etch pits may take place either by spontaneous opening up, by a repeated two dimensional nucleation process at edge dislocation or by unwinding of spiral turns of screw dislocation. The strain energy of dislocations is responsible for the spontaneous non-stationary

dissolution. But the later mechanism, involving stationary dissolution, is due to the geometrical arrangement of atoms/ molecules layers that localizes energy around them. It was suggested by Cabrera [21] that the transition from stationary to spontaneous non-stationary dissolution takes place at a critical value of under saturation. The verification of the Cabrera's model in the case of KDP crystals was carried out by Koziejowska and Sangwal [59]. They have found that existence of an under saturated barrier above which dislocation etch pits were easily formed. For the (001) and (110) faces of KDP, the values of these under saturations were found to be 9 % and 6.4 %, respectively. They concluded that the preferred occurrence of dissolution of crystal edges indicated that the surface dissolution took place by surface nucleation process, consequently, the Cabrera's theory of etch pit formation held good in the case of KDP.

7.6 Chemical Etching Procedure

The pure and amino acids doped KDP crystals were grown by slow solvent evaporation technique, which has been already explained in chapter II. The (100) face of pure and amino acids doped KDP crystals selected for the chemical etching studies. The etchant used for all crystals were AR grade glacial acetic acid (CH_3COOH). For every etching process, fresh etchant was used. The etching time was selected 10 second. For high temperature etching, the beaker containing etchant was heated by using suitable water bath of $\pm 0.1\ ^0$C accuracy and the crystal was dipped into the etchant for 10 seconds and, thereafter, removed and air dried before observation under microscope. A soft tissue cleaning was also done before air drying. The etching temperature was varied

from 25 ^{0}C to 40 ^{0}C with increment of 5 ^{0}C. The etch pits were observed by using Carl Zeiss NU2 microscope. For the measurements of etch pits width a filar eye-piece attached with microscope was used. Figure (7.2) shows the photograph of Carl Zyss microscope.

Figure: 7.2 Photograph of Carl Zyss microscope.

7.7 Etching Studies of Pure and Amino Acids Doped KDP Crystals.

Photomicrographs of etch pits observed on (100) face of pure and 0.3 wt % L – histidine, L-threonine and DL-methionine doped KDP crystals etched at 30 ^{0}C and 40 ^{0}C are shown in figures (7.3 a-h).

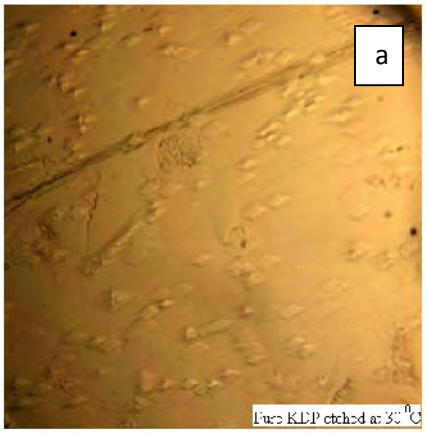

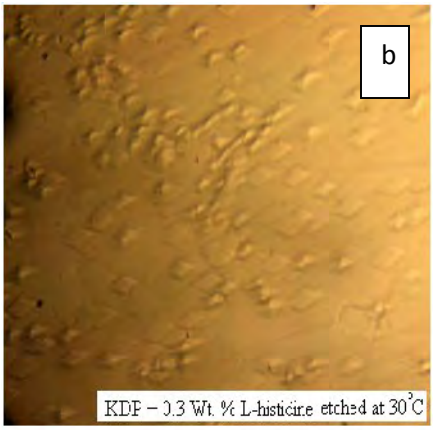

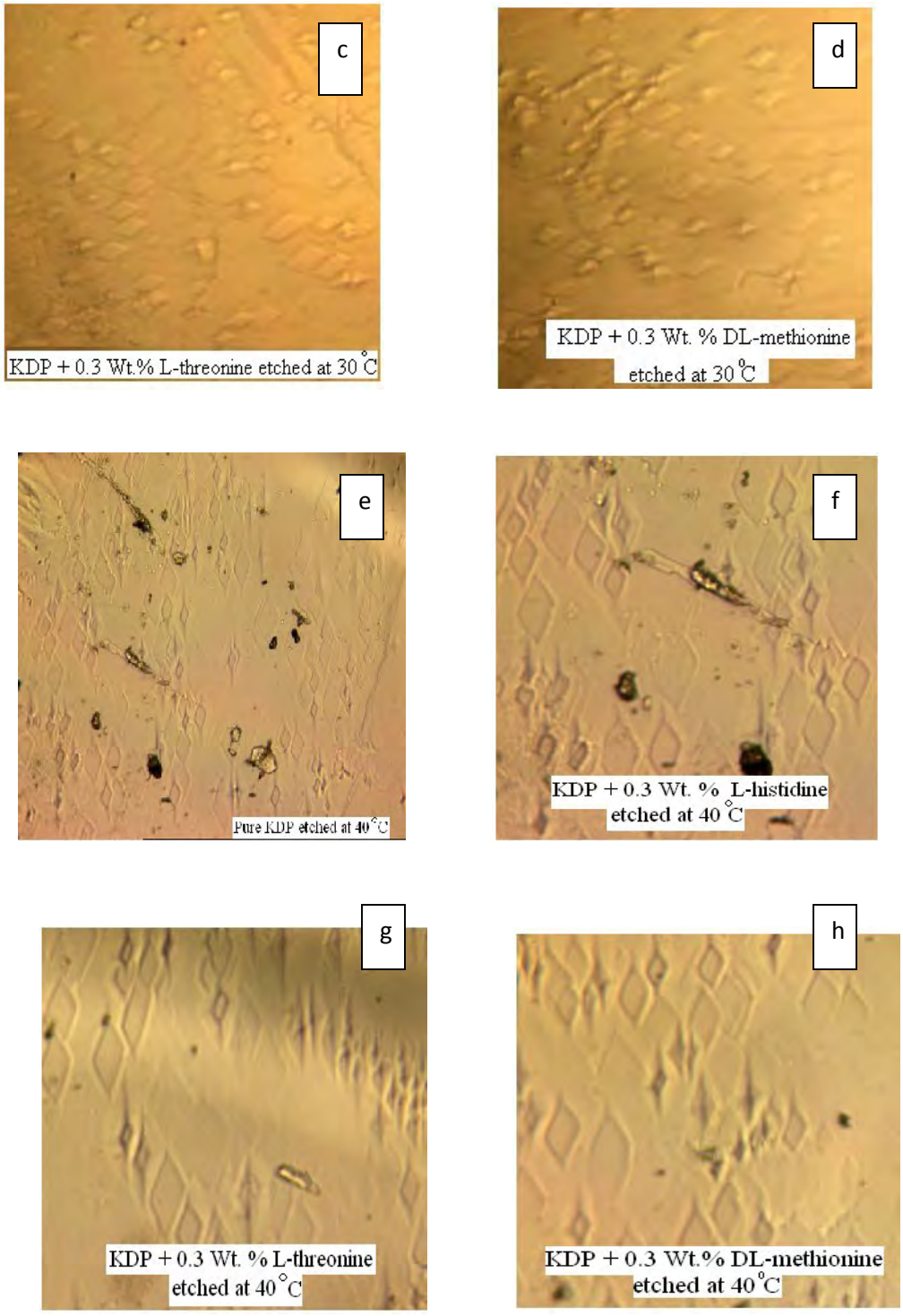

Figure: 7.3 Etched (100) face of pure KDP crystal (a &b), 0.3 wt % L – histidine (c& d), L-threonine (e & f) and DL-methionine (g & h) doped KDP crystal etched at 30 ^{0}C and 40 ^{0}C, respectively.

From the figures (7.3 a- h) of pure and 0.3 wt % aof these selected amino acids doped KDP crystals, one can see that the etch pits are rhombic in nature. Some of the etch pits are flat bottom and with blunt edges, which are likely to be due to doped impurities and thus may decorate the presence of doped compounds.

7.7 Kinetic Parameters

During the etching study of alkali halide crystals by various solutions, it has been found that nature of solvent, nature and concentration of impurities**,** temperature, stirring, under saturation, crystallographic orientation of the surface being etched, segregation of impurities at dislocations and kind of dislocations affect the formation of etch pits [58]. Moreover, Sangwal [15] has reported the roles of crystal structure, solvent surface orientation, additive impurities and reaction products in etching.

Altogether, there are different situations where solution of KDP is used as an etchant. The defect characterization of solution-grown single crystal of magnesium sulphate heptahydrate using chemical etching technique was reported by Karan and Sen Gupta [61], where double distilled water, $FeCl_3$, HCl, under saturated solution of KDP and saturated solution of KDP were used as an etchants.

Various authors have reported dislocation and etch pits by using different etchants on various crystals. It is very laborious to compile all details of etching, however, Joshi [62] has attempted to compile the details up to a certain extent. In the present author's laboratory dislocation etching has been studied extensively on various crystals, for examples, Bismuth single crystals [63-66], antimony

single crystal [67-70], anthracene single crystals [71,72], calcite crystal cleavages [73-78], Mn^{+2} and Cu^{+2} doped calcium L- tartrate crystals [79].

The Arrhenius equation is usually used today to interpret kinetic data, the problem of temperature dependence of reaction was of great deal of controversy and discussion during 1850 to 1910. Several empirical relations are well reported and discussed in details by Laidler [80, 81]. The following reactions can be considered for etch pits. Berthelot [82] proposed the equation,

$$W = Ae^{DT} \tag{7.13}$$

Where, *W* is the average width of etch pit, *T* is the absolute temperature, *A* and *D* are constants. This equation was supported by results of Hood [83] and the parameters could be determined by a plot of *log W* versus *log T.*

Harcourt and Esson [84] made their contributions to chemical kinetics by formulating and applying the method of integration and suggested an equation for temperature dependence in the following form:

$$W = AT^{m} \tag{7.14}$$

Where, *W* is the average width of etch pit, *T* is the absolute temperature, *A* and *m* are constants.

The parameters can be evaluated from the plots of *log W* versus *log T.* In 1898, Van't Hoff [85] pointed out that most of the equations that had been proposed for temperature dependence were special case of the following type three parameter equations.

$$W = AT^{m} \exp -\left\{\left(B - DT^{2}\right)/T\right\} \tag{7.15}$$

By about 1910 the only one-parameter temperature dependence equation to survive was the Arrhenius equation [82]. This was not because it was empirically the best, but it provides an insight into how the reactions proceed.

$$W = Ae^{-E/RT} \quad \text{or} \quad \log W = \log A - E/RT \tag{7.16}$$

Where, W = Average width of etch pit, A = Pre-exponential factor, E = Activation energy of the reaction, R = Gas constant, T = Absolute temperature

The Pre-exponential factor or frequency factor is related to the collision frequency and the steric factor. Boikess and Edelson [86] describe that the value of A increases if the steric factor increases or collisions frequency increases. In other words, a reaction will be faster if there is more collision or a higher percentage of the collisions which have the proper orientation required for product formation. The specific rate constant is high for fast reactions. It is evident from the above expression that as E, the activation energy, increases, the value of W decreases and consequently the reaction rate decreases. The activation energy is considered as a barrier to be surmounted to form the reaction product. Therefore, the higher values of activation energy show slower reaction rates.

In the present investigation, the flat bottom Rhmobus etch pits were obtained in all cases including pure KDP. More than 25 etch pits were measured to find the average etch pit width at each temperature.

Table: 7.1 The values of activation energy and pre-exponential factor for pure and amino acid doped KDP crystals.

Sample	Activation energy kJ/mol	Pre-Exponential Factor
Pure KDP	21.95	1.96×10^{9}
KDP + 0.3 Wt.% L- histidine	19.59	2.75×10^{6}
KDP + 0.4 Wt.% L- histidine	20.33	5.39×10^{6}
KDP + 0.5 Wt.% L- histidine	19.82	3.58×10^{6}
KDP + 0.3 Wt.% L- threonine	18.63	1.40×10^{6}
KDP + 0.4 Wt.% L- threonine	18.43	1.23×10^{6}
KDP + 0.5 Wt.% L- threonine	18.51	1.36×10^{6}
KDP + 0.3 Wt.% DL-methionine	17.54	4.09×10^{5}
KDP + 0.4 Wt.% DL-methionine	17.21	4.48×10^{5}
KDP + 0.5 Wt.% DL-methionine	17.47	5.67×10^{5}

Table 7.1 summarizes the values of activation energy and pre-exponential factors, calculated for pure and amino acids doped KDP crystals. The Arrhenius plots of logarithm of average pit width *W* versus reciprocal of absolute temperature *T* for pure KDP crystal and various weight percentage amino acids (L-histinine, L- threonine & DL-methionine) doped KDP crystals respectively, are shown in figures (7.4-7.6). From the slope of the plots the values of activation energy and pre-exponential factors were calculated.

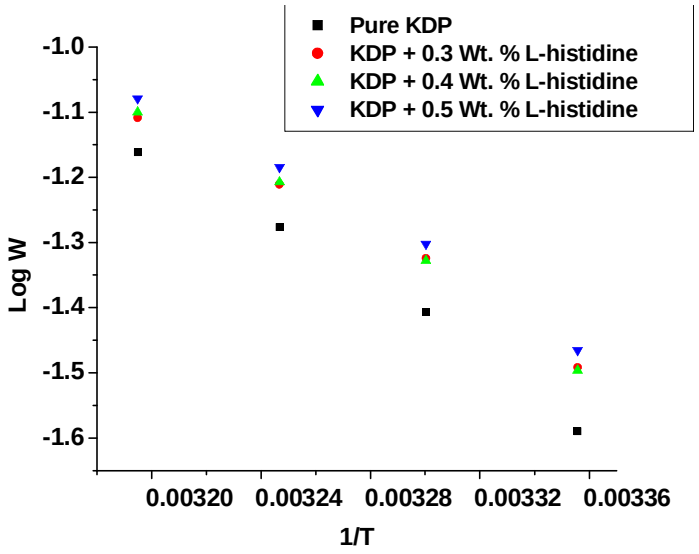

Figure: 7.4 Plots of log W → 1/T for pure and L-histidine doped KDP crystal.

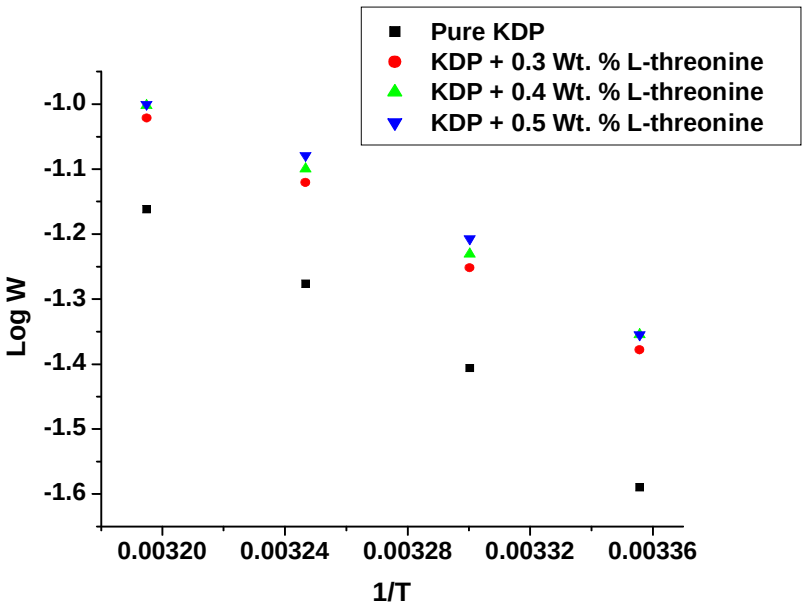

Figure:7.5 Plots of log W → 1/T for pure and L-threonine doped KDP crystal.

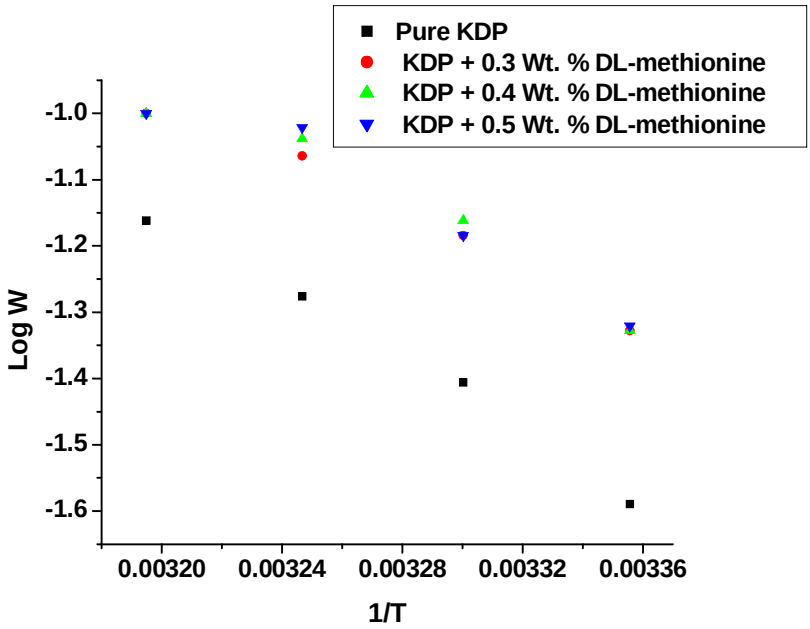

Figure :7.6 Plots of log W → 1/T for pure and DL-methionine doped KDP crystal.

From table 7.1, one can observe that the activation energy is highest for pure KDP crystals compared to amino acids doped KDP crystals. Further, the activation energy slowly decreases from L-histidine to L-threonine and then to DL-methionine. The lower values of activation energy for amino acids doped

KDP crystals compared to pure KDP crystals indicates higher reaction rate for doped crystal. The doping of amino acid is expected to increase the reactivity at line defects by facilitating preferential chemical reaction. But for a particular dopant, the activation energy remains practically constant even if the concentration of that dopant changes, while the pre-exponential factor does not show any systematic variation. But this factor is higher for pure KDP crystals, compared to the doped crystals. In doped crystals the pre-exponential factor is found higher for L-histidine doped KDP crystals and then it drops for L-threonine and it has the minimum values for DL-methionine doped crystals. It has been observed by Joshi and Shah [87] that the shape of molecule and its reactivity plays important roles in reactivity at line defects. They have studied the effect of n-propyl alcohol and iso-propyl alcohol containing etchants and found that the branched iso-propyl alcohol containing etchant exhibits lower reaction rate the higher values of activation energy compared to n-propyl alcohol.

In the present study, the three selected amino-acids viz. L-histidine, L-threonine and DL-methionine doped KDP crystals have shown different values of activation energy, as this can be seen from table (7.1). The values of activation energy are higher for L-histidine containing KDP crystals than the other two amino acids containing KDP crystals. The molecular structure of amino acids are shown in Chapter-6, indicating that L-histidine has closed structure with imidazole group attached to it and possess basic nature, while L- threonine has linear structure having hydrophobic nature and unchanged or non-ionic polar side chains and DL-methionine has also linear structure with non-polar side chains

and possess hydrophobic nature. It can be conjectured that the closed structure with attached branch of L-histidine offers steric hindrance and exhibits lower reactivity with etchant containing acetic acid and offer lower reactivity with etchant containing acetic acid and offer high activation energy among all the three amino acids studied. The hydrophobic nature and non-polar side chain of DL-methionine has offered higher reactivity compared to its linear counter part with polar side chain- L- threonine to the reacting etchant.

7.8 Thermodynamic Parameters

The thermodynamic parameters can be estimated for the motions of ledges of etch pits. Various thermodynamic parameters are obtained from the following standard relations [81]. The standard enthalpy of activation ($\Delta^{\#}H^{o}$) was calculated by using the following relation,

$$\Delta^{\#}H^{o} = E - 2RT \qquad (7.17)$$

The standard change in entropy of activation ($\Delta^{\#}S^{o}$) could be calculated by using the following formula,

$$W = \frac{kT}{h} \text{ x } \exp\left(\Delta^{\#}S^{0}/R\right) \text{ x } \exp\left(\Delta^{\#}H^{0}/RT\right) \qquad (7.18)$$

Where, W = Average width of etch pit, k = Boltzmann constant, h = Planck's constant, T = Absolute temperature, R = Gas constant

The standard change in Gibbs free energy of activation ($\Delta^{\#}G^{o}$) is possible to estimate from the following equation

$$\Delta^{\#}G^{o} = \Delta^{\#}H^{o} - T\Delta^{\#}S^{o} \qquad (7.19)$$

The standard change in the internal energy in passing from the initial to the activated state $(\Delta^{\#}U^{o})$ can be represented as,

$$E = RT + \Delta^{\#}U^{o} \quad (7.20)$$

Enthalpy is a state function whose absolute value cannot be known easily; it $(\Delta^{\#}H^{o})$ can be ascertained, either by direct method or indirectly. An increase in the enthalpy of a system, for which $\Delta^{\#}H^{o}$ is positive, is referred to as an endothermic process. Conversely, loss of heat from a system, for which $\Delta^{\#}H^{o}$ has negative value, is referred to as an exothermic process.

Table: 7.2 Thermodynamics parameters for pure and amino acids doped KDP crystals.

Sample	**Standard Entropy $\Delta^{\#}$ S° JKMol^{-1}**	**Standard Enthalpy $\Delta^{\#}$ H° kJ Mol $^{-1}$**	**Standard Gibbs free energy $\Delta^{\#}G^{o}$ kJ Mol $^{-1}$**	**Standard change in internal energy $\Delta^{\#}$ U° kJ Mol $^{-1}$**
Pure KDP	-45.9311	16.920	30.837	19.434
KDP+0.3 Wt.% L-histidine	-53.2603	14.560	30.698	17.074
KDP+0.4 Wt.% L-histidine	-50.6894	15.300	30.659	17.814
KDP+0.5 Wt.% L-histidine	-52.4012	14.790	30.667	17.304
KDP+0.3 Wt.% L-threonine	-56.9187	13.598	30.844	16.112
KDP+0.4 Wt.% L-threonine	-57.7279	13.400	30.891	15.914
KDP+0.5 Wt.% L-threonine	-57.3492	13.480	30.857	15.994
KDP+0.3 Wt.% DL-methionine	-63.7978	12.110	31.440	14.624
KDP+0.4 Wt.% DL-methionine	-63.4041	12.180	31.391	14.694
KDP+0.5 Wt.% DL-methionine	-62.1054	12.440	31.258	14.954

Entropy is a thermodynamic property of a system. It is a state function and it is defined in terms of entropy change rather than its absolute value. A spontaneous process has a natural tendency to occur, without the need for input work into the system. In contrast to this, the non-spontaneous process does not have a natural tendency to occur.

The values of the standard change in Gibbs energy of activation remain more-or-less constant for particular doping of amino acid in KDP. Any effect, for example, that leads to a stronger binding between a solute molecule and solvent molecules will lower the enthalpy; it will lower entropy by restricting the freedom of vibration and rotation of the solvent molecules. This has been observed for amino acid doped crystals, where the values of standard change in enthalpy and entropy are lower compared to pure KDP crystals. However, change of substituent and solvent often exert their influence on $\Delta^{\#}H^{o}$ in a rather complex manner, but the partial compensation between $\Delta^{\#}H^{o}$ and $T\Delta^{\#}S^{o}$ is of such a nature that their influence on $\Delta^{\#}G^{o}$, is much simpler [84]. In the present study the negative values of $\Delta^{\#}S^{o}$ and moderate values of frequency factor *A* indicate the formation of the intermediate complex compound in etching, which has been observed earlier [88,89] and also may be the rate determining.

Conclusion

1. Glacial acetic acid as an etchant revealed dislocations on the (100) surfaces of pure KDP crystals as well as selected amino acids (L-histidine, L-threonine and DL-methionine) doped KDP crystals.
2. The shape of the etch pits did not vary upon the change of temperature from 25 ^{0}C to 40 ^{0}C and also remained invariant for pure and selected amino acids doped KDP crystals.
3. The activation energy was highest for the pure KDP crystals, while its value slightly decreased in the successive manner with the doping of L-histidine, L-threonine and DL- methionine, respectively. This suggested that the most stable nature of KDP crystals and on doping of amino acids it enhanced the reactivity at line defects by facilitating the extra sites for chemical reaction. The chemical structure of amino acids also played important role.
4. The pre-exponential factor value was highest for pure KDP crystal, whereas, the lower values for amino acids doped KDP crystals were observed. The pre exponential factor dropped in its value from $\approx 10^9$ for pure KDP crystals to amino acids doped KDP crystals to $\approx 10^6$, without much affecting the activation energy. The pre-exponential factor is dependent on the collision frequency and the steric factor. Therefore, it can be conjectured that the dopant amino acids reduce the steric hindrance giving rise to increased reactions sites for the attacking etchant might be due to increased steric factor and the non coplanar NH_2 in

various amino acid structure. Further the pre-exponential factor also decreased in successive manner for L-histidine, L-threonine and DL-methionine doped KDP crystals, respectively. The molecular structure of amino acid played important role.

5. There was a systematic downward trend for standard change in enthalpy and the standard change in entropy from pure KDP and selected amino acids doped KDP crystals. Therefore, it can be inferred that the influence of amino acid doping was such that the value of $T\Delta^{\#}S^{o}$ and $\Delta^{\#}H^{o}$ compensated each other so that $\Delta^{\#}G^{o}$ remained practically constant for the particular amino acid doping in KDP crystals.

References:

1. J. J. Gilman, W.G. Johnston, *J. Appl.Phys*. **27** (1956) 1018.
2. V. Venkataramanan, G. Dhinaraj, V.K. Wadhawan, J.N. Sherwood, H.L. Bhatt, *J. Cryst. Growth* **154** (1995) 92.
3. F.J. Rethimanam, D. Arivuoli, S. Ramasamy, P. Ramasamy, *Mater. Res. Bull*. **29** (1994) 309.
4. N. Nakatani, *Japanese J. Appl. Phys*. **L1961** (1991) 30.
5. I. Owezarek, K. Sangwal. *J. Mater. Sci. Lett*. **9** (1990) 440.
6. D. Rugar, P.K. Hansma, *Phys. Today* **43** (1990) 23.
7. A. J. Gratz, S. Manne, P. K. Hansma, *Scince* **251** (1993) 1343.
8. V. B. Paritskii, S. V. Lubenets, V. I. Startsev, *Sov. Phys. Solids State* **8** (1966) 976.
9. J. J. Gilman, W. G. Johnson, G. W. Sears, *J. Appl. Phys*. **29** (1958) 747.
10. J. W. Faust , Jr, "*The Surface Chemistry of Solids*", Wiley, New York (1960).
11. B. D. Cuming, A. J. W. Moore, *J. Australian Inst. & Metals* **3** (1958) 124.
12. W. K. Burton, N. Cabrera and F. C. Frank, *Phil. Trans. Roy. Soc. London* **A243** (1951) 299.
13. J. J. Gilman, W. G. Johnson, *J. Appl. Phys*. **29** (1958) 877.
14. N. Cabrera, M. M. Levine, *Phil. Mag*. **1** (1956) 458.
15. K. Sangwal, *J. Mater Sci*. **17** (1982) 2227
16. R. B. Heimann, *Auflosung von kristallen*, *Springer-Verlag, Wien***,** New York, (1975).
17. K. Sangwal, *J. Mater*. *Sci*. **15** (1980) 237.

18. N. Cabrera, *J. Chem. Phys*. **53** (1956) 675.

19. N. Cabrea, M. M. Levine, *Phil. Mag*. **1** (1956) 450.

20. W. Schaarwachter, *Phys. Status Solidi* 12 (1965) 375.

21. N. Cabrera, "*The Surface Chemistry of Metals and Semiconductors*", Wiley, New York (1960).

22. M. B. Ives, D.D. McAusland, *On the slope of Etch pits, Technical Report*, no.11, U.S. Office of Naval Research, Jan, (1968).

23. I. N. Stranski, *Phys. Chem*. **11B** (1931) 342.

24. J. P. Hirth, G. M. Pound, *J. Chem. Phys*. **26** (1957) 1216.

25. M. B. Ives,J. P. Hirth, *J. Chem. Phys.* **33** (1960) 517.

26. W. G. Johnson, *Progress in Ceramic Sci.* **2** (1961)9.

27. J. J. Gilman, "*The surface chemistry of metals and Semiconductors",* Wiley, New York (1960).

28. S. N. Andreev, V. G. Khaldin, *Dokldy Akad. Nauk, SSSR,* **134** (1962) 335.

29. S. N. Andreev, O. V. Sapozhnikova, *Zn. Neorg. Khimi* 13 (1968) 1548.

30. J. Bjerum, G. Schwarzenbach, L. G. Silline, *Stability Constants*, Part II, Chemical Society, London (1958).

31. F. L. Vogel, W. O. Pfann, H. E. Corey, E. E. Thomas, *Phys. Rev*. **90** (1953)489.

32. F. L. Vogel, *J. Metal.* **8** (1956) 746.

33. R. Gevers, S. Amelinckx, W. Dekeyer, *Naturwissenschaften* **39** (1952) 448.

34. R. Gevers, *J. Chim. Phys*. **50** (1953) 321.

35. J. J. Gilman, *J. Appl. Phys.* **31** (1960) 936.

36. D. A. Young, *Nature* **182** (1985) 375.

37. K. Sangwal, *Key Engg, Mater.* **58** (1991) 187.

38. J. J. Gilman, W.C. Johnson, "*Dislocations and Mechanical properties of Crystals"*, Wiley, New York (1957).

39. K. Sangwal, "*Etching of Crystals: Theory, Experiments and Applications*", North Holland (1987).

40. A. Amelinckx, "*The Direct Observation of Dislocations"*, Academic press, London (1964)

41. W. G. Johnson, "P*rogress in ceramic sciences"*, Vol 2, Pergamon press, Oxford (1962).

42. R. B. Heimann, "*Principles of Chemical etching– the arts and science of Etching Crystals",* Springer,1982

43. S. Amelinckx, *Acta. Met*. **2** (1954) 848.

44. F. L. Vogel, *Acta Met*. **3** (1955) 95.

45. W. R. Hibbard, C. G. Dann, *Acta. Met.* **4** (1956) 30.

46. J. J. Gilmann, W. C. Johnson, *"Dislocations and Mechanical properties of Crystals*", Wiley, New York (1957).

47. S. Amelinckx; *Phil. Mag.* **1** (1956) 269.

48. S. Balamurugan, G. Bhagavannarayana, P. Ramasamy, *Mater. Lett.***62(24)** (2008)3963.

49. S. Balamurugan, P. Ramasamy, *Mater. Chem & Phys.***112** (2008)1.

50. G. Ravi, A.S. H. Hameed, P. Ramasamy, *J. Cryst. Growth* **207** (1999)319.

51. Z. De-Gao, T. Biny, D. S. Ming, W. Qing-Guo, Z. Yan-Shuai, H. Wan-Xia, Yu Tao, *Cryst. Res. Technol.* **44** (2009) 500.

52. P. Feng, L. Jin Kai, S. U. Genbo, He youping H. B. Ring, H. Yisen, Z. Ceinglan, *Cryst. Res.Technol*. **26** (2006) 289

53. S. S. Gupta, T. Kar, S. P. Sen Gupta, *Appl. Phy.* **32** (1993) 1160.

54. S. S. Gupta, S.P. Sen Gupta, *Jpn. J. Appl. Phy.* **35** (1996) 6180.

55. S. Javidi, H. Faripour, M. Esmaeil Nia, K. F. Sepehri, N. Ali Akbari, semicond. *Phys Quant Electra & Optoelectr.* **11** (2008) 248.

56. E. K. Wheeler, P. K. Whitman, T. A. Land, C. B. Thorsness, J. H. McWhirter, M. L. Hanna, E. L. Miller, *Appl. Phys*. *A.* **74** (2002) 813.

57. P. Whitman, J. DeYoreo, T. Land, E. Miller, T. Suratwala, C. Thorness, E. Wheeler, Tech. Rep, Lawrence Livermore National Laboratory, CA, USA, UCRL-ID-134532-REV-1,(2001).

58. K. Sangwal, G. Zaniewska, *J. Mater. Sci*. **19** (1984) 1131.

59. A. Koziejowska, K. Sangwal J.Mater. Sci. **23** (1988) 2989.

60. A. J. Nelson, T. van Buuren, Eric Miller, T. A. Land, C. Bostedt, N. France, P. K. Whitman,P. A. Baisden and L. J. Terrninello and T.A. Callcott, “X-ray absorption analysis of KDP optics”UCRL VG-138950, submitted to *J. Electron Spectrosc. Related Phenomena (2001).*

61. S. Karan, S. P. Sen, Gupta, *Indian J. Phys*. **76A** (2002) 561.

62. M. J. Joshi, *Ph. D. Thesis*, Saurashtra University, Rajkot, India(1986).

63. K. C. Poria, M. J. Joshi, B. S. shah, *Indian J. Phys*. **7lA** (1997) 593.

64. B. S. Shah, M. J. Joshi, L. K. Maniar, *Indian J. Phys*. **65A** (1991) 113.

65. P.C. Shah, B. S. Shah, *Indian J. Pure and Appl. Phys*. **30** (1992) 176.

66. B.S. Shah, M.J. Joshi, L. K. Maniar, *Cryst. Latt. Def. and Amorph Mat*. **17** (1988) 417.

67. A. H. Raval, M. J. Joshi, B. S. Shah, *Indian J. Phys*. **70A** (1996) 569.

68. A. H. Raval, M. J . Joshi, B. S. Shah, *Cryst. Res.Technol.* **30** (1995) 1003.

69. A. H. Raval, M. J. Joshi, *Indian J. Phys*. **68A** (1994) 113.

70. C. P. Maniar, A.H. Raval, M. J. Joshi, *Indian J. Phys*. **75A** (2001) 525.

71. R. M. Vaishnav, L. K. Maniar, M. J. Joshi, R. M. Dabhi, *Indian J. Phys*. **74A** (2000) 581.

72. R. M. Vaishnav, B. J. Mehta and B. S. Shah*, Rev. Latin. de Metaly Mater* **2** (1982) 153.

73. B. J. Mehta, G. R. Sidapara, *Cryst. Res. Technol.* **25** (1990) 81.

74. B. T. Thumar, B. J. Mehta. *Cryst..Res. Technol*. **19**(1984) K57.

75. B. J. Mehta, *Cryst .Res. Technol.* **l6** (1981) 1097.

76. B. J. Mehta, *Surfuce Technol.* **13** (1981) 33.

77. B. J. Mehta, *Surface Technol*. **12** (1981) 253.

78. B. J. Mehta, *Surface Technol.* **11** (1980) 301.

79. S. R. Suthar, *Ph. D. Thesis*, Saurashtra University, Rajkot (2007).

80. K. J. Laidler, *Chem. Edu*. **49** (1972) 343.

81. K. J. Laidler, "*Chemical Kinetics*", Harper & Row, New York(1987).

82. M. Berthelot, *Am. Chem. Phys*. **66(3)** (1862)5.

83. J. J. Hood, *Philos. Mag*. **20(5)** (1885) 323.

84. A. V. Harcourt and W. Esson, *Philos Trrans.* **186** (1895) 817.

85. J van't Hoff *"Lectures on theoretical and Physical chemistry",Pt -1,* "Chemical Dynamics", Edward Arnold, London(1898).

86. R.S. Boikess, E. Edelson, "*Chemical principle",* Harper & Row, New York (1978).

87. M. J. Joshi, B. S. Shah, *Cryst. Lett. Def. & Amorph. Mater.* **11** (1985) 229.

88. H. H. Garcher, P. H. Parsania, *Proc. Indian Acad. Sci. (Chem. Sci.)* **107**(1995)593.

89. K. C. Poria, M. J. Joshi, B. S. Shah, *Indian J. Phys*. **71a**(1997)593.

Chapter VIII

Micro-hardness Studies of Pure and Amino Acids Doped KDP Crystals

8.1 Introduction:

The concept of hardness varies with situation. A convenient definition is generally given by one's own perception and thoughts; the hardness in terms of sawing, drilling or filing or the hardness in terms of wearing a job as a machinist thinks; while an engineer grades his material on the basis of the depth of penetration of a hard indenter as it is forced into a surface with specific force.

The resistance offered by material to indentation by a relatively harder body is known as hardness. The most common method of determining hardness consists of indenting a solid surface by a loaded indenter of a definite geometrical shape and measuring the contact area between the indenter and the material. The ratio of the load and the contact area is the experimental definition of hardness. Most of the techniques for the determination of hardness are essentially means of giving a quantitative value to the materials ability to resist load deformation [1]. Hardness is defined alternatively as resistance against lattice destruction [2] and also stated as the resistance offered by a solid to permanent deformation.

Nevertheless, attempts have been made to define hardness in numerous ways such as: "Hardness is like the storminess of the sea, easily appreciated but not readily measured (or defined) [3]". "The hardness is not a single property but rather a complex of mechanical properties and at the same

time a measure of intrinsic bonding of the material [4]". "There are clear connections between chemical bonding, hardness and dislocation mobility [5]". The precise definition of hardness depends entirely on the method of measurement [6]. Resistance to the movement of dislocations will determine the hardness of the materials [7].The above quotes suggest a complexity in defining the hardness.

For quite some time, only metallurgists and mineralogists were interested in hardness. However, in the last several decades, physicists and chemists also have involved themselves in studies of hardness. Discussion of various aspects of hardness and data on a large number of materials are found in books [3-6], compilations [7-13] and also in several articles strewn over many scientific journals.

Several methods are available for the measurement of hardness. Shaw [11] has listed various hardness tests and categorized them. Nevertheless, the most commonly used form of measuring hardness of sample is the indentation type. An elaborate description of these methods, with their relative merits and demerits, is given in the books by Tabor [3] and Mott [6]. In order to describe the ISE (Indentation Size Effect) and RISE (Reverse Indentation Size Effect) behaviors of materials, several models for relation between applied indentation test load and indentation diagonal length have been reported in the literature [3] and in this chapter it has been explained with the help of Meyer's law [6] and Kick's law [13], Hays and Kendall's [14] approach and Proportional Specimen Resistance (PSR) model proposed by Li and Bradt [15].

8.2 Methods of Hardness Testing

Various hardness tests can be briefly reviewed as follows on the basis of compilations of Tabor [3] and Mott [6].

8.2.1 Dynamic Hardness

In this type of test an indenter is dropped from a given height on the surface and the depth of the impression produced is measured. The hardness is expressed in terms of energy of the impact and the depth and size of the indentation.

1. Scratch hardness

This test is the oldest form of hardness measurement and was probably developed by mineralogists. In the first test one merely observes whether the selected material is capable of scratching another. In the second form of this method, the hardness number is expressed in terms of width or depth of a scratch made with a diamond or a steel indenter, under a definite load traversing the surface at a steady rate.

2. Rebound hardness

The hardness is given by the height of rebound of diamond tipped weight falling on the surface from a fixed height. The shore Scleroscope is an instrument of this type.

3. Plowing hardness

In which a blunt element is moved across a surface under controlled conditions of load and geometry and the width of the groove is the measure of hardness. The Bierbaum test is of this type.

4. Cutting hardness

Sharp tool of a given geometry is caused to remove a chip of standard dimensions.

5. Damping hardness

In this test, change in amplitude of a pendulum having hard pivot resting on test surface is the measure of hardness. The Herbert pendulum test is of this type.

6. Abrasion hardness

Specimen is loaded against a rotating disk and the rate of wear is taken as a measure of hardness.

7. Erosion hardness

Sand or abrasive gram is caused to impinge upon the test surface under standard conditions and loss of material in given time is taken as the measure of hardness.

In the present chapter, the author describes micro-hardness using a Vickers hardness tester, which falls under the static hardness category. A brief account on various static indentation tests is presented here.

8.2.2 Static Indentation Tests

For an indentation method, when a loaded indenter is pressed against the surface of the material, it creates dislocations. As the indentation continues, newly created dislocations push the dislocations created earlier. These dislocations move in some preferred direction in the crystal depending on the slip systems. This motion of dislocations is obstructed by at least four factors, viz.

1. Impurities and precipitates present in the material (impurity hardening)
2. Other dislocations present in the material (dislocation hardening)

3. Grain boundaries (grain boundary hardening)

4. The chemical forces in the lattice of the material (intrinsic hardness).

Thus, the hardness of a pure (free from impurities) and well-annealed (free from excessive number of dislocations and grain boundaries) crystal represents the intrinsic hardness, which reflects the bond strength. Creation of hardness indentation and obstacles are shown in the form of schematic diagram in Figure (8.1). The low-load indentation method of hardness testing is popular because it offers several advantages viz.:

1. It is simple and does not consume much time
2. It can be used on samples with small areas, e.g. small crystals
3. It can be used on brittle materials which cannot withstand large loads, e.g. glasses.

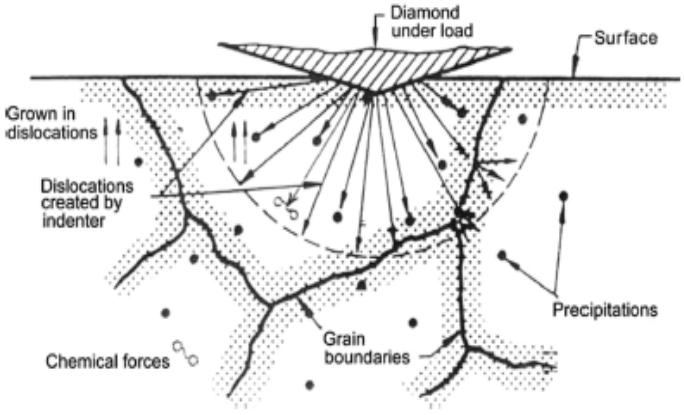

Figure:8.1 Schematic diagram of resistance to motion of dislocation [13].

To cover a broad range of materials with a wide range of testing conditions, the static indentation tests are the most favored ones and give much insight in studying the properties of a given material. The four main tests in this category are as follows:

1. Brinell Test

It is perhaps the first scientific technique to measure hardness of materials. In a standard Brinell test [16] a hard steel ball of about 1 cm. diameter is pressed normally on the surface of metal under examination for a standard period of 30 sec. After the removal of the load, the indentation impression is measured. The impression may not be circular due to some reasons necessitating the measurement of two diagonals at right angles and using the mean value for estimating the hardness number. To reduce various errors, usually, the geometrical similarity of indentation marks should be preserved and hence the diameter of the impression mark should be kept within the range of 0.25 to 0.50 times the diameter of the ball.

The Brinell hardness number, or simply the Brinell number, can be obtained by dividing the load used, in kilograms, by the actual surface area of the indentation, in square millimeters. The result is a pressure measurement, but the units are rarely stated. The Brinell hardness test uses a desk top machine to press a 10 mm diameter, hardened steel ball impressed onto the surface of the test specimen. The machine applies a load of 500 kilogram for soft metals such as copper and brass. A 1500 kilogram load is used for aluminum castings and a 3000 kilogram load is used for materials such as iron and steel. The load is usually applied for 10 to 15 second. After the impression is made, a measurement of the diameter of the resulting round impression is taken. The hardness is calculated by dividing the load by the area of the curved surface of the indention. Among the three hardness tests, the Brinell ball makes the deepest and the widest indentations, so the test averages hardness over a wider amount of material, which is more accurate

to be account for multiple grain structures and any irregularities in the uniformity of the alloy.

The test has its demerits when it is applied for materials with hardness greater than 500 kg/mm^2; the deformation of the ball and in turn erratic measurements occur. An ultrasonic hardness tester – a modified version of the Brinell test has been developed to enable instantaneous and automatic read out by Szilard [17].

2. Rockwell Test

In this test a spherical or conical diamond indenter with a spherical tip is used. First a small preliminary load is applied and the dial guage is set to zero, then the main load is applied, upon removal of the load the depth of the residual indentation is measured, which is directly read off on the dial guage quoted as Rockwell Numbers. The advantage of this method lies in the rapidity with which it can be carried out and also because it does not involve optical measurements; which makes it very favorable in industries.

The main disadvantage of this test lies with the piling up, sinking in and the elastic recovery upon removal of the load. A possible solution is due to the area of the indentation formed under the load is deduced from the acoustic impedance of the indenter-metal interface [18]. Again the dial reading is taken for hardness number, but it is based on the area of the indentation not on its recovered depth.

3. Vickers Test

In the Vickers test, Smith and Sandland [19] have used a diamond pyramidal indenter. The diamond is the hardest material; it is applicable to determine the hardness of extremely hard materials. This test has the advantage of geometrical similarity of impression at different loads.

Smith and Sandland [20] observed that the size of ideal ball impression such that its diameter was 0.375 times the diameter of the ball in a Brinell test. They choose 136^0 as the angle for the diamond indenter, which corresponds to the tangential angle of the ball impression.

The procedure to measure hardness is the same as in the Brinell test. The Vickers Diamond Pyramid Hardness (DPH) number or simply Vickers Hardness Number (H_v) is defined as

$$\text{DPH or } H_V = \frac{Load}{Pyramidal\ area\ of\ the\ indentation\ mark} \quad (8.1)$$

For an applied load *P* in kilogram, if the diagonal of the impression mark is *d* mm, then,

$$H_v = P / (1/2)\, d^2 \sin [(1/2)\,(136^0)] \quad (8.2)$$

$$= 1.8544\, (P/d^2)\ MPa \quad (8.3)$$

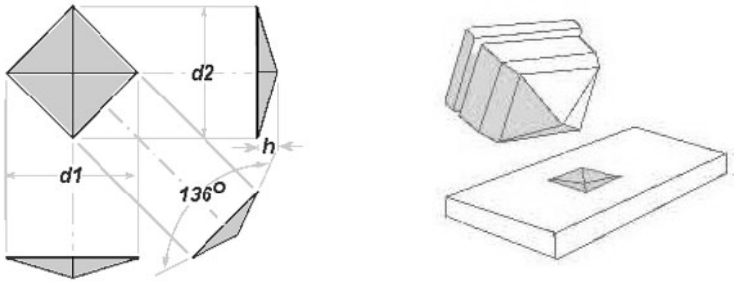

Figure: 8.2 Schematic Diagram of Vickers Identation Mark.

Where, *P* is the applied load (measured in N) and d^2 is the area of the indentation (measured in meter square). The Vickers test is reliable for measuring the hardness of metals and also used for ceramic materials. The impression left by the Vickers penetrator is a dark square on a light background. Several loadings give practically identical hardness numbers on uniform material, which is much better than the arbitrary changing of scale with the other types of hardness testing machines. A filar microscope is

swung over the specimen to measure the square indentation to a tolerance of plus or minus 1/1000 of a millimeter. The measurements taken across the diagonals to determine the area and are averaged. The correct Vickers hardness is designated as the number followed H_v (Hardness Vickers). The Vickers hardness test provides extremely accurate readings and just one type of indenter is used for all types of metals and surfaces. This method is adaptable and very precise for testing the softness and hardness of all the materials, under the varying loads. The Vickers machine is a floor standing unit that is rather more expensive than the Brinell or Rockwell machines. The present author has used Vaiseshikha Vickers micro-hardness tester.

The geometry of the indentation made with Vickers pyramid is independent of the depth and hence the hardness should be independent of the load. This is not the case as in the Brinell test.

4. Knoop Test

Knoop et al [21] have modified the Vickers test. In this test, a diamond indenter is used but its shape is such that it forms an elongated pyramidal impression, with the angles between the long and short edges being 172^0 30' and 130^0 respectively. The shape of the impression is that of a parallelogram for which one diagonal is about seven times the length of the other. The knoop test is very useful in studying the effect of crystal orientation on hardness.

The Knoop hardness (H_k) is obtained from the following formula:

$$H_k = 14.229\ (P/d^2) \qquad (8.4)$$

Where, *P* is the applied load (measured in N) and d^2 is the area of the indentation (measured in square meter). The Knoop hardness numbers are often cited in conjunction with specific load variation. Aside from a minor

savings of time, one of the main advantages of the Knoop test is that it can test thin layers more easily. For surfaces with varying hardness, such as in case of hardened parts, the Knoop indents can be spaced closer than Vickers indents. Thus, a single Knoop traverse can define a hardness gradient more simply than a series of two or three parallel Vickers traverses in which each indent is made at different depths. Furthermore, if the hardness varies strongly with the depth, the Vickers indent is distorted by this change; i.e., the diagonal parallel to the hardness change is affected by the hardness gradient, while the diagonal perpendicular to the hardness gradient remains unaffected.

5. Nano-identation

The nano-indentation is used for measuring hardness at very small length scales. The commonly used indenter for nano-indentation is the Berkovich diamond indenter which is a triangular diamond pyramid. In this, the lateral dimension of the contact impression is approximately seven times the depth. So, the measurements are possible for contact impressions with lateral dimensions 0.1 μm. A detailed procedure for the determination of mechanical properties of very thin coatings and films using the nano-indentation technique was first described by Oliver and Pharr [12].

8.3 Experimental Technique

Pure and various amino acids ((L-histidine, L-threonine, DL-methionine) doped KDP crystals were subjected to Vickers micro-hardness studies. Indentations were made on smooth (100) faces. The Vickers micro-hardness tester is shown in figure (8.3 a). The instrument comprises of microscope with a filar micrometer eyepiece (least count 0.0001428 mm) mounted on a stand. A loading and unloading mechanism is attached to the

microscope for taking indentation of a diamond indenter on a specimen surface under certain loads in gram. An illumination system is mounted on the microscope with a rotating table. The set up is having accuracy of ± 20 Vicker. In the present study, the Vickers indenter loads were varied from 0.298 N to 0.98 N in order to study the effect of load on micro-hardness. The indentation time of 15 second was kept constant throughout the experimental work. The size of the impression was measured using a filar micrometer eyepiece.

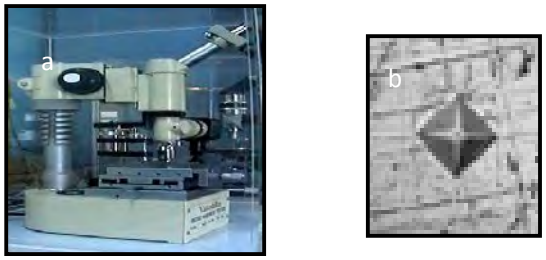

Figure: 8.3a, b Vaiseshika Vickers micro-hardness tester and indentation mark.

Between the two neighboring indentation marks on the same surface, a separation of at least five indentations was maintained to avoid the effect of interference.

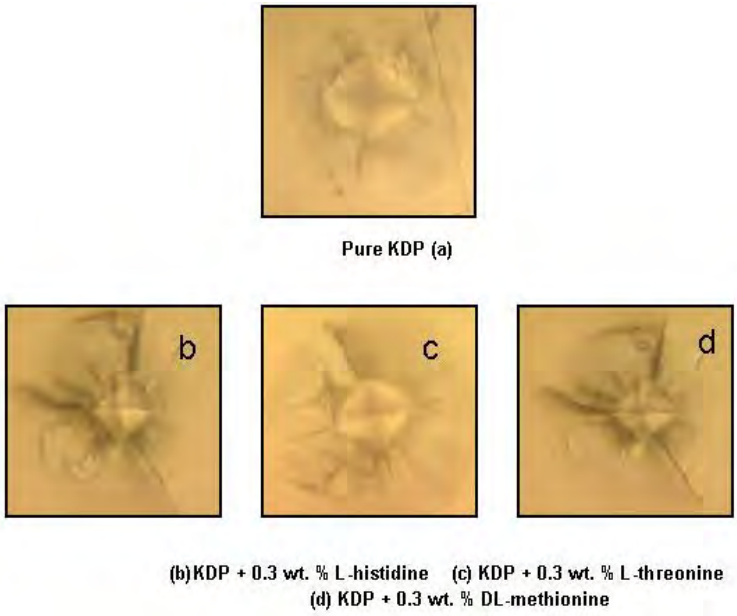

Figure: 8.4 Typical Vickers indentation mark on (100) faces of pure and 0.3 wt. % various amino acids doped KDP crystals at a load of 50 g.

Figure (8.4) shows the typical Vickers indentation mark obtained on (100) face of pure and amino acids doped KDP crystals at a load of 50 g. One can observe that the cracks are produced; the analysis of cracks is given in section (8.8) of this chapter.

8.4 Effect of Load on Vickers Micro-hardness

Hardness is not an intrinsic property of material directed by precise definitions in terms of fundamental units of mass, length, and time. Hardness is independent of load but it is true only for large indentations. The Micro-hardness number may increase with decreasing load for small loads, since fewer numbers of dislocations become available for slip in such small volumes of the crystal. If more than one slip system exists, increasing the load may activate a secondary system, thereby decreasing the hardness of the material.

The impurity has prominent effect on hardness. It is a well-known fact that dilute addition of divalent impurity has an appreciable effect on the hardness of alkali halide crystals. For each divalent ion introduced in to the lattice a positive ion vacancy is formed and these defects are distributed in various ways. The impurity ions and vacancies could be present as individual defects independent of one another or they may be present as impurity vacancy complexes or as larger aggregates. All these defects act as obstacles to dislocation motion, therefore, increasing the hardness of the crystals. Rao and Haribabu [22] have studied the effect of the distributed impurities and their state of dispersion on hardness of crystals from micro-hardness measurements on KCl crystals doped with Ca, Ba, and Sr. It has been observed that small addition of impurity increases the hardness; whereas at high concentration of impurity, visible precipitates are observed

which result in the decrease of hardness. Recently, it has been found that in NLO material L–arginine dihydrogen phosphate crystals, the metal doping showed harder crystals than the pure and amino acid substituted crystals [23].

The variation in the Vickers micro-hardness number with load has been studied widely on large number of materials [24-26]. However, some of the reported results indicate that the micro-hardness of a given material is constant above a critical size of penetration of the indenter impression, but below this size a steady increase in micro-hardness occurs as the load decreases. [6, 27-30]. Gane and Cox [31] have put forward an alternative explanation suggesting that the increase in micro-hardness at small indentation size is due to an increase in the stress necessary to operate dislocation sources in a perfect crystal region. The size of the dislocation of the rosette produced around micro-indentation is useful and convenient test for determination of mechanical strength of single crystals. Palanisamy [32] has studied the indenter impression at different loads on Li_2CO_3 crystals and subsequently etched them. Micro-indentation hardness along with chemical etching has been reported on many organic molecular crystals [33-36]. Moreover, the variation of Vickers micro-hardness with load has been studied at different temperatures in antimony single crystals [37]. The positions of the peaks in the micro-hardness versus load curves were identified by slip systems operative. Earlier, the nature of Vickers micro-hardness variation with load was studied by Vaghari [35] and Joshi [36] for bismuth single crystal cleavages. The variation of micro-hardness with applied load was also studied on many organic molecular crystals like anthracence and benzoic acid [39-42]. Altogether, the variation of Vickers micro-hardness with load was studied for KDP crystals grown with organic additives; it was found that the hardness

values increased for different additive values [43]. According to Patel and Arora [44], Vickers hardness increases as load increases for strontium tartrate crystals. Apart from this, the variation of Knoop hardness with load and the orientation of strontium tartrate crystals was studied by Joseph [45]. However, there are recent studies on the temperature and dwell time effect on hardness [46] and hardness variation across bulk metallic glass [47].

Almost three decades back the micro-hardness studies on KDP crystals were reported by Kishan Rao and Sirdeshmukh [48], Joshi and Antony [49] as well as by Joshi et al [50] and Anbukumar et al [51]. Kishan Rao and Sirdeshmukh [48] have found two different values of hardness for normal to (100) and (001) planes, which are 1.43 GPa and 1.29 GPa, respectively. Joshi and Antony [49] as well as Joshi et al [50] have studied dependence of hardness on indentation load and anisotropy of (100) and (011) planes of KDP crystals. They also indicated the presence of crack patterns around the indentation mark; which were found to be dependent on the indenter orientation [50]. Anbukumar et al [51] have measured Vickers micro-hardness on (100) planes of KDP within the load range from 5 to 50 g and found the variation of hardness from 1.77 to1.57 GPa. They have also observed that the indentation increased with increase in applied load.

Micro-hardness studies on (100) face of gel growth KDP and ADP crystals are reported by Sengupta and Sengupta [52]. They observed slip lines on the (100) face of ADP crystal at corners of the impression mark. However, the micro-crack were observed around the indentation on (100) face of KDP crystals from 10 g load, which spread out as the load increased. The Vickers micro-hardness decreased as applied load increased for both crystals and the work hardening coefficient was less than 2, which indicated the soft

material nature using Wooster's empirical relation; they also calculated the values of C_{11} from micro-hardness, where C_{11} is first order elastic stiffness constant. Kannan et al [53] have studied the influence of La^{+3} ions on growth of KDP crystals. They confirmed by using Vickers micro-hardness that the presence of La^{+3} ions in the superfacial crystal growth layers produced weak lattice stress. Recently, Ramakrishna Murthy and Venkateshwar Rao [54] have reported the study of He^{+} ion beam modification of the (100) surfaces of KDP and ADP crystals relative to the as grown to assess, the nature and extent of radiation damage. The measurements of micro-hardness studies on planar plastic anisotropy in as grown surfaces relative to ion bombarded surfaces have been made by the employing the Knoop indenter. The results have been interpreted in terms of the nature of bonding, bond strength and radiation damage on the ion bombardment. Also, they have observed plastic anisotropy in these surfaces which is found to be in conformity with (100) plane on which indentations are made. The micro- indentation technique has recently been employed to characterize the KDP crystals grown by Sankaranarayan Ramasamy (S-R) method. Balamurugan et al [55] have studied the micro-hardness of S-R method grown (001) directed KDP crystals. Moreover, Balamurugan et al [56] have studied the effect of KCl and measured the micro-hardness of KDP crystals.

Altogether, attempts have been made to study the micro-hardness of KDP-ADP mixed crystals. Srinivasan et al [57] have studied Vickers micro-hardness of different 19 compositions of KDP-ADP mixed crystals. Apart from this, Sengupta and Sengupta [58] have reported results of micro-hardness studies of ADP-KDP single crystals. Rajesh et al [43] have reported that the organic additives improved the mechanical strength of KDP crystals. Pritula et

al [59] have reported room temperature Vickers micro-hardness studies on (100) and (001) planes of KDP crystals grown from urea doped solutions. They found increased in hardness values for doped crystals compared to pure KDP crystals. Similarly, Podder [60] earlier concluded in his study that Vicker micro-hardness exhibited higher mechanical stability of urea doped crystals than KCl doped.

The values of Vickers hardness H_v calculated using equation (8.1) is compiled in table (8.1). The plots of H_v *Vs* load for pure and 0.3 wt. %, 0.4 wt. % and 0.5 wt. % amino acids (L-histidine, L-threonine, DL-methionine) doped KDP crystals are shown in figure (8.5a -8.5c). From these figures it is observed that the micro-hardness decreases rapidly with increasing load and then attains nearly a constant value. During indentation, the indenter first penetrates the distorted zone of the surface layer. Therefore, one observes a decrease in the hardness of the material for increasing load. As the depth of indentation increases with load, the effect of the inner layers become more and more prominent than the surface layer and the indenter reaches a depth at which undistorted material exists and hence, no change is observed in the value of hardness with load [61]. From figure (8.5 a,b,c) one can also observe that as the doping of amino acids increase the Vickers micro-hardness value decrease slightly with comparison to pure KDP. It can be conjectured that the doping of amino acid softens the KDP crystal up to a marginal extent. The effect of doping of amino acids on Vickers micro-hardness of KDP crystals can be studied from table (8.1).

Table (8.1): Values of Vickers micro-indentation hardness in (MPa) at different loads for pure and amino acid doped KDP crystals

Load (N)	Pure KDP	KDP + L-histidine			KDP + L-threonine			KDP + DL-methionine		
		0.3 %	0.4 %	0.5 %	0.3 %	0.4 %	0.5 %	0.3 %	0.4 %	0.5 %
0.294	1884.5	1854.23	1838.34	1831.34	1864.93	1862.32	1852.32	1861.87	1859.87	1849.17
0.491	1652.9	1632.46	1624.47	1622.81	1643.86	1640.86	1639.12	1647.27	1638.17	1630.19
0.588	1515.2	1395.59	1392.82	1385.12	1404.22	1394.22	1381.51	1400.54	1391.54	1389.04
0.686	1416.6	1349.12	1348.5	1333.71	1352.44	1342.44	1335.21	1352.96	1349.26	1339.11
0.784	1358.4	1320.58	1320.11	1315.05	1324.58	1320.12	1319.11	1323.21	1318.03	1315.93
0.981	1296.3	1294.56	1292.19	1288.93	1294.56	1289.51	1288.09	1292.41	1288.01	1284.25

One can notice that, for particular applied load, the Vickers micro-hardness decreases as the amount of doping of particular amino acid increases. This indicates that the doping of amino acids reduces the Vickers micro-hardness for a particular load.

Suthar [62] has observed that as the amount of doping of Mn^{+2} and Cu^{+2} increases, the Vickers micro-hardness value decreases for Calcium levo-tartrate tetrahydrate crystals at high load region. The doping of metallic impurity facilitated the slip mechanism and made the samples softer.

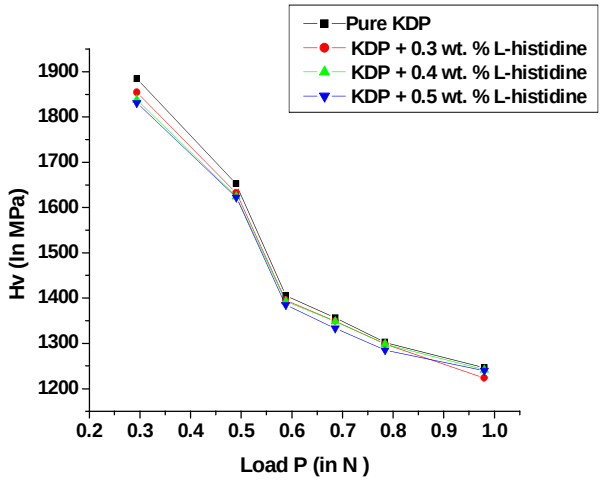

Figure: 8.5a Plot of H_v *Vs* load for pure and L-histidine doped KDP crystals.

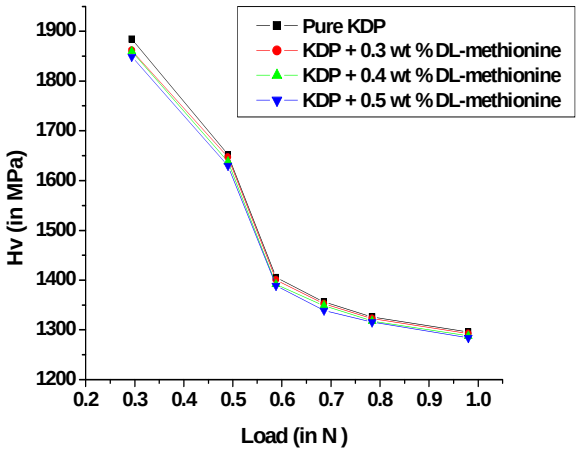

Figure: 8.5b Plot of H_v *Vs* load for pure and DL-methionine doped KDP crystals.

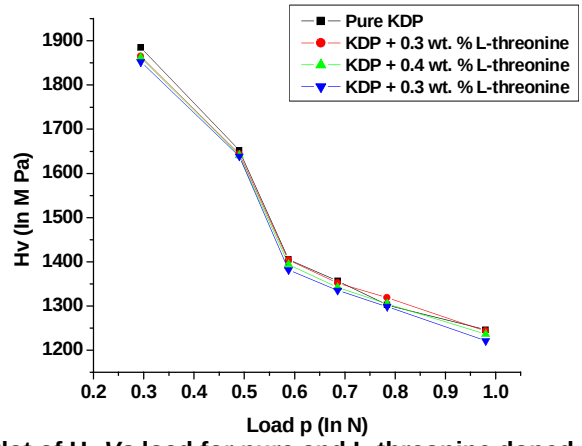

Figure: 8.5c Plot of H_v *Vs* load for pure and L-threonine doped KDP crystals.

The hardness is related to yield stress by

$$H = 2.78\sigma_y \qquad (8.5)$$

This has been used for the materials that do not work-harden appreciably [63]. It is found experimentally that best fit values are obtained for the following equation [64].

$$H = 3\sigma_y \qquad (8.6)$$

The yield stress calculated for high load region for pure and amino acid doped KDP crystals and tabulated in table (8.2).

The first order elastic stiffness constant (C_{11}) has been evaluated for pure and amino acid doped KDP crystals using Wooster's empirical relation [65] as follow:

$$\log C_{11} = (7/4) \log H_v \quad (8.7)$$

Where, H_v is micro-hardness. The values of C_{11} are tabulated in table (8.2).

This supports the concept of Onitsch [66], that if $n < 2$ the micro-hardness number decreases as the load increases. In low-load regions the resistance offered by material may be comparable with the applied load, resulting in a higher value of hardness. However, at higher load the plastic flow of the material may be higher and hence the resistance offered by the material is negligible, thus the value of hardness decreases with increase in the value of applied load.

8.5 Study of Mayer's law or Kick's law:

Variation of micro-hardness with applied load is usually explained for spherical indenter by Meyer's law [6] and pyramidal indenter by Kick's law [13]. Later on Kick's law was modified by Hay and Kendall [14], which is discussed in next section of this chapter. For pyramidal indenter Kick's law is given as,

$$P = ad^n \quad (8.8)$$

Where, *P* is the applied load in gram (or Newton), *d* is the observed diagonal length of indentation mark, and *n* is the constant for a given material. Kick postulated a constant value of *n= 2* for all the indenters and for all geometrically similar impressions. Nevertheless, Kick's law did not receive wide acceptance on account of the fact that *n* usually has a value less than *2*, particularly in the low load regions. If *n* is less than *2*, the hardness number increases with decreasing load, and if *n* is greater than *2*, it decreases as the

load is decreased [13]. The constant '*a'* is also known as the standard hardness.

$$\log P = \log a + n \log d \qquad (8.9)$$

The values of constants *a* and *n* are obtained from the plot of log *P Vs* log *d*. Since the relation between log *P* and log *d* is linear, the slope of this line gives the value of constant *n* and the intercept on log *P* axis gives the value of log *a* and hence the value of *a*.

In order to analyze the ISE in the hardness testing, one needs to fit the experimental data according to Kick's law. The behavior of the change in micro-hardness with the applied load can also be studied by obtaining the value of *n*. The variation of micro-hardness with load and its nature of the value of *n* are widely studied for various materials. From the observations of the variations of *P* with *d* Haneman and Schultz [67] have reported that in the low load region, *n* generally has a value less that *2*. Onitsch [68] also found such low values of *n* by observing variation of micro-hardness with load, while Grodzinski [69] had found variation of *n* values from 1.3 to 4.9 of various materials. Knoop [70] observed an increase in hardness with decrease in load where as, Campbell et al [71] and Mott et al [72] observed a decrease in hardness with decrease in load. On the other hand, Taylor [73] and Toman et al [74] have reported no significant change in the micro-hardness value with variation of load. Such contradictory results [75] may be due to the effect of the surface layers and vibrations produced during the test. Gane et al [31] studied the micro-hardness at very small loads. They observed a sharp increase in micro-hardness at small indentation size suggested that this increase might be due to the high stresses required for homogeneous nucleation in small dislocation free regions indented. On the contrary, Ivan'ko

[76] found that a micro-hardness decreased with decrease in load and concluded that this dependence was due to the relative contributions of plastic and elastic deformations in the indentation process. In view of these different observations, it has become rather difficult to establish any definite relationship of general validity between *P* and *d* or *H* and *P*. The Kick's law was applied to variation of Vickers micro-hardness with load in several organic molecular crystals and it was found that *n=2* for anthracene and benzoic acid crystals but *n=1.8* for phenanthrene crystals [36]. In case of several non linear optical (NLO) crystals, such as L-histyidineium perchlorate (LHPC), L-histyidineium bromide monohydrate (LHB), L-histyidineium dihydrogen phosphate orthophosphoric acid (LHDP) and L-arginium bis (Dihydrogen phosphate) (LADP), the application of Kick's law to the variation of hardness with load gave the work hardening coefficient less than 1, but for LHPC it gave more than *2* [*77*]. Also, Vaidya [78] applied Kick's law to the Vickers hardness profile with applied load for bismuth and bismuth-zinc systems. Notwithstanding, some studies have suggested more than one value of coefficient *n.* Saraf [79] has obtained two different values of *n* for higher and lower load regions in the case of baryte crystals. Ambujam [80] has reported the profile of Vickers micro-hardness variation with load for γ-glycine crystals. The RISE was predicted from the Kick's law plots of *log P* verses *log d*. The work hardening coefficient or the Meyer index *n* was found to be *2.58*. The RISE suggests that the apparent micro-hardness increases with increasing applied test loads, which has been critically examined by Sangwal [81-82] for a number of crystals. This RISE has been examined in terms of the existence of a distorted zone near the crystal- medium interface, effect of vibrations and indenter bluntness at low loads, the applied energy loss as a

result of specimen chipping around the indentation and the generation of median or radial cracks during the indenter loading half-cycle. In case of RISE, a specimen does not offer resistance or undergo elastic recovery, as postulated in some of the models, but undergoes relaxation involving a release of the indentation stress along the surface away from the indentation site. This leads to a large indentation size and hence to a lower hardness at low loads. It was found that the RISE phenomenon occurs only in materials in which plastic deformation is predominant. Vaidya [78] also observed the RISE in certain Bi-Zn crystals. An empirical procedure for correcting micro-hardness values for the size effect has been discussed in detail by Tirupatiah and Sundrararajan [86] in the low load region.

Figure (8.6) are plots of log *P* versus log *d* for pure and different amino acids (L-histidine, L-threonine, DL-methionine) doped KDP crystals.

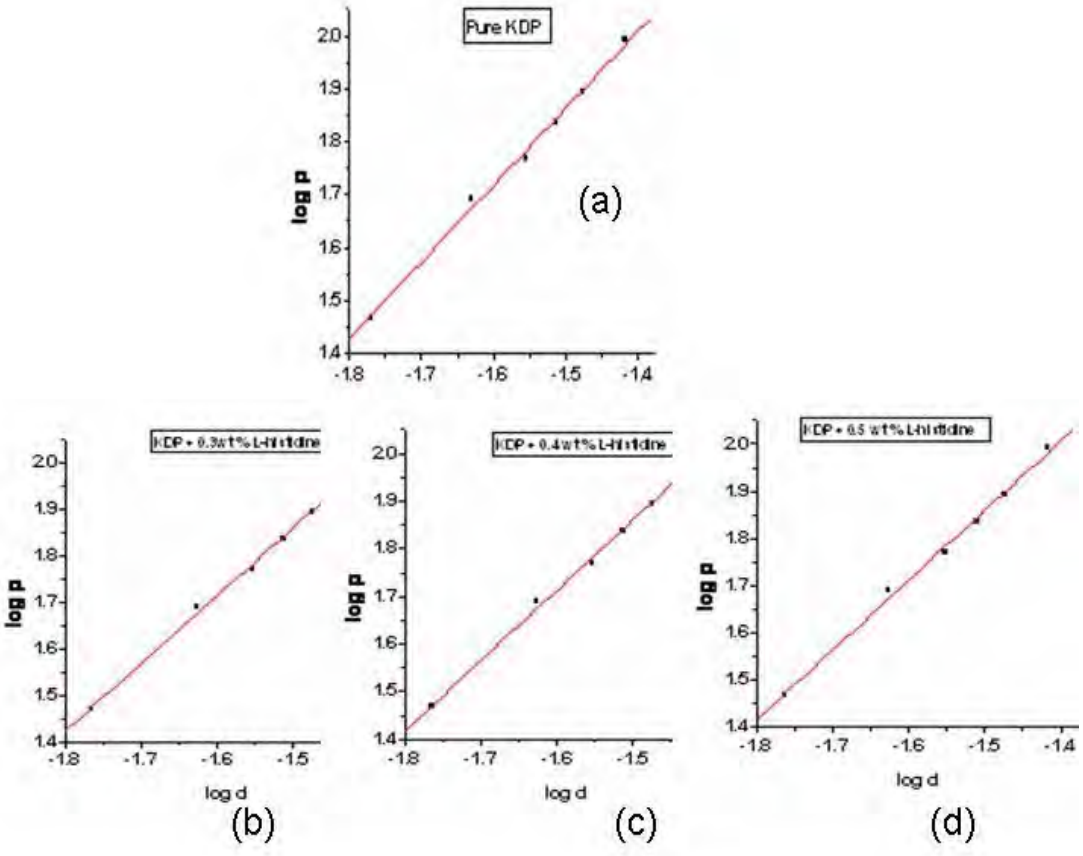

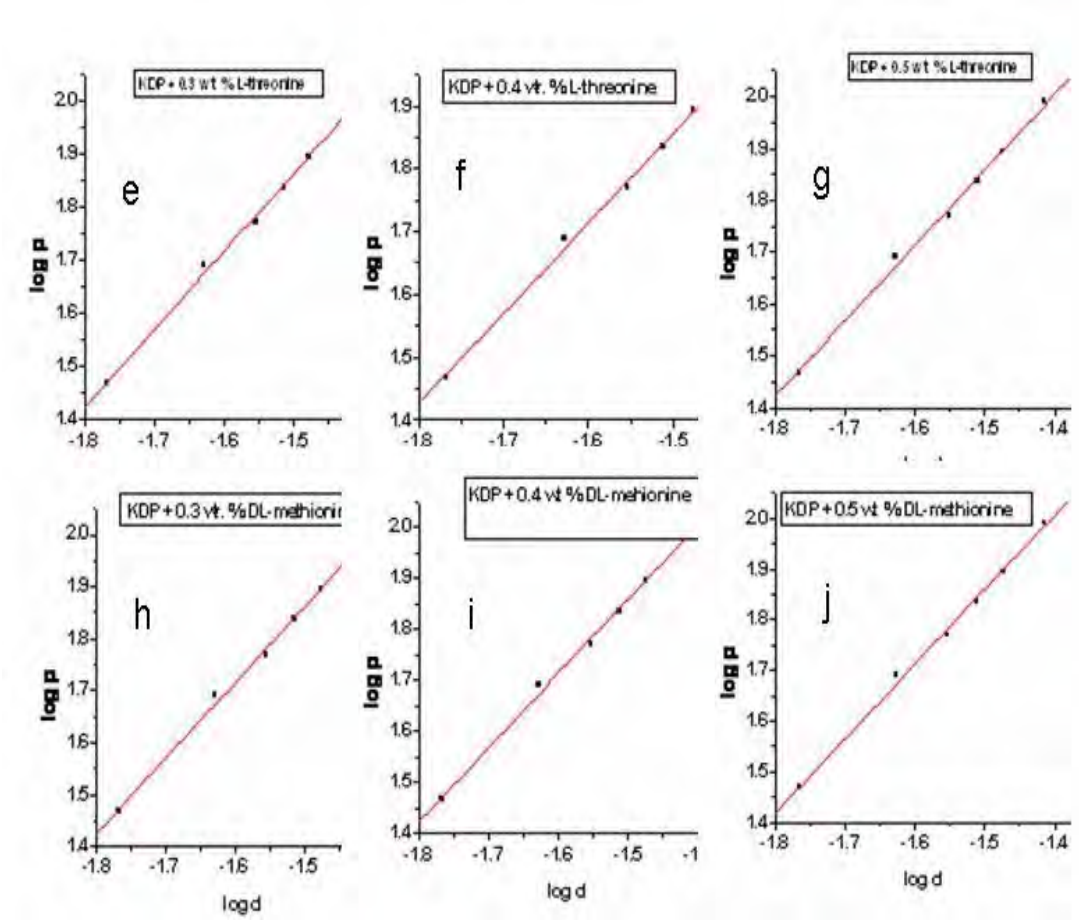

Figure: 8.6 Plots of log P Vs log d for pure (a) and 0.3,0.4 & 0.5 wt % L-histide (b-d), L-threonine (e-g) and DL-methionine (h-J) doped KDP crystals,respectively.

It can be seen that the plots exhibit a straight line nature and the value of n calculated and listed in table (8.2).

The values of *n* being less than 2 indicate that the Vickers micro-hardness values are increasing with decreasing the appiled load in low load region.

The values of standard hardness are slightly less in amino acid doped KDP crystals than pure KDP crystals. Also, marginal changes in the work hardening coefficient and the standard hardness are found for different amino acid doped KDP crystals.

Table: 8.2 Yield stress, first order elastic stiffness constant at 100g load, work hardening coefficient and standard hardness values for pure and amino acid doped KDP crystals.

Samples	Yield Stress σ_y (MPa)	First Order Elastic Stiffness Constant C_{11} (MPa)	Work Hardening Coefficient *n*	Standard Hardness *a* (MPa)
Pure KDP Crystal	432.1	280049.4	1.461	12887
KDP + 0.3% L-histidine	431.5	279391.9	1.468	12643
KDP + 0.4% L-histidine	430.7	278497.4	1.472	12601
KDP + 0.5% L-histidine	429.6	277269.0	1.474	12552
KDP + 0.3% L-threonine	431.5	279391.9	1.463	12604
KDP + 0.4% L-threonine	429.8	277487.4	1.484	12585
KDP + 0.5% L-threonine	429.4	276952.9	1.497	12501
KDP + 0.3% DL-methionine	430.8	278580.4	1.469	12504
KDP + 0.4% DL-methionine	429.3	276922.8	1.472	12452
KDP + 0.5% DL-methionine	428.0	275509.6	1.499	12360

8.6 Hays and Kendall law

In the present study, the micro-hardness has a relatively larger value at low loads. The micro-hardness shows a steep decrease with increasing loads up to about 0.294 N and, thereafter, the micro-hardness becomes almost constant. Mott [6] quotes several reports where such behaviors have been observed. Pratap and Hari Babu [84] in their study of ammonium halide crystals and Kotru [85] in his study of rare earth compound crystals observed similar load dependence. Suthar [62] applied Hays and Kendall law to Mn^{+2} and Cu^{+2} doped calcium levo-tartrate tetrahydrate crystals.

According to the approach of Hays and Kendall [14] this type of load variation can be due to the sample exerting a Newtonian pressure on the loaded indenter. This resultant pressure (*W*) is a function of the material being

tested and represents the minimum applied load to cause an indentation as the load (*P*) will allow no plastic deformation. With this approach it may be written as,

$$P - W = K d^2 \qquad (8.10)$$

Where, *K* = Constant, *d* = Diagonal length, *W* =Pressure and *P* = Load

The plot of *P Vs* d^2*,* in such a case has a positive intercept on the *P*-axis. This intercept represents the value of *W.* With the applied load *P* reduced by the

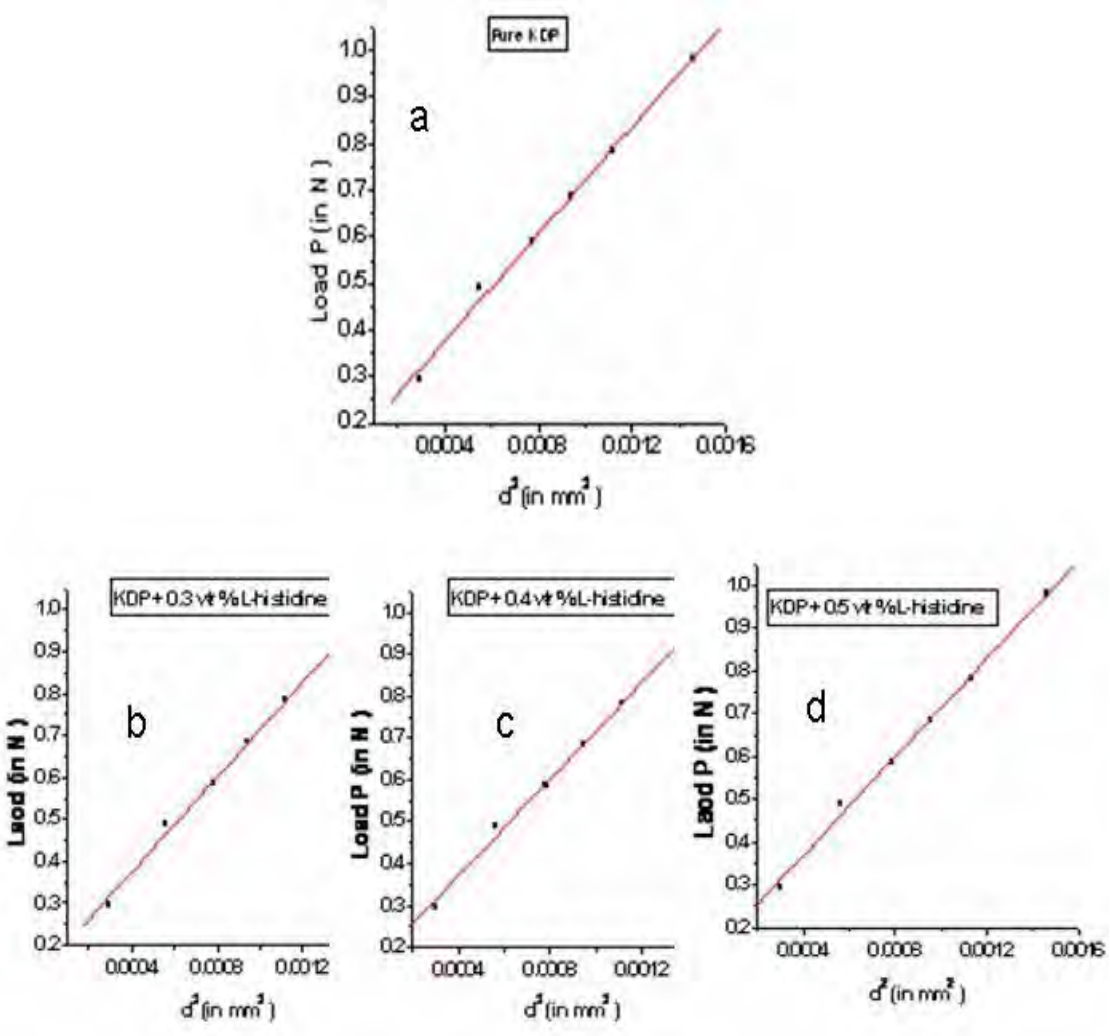

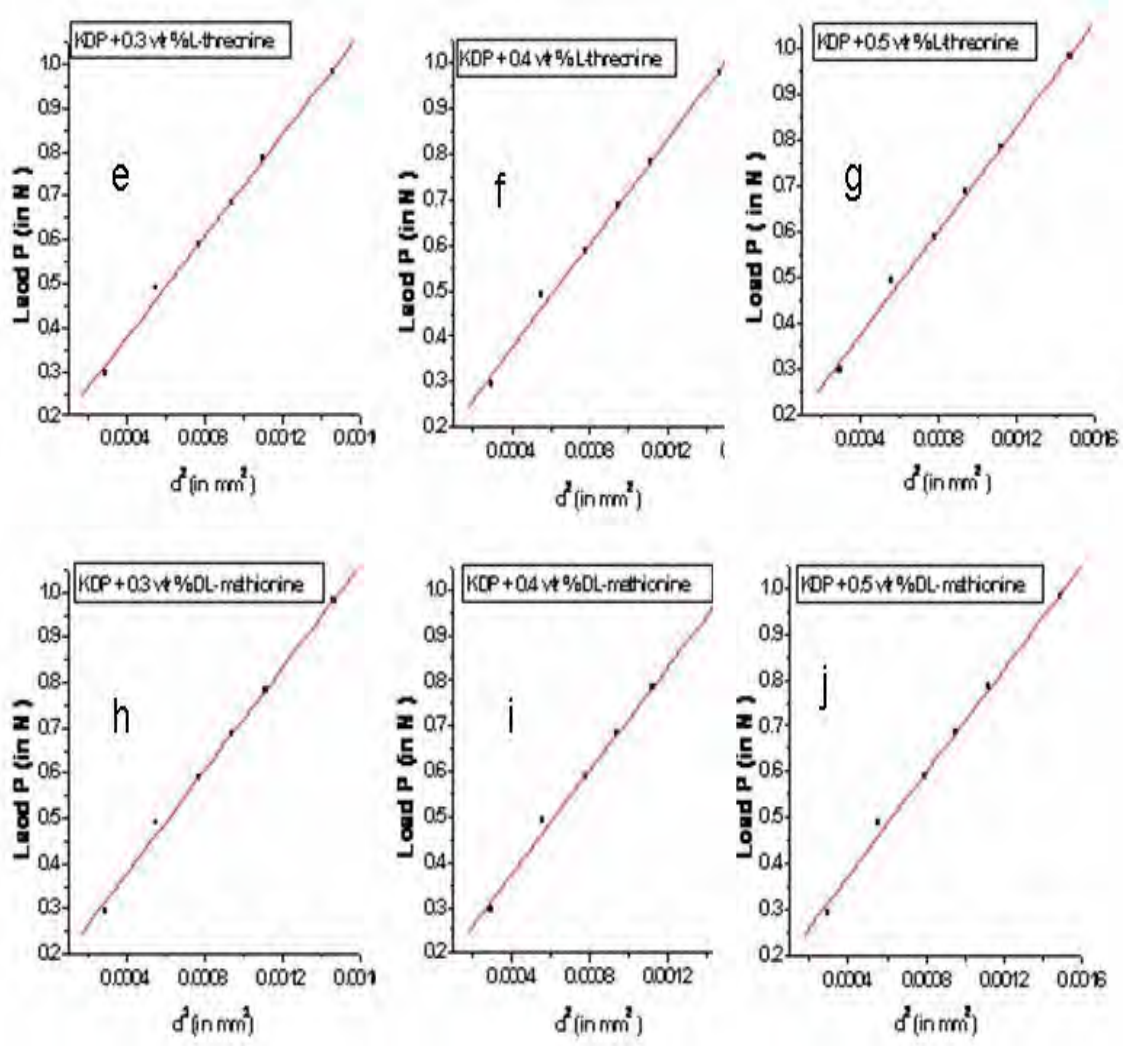

Figure: 8.7a-j Plots of P *Vs* d^2 for pure (a) and 0.3,0.4 & 0.5 wt % doped various amino acids (L-histide (b-d), L-threonine (e-g) and DL-methionine (h-J)) doped KDP crystals.

term *W*, the hardness is calculated from,

$$H_v = 1.8544\ (P - W)/\ d^2 \qquad (8.11)$$

It is load independent and represents the true value.

Figure (8.7) is the plot of load (*P*) *Vs* d^2 for pure and doped KDP crystals. From these plots the slope and the intercept (*W*) on the load axis are obtained, which are compiled in table (8.3).

8.7 Proportional Specimen Resistance (PSR) model

Bradt [15] explained the ISE with the help of the general model i.e. "Proportional Specimen Resistance" (PSR). According to PSR model micro-hardness can be described with two components, which are the frictional forces between the test specimen and the indenter faces and the elastic resistance of the test specimen. The indentation load *P* is related to indentation size *d*, as,

$$P = a_1 d + a_2 d^2 \qquad (8.12)$$

Where, the coefficient a_1 is contribution of proportional specimen resistance to apparent micro-hardness and a_2 coefficient is related to the load independent micro-hardness or load independent constant. The parameter a_1 characterizes the load dependence of hardness [15] and it is suggested that the a_1/a_2 can be considered as measure of the residual stress and these are connected with defect. The term $a_1 d$ has been attributed to the specimen surface energy [86], the deformed surface layer [87], the indenter edges acting as plastic hinges [88] and the proportional specimen resistance [15, 89]. Modifying equation (8.12),

$$P/d = a_1 + (P_c / d_0^2)\, d \qquad (8.13)$$

Where, P_c is the critical applied test load above which micro-hardness become load independent and d_o is the corresponding diagonal length of the indentation. The applicability of the PSR model to describe the observed ISE in relatively wide range of applied test loads can be examined by the linearity between *P/d* and *d*. The term a_2 is not related to ISE. Rather, it is related to the load independent micro-hardness and is equal to P_o/d_0^2 [90]. Plot of *P/d*

versus *d* should be a straight line and its slope which gives the value of load independent hardness. Applying PSR model to pure and doped KDP crystals, it has been observed that, a plot of *P/d* versus *d* gives a straight line as shown in figure (8.8). This linear relation confirms that PSR model is applicable in these samples.

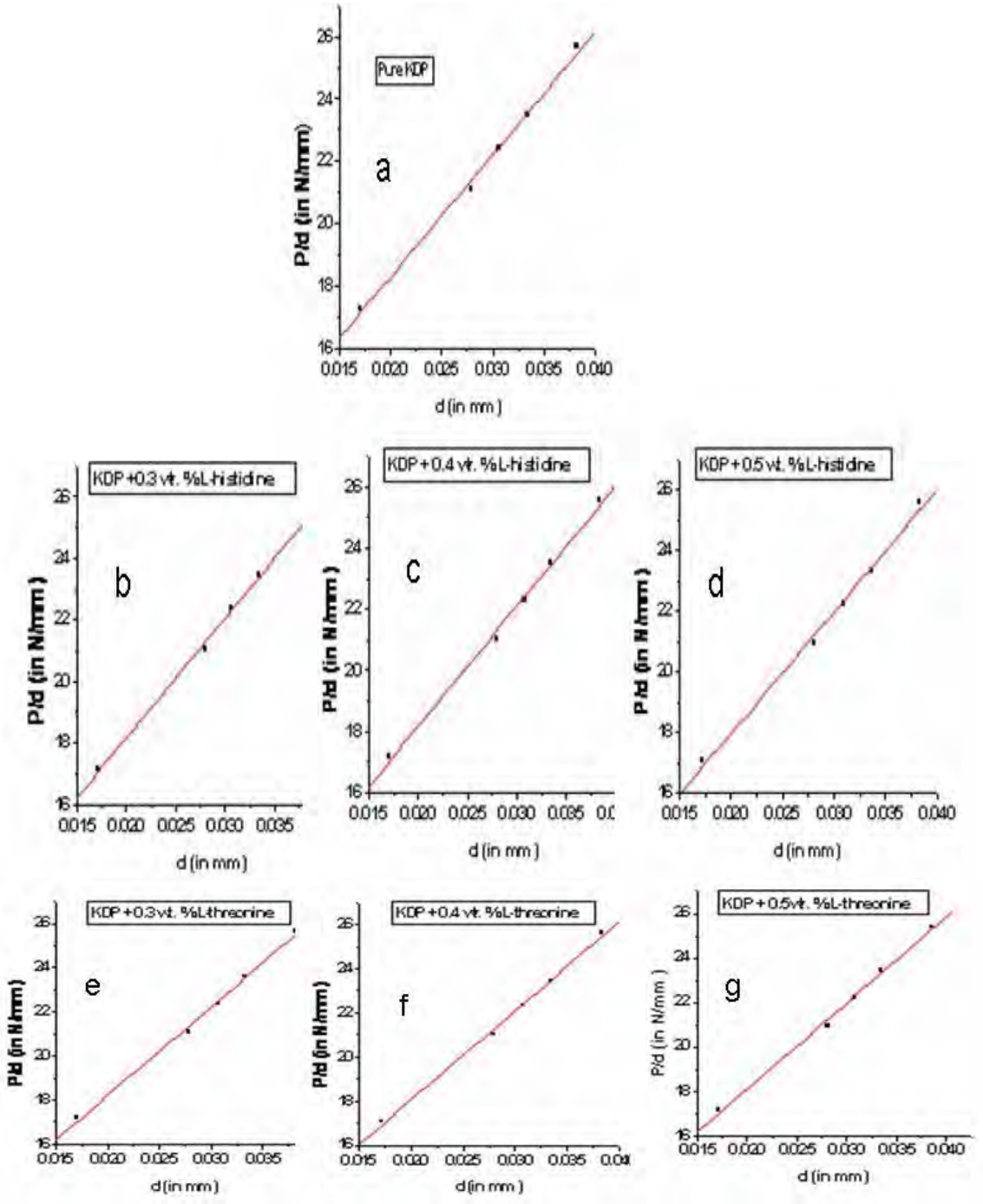

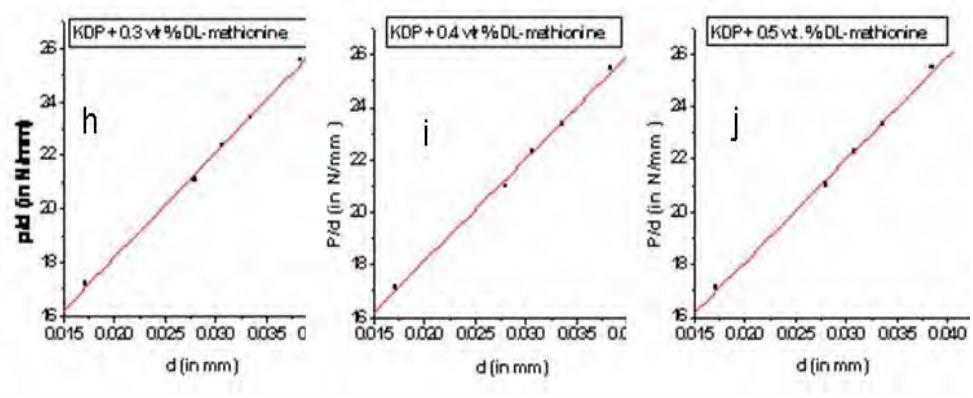

Figure: 8.8 Plots of *P/d Vs d* for pure (a) and 0.3,0.4 & 0.5 wt % L-histide (b-d), L-threonine (e-g) and DL-methionine (h-J) doped KDP crystals.

The values of load independent hardness and intercept are tabulated in table (8.3). It is observed that very less variation is found in load independent hardness for different doped KDP crystals. However, the values are slightly higher in pure KDP crystal.

From the table (8.3) one can notice that the load independent hardness H_v obtained from Hays and Kendall law is the highest in pure KDP crystals and decreases progressively as the doping of amino acids increases in KDP crystal.

The slope (P_o/d_0^2) and intercept (a_1) of the plot of *P/d Vs d* are listed in table (8.3) for pure and amino acid doped KDP crystals. These values are slightly higher in pure KDP crystals and the same decreases on increasing the doping of amino acids. It should be noted that in the case of $a_1 > 0$ the normal ISE is obtained where the H_v decreases with increase in load. Notwithstanding, for $a_1 < 0$ a RISE is obtained, where the H_v increases with increase in load.

Table: 8.3 Values of load independent (H_v), the intercept on load axis (W), Standard hardness slope (P_c/d_0^2) and intercept (a_1) values for pure and amino acid doped KDP crystals.

Samples	Load Independent Average *Hv* (Pa/m^2)	Intercept on P axis *W* (Pa/m^2)	Standard Hardness Slope P_c/d_0^2 (N/m^2)	Intercept a_1 (N/m)
Pure KDP Crystal	1486.9	15.00	385.7	11.29
KDP + 0.3% L-histidine	1474.4	14.82	383.6	11.11
KDP + 0.4% L-histidine	1469.4	14.46	379.6	10.96
KDP + 0.5% L-histidine	1462.8	14.40	373.6	10.89
KDP + 0.3% L-threonine	1480.7	14.80	385.1	11.09
KDP + 0.4% L-threonine	1474.9	14.41	380.1	11.02
KDP + 0.5% L-threonine	1469.2	14.23	371.7	11.01
KDP + 0.3% DL-methionine	1479.7	14.76	382.9	11.13
KDP + 0.4% DL-methionine	1474.1	14.31	377.7	11.05
KDP + 0.5% DL-methionine	1467.9	14.19	370.3	11.02

This leads to a reduction in the value of *d* upon unloading. This implies that the values of *a* are negative when the elastic surface stresses are tensile, which leads to a relation of these surface stresses introduced by indentation.

8.8 Crack Measurement and Fracture Toughness

Indentation hardness testing has been finding applications in the scientific investigations of damage processes in highly brittle solids [4]. A suitably chosen sharp indenter tip concentrates very high levels of stresses,

particularly in shear and hydrostatic compression, and thus induces irreversible deformation in localized regions of a test surface. In many brittle materials the mean contact pressure can be as much as a tenth of an elastic modulus [91] which indicates that the intrinsic bond strength of the lattice itself is exceeded. One of the important aspects of indentation damage is cracking. An understanding of indentation fracture is important for many practical as well as academic interests [92]. Brittle materials are used in industries quite commonly. For example, in the aerospace industry, the components of brittle materials face problems of strength degradation and material removal by crack growth under erosive conditions. The contact of erosive particles, including both solids and liquid drops, generates intense local stress concentrations, which give rise to characteristic indentation fracture patterns. Erosion studies of brittle materials are aimed towards understanding of the role of plastic deformation in production of these crack systems [93-95]. The cracks propagate into surrounding elastic hinterland. For crystalline solids, deformation processes may also be required for the propagation of non-cleavage (radial) cracks in ionic solids. Surface micro-flaws formed in an indentation with a sharp or blunt indenter have been studied in contest to evaluations of surface damage resistance, fracture toughness and wear resistance of brittle materials. Such micro-flaws are regarded as similar to typical fracture-strength-controlling flaws produced in manufacturing processes such as forming, grinding, cutting and handling. Therefore, it is important to study the mechanism of flow formation in indentations. In glasses a simple crack (Hertzian Crack) is usually produced by blunt indenter. In sharp indenters, such as Vickers or Knoop diamond pyramid, however, the crack formation mechanism is complicated because an

irreversibly deformed zone, affecting the stress field for crack formation, appears beneath the indenter. The primary cracks produced by indentation with Vickers diamond pyramid for glasses are radial, medial and lateral types. The radial and median cracks are particularly important because they control the fracture strength of the indented specimen under bending or tensile loading conditions. The different types of cracks are shown in figure (8.9). The cracking mechanism about Knoop and Vickers indenters in Al_2O_3 and SiC has been reported by Lawn and Swain [93]. With Vickers indented specimens, the cracks were always observed radially extended outwards from the corners of the indentations.

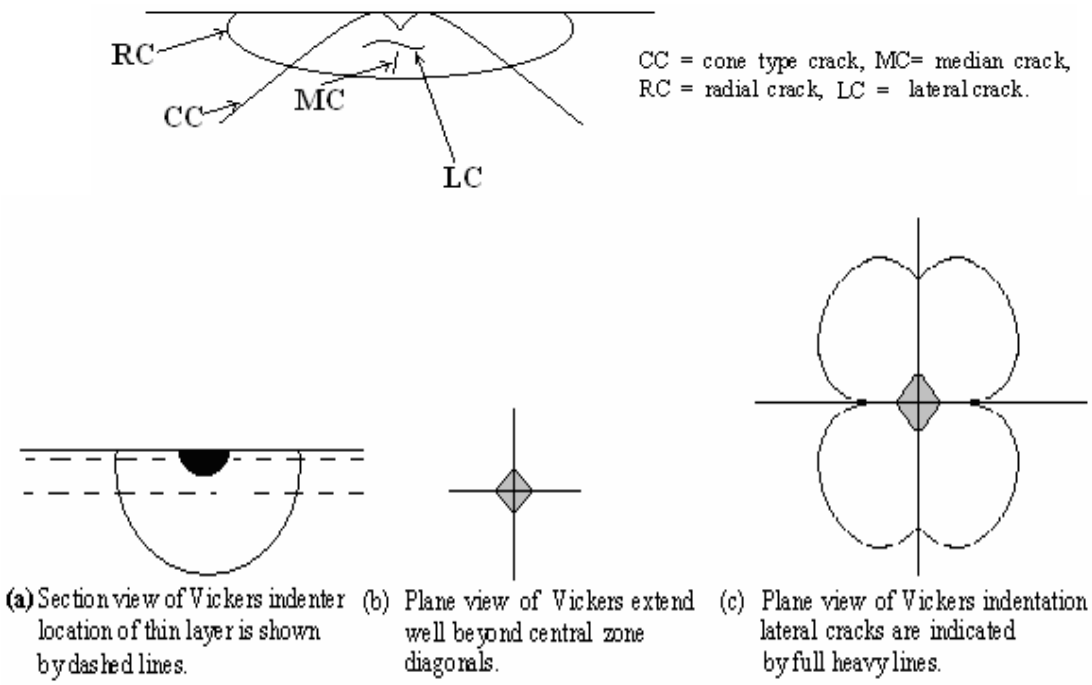

Figure: 8.9 Schematic diagram depicting the types of cracks.

Basically, two distinct stages of crack formations are proposed [95], which are cracks occurring during loading and cracks occurring during unloading. During unloading, just before removal of the indenter, the new cracks initiate at the deformation zone and extend sideways into a shallow-

saucer-shaped configuration, modified into some extent by the presence of median vents. In certain cases fringes are generated by the interference between slightly mismatched, simultaneously diffracting portions of crystal across the crack interfaces. These are considered as the thickness fringes [96].

Hockey and Lawn [96] studied cracking around indentation by electron microscope in aluminum oxide and silicon carbide (SiC). In semi quantitative information on geometry of residual cracks about micro-indentations, they obtained interesting information. The information obtained is related to the history of the crack propagation and not the initiation of the cracks. The electron microscopy is not capable to tell how the cracks originally nucleated and formed. It has been known from the etching examination [92] that median and lateral-vent initiation both tied up intimately with events within gross deformation zone immediately surrounding the indenter, unfortunately, this region of lost resolution does not give clear pattern. The authors have also discussed in detail the important aspect of crack healing. Lawn and Fuller [97] suggested that the toughness, K_c can be related to the indenter load P, and radius of median crack, C, by

$$K_c = \chi_c P C^{3/2} \qquad (8.14)$$

Where χ_c is the number dependent upon the indenter geometry for Vickers indenter, it is assumed to be *0.0726.*

Evans and Charles [98] have employed the dimensional analysis and obtained correlation with conventional fracture toughness measurements. In this analysis the functional dependence on the *E/H* is introduced to account for elastic/plastic stress with indentation

$$K_c = \chi (E/H)^{0.4} P C^{3/2} \qquad (8.15)$$

Where, *E* is the Young's modulus and *H* is the hardness.

However, there are several reports on cracking around indentations in several materials. PETN and RDX are important plastic explosive materials. The fracture mechanism of indentation cracks was studied by Hagan and Choudhari [99] by using the formulation suggested by Lawn and Fuller [97] as follows:

$$\chi P\, C^{3/2} = ((2\gamma\, E/(1-v^2))^{1/2} \qquad (8.16)$$

Where, *P* is the load of indenter, *C* is the length of crack, *E* is the Young's modulus, *v* is the Poisson's ratio and χ is the coefficient of function between the indenter and indented material, which is generally obtained by rubbing against standard hard surface. The fracture toughness of ferrites has been studied by Johnson et al. [100]. They used Vickers indenter and applied the formula proposed by Evans and Charles [98]. Moreover, they hypothesized that the large cations, Ca^{+2} and Fe^{+2} on the grain boundaries cause locally-distorted structure which is an easy fracture path. Ferrites exhibit high strength and fracture toughness but also experience grain boundary fracture in contrast to trans-granular fracture in weaker counterparts. Altogether, fracture toughness of doped bismuth oxide electrolytes have been reported by Sammes [101]. Burnett and Page [102] have studied crack propagation and patterns around Vickers indentation mark on sapphire and glass with and without ion implantations. They also determined the fracture toughness K_c by using the relation proposed by Lawn and Co-workers [103-104] as follows:

$$K_c = 0.0139\, (E/H)^{1/2}\, P/C^{3/2} \qquad (8.17)$$

Where, *H* is the hardness, *E* is the modulus of the elasticity, *P* is the load and *C* is the crack length.

A statistical model for ideal crack initiation using Vickers indentations has been suggested by Dal Maschio et al [105]. Using such model it is possible to calculate the threshold load, defined as the load at which there is a 50% fracture probability, from experimental evaluations.

The toughness of a material denotes its resistance to fracture. For a solid containing a well-developed crack of specified dimension, the fracture toughness, K_c determines the fracture stresses in uniform tensile loading. The fracture mechanics of the indentation process has provided an equilibrium relation for well-developed crack extending under a center-loading condition.

$$\frac{P}{l^{3/2}} = \beta_0 . K_c \qquad \text{for } l > d/2 \tag{8.18}$$

Where, *P* is the load, *l* is the crack length measured from the center of the indenta-tion mark to the crack end, *d* the diagonal length of the indentation impression and β_0 the indenter constant equal to *7* for the Vickers indenter [106-108].

Shaskol'skaya et al [109] and Guin et al [110] have reported measurements of both hardness and cracking in KDP and deuterated KDP crystals. They also identified two types of slip systems in KDP; the first system consisted of slip planes (110), (101), (112) and (123) with common Burgers vectors <111>/2; the second slip system was identified as (010). Marion [111] has reported values of fracture toughness in KDP crystals as 0.2 $MPa.m^{1/2}$.

More recently, Fang and Lambropoulos [112] studied Vickers and Knoop hardness of KDP crystals on (100) and (001) faces. The cracks were observed for large loads values on the both faces, however, the cracks were longer on the (100) faces than the (001) faces. Assuming the elastic and plastic isotropy the crack sizes were analyzed and fracture toughness K_c were measured. They

concluded that the effect of isotropic assumption on the extracted fracture toughness was 33% with 23% contribution resulting from the elastic anisotropy and 10% from the slip system plastic anisotropy.

Vickers indentation was used to access the fracture toughness on the (100) faces of pure and amino acids doped KDP crystals at room temperature. Well formed straight radial cracks emanate from the corners of the indents for load exceeding ~ 0.25 N were observed, which is in agreement with Fang and Lambropoulos [112]. The present author employed load in the range of 0.294 N to 0.98 N and each load was applied for 15 sec. Five indents were made at each load for better averages. The indentation diagonal *d* and crack size *2c* (tip to tip) were measured with an optical microscope with filar eye piece as described in section (8.3).

However, no analysis is available to convert measured micro-indentation crack size to fracture toughness in tetragonal system like KDP. The only available analysis is for isotropic materials such as glasses or polycrystalline ceramics [113]. To convert the direct measurements of indentation crack size to a fracture toughness, it is assumed that KDP possesses an equivalent isotropic young's modulus E = 38.7 GPa [114]. The KDP crystals have been studied by Evans [115] and Anstis et al [116].

Evans [115] applied dimensional analysis and curve fitting over a range of *c/(d/2)* from 1.5 to 7. As per this model,

$$K_c = H\,(d/2)^{1/2}\,(E/H)^{0.4}\,10^{f(x)} \qquad (8.19)$$

$$f(x) = -1.59 - 0.34 - 2.02\,x^2 + 11.23\,x^3 - 23.97\,x^4 + 16.23\,x^5 \qquad (8.20)$$

Where, K_c is the fracture toughness, *H* is the hardness, *d* is the indentation diagonal, *E* is the Young's modulus and *C* is the half crack size.

According to Anstis et al model[119],

$$K_c = (0.016 \pm 0.002) (E/H)^{1/2} P/c^{3/2} \quad (8.21)$$

The model proposed by Anstis et al [116] is based on the assumption that the observed surface cracks are surface traces of sufficiently large radial cracks, on the other hand, the Evans model [115] is applicable for both shorter near surface cracks, where $c \sim P$, as well as for deeper radial cracks.

The cracks observed on the (100) surface of the pure and amino acid doped KDP crystals are shown in figures (8.4a -8.4d). The cracks for different loads were measured and the fracture toughness (K_c) of pure and amino acids doped KDP crystals were calculated with the help of equation (8.21). Figure (8.10a -8.10c) show plots of fracture toughness *Vs* load for pure and amino acids doped KDP crystals, which show that as the load increases obviously the crack length increases. The values of fracture toughness K_c for pure and doped KDP crystals are listed in table (8.4) for various loads.

Table: 8.4 Values of Fracture toughness K_c at different loads for pure and amino acid doped KDP crystals.

Load (N)	Pure KDP	KDP + L- histidine In MPa			KDP + L-threonine In MPa			KDP +DL-mehtionine In MPa		
		0.3 %	0.4 %	0.5 %	0.3 %	0.4 %	0.5 %	0.3 %	0.4 %	0.5 %
0.294	0.257	0.223	0.184	0.173	0.222	0.198	0.185	0.240	0.210	0.183
0.491	0.256	0.232	0.211	0.202	0.222	0.208	0.185	0.243	0.221	0.202
0.588	0.230	0.203	0.196	0.189	0.209	0.195	0.179	0.211	0.196	0.182
0.686	0.190	0.182	0.166	0.162	0.178	0.175	0.160	0.171	0.161	0.149
0.784	0.156	0.144	0.131	0.126	0.145	0.137	0.132	0.160	0.141	0.131
0.981	0.167	0.154	0.143	0.135	0.157	0.151	0.147	0.167	0.164	0.154

Figures (8.11a -8.11c) are plots of variation of fracture toughness with applied load. From figures (8.11a -8.11c) one can observe that as the load increases from 0.5 to 0.8 N the fracture toughness of various crystalline samples decreases rapidly. The fracture toughness of various amino acids doped KDP crystals progressively decrease as the doping concentration increases. This indicates that the doping of amino acid into KDP reduces the fracture toughness of crystals. It is also observed that for higher concentration of amino acids the fracture toughness slightly increases on increasing load in the region of 0.3 to 0.5 N.

Shaskol'skaya et al [109] and Guin et al [110] have analyzed the data by the Evans model with E = 38.7 GPa and the values of K_c was obtained as 0.24 ± 0.04 MPa.m$^{1/2}$ at 200 g load, whereas, the Anstis model gave the K_c as 0.17 ± 0.03 MPa.m$^{1/2}$ for the same load. However, Anstis model predictions are in agreement with reported values by Marion [111]. Comparing the models by Evans [115] and Anstis et al [116], both results were based on using young's modulus E = 38.7 GPa. It was observed that the Evans model predicted fracture toughness that was a factor 1.2 to 1.45 times higher than the predictions of the Anstis model; however both models gave the same qualitative ranking of the data. In the present study the values of fracture toughness corresponds to the Evan's Model/ Anstis Model for pure KDP crystals. The effect of amino acid doping in KDP decreases the fracture toughness values for particular load.

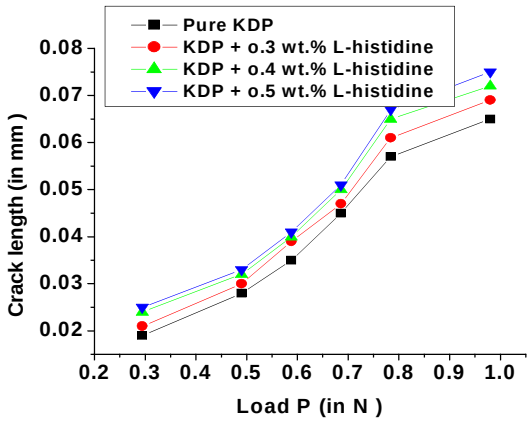

Figure : 8.10a: Plot of crack length *Vs* load for pure and L-histidine doped KDP crystals.

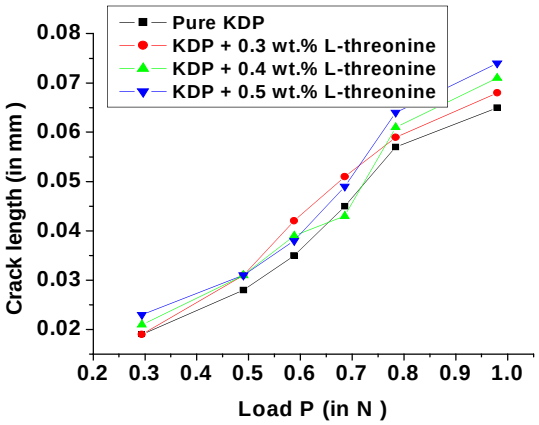

Figure: 8.10b Plot of crack length vs load for pure and L-threonine doped KDP crystals.

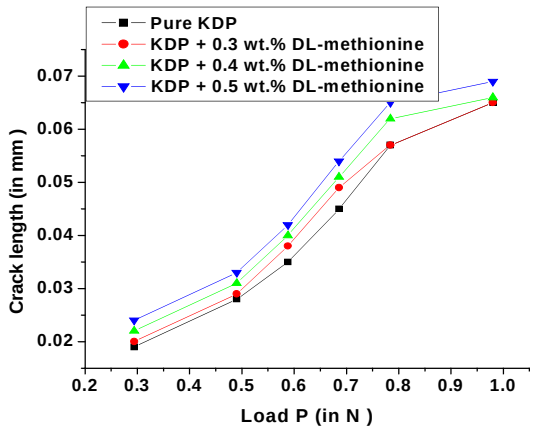

Figure: 8.10c Plot of crack length vs load for pure and DL-methionine doped KDP crystals.

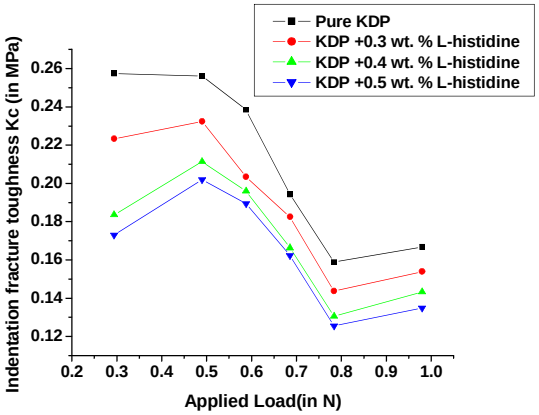

Figure: 8.11a Plot of fracture toughness *Vs* load for pure and L-histidine doped KDP crystals.

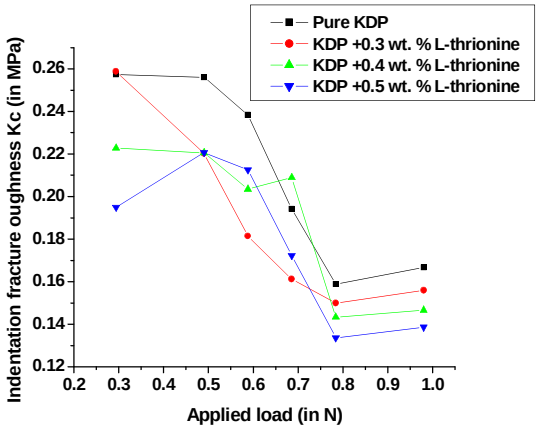

Figure: 8.11b: Plot of fracture toughness vs load for pure and L-threonine doped KDP crystals.

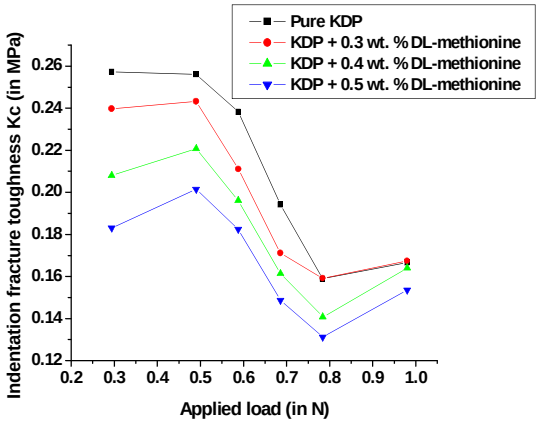

Figure (8.11c): Plot of fracture toughness *Vs* load for pure and DL-methionine doped KDP crystals.

Conclusions

1. The Vickers micro-hardness of pure and amino acids doped KDP crystals is a load dependent quantity and the variation is prominent in low load regime. Initially the Vickers micro-hardness decreased with increasing the load very steeply and then for higher loads it decreases rather gradually and became virtually independent of load. Thus the Indentation size effect (ISE) was observed for both the pure and amino acid doped KDP crystals.
2. With increase in the concentration of a dopant (amino acids) the Vickers micro-hardness also reduced at a considered load value in KDP crystals. The Vickers micro-hardness decreased as amino acid doping level was increased indicating that the KDP crystals became softer.
3. The ISE has been verified by using the Kick's law. From the plots of log *P* versus log *d*, the values of work hardening coefficient '*n*' and the standard hardness '*a*' were obtained. The values of '*n*' and '*a*' were constant and these values changed marginally with increased concentration of doping in random manner. The variation of Vickers micro-hardness with load agreed well with the nature obtained by the other workers on the (100) faces of pure KDP crystals.
4. The values of the load independent hardness and the Newtonian pressure (W) were higher in pure KDP crystals than the amino acids doped KDP crystals. It was found that as the doping concentration of amino acids increased the values of load independent hardness and Newtonian pressure decreased. This further indicated that the doping of amino acids had softened the KDP crystals slightly.

5. According to Hays and Kendall law, the plots of d^2 *Vs* load *P* are straight lines for pure as well as amino acids doped KDP crystals. From the application of PSR model, the linear relation between *P/d* and *d* was observed for both pure and amino acids doped KDP crystals. This suggested the ISE behavior. The standard hardness '*a*' was obtained. It was observed that for pure KDP the values of P_o/d_o^2 and '*a*' is higher compared to the amino acids doped KDP crystals.
6. For the indentation greater than loads ~ 0.25 N cracks were observed on the (100) faces of pure and amino acid doped KDP crystals. The crack length 'c' was found to be approximating to 3/2 power of the load *P* and Anstis model was applied to obtain the values of toughness fracture $K_{c..}$ It can be concluded that as the doping concentration increased the Vickers micro-hardness values decreased and also the fracture toughness decreases, this suggested that the doping of different amino acids in KDP crystals made them slightly soft and also more fragile to produce cracks easily.
7. As the load increased the fracture toughness decreased in the case of pure and amino acids doped KDP crystals. This supported the ISE behavior. Further, with the increase in dopant concentration the value of fracture toughness decreased for all the three dopants viz. L-histidine, L-threonine, DL-methionine for different values of load. This effect was more prominent at low loads suggesting surface effect due to the dopants.

References

1. C. W. Stillwel, "*Crystal Chemistry* ", McGraw Hill, New York (1983).
2. N. A. Ashby, *NZ Eng* **6** (1951) 33.
3. D. Tabor, "*Hardness of Metals"*, Clarendon, Oxford (1951).
4. J. H. Westbrook, H. Conrad, "*The Science of Hardness Testing and its Research Applications American Society of Metals*," Ohio (1973).
5. J. J. Gilman, *American Society of Metals,* Ohio (1973).
6. B. W. Mott, "*Microhardness Indentation Testing"*, Butterworths", London (1956)
7. J. N. Plendl, P. J. Gielisse, *Phys. Rev*. **125** (1962) 828.
8. D. B. Sirdeshmush, K. G. Subhadra, K. Kishan Rao, T. Thiramal Rao, *Cryst. Res. Technol*. **30** (1995) 861.
9. D.B. Sirdeshmukh, L. Sirdeshmukh, K.G. Subhadra, "*Alkali Halides"*, Springer, Berlin Heidelberg, New York (2001).
10. J. Grunzeig, I. M. Longman, N. J. Petch, *J. Mech. Phys. Solids.* **2** (1954) 81.
11. M.C. Shaw, "*The Science of Hardness Testing and its Research Applications"*, American Society of Metals, Ohio (1973).
12. W. C. Oliver, G. M. Pharr, *J. Mater. Res.* **7** (1992)1564.
13. F. Kick, "*Das Gesetzder Proportionalen Winderstande and Science anwendung*, Leipzig", Felix (1885).
14. C. Hays, E.G. Kendall, *Metallography* **6** (1973) 275.
15. H. Li, R.C. Bradt, *J. Mater. Sci*. **28** (1993) 917.
16. J.A. Brinell, *2nd Cong. Inst. Methods d'Essai*, Paris(1920).
17. J. Szilard, *Ultrasonics* **22** (1984) 174.
18. C. Kleesattel, *J. Acoust. Soc. Am.* **39** (1966) 404.

19. R. Smith, G. Sandland, *J. Iron. St. Inst.* **111** (1925) 285.

20. R. Smith, G. Sandland, *Proc. Instn. Mech. Engr.* London **1** (1922) 623.

21. F. Knoop, C. G. Peters, W. B. Emerson, *J. Res. Nat. Bur. Stand.* **23** (1939) 39.

22. M. L. Rao, V. Haribabu, *Indian J. Pure & Appl. Phys.* **16** (1978) 821.

23. A. Joseph Arul Pragasam, *Ph. D. Thesis,* University of Madras, India (2004).

24. S. K. Arora, G. S. Trivikram Rao, M. M. Batra, *J. Mater. Sci.* **19** (1984) 297.

25. G. R. Pandya, D. D. Vyas, C. F. Desai, *Surface Technol.* **22** (1984) 38.

26. B. S. Shah, *Cryst. Res. & Technol.* **17** (1982) K27.

27. H. Buckle, *Metal Rev. Inst. Metals*, London **4** (1959) 49.

28. M. S. Joshi, V. V. Joshi, A. L. Chaudhari, R.G. Kanitkar, *J. Mater. Sci.* **19** (1984) 3337.

29. J. R. Pandya, L. J. Bhagia, A. J. Shah, *Bull. Mater. Sci*. **5** (1983) 79.

30. C. C. Desai, J. L. Rai, *Bull. Mater Sci.* **5** (1983) 453.

31. N. Gane , J. M. Cox, *Phil. Mag.* **22** (1970) 881.

32. M. Palanisamy; *Ph. D. Thesis*, Anna University, Chennai, India(1985).

33. B. S. Shah, J. N. Sherwood, *Trans. Farady Soc*. **69** (1971) 1200.

34. P. J. Halfpenny, K. J. Roberts, J. N. Sherwood, *J. Mater. Sci.* **19** (1984) 1629.

35. D.J. Vaghari, *Ph. D. Thesis,* M. S. University, Vadodara, India (1971).

36. M. J. Joshi, B. S. Shah, *Cryst. Res. & Technol*. **19** (1984) 1107.

37. A. H. Raval, M. J. Joshi,B. S. Shah, *Indian J. Engng. & Mater. Sci.* **9** (2002) 79.

38. M. J. Joshi, *Ph. D. Thesis*, Saurashtra University, Rajkot, India (1987).

39. N. Vaidya, B. S. Shah, *Indian J. Pure & Appl. Phys*. **34** (1996) 915.

40. N. Vaidya, B. S. Shah, *Indian J. Phys*. **71A** (1996) 57.

41. R. K. Marwaha, B. S. Shah, *Indian J. Pure and Appl. Phys*. **34** (1996) 987.

42. R. K. Marwaha, B. S. Shah, *Indian J. Pure and Appl. Phys*. **71A** (1996) 53.

43. N. P. Rajesh, V. Kannan, P. Santhana Ranghavan, P. Ramasamy, C. W. Lan, *Mater. Lett.* **52** (2002) 326.

44. A. R. Patel, S. K. Arora, *J. Mater. Sci.* **12** (1997) 2124.

45. S. Joseph, *Ph. D. Thesis,* Saurashtra University, Rajkot India (1997).

46. F. AbdEL – Salam, L. A. Wahab, R. H. Nada, H. Y. Zarhran, *J. Mater. Sci.* **42** (2007) 3661.

47. R. Chem, F. Yans, G. Fan, P. K. Liaw, *J. Mater. Sci.* **42** (2007) 2208.

48. K. K. Rao, D. B. Sirdeshmukh, *Indian J. Pure & Appl. Phys.* **16** (1978) 860.

49. M. S. Joshi, A. V. Antony, *Bull. Mater. Sci.* **2** (1980) 31.

50. M. S. Joshi, A. V. Antony, P. Mohan Rao, *Kristall and Technik* **15** (1980) 743.

51. S. Anbukumar, S. Vasudevan, P. Ramasamaj, *Ind. J. Phys* **61A** (1987) 397.

52. S. Sengupta and S. P. Sengupta, *Bull Mater. Sci.* **15** (1992) 333.

53. V. Kannan, R. Bairava Ganesh, R. Sathyalakshmi, N.P. Rajesh, P. Ramaswamy, *Cryst. Res. & Technol.* **41** (2006) 678.

54. M. Ramakrishna Murthy, E. Venkateshwar Rao, *Indian J. Phys.* **84** (2010) 193.

55. S. Balamurugan, P. Ramasamy, S.K. Sharma, Y. Inkong, P. Manyan, *Mater. Chem. Phys.* **117** (2009) 465.

56. S. Balamurugan, P. Ramasamy, Y. Inkong, P. Manyan, *Mater. Chem. Phys.* **113** (2009) 622.

57. S. Srinivasan, P. Ramasamy, A. Cantoni, G. Bocelli, *Mater. Sci. Eng.* **52** (1998) 129.

58. S. Sengupta, S.P. Sengupta, *J. Mater. Sci. Lett.* **15** (1996) 525.

59. I. Pritula, A. Kosinova, M. Kolybayeva, V. Puzikov, S. Bondarenko, V. Tkachenko, V. Tsurikov, O. Fesenko, *Mater. Res. Bull.* **43** (2008) 2777.

60. J. Podder, *J. Cryst. Growth* **237** (2002) 70.

61. X.S. Shajan, C. Mahadeven, *Bull. Mater. Sci.* **27** (2004) 327.

62. S. Suthar, *Ph.D. Thesis*, Saurashtra. University, Rajkot, India. (2008).

63. M. Neuberger, "*Handbook of Electronic Materials",* Vol-5 IFT/Plenum (1971).

64. R. Wytt," *Metal Ceramics & Polymers"*, Cambridge University Press, London (1974).

65. W. A. Wooster, *Widersande and Science Anwendung, Rep Prog. Phys*. **1** (1953) 62.

66. P. M. Onitsch, *Mikroskopie* **2** (1974) 131.

67. H. Haneman, F. Scultz, *Metalkunde* **33** (1947) 122.

68. E.M. Ointsch, *Schweiz. Arch. Angew. Wiss* **19(**1953) 320.

69. P. Grodzinski, *Schwaiz, Arch. Angew. Wiss* **18** (1952) 282.

70. F. Knoop, *Tech. Blatter* **27 (**1937) 472.

71. R. F. Campbell, O. Henderson and M. R. Donlevy, *Trans. A.S.M.* **40 (**1948) 954.

72. W. B. Mott, S. D. Ford, I.R.W Jones, *A.E.R.E, Harwell Report,* **Ir-1** (1952) 945.

73. E.W. Taylor, *J. Inster. Metals* **74** (1948) 183.

74. L. Toman, W.F. Nye, and A. J Gelas, *5th Int. Cong. Electron Microscopy*, **1** (1962)143.

75. P. Grodzinski, *Indust. Diam. Rev*. **12** (1952) 209.

76. A. A Iva'ko, "*Handbook of Hardness Data"*, Ed. GV Samsonov (1971).

77. R. Ittyacchen, *Ph. D Thesis*, University of Madras , India(2003).

78. D. J. Vaidya, *Ph.D. Thesis*, Veer Narmad South Gujarat University, Surat, India. (2005).

79. C. L. Saraf, *Ph.D. Thesis*, M.S. University, Baroda, India (1971).

80. K. Ambujam, *Ph.D. Thesis*, University of Madras, India (2005).

81. K. Sangwal, *J. Mater. Sci*. **24** (1989) 1128.

82. K. Sangwal, *Mater. Chem. and Phys.* **63** (2000) 145.

83. Y. Tirupatiah, G. Sundararajan, *Wear* **110** (1986) 183.

84. K. J. Pratap, V. Hari Babu, *Bull. Mater .Sci*.**2** (1980) 43.

85. P. N. Kotru, "II *National Seminar on Crystal Growth"* Madras, (1984).

86. B.D. Michels, G.H. Frischat, *J. Mater. Sci*. **17**(1982) 329.

87. W.C. Oliver, R. Hutchings and J.B. Pethica, "*Microindentation Techniques In Materials Science and Engineering",* (Eds) P. J. Balu and B. R. Lawn, Astm, Philadenphila (1986).

88. Q. Ma, D. R. Clarke,*J Mater. Res*.**10** (1995) 853**.**

89. H. Li, Y. H. Han, R. C. Bradt, *J. Mater. Sci*.**29** (1994) 5641.

90. H. Li, A. Ghosh, Y. H. Han, R.C. Bradt, *J. Mater. Res.* **8**(1993) 1028.

91. A. Kelley; "*Strong Solids"*, Clarendon Press, Oxford (1966).

92. B. R. Lawn, T. R. Wilson, *J. Mater. Sci*. **10** (1975) 1049.

93. B. R. Lawn, M. V. Swain, *J. Mater. Sci*. **10** (1975) 113.

94. J. T. Hagan, M. V. Swain, J*. Phys.* **D14** (1978) 2091.

95. B. R. Lawn, D. B. Marshall, "*Fracture Mechanics of Ceramics"*, Vol.3, Eds. R. C. Brookes, D. P. H. Flasselman, F. F. Lange; Plenum, New York (1978).

96. S. J. Hockey, B. R. Lawn, *J. Mater. Sci*. **10** (1975) 1275.

97. B. R. Lawn, E. R. Fuller, *J. Mater. Sci*.**10** (1975) 2016.

98. A. G. Evans, E. A. Charles, *J. Amer. Ceram. Soc*. **59** (1976) 371.

99. J. T. Hagan, M. M. Choudhari, *J. Mater. Sci*. **12** (1977) 1055.

100. D. W. Johnson, E. M. Vogel, B. B. Ghate, *Ferrites: Proceeding of International conference,* Sept-Oct 180 Japan, p-285.

101. N. M. Sammes, *J. Mater. Sci. Lett.* **12** (1993).

102. P. J. Burnett,T. F. Page, *J. Mater. Sci.* **20** (1985) 4624.

103. B. R. Lawn, A. G. Evans, D.B. Marshall, *J. Amer. Ceramic Soc*. **63** (1980) 574.

104. G. R. Anstis, P. Chantikul, B.R. Lawn, D. B. Marshall, *J. Amer Ceramic Soc*. **64** (1981) 533.

105. R. Dal Maschio, A. Maddalena, I. Calliariri, *Mat. Chem. & Phys.* **11** (1984) 443.

106. R. G. Wilson, W. Kobis, M. F. Fine, *J. Appl. Phys*. **37** (1966) 704.

107. B. Vengatesan, N. Kanniah, P. Ramasamy, *J. Mater. Sci. Lett.* **5** (1986) 595.

108. K. Blaarishnan, B. Vengatesan, N. Kanniah, P. Ramasamy, *J. Mater. Sci. Lett.* **9** (1990) 785.

109. M. P. Shaskol'skaya, H. K. Ch'ang, M. D. Katrich, Izv Akad Nauk SSR Neorg. Mater **14** (1978) 716.

110. C.H. Guin. *Krist and Technik* **15** (1989) 479.

111. J.E. Marion, *J. Appl. Phys*. **62** (1987) 1595.

112. T. Fang, J.C. Lambropoulos, *J. Am. Ceramic* **174**(2002)85.

113. R. Hill, *Proc.Phys.Soc.* 65A (1952) 349

114. LLE Rev. **86** (2001)101.

115. A.G. Evans, "*In Fracture Mechanics Applied to Brittle Materials"*, Ed. S.W. Freiman, ASTM, **678** (1979).

116. G. R. Anstis, P. Chanticul, B. R. Lown, D.B Marshall, *J. Am. Ceram. Soc.* **64** (1981) 533.

Chapter IX

General Conclusion

As it has been already discussed in the present thesis, KDP crystals play very prominent role in NLO applications. In India, majority of research is carried out on characterization of NLO materials crystals, nevertheless, only few research work is reported on the device applications. It is interesting to note that in Raja Ramanna Centre for Advanced Technology (RRCAT), Indore, the growth of 75 x 75 x 125 mm^3 KDP crystals is reported. The optical homogeneity of KDP crystals was assessed by Mach-Zahnder interferometer [1, 2]. The elctro-optic modulator using DKDP crystal has been fabricated at RRCAT. Moreover, Type-II SHG cell using KDP, with clear aperture of 50 mm and length of 25 mm have been devised at the same institute for doubling Nd:YAG laser.

There are certain characterizations based on very simple techniques but provide very interesting information. Michelson interferometer has been used for imaging the surface micro-morphology of prismatic and pyramidal faces of KDP. The spiral growth mechanism, which has been discussed in chapter – II, has been imagined in form of concentric fringes of equal thickness. These fringes originated from the screw dislocation - generated hillocks on the crystal face were discussed [3].

Another technique employed to study the convection during the growth of KDP crystals is the Shadow-graphy. This technique was employed to map convection around growing crystal. The shadow-graph images are helpful to quantify the free convection in terms of Grashof number and

establish a range beyond which the crystal quality becomes sensitive to fluctuation in concentrations [4, 5].

Doping of suitable compound or element is carried out to engineer and modify the properties of the parent material. This has achieved miraculous results in case of doping in semiconductor crystal. However, in the same line the material scientists and crystal growers have doped several compounds in crystals of their interests. Doping of several compounds has been reported in KDP crystals, which has been discussed elaborately in earlier chapters 3 to 8. After the boom of the nanotechnology, notwithstanding, the doping of nano-materials in KDP is achieved in recent past. The synthesis and non-linear optical properties of KDP crystals containing TiO_2 nano-particles is reported by Prytula et al.[6] Also ZnSe nano-crystals were embedded in KDP crystals by adding it in the mother solution during the growth of KDP crystals[7].

Molds are prepared for different material applications, including normal medical and household applications. For dental treatment, the molds are prepared for making denture. However, this simple technique is ingeniously applied to study the elementary steps on crystals. Replica molding with elastomeric polymers has been used to replicate features less than 10nm size. Because the theoretical limit of this technique is set by polymer-surface interactions, atomic radii and accessible volumes, the replication at sub-nanometer length scale is possible. Using polydimethylsiloxane to create a mold and polyurethrane to form the replica, Elhadj et al. [8] have demonstrated the replication of elementary steps of 3-5 Å in height to define the minimum separation between

molecular layers in lattice of KDP. This technique, however, establishes the operation of replica molding at molecular scale.

The summary of the study carried out by the present author on pure and amino acids, viz., L-histidine, DL-methionine and L-threonine, doped KDP crystals is presented hereby.

1. The solubility of amino acids doped KDP crystals was more than the pure KDP crystals at any particular temperature.
2. The doping of amino acids had affected the nucleation process, which was found by increase in the value of induction period for amino acids doped systems.
3. It was found that the nucleation parameters, viz., interfacial tension, energy of formation of critical nucleus and radius of critical nucleus, decreased as super-saturation increased.
4. The values of nucleation parameters were larger for amino acids doped KDP crystals than the pure KDP crystals. This might be due to formation of specks of amino acids earlier than KDP resulting into accelerated nucleation.
5. CHN analysis and Paper Chromatography confirmed the presence of amino acids in KDP crystals.
6. The FT-IR spectra indicated the presence of C=O stretching, N-H symmetric and asymmetric stretching vibrations, which were absent in pure KDP crystals. This provided indication of presence of amino acids in KDP crystals.
7. The frequency of absorption related to O=P-OH symmetric stretching, O-P-OH symmetric stretching and O=P-OH bending were altered in the

case of amino acids doped KDP crystals, which indicated the interaction of dopant through hydrogen bond of KDP.

8. The Thermo-gravimatric analysis suggested that amino acids doped KDP crystals were slightly less stable than pure KDP crystals. The higher values of activation energy and standard entropy of activation suggested more stable condition for pure KDP crystals than amino acids doped KDP crystals.
9. The dielectric constant was found to be lower in amino acids doped KDP crystals than the pure KDP crystals, which might be due to generation of L-defects upon addition of amino acids.
10. As the doping of amino acids increased, the dielectric loss of KDP crystals decreased, which indicated that the doping of amino acids did not bring major defects.
11. The significant lowering of the dielectric constant on doping of amino acids can make KDP crystals good candidates for electro-optic applications.
12. As the doping of amino acids increased, the SHG efficiency increased.
13. The UV cut off limit decreased slightly on doping amino acids in KDP crystals, however, for L-threonine doping, it remained almost unaltered. Looking at SHG efficiency data and UV cut off limit, it could be concluded that the L-threonine doping in KDP crystals was a better option.
14. In chemical etching studies by glacial acetic acid, the highest activation energy for the lateral motion of ledges of etch-pits for pure KDP was obtained compared to amino acids doped KDP crystals. This

suggested the most stable nature of KDP crystals and doping of amino acids enhanced the reactivity at line defects by facilitating the chemical reaction.

15. The molecular structure of amino acids played important role in chemical etching.
16. The Vickers micro-hardness decreased as the amino acids doping increased in KDP crystals. This indicated that amino acids doping made KDP crystals softer. As the doping concentration of amino acids increased, the load independent hardness and the Newtonian pressure decreased, further indicated that doping had made KDP crystals softer.
17. For the indentations greater than 0.25N loads, the cracks were observed. The fracture toughness values were obtained by applying Anstis model. It was found that as the doping concentration increased, the Vickers micro-hardness decreased and also the fracture toughness decreased. This suggested that the doping of amino acids in KDP crystals made them slightly soft and also more fragile to produce cracks easily.
18. From various characterization results, the author is led to conclude that the amino acids doping in KDP crystals is beneficial from better SHG and better transparency point of view. However, the sacrifice has to be given in terms of slightly less thermal stability, less UV cut off limit and less fracture toughness.
19. From the comparative results of all the three amino acids, L-threonine doping poses a better option in terms of unaltered UV cut off limits.

Suggestions for Future Work

The future work in continuation to the present work may be pursued as follows:

1. It will be interesting to measure different non-linear parameters for amino acids doped KDP crystals, such as Birefringence, damage threshold, NLO susceptibility coefficient, Non-linear index of refraction, effective Non-linear coefficient and optical homogeneity. This study is expected to give complete picture of utility of amino acids doped KDP crystals in devices.
2. It is also required to study in future other parameters such as, beam walk off, phase matching conditions, angular acceptance width, coherence length and conversion efficiency for amino acids doped KDP crystals.
3. It is also interesting to study the higher order of optical susceptibility by techniques like Z-scan for amino acids doped KDP crystals.
4. It will be interesting to carry out further characterization studies on higher order of amino acids doping concentrations in KDP to find of the optimum the limit of doping.
5. A single crystal XRD study can also be conducted in future to find out the exact position of dopant molecules in KDP lattice and their interaction with KDP molecules in lattice.

References

1. S. Dinakaran, S. Verma, S. J. Das, S. Kar, K. S. Bartwal, P.K. Gupta, *Physica B* **405** (2010) 1809.
2. S. Dinakaran, S. Verma, S. J. Das, G. Bhagavannarayana, S. Kar, K.S. Bartwal, *Appl. Phys.* (2010) Doi. 10.1007/s00339-010-5551-1.
3. S. Verma, K. Muralidhar, *Recent Research Development in Crystal Growth* **5** (2009) 141.
4. S. Verma, K. Muralidhar, V. K. Wadhwan, *Ferroelectrics* **323** (2005) 25.
5. S. Verma, *Ph.D. Thesis*, IIT Kanpur, India (2007).
6. I. Prytula, V. Gayvoronsky, M. Kopylovsky, V. Tkachenko, V. Tsurikov, *ISLNOM – 5,* 3-5 sept., RRCAT, Indore, India (2009).
7. A. Bensouici, O. Halimi, A. Chaieb, M. Sebais, *Mediterranean Winter* (2008), DoI: 10.1109/ICTONMW.2008.4773106.
8. S. Elhadj, R. M. Rioux, M. D. Dickey, J. J. De Yoreo, G. M. Whitesides, *Nano. Lett.***10** (2010) 4140.

Bull. Mater. Sci., Vol. 30, No. 2, April 2007, pp. 105–112. © Indian Academy of Sciences.

Thermal, FT–IR and SHG efficiency studies of L-arginine doped KDP crystals

K D PARIKH, D J DAVE, B B PAREKH† and M J JOSHI*

Department of Physics, Saurashtra University, Rajkot 360 005, India
†Institute of Diploma Studies, Nirma University of Science and Technology, S.G. Highway, Ahmedabad 384 481, India

MS received 22 January 2007; revised 12 March 2007

Abstract. Potassium dihydrogen phosphate (KDP) is a well known nonlinear optical (NLO) material with different applications. Since most of the amino acids exhibit NLO property, it is of interest to dope them in KDP. In the present study, amino acid L-arginine was doped in KDP. The doping of L-arginine was confirmed by FT–IR and paper chromatography. Thermogravimetry suggested that as the amount of doping increases the thermal stability decreases as well as the value of thermodynamic and kinetic parameters decreases. The second harmonic generation (SHG) efficiency of L-arginine doped KDP crystals was found to be increasing with doping concentration of L-arginine. The results are discussed here.

Keywords. NLO material; solution growth; doping; FT–IR; TGA; kinetic parameters; thermal parameters; SHG efficiency.

1. Introduction

Potassium dihydrogen phosphate (KH_2PO_4, KDP) and its isomorphous deuterated form, DKDP (KD_2PO_4), are popular due to their applications in frequency converters, electro-optic switching and modulators (Lu and Sun 2002; Sun *et al* 2002). KDP and DKDP crystals have been grown in very large sizes up to 57×57 cm^2 in cross-section and about 55 cm in height (Zaitseva *et al* 1997). KDP and DKDP crystals have been developed for the world's most powerful laser systems (De Yoreo 2002). In order to get good quality crystals rapidly, many techniques have been introduced by several workers (Wang *et al* 1987; Zaitseva *et al* 1999; Dixit *et al* 2001).

Several authors have doped KDP crystals by KI, NaI and Au^+ (Ananda Kumari and Chandramani 2003), ammonium compounds (Freeda and Mahadevan 2000) and urea and thiourea (Priya *et al* 2001). It was found that the doping increased electrical conductivity of KDP crystals. Similarly, light scattering in KDP is found to be due to bacteria (Yokotani *et al* 1988), organic materials (Singleton *et al* 1988) and some indissoluble impurities (Yan *et al* 1986). Since all of amino acids, except glycine, exhibit NLO properties, the present communication is a part of the extensive studies being carried out on the effect of different amino acids doping on the properties of KDP. It has been reported that doping of L-arginine in KDP increases NLO properties of KDP in terms of increase in second harmonic generation efficiency (SHG) (Kumaresan *et al* 2004). In that regard, the effect of doping of amino acid L-arginine on the thermal stability of grown crystals and the kinetic and thermodynamic parameters of dehydration as well as SHG efficiency is reported.

2. Experimental

2.1 *Crystal growth*

Slow evaporation technique was employed to grow crystals. The solubility curve of KDP in double distilled water was experimentally confirmed with the available one in the literature. The doping of L-arginine into KDP was achieved by adding 0·3 and 0·4 wt% solution into saturated KDP solution. The mixture was thoroughly stirred for 8 h for homogenization. Seed crystals were harvested in conventional manner. Best seed crystals of respective doping were selected and placed in appropriate solution for growth. The vessel containing the solution was closed with perforated cover and kept in a constant temperature bath at 40°C to allow slow evaporation of the solvent. Figure 1 shows a photograph of 0·3% L-arginine doped KDP crystal.

2.2 *Characterization*

The crystals were characterized by FTIR spectroscopy, powder XRD and thermogravimetric analysis (TGA). The

*Author for correspondence (mshilp24@rediffmail.com)

Modern Physics Letters B, Vol. 23, No. 12 (2009) 1589–1602

World Scientific
www.worldscientific.com

CRYSTAL GROWTH, THERMAL, OPTICAL, AND DIELECTRIC PROPERTIES OF L-LYSINE DOPED KDP CRYSTALS

KETAN D. PARIKH*,†, DIPAK J. DAVE and MIHIR J. JOSHI
Physics Department, Saurashtra University, Rajkot 360005, India
**ketandparikh@yahoo.co.in*
†*ketandparikh@gmail.com*

Received 1 August 2008
Revised 19 October 2008

Single crystals of pure and various amount of L-lysine doped KDP crystals were grown from aqueous solution. The doping of L-lysine was confirmed by CHN analysis and FT-IR spectroscopy. Powder XRD was carried out to assess the single phase nature of the samples. The effect of doping on thermal stability of the crystals was carried out by TGA and the kinetic and thermodynamic parameters of dehydration were evaluated. It was found that as the amount of doping of amino acid, L-lysine, increased the thermal stability of the grown crystals decreased. However, the second-harmonic generation (SHG) efficiency of Nd:YAG laser and UV-vis spectroscopy studies indicated that as the L-lysine doping increased in KDP crystals the SHG efficiency and optical transmission percentage increased. The dielectric constant and the dielectric loss of L-lysine doped KDP crystals are lower than the pure KDP crystals. Hence L-lysine doped KDP crystals are found to be more beneficial from an application point of view as compared to pure KDP crystals. The results are discussed.

Keywords: NLO materials; crystal growth; FT-IR; CHN; powder XRD; TGA; UV-vis; dielectric study; SHG.

1. Introduction

Potassium dihydrogen phosphate (KDP) crystal exhibits excellent electro-optical and nonlinear optical properties. Easy growth of large single crystals, a broad transparency range, a high optical damage threshold, and relatively low production cost are all qualities that make KDP crystals attractive candidates for a variety of optical applications. KDP is the only nonlinear optical (NLO) material, which has been grown in large sizes, 50–80 cm at a growth rate of 12–15 mm/day, for laser fusion experiments.[1]

Organic NLO crystals offer flexibility of molecular design and high damage resistance to optical radiation. However, the mechanical strength of organic crystals is very low. In general, the complex of organic–inorganic (semi-organic materials) exhibits the benefits of both organic and inorganic nonlinear optical materials.

*Corresponding author.

Titre du document / Document title

Growth and spectroscopic, thermal, dielectric and SHG studies of L- threonine doped KDP c

Auteur(s) / Author(s)

DAVE D. J. ; PARIKH K. D. ; PAREKH B. B. ; JOSHI M. J. ;

Résumé / Abstract

Potassium Dihydrogen Phosphate (KDP) crystals are one of the most popular crystals used
acids also exhibit NLO property; therefore, the effect of doping of one of the amino acids,
Pure and L - Threonine doped KDP crystals were grown by slow solvent evaporation solutio
0.4 weight percent solutions of L - Threonine was added to aqueous solution of KDP. Good
days. Doping of amino acid in grown crystals was confirmed by paper chromatography, (
powder XRD suggested the single phase nature and the unit cell parameters were not altere
was studied by employing TGA. It was observed that on increasing the amount of doping
temperature than that of the pure KDP crystals. The dielectric constant and the dielectric lo
the pure KDP crystals. Increment in the values of the second harmonic generation (SGH) e
to the pure KDP crystals. The percentage optical transmission increased with increasing th
doping of L -Threonine does not alter the physical properties of KDP by large extent, a
discussed.

Revue / Journal Title

Journal of optoelectronics and adavnced materials **ISSN** 1454-4164

Source / Source

2009, vol. 11, n°5, pp. 602-609 [8 page(s) (article)]

Langue / Language

Anglais

Editeur / Publisher

INOE 2000, Bucuresti, (1999) (Revue)

Localisation / Location

INIST-CNRS, Cote INIST : 27497, 35400018825431.0110

N° notice refdoc (ud4) : 21535380

Modern Physics Letters B, Vol. 24, No. 8 (2010) 735–747

DOI: 10.1142/S0217984910022810

GROWTH AND CHARACTERIZATION OF BIS-THIOUREA STRONTIUM CHLORIDE SINGLE CRYSTALS

R. R. HAJIYANI*, D. J. DAVE, C. K. CHAUHAN, P. M. VYAS and M. J. JOSHI†

Crystal Growth Laboratory, Department of Physics, Saurashtra University, Rajkot 360 005, India
**hajiyanirakesh@gmail.com*
†*mshilp24@rediffmail.com*

Received 5 June 2009
Revised 12 July 2009

Bis-thiourea strontium chloride was synthesized and single crystals were grown by the slow solvent evaporation technique using aqueous solvent. The solubility curve was obtained and the determination of the induction period as well as the evaluation of kinetic parameters of nucleation was carried out. The powder XRD analysis suggested orthorhombic crystal structure. The FT-IR spectrum confirmed the presence of various functional groups. The thermo-gravimetry analysis was carried out and the crystals were found to be stable up to 170°C. Applying Coats and Redferm relation to the thermogram, the kinetic and thermodynamic parameters of dehydration were calculated. The dielectric study was carried out in the frequency range of applied field from 500 Hz to 1 MHz. The variations of dielectric constant, dielectric loss, AC resistivity and AC conductivity were studied with frequency. It was found that the dielectric constant and the dielectric loss decreased as the frequency of applied field increased, whereas the AC resistivity increased as the frequency increased.

Keywords: Bis-thiourea strontium chloride; induction period; nucleation parameters; powder XRD; TGA; dielectric study.

1. Introduction

Nonlinear Optical (NLO) materials crystals are in great demand because of their various applications in science and technology, such as different harmonic generators, sum and difference generators and parametric oscillators.[1,2] There are inorganic and organic class of NLO materials available with different merits and demerits.[3,4] however, another class of NLO materials are the semi-organic materials, which possess the properties of both organic and inorganic NLO materials[5–7] such as a wide range of electronic characteristics, mechanical hardness, and thermal stability and, on the other hand, structural variety, large polarizability, and easy processing of the organic molecules. Metal complexes of urea and urea analogs have been explored.[7] Bis-thiourea cadmium chloride[8] and bis-thiourea zinc chloride[9] crystals have been synthesized, grown and characterized, which exhibit good NLO properties. Bis-thiourea cadmium chloride exhibits the highest laser-induced

Effect of Different Amino Acids Doping on Various Characterization of KDP Single Crystals

Mihir J. Joshi[†], Dipak J. Dave[*] and Ketan D. Parikh[†]
[†]Department of Physics, Saurashtra University, Rajkot, 360 005

Email: mshilp24@rediffmail.com

Abstract

Potassium dihydrogen phosphate (KDP) crystals are very popular for Non-linear Optical (NLO) applications. Majority of amino acids also exhibit NLO properties, therefore, the doping of selected amino acids (L- lysine, L- threonine , L- arginine , L – alanine and DL- methionine) in KDP crystals has been investigated. Good quality pure and amino acids doped KDP crystals were grown by slow solvent evaporation technique. For growing the doped KDP crystals, 0.3and 0.4 weight percent solutions of selected amino acids were added to the aqueous solution of KDP. Doping of amino acids in grown crystals was confirmed by the paper chromatography, the C H N analysis and the FT – IR spectroscopy studies. The powder XRD indicated the single phase nature of samples and the unit cell parameters were not altered much due to doping. The second harmonic generation (SHG) efficiency and percentage optical transmission in UV – Vis spectra increased as the doping of amino acids increased in KDP crystals. It was found that the doping of amino acids enhanced the optical properties. The reactivity at line defects in pure and doped KDP crystals were studied by carrying out chemical etching. The values of dielectric constant and the dielectric loss of amino acids doped KDP crystals were lower than the pure KDP crystals.

INTRODUCTION

The Non-linear Optical (NLO) materials crystals have placed themselves at the forefront in technological advancements. As per one survey the total market for NLO materials in 2000 was $425.3 million [1] and was expected to reach $1.66 billion in 2009 [2] and out of which KDP(potassium dihydrogen phosphate) and ADP (ammonium dihydrogen phosphate) and other crystals will have share of $415.6 million. KDP crystal exhibits excellent electro-optical and nonlinear optical properties. Easy growth of large single crystals, a wide and high frequency conversion efficiency, a broad transparency range, a high optical damage threshold against high power laser, and relatively low production cost are all qualities which make KDP crystals attractive candidates for a variety of optical applications. KDP is the only NLO crystal, which has been grown to the sizes 50 –80 cm at a growth rate of 12-15 mm/day needed for laser radiation in high energy inertial confinement fusion experiments [3]. Several modifications in growth techniques have been made to grow good quality KDP crystals. A set up designed and fabricated having bi-directional accelerated seed rotation controller for solution growth was employed for the growth of KDP crystals [4], which was found useful for forced convection configurations to maintain a higher homogeneity of the solution. Using 5 liter capacity crystallizer with accelerated crucible rotation technique (ACRT) and simulated platform geometry to control the hydrodynamic conditions, Dixit et al [5] reported rapid growth of KDP crystals along [100] and [001] directions. Also, KDP crystals were grown along < 001 > direction by using the Sankarnarayana- Ramasamy method in a quest to grow the longest crystal [6].

Doping of various impurities in known amount is usually carried out to engineer various properties of crystals for different applications. Various impurities, when added in known amounts can be called additives, considerably influence the growth kinetics, morphology and quality of grown crystals. They also strongly affect the various physical properties of crystals. Many workers have reported doping of various impurities in KDP crystals, for instance, Mg^{+2} ,Cu^{+2} ,Ca^{+2} and Ni^{+2} doping [7], L-arginine doping [8], metal ions and dyes doping [9], Cerium doping[4] as well as urea and KCl doping [10].

A brief review is made on the work carried out in the present authors' laboratory to study the effect of doping different amino acids in KDP crystals. The aim of doping amino acids was to increase the SHG efficiency of KDP crystals without sacrifice of other properties. The effect of five different amino acids, viz., L- lysine, L- threonine , L-arginine , L – alanine and DL- methionine, on different characterizations of KDP crystals have been discussed hereby.

EXPERIMENTAL

The doping of five different amino acids (L- lysine , L-threonine , L- arginine , L – alanine and DL- methionine)

Cryst. Res. Technol., 1 – 8 (2010) / **DOI** 10.1002/crat.201000019

Growth and characterization of L-alanine doped KDP crystals

K. D. Parikh*[1,2], D. J. Dave[2], B. B. Parekh[3], and M. J. Joshi[2]

[1] M. P. Shah Arts and Science College, Surendranagar, 363 001, India
[2] Crystal Growth Laboratory, Department of Physics, Saurashtra University, Rajkot, 360 005, India
[3] Pandit Deendayal Petroleum University, Gandhinagar, 382 007, India

Received 16 January 2010, revised 11 March 2010, accepted 29 March 2010
Published online 16 April 2010

Key words nonlinear optical crystal, FTIR, TGA, powder XRD, UV-Vis, SHG, dielectric study.

Potassium Dihydrogen Phosphate (KDP) is an excellent inorganic nonlinear optical (NLO) material with different device applications. Most of amino acids possess NLO property; therefore, it is of interest to dope them in KDP crystals. In the present study, amino acid L-alanine doped KDP crystals were grown by slow aqueous solvent evaporation technique. The doping of L-alanine was confirmed by the paper chromatography, the CHN analysis and the FT-IR spectroscopy. The powder XRD was carried out to assess the single phase nature of the samples. The effect of doping on thermal stability of the crystals was studied by TGA and the kinetic and thermodynamic parameters of dehydration were evaluated. As the amount of doping increased the thermal stability of crystals decreased. However, the second harmonic generation (SHG) efficiency and the UV-Vis spectroscopy studies indicated that as the L-alanine doping increased the SHG efficiency and optical transmission percentage increased. The dielectric behavior of the samples has been studied. The variation of dielectric constant, dielectric loss (tanδ), a.c.resistivity and a.c.conductivity with frequency of applied field in the range from 100 Hz to 100 kHz was studied. The dielectric constant and dielectric loss decreased with increase the value of frequency of applied field. The dielectric constant and the dielectric loss values of L-alanine doped KDP crystals were lower than the pure KDP crystals. The results are discussed.

1 Introduction

Potassium Dihydrogen Phosphate (KH_2PO_4 or KDP) single crystals have a high laser damage threshold, a large non-linear optical coefficient, good structural quality and mechanical properties. KDP crystals find several device applications. The electro-optic effect in KDP is used to obtain phase and amplitude modulations [1,2]. The acousto-optic tunable filters have been developed using KDP [3]. For the inertial confinement fusion (ICF) experiments the performance of large aperture switches based on KDP have been assessed for high power laser experiments [4,5]. Rapid growths of large size (40-55 cm) KDP crystals [6] as well as rapid growth of KDP crystals with additives [7] have facilitated to obtain perfect KDP crystals for device application on large scale. But recent interest is focused on the development of new semi-organic NLO (non-linear optical) materials. These materials posses the advantage of both organic and inorganic materials in terms of high thermal and mechanical stability as well as broad optical frequency range, higher SHG (second harmonic generation) efficiency and high damage threshold [8-10]. The family of semi-organic NLO materials has been growing larger and larger by addition of new compounds.

Amino acids exhibit specific features of interest [11] such as (i) molecular chirality, which secures non-centro symmetric crystallographic structure, (ii) absence of strongly conjugated bonds, which leads to wide transparency ranges in the visible and UV spectral regions, and (iii) zwitter ionic nature of the molecule, which favors crystal hardness for applications in devices. The growth of amino acid L-alanine (CH_3CHNH_2COOH) single crystal is reported in the literature. L-alanine was first crystallized by Bernal [12] in 1931 and later on crystal structures were studied at room temperatures and lower temperatures [13, 14]. The unit cell parameters of L-alanine are; a = 6.320 Å, b = 12.343 Å, c = 5.784 Å, $\alpha = \beta = \gamma = 90°$. The growth of pure L-alanine crystals was reported by Vijayan et al. [15] and found higher damage threshold than KDP. The doping of lithium in L-alanine crystals increased the second harmonic generation (SHG) efficiency, but it remained lower

* Corresponding author: e-mail: ketandparikh@yahoo.co.in, ketandparikh@gmail.com